THE ROLE OF THE INTESTINE-LIVER AXIS IN TCDD-ELICITED NON-ALCOHOLIC FATTY LIVER DISEASE IN MICE

By

Kelly A. Fader

A DISSERTATION

Submitted to
Michigan State University
in partial fulfillment of the requirements
for the degree of

Biochemistry and Molecular Biology – Environmental Toxicology – Doctor of Philosophy

2018

ABSTRACT

THE ROLE OF THE INTESTINE-LIVER AXIS IN TCDD-ELICITED NON-ALCOHOLIC FATTY LIVER DISEASE IN MICE

By

Kelly A. Fader

Non-alcoholic fatty liver disease (NAFLD), a spectrum of liver disorders in which simple hepatic lipid accumulation (hepatic steatosis) progresses to steatohepatitis with fibrosis, is approaching epidemic prevalence in the United States. Often considered to be the hepatic manifestation of metabolic syndrome (MetS), NAFLD increases the risk of developing other complex metabolic disorders (e.g. diabetes, cardiovascular disease, hepatocellular carcinoma) and was recently identified as the second leading cause for requiring a liver transplant. Several factors are known to contribute to NAFLD development including genetic determinants, diet, lifestyle choices, and age. Recently, disruptions in circadian rhythm such as shift work, jet lag, and binge eating have also been associated with NAFLD. Moreover, accumulating evidence demonstrates that exposure to environmental contaminants such as 2,3,7,8-tetrachlorodibenzo-*p*-dioxin (TCDD) and related aryl hydrocarbon receptor (AhR) agonists plays an underappreciated role in the development of metabolic disorders. In rodent models, TCDD-elicited AhR activation causes hepatotoxic features resembling human NAFLD including hepatic lipid accumulation, inflammation, and fibrosis, while chronic exposure increases the incidence of hepatocellular carcinoma. Hepatic and intestinal homeostasis are closely linked by portal and enterohepatic circulation, and thus dysregulation of this intestine-liver axis has been associated with NAFLD and other complex metabolic disorders. However, AhR-mediated transcriptional and functional changes along the intestinal tract have not been thoroughly investigated.

This report evaluates the role of the intestine-liver axis in the development and progression of AhR-mediated NAFLD in mice orally gavaged with TCDD every 4 days for 28 days. High throughput analyses such as RNA-Sequencing, AhR chromatin immunoprecipitation (ChIP)-

Sequencing, and metabolomics were integrated with targeted assessments including protein measurements, serum biochemistry, microbial gene quantification, and functional assays. TCDD-elicited segment-specific changes along the intestinal tract suggest: (i) dysregulation of dietary iron absorption in the duodenum leads to systemic iron overloading, (ii) enhanced lipid digestion and absorption in the jejunum contributes to hepatic lipid accumulation, (iii) increased bile acid reabsorption in the ileum dysregulates enterohepatic circulation, and (iv) increased microbial bile acid metabolism in the colon results in accumulation of hepatotoxic secondary bile acids. AhR activation also increased paracellular permeability in the gastroduodenal and colonic regions, decreased gut motility, and depleted antigen-presenting cells in the intestinal lamina propria, which may promote hepatic inflammation. Moreover, TCDD dampened the rhythmic expression of core hepatic clock regulators and impaired cues (e.g. heme) which entrain hepatic cycling to nutrient availability. In turn, the rhythmicity of the hepatic transcriptome and metabolome was abolished, decoupling hepatic metabolism from feeding/fasting cycles and reducing metabolic efficiency. Collectively, TCDD-elicited alterations along the intestine-liver axis promote several features of AhR-mediated NAFLD including dietary lipid accumulation, oxidative stress, inflammation, bile acid accumulation, and metabolic reprogramming. These studies provide novel insight into the underlying mechanisms involved in AhR-mediated NAFLD, while highlighting the importance of intestine-liver and host-microbiota relationships in complex metabolic disorders.

ACKNOWLEDGMENTS

Completing my PhD would not have been possible without the encouragement and guidance of so many in my life and thus I extend my sincerest gratitude to everyone who has supported me in this process.

To my advisor Dr. Zacharewski, thank you for offering me a place in your lab over the past 6 years. I could not have asked for a better mentor - I have learned so much from you during my graduate career. You have made me an independent, critically-thinking scientist and have provided me with countless opportunities to present my research. And thank you for always smuggling All Dressed chips across the border! I would also like to thank Jana, Lara, and Nic for always inviting me to spend the American holidays with your family.

To my committee, Dr. DeWitt, Dr. Kaminski, Dr. McCabe, and Dr. Wang, thank you for your expertise, guidance, and insight into my project, and for pushing me to think outside the box. I appreciate all the time you have devoted to my scientific career.

To all the past and current members of the Zacharewski lab, thank you for your help, scientific discussions, and advice. Rance and Ania, I would not have made it through this process without your mentorship, reassurance, optimism, and most importantly friendship, and I am incredibly grateful for this. Agnes, thank you for teaching me to pipette and for inspiring me to go to grad school. I would also like to thank Claire for helping me fight the war over the thermostat, Dustin for putting up with my color-coding, and Russ for guiding me through the complex world of untargeted mass spectrometry analysis.

To the Biochemistry and Molecular Biology Department and the Institute for Integrative Toxicology, thank you for providing me with financial support, career building opportunities, and excellent seminars. Thank you to the Canadian Institutes of Health Research (CIHR) for supporting my research in the United States. Also, Jessica Lawrence, thank you for all your patience and hard work in helping me navigate the unique circumstances of this fellowship and for always finding a way to obtain the elusive parking pass.

To my friends, thank you for reminding me what's important in life. To Chloe for making me jump out of an airplane, to Emily and Lorna for driving 5 hours to see 'Waitress' with me, to Sarah and Sean for waiting while I took a picture of every piece of memorabilia at the Bond exhibit, to Dan for always recognizing my quotes from 'The Office', and to Brian for telling me like it is – thank you!

To my parents, it is impossible to put into words how grateful I am for your unwavering love and encouragement over the past 28 years. You have supported me at every stage in my education and life - this has meant the world to me and I would not have made it here without you. And to my sister and nieces, thank you for always having my back and for creating one-of-a-kind artwork for my condo.

To Jem and Scout, thank you for making sure I never wrote alone.

Lastly, to the Blue Jays, thank you for finally breaking your 22-year long playoff drought and for waiting until I was living in a different country to do so… we'll get 'em next year (or the year after)!

TABLE OF CONTENTS

LIST OF TABLES

LIST OF FIGURES

KEY TO ABBREVIATIONS

AFLD	alcoholic fatty liver disease
AhR	aryl hydrocarbon receptor
ARNT	aryl hydrocarbon receptor nuclear translocator
BCA	bicinchoninic acid
bHLH	basic helix-loop-helix
BMD	benchmark dose
BMDL	benchmark dose lower confidence limit
BMR	benchmark response
βNF	β-naphthoflavone
ChIP	chromatin immunoprecipitation
DAVID	Database for Annotation, Visualization, and Integrated Discovery
DC	dendritic cell
DEG	differentially expressed gene
DRE	dioxin response element
ED_{50}	median effective dose
ES	enrichment score
FC	fold change
FDR	false discovery rate
Fe	iron
FICZ	6-formylindolo[3,2-b]carbazole
GEO	Gene Expression Omnibus
GO	Gene Ontology
gWAT	gonadal white adipose tissue

H&E	hematoxylin and eosin
HAH	halogenated aromatic hydrocarbon
HSV	hue, saturation, value
ILC	innate lymphoid cell
LPS	lipopolysaccharide
MetS	metabolic syndrome
MS	mass spectrometry
MSS	matrix similarity score
NAFLD	non-alcoholic fatty liver disease
NASH	non-alcoholic steatohepatitis
ORO	oil red O
PAH	polycyclic aromatic hydrocarbon
PAS	Per-Arnt-Sim
PCB	polychlorinated biphenyl
PCDD	polychlorinated dibenzo-*p*-dioxin
PCDF	polychlorinated dibenzofuran
pDRE	putative dioxin response element
PND	postnatal day
POP	persistent organic pollutant
PSR	picro-sirius red
PWM	position weight matrix
qRT-PCR	quantitative real-time polymerase chain reaction
QuHAnT	Quantitative Histological Analysis Tool
RgWATW	relative gonadal white adipose tissue weight
RLW	relative liver weight

ROS	reactive oxygen species
RTSF	Research Technology Support Facility
SCN	suprachiasmatic nucleus
SEM	standard error of the mean
TAG	triacylglycerol
TCDD	2,3,7,8-tetrachlorodibenzo-*p*-dioxin
TCDF	2,3,7,8-tetrachlorodibenzofuran
TEF	toxic equivalency factor
TSS	transcription start site
UTR	untranslated region
ZT	zeitgeber time

CHAPTER 1: LITERATURE REVIEW

INTRODUCTION

Non-alcoholic fatty liver disease (NAFLD) is a spectrum of disorders in which hepatic lipid accumulation (steatosis) progresses to chronic steatohepatitis (steatosis with inflammation) and fibrosis [1, 2]. Recently identified as the second leading cause for requiring a liver transplantation, NAFLD is approaching epidemic prevalence in the United States [3-5]. Accumulating evidence suggests that the environmental contaminant 2,3,7,8-tetrachlorodibenzo-*p*-dioxin (TCDD) and related aryl hydrocarbon receptor (AhR) agonists play an underappreciated role in NAFLD development [6-9]. In rodent models, a single bolus dose of TCDD induces hepatic steatosis [10], with progression to steatohepatitis and fibrosis following repeated treatment [11, 12].

Hepatic and intestinal homeostasis are closely linked through portal and enterohepatic circulation, where factors which cross the intestinal barrier (e.g. nutrients, minerals, microbial products) are directly delivered to the liver for metabolism or detoxification. As a result, perturbations along the intestine-liver axis, including changes in intestinal permeability and motility, nutrient absorption, bile acid homeostasis, and the gut microbiome, promote the development and progression of NAFLD [13-15]. Moreover, NAFLD has recently been associated with disruptions in circadian rhythm, where hepatic metabolism becomes decoupled from feeding/fasting cycles and nutrient availability [16-18]. To date, AhR-mediated transcriptional and functional changes along the intestinal tract have not been thoroughly investigated. Furthermore, little is known about the effects of AhR activation on the circadian regulation of hepatic metabolism. Understanding the intestine's role in AhR-mediated NAFLD will not only provide novel insight into the molecular mechanisms of toxicity but may also identify novel targets for the treatment of chronic liver diseases and complex metabolic disorders.

ARYL HYDROCARBON RECEPTOR SIGNALING

The AhR is a ligand-activated transcription factor best known for serving as an environmental sensor to xenobiotics and drugs [19]. It is well established that the AhR regulates

the expression of several xenobiotic-metabolizing enzymes including cytochrome P450s (e.g. *Cyp1a1*, *Cyp1b1*, and *Cyp1a2*), glutathione-S-transferases (GSTs), and UDP-glucuronosyltransferases (UGTs), which not only facilitates an adaptive response to a chemical insult but may also promote the chemical's toxicity [20]. Beyond its role as an xenobiotic sensor, studies involving AhR-null animals demonstrate that it serves an underappreciated role in normal physiology and organ development, regulating cell differentiation, proliferation, adhesion, and migration [21-24].

In the canonical pathway, ligand binding to the cytoplasmic AhR causes dissociation from heat shock protein 90 (HSP90), AhR-interacting protein (AIP; aka XAP2), and p23 chaperone proteins, followed by translocation to the nucleus and heterodimerization with the aryl hydrocarbon receptor nuclear translocator (ARNT). The AhR/ARNT complex binds to dioxin response elements (DREs; 5'-GCGTG-3' core sequence) and recruits transcriptional co-regulators, leading to differential expression of target genes (Figure 1) [25, 26]. Beyond the canonical pathway, accumulating evidence demonstrates DRE-independent mechanisms of differential gene expression including non-consensus xenobiotic response elements (NC-XREs), tethering to other transcription factors, and alternative binding partners (e.g. Krüppel-like factor 6 (KLF6)) [27-30]. The 'AhR gene battery' refers to a group of classic AhR target genes which are differentially expressed in most tissues and species including *Cyp1a1*, *Cyp1a2*, *Cyp1b1,* TCDD-inducible poly(ADP-ribose) polymerase (*Tiparp*), NAD(P)H dehydrogenase quinone 1 (*Nqo1*), and *Ugt1a6* [31]. However, target genes from a wide range of metabolic pathways and biological processes have been identified including lipid metabolism, gluconeogenesis, redox homeostasis, differentiation/development, apoptosis, and immunological responses [10].

Both AhR and ARNT are members of the basic helix-loop-helix (bHLH) Per-Arnt-Sim (PAS) family [32]. The peptide sequence of the mouse AhR contains 805 amino acids organized into the following structural domains: (i) a bHLH domain near the amino-terminus, (ii) a PAS domain consisting of PAS-A and PAS-B motifs, and (iii) a transactivation domain near the

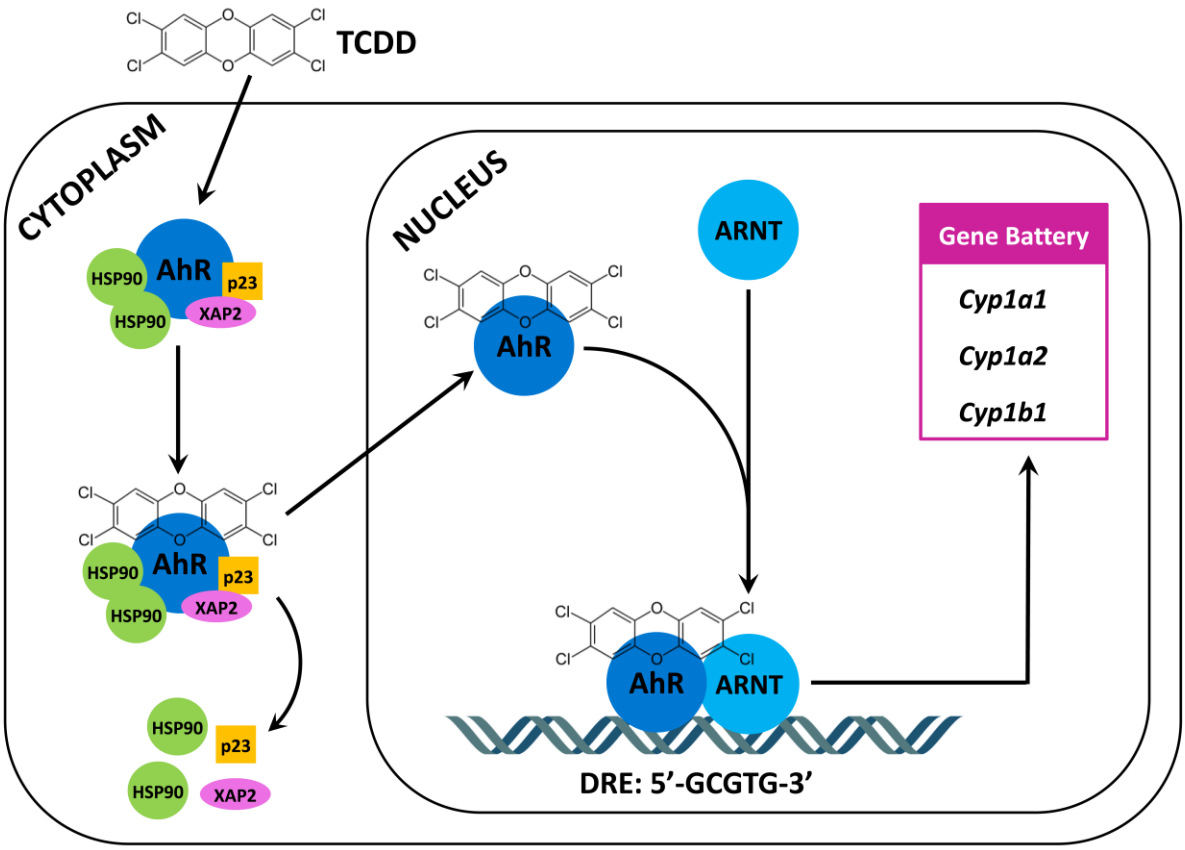

FIGURE 1. THE CANONICAL SIGNALING PATHWAY OF THE ARYL HYDROCARBON RECEPTOR

carboxy-terminus [33, 34]. The bHLH domain of AhR facilitates heterodimerization with ARNT and is responsible for binding DNA at specific response elements [35]. The PAS-A motif is also involved in dimerization with ARNT [36], while PAS-B forms the ligand-binding region and enables binding with chaperone proteins [35, 37]. The glutamine-rich transactivation domain is responsible for recruiting transcriptional co-activators [38]. Although functionally similar to nuclear receptors such as the estrogen (ER), thyroid hormone (THR), and retinoic acid (RAR) receptors, the AhR does not contain the structural domains required for membership within the nuclear receptor superfamily [39].

AhR-mediated differential gene expression elicits a broad spectrum of toxic responses in a cell-, tissue-, species-, sex-, and ligand-specific manner [40, 41]. Suppression of the immune system is one of the most sensitive endpoints of AhR activation, involving direct impairment of B lymphocyte differentiation and IgM antibody secretion, as well as thymic atrophy [42-45]. Although most AhR ligands are not directly genotoxic themselves, AhR activation promotes tumorigenesis in several tissues (e.g. liver, lung, skin, and thyroid) by impairing apoptosis of preneoplastic cells and dysregulating growth-related signaling pathways [46-49]. Additionally, AhR activation elicits dermal lesions such as chloracne [50], reproductive toxicity [51, 52], teratogenicity [53, 54], and altered mineralization in bones and teeth [55, 56]. Furthermore, AhR activation causes hepatotoxicity involving lipid accumulation, immune cell infiltration, and collagen deposition, which will be the focus of this report [10, 11, 57]. Although the canonical AhR signaling pathway is well established, the initial target genes and downstream sequence of events leading to these toxic endpoints remain poorly understood.

TCDD AND RELATED AHR AGONISTS

The AhR can be bound and activated by a wide range of structurally diverse ligands. This suggests that the ligand binding domain of AhR is quite promiscuous, providing the organism with the ability to detect a broad range of chemicals [58, 59]. There are two major classes of AhR

ligands: (i) synthetic ligands produced through anthropogenic activity, and (ii) naturally occurring ligands formed in biological organisms (Figure 2). To date, most high affinity AhR ligands are classified as synthetic, including planar halogenated aromatic hydrocarbons (HAHs) (e.g. polychlorinated dibenzo-*p*-dioxins (PCDDs), dibenzofurans (PCDFs), and biphenyls (PCBs)) and polyaromatic hydrocarbons (PAHs) (e.g. benzo[a]pyrene (BaP), benz[a]anthracene, benzoflavones, and 3-methylcholanthracene (3MC)) (Figure 2) [60-62]. HAHs are more metabolically stable and potent than PAHs, with binding affinities in the pM to nM range compared to HAH binding affinities that typically fall in the nM to μM range [58, 63]. More recently, several synthetic ligands have been identified with structures that differ drastically from the classical PAHs and HAHs including thiabendazole and 1-methyl-1-phenylhydrazine, however most of these 'nonclassical' ligands are relatively weak inducers of *Cyp1a1* expression with low affinity for AhR [58, 64].

The ubiquitous environmental contaminant TCDD is the most potent AhR agonist and is classically considered to be the prototypical ligand of the AhR. The relative potency of other synthetic AhR ligands, termed 'toxic equivalency factors' (TEFs), are therefore typically determined relative to TCDD, allowing the hazard of HAH mixtures to be estimated during risk assessment [60, 62]. TCDD was never intentionally manufactured, but rather is formed as a contaminant during industrial processes including pulp bleaching at paper mills, waste incineration, and organochlorine pesticide/herbicide manufacture [65, 66]. TCDD achieved notoriety for its presence as a contaminant in the defoliant Agent Orange used during the Vietnam War during the late 1960s, exposing military personnel and Vietnamese civilians to high levels of the toxicant [67-69]. Additional incidents involving accidental exposure to high concentrations of TCDD include: (i) the explosion of a 2,4,5-trichlorophenol reactor at a chemical plant near Seveso, Italy in 1976 [70, 71], (ii) two separate incidents (1953 and 1988) at the Baden Aniline and Soda Factory (BASF) chemical company in Germany, leading to acute, high-dose exposure to employees [72, 73], (iii) spraying dirt roads in eastern Missouri (Times Beach, Quail Run Trailer

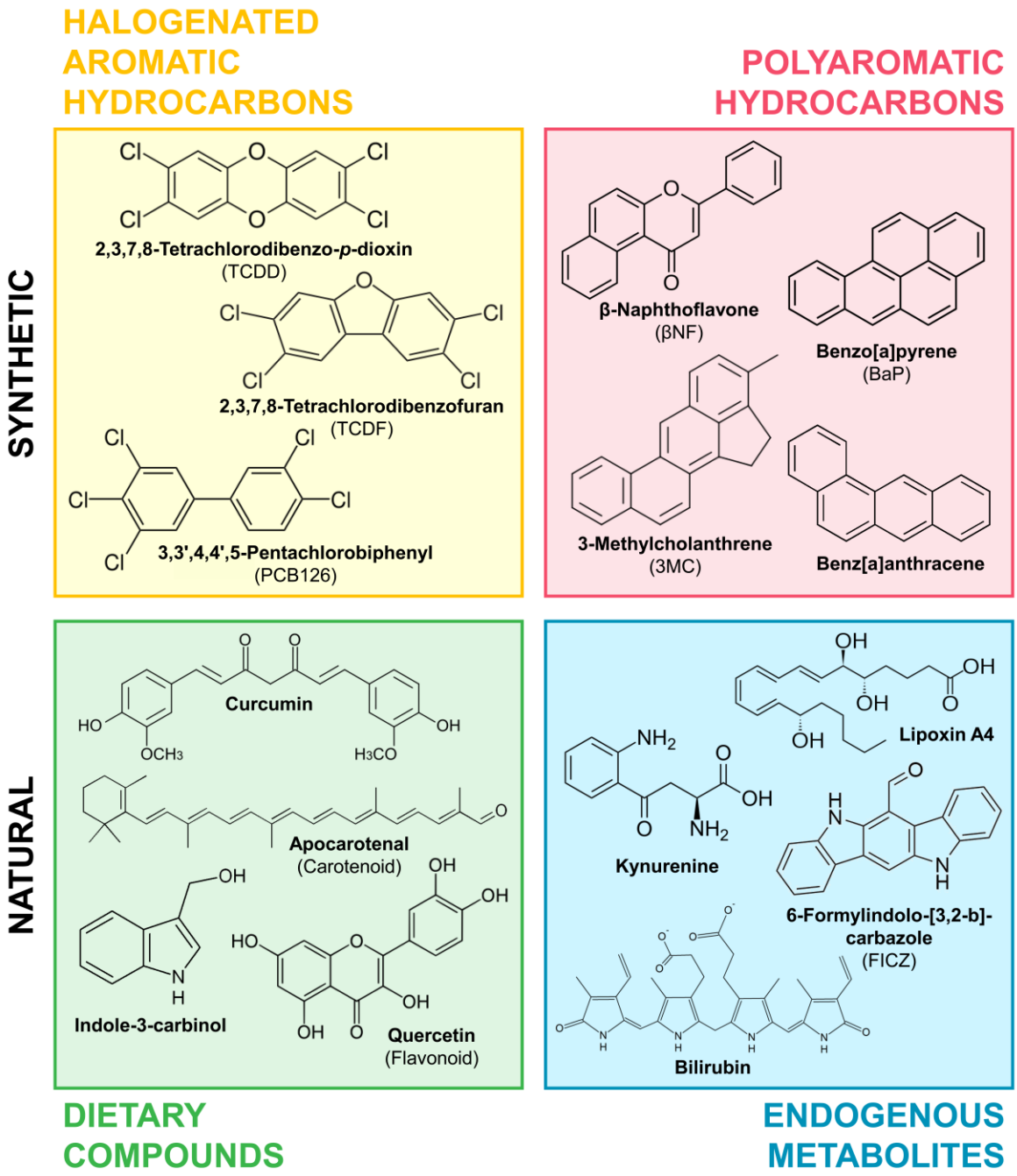

FIGURE 2. DIVERSITY OF SYNTHETIC AND NATURAL AHR LIGANDS

Park) with TCDD-contaminated oil [74, 75], and (iv) the occupational exposure of employees at herbicide and chemical manufacturing plants such as Dow Chemical and Monsanto [76, 77]. Furthermore, a few cases of intentional poisoning have been reported, including the 2004 poisoning of Viktor Yushchenko during the Ukrainian presidential election, leading to dermal lesions termed chloracne [78].

Beyond the contribution from industrial sources, TCDD is also released into the environment through combustion processes such as fuel burning (e.g. wood, coal, oil), forest fires, and volcanic eruptions [65]. As a result of its lipophilic nature and high degree of chlorination, TCDD is highly persistent in the environment, where it biomagnifies through the food chain and bioaccumulates within the fat-depots of animals [79, 80]. Today, the primary source of TCDD exposure for the general public is through the consumption of animal-derived foods including fish, meat, milk, and eggs [81, 82]. Once consumed, TCDD is stable within the body due to negligible metabolism [80]. Although levels of TCDD and related dioxin-like compounds in the environment are decreasing, the cumulative exposure to all potential synthetic AhR ligands such as PAHs and polybrominated HAHs (e.g. polybrominated flame retardants) may be increasing [83-85], and thus the adverse effects of inappropriate AhR activation remain a relevant health concern.

Naturally occurring AhR ligands consist of both natural exogenous compounds consumed through the diet and endogenously synthesized metabolites (Figure 2). The intestinal lumen is a rich source of natural AhR ligands including both dietary compounds and microbially-derived products, which may exhibit agonistic or antagonistic effects on the canonical pathway [86]. The potential for these gut-derived ligands to affect AhR signaling depends on their absorption, metabolic stability, and plasma half-life. The majority of dietary AhR ligands originate from plant materials such as vegetables, fruits, or teas including indole-3-carbinol (I3C) [87], curcumin [88], carotenoids (e.g. apocarotenal) [89], and flavonoids (e.g. quercetin) (Figure 2) [90]. I3C, generated from glucobrassicin in cruciferous vegetables, undergoes acid condensation within the mammalian intestinal tract to yield indolo[3,2-b]carbazole (ICZ), which is the most potent natural

AhR ligand identified to date [87]. The gut microbiome also contributes to the pool of intestine-derived AhR ligands, where bacterial metabolism of tryptophan yields indoles capable of stimulating AhR activity including indole-3-aldehyde and indole-3-acetate [91, 92].

Despite accumulating evidence that AhR serves a physiological role in cell differentiation and proliferation, no high-affinity endogenous ligand has been identified to date and thus the AhR is often classified as an 'orphan receptor'. However, several studies have identified endogenous chemicals capable of binding AhR with relatively low affinity and weakly activating AhR-dependent gene expression (Figure 2), many of which are metabolized by the detoxification enzymes they induce [58]. Several endogenous tryptophan metabolites have been shown to activate AhR including 6-formylindolo[3,2-b]carbazole (FICZ), tryptamine, indole acetic acid, kynurenine, indigo, and indirubin [93-96]. FICZ, which is structurally similar to diet-derived ICZ, is a photo-oxidation product of tryptophan. It is hypothesized that FICZ may serve as a chemical messenger of light formed in the skin of UV-irradiated mammals, relaying the periodicity of the solar cycle [97]. Interestingly, accumulating evidence suggests that AhR may play a physiological role in circadian regulation, while other PAS proteins such as aryl hydrocarbon receptor nuclear translocator-like (ARNTL), circadian locomotor output cycles kaput (CLOCK), and period (PER) are core regulators of circadian rhythm [98, 99]. Given that AhR activation is reported to disrupt heme biosynthesis [100], it is not surprising that tetrapyrrole metabolites have been found to bind to the AhR. For example, bilirubin, the primary product of heme degradation, induces AhR-dependent gene expression, thereby stimulating its own detoxification through UGT1A1- and CYP1A1/1A2-dependent metabolism [101]. Additionally, arachidonic acid metabolites including lipoxin A4 and prostaglandin G_2 have been shown to bind AhR and activate DRE-dependent gene expression [102, 103], providing further evidence that AhR plays a role in regulating eicosanoid signaling [104]. Recently, homocysteine was identified as a novel endogenous agonist of the AhR, where hyperhomocysteinemia promotes hepatic lipid accumulation through induction of the *Cd36* fatty acid transporter [105]. High throughput screening bioassays and virtual screening of ligand

libraries are currently being employed to identify additional exogenous and endogenous ligands for the AhR, providing further insight into its physiological role [106-108].

NON-ALCOHOLIC FATTY LIVER DISEASE

Fatty liver disease is a spectrum of liver disorders in which hepatic lipid accumulation (steatosis) progresses to chronic steatohepatitis (steatosis with inflammation) and fibrosis (collagen deposition) (Figure 3) [1, 2]. Although hepatic steatosis is benign and completely reversible, hepatic inflammation and fibrosis are considered to be more severe as they are largely irreversible and may lead to cirrhosis and/or hepatocellular carcinoma [109, 110]. Fatty liver disease is typically classified as either ‘alcoholic’ (AFLD) or ‘non-alcoholic’ (NAFLD) depending on whether or not it is linked to excessive alcohol consumption (20-40 g/day for men; 20g/day for women), however both sub-types present similar histopathological features [111].

In 2013, NAFLD became the second leading cause for requiring a liver transplant after hepatitis C virus, with the number of NAFLD patients awaiting a liver transplant nearly tripling since 2004 [3]. Additionally, non-alcoholic steatohepatitis (NASH) has been identified as the most rapidly increasing cause of hepatocellular carcinoma in Western countries [112]. Often considered to be the hepatic manifestation of metabolic syndrome (MetS), NAFLD progression increases the risk of developing complex systemic metabolic diseases including cardiovascular disease (CVD) and type II diabetes [109, 110, 113]. The prevalence of NAFLD is continuously increasing both in the United States and worldwide [4], currently affecting approximately 27-34% of Americans [5, 114]. Elucidation of contributing factors and mechanisms involved in NAFLD development may lead to novel therapeutic strategies, which would be of great value to public health.

Several factors are known to contribute to the development of NAFLD, including genetics, high caloric diet, sedentary lifestyle, and age [115-117]. Recently, dysregulation of circadian rhythm resulting from disrupted sleep/wake and feeding/fasting cycles (e.g. shift work, jet lag) has also been associated with metabolic diseases such as NAFLD, diabetes, and cancer [16-18].

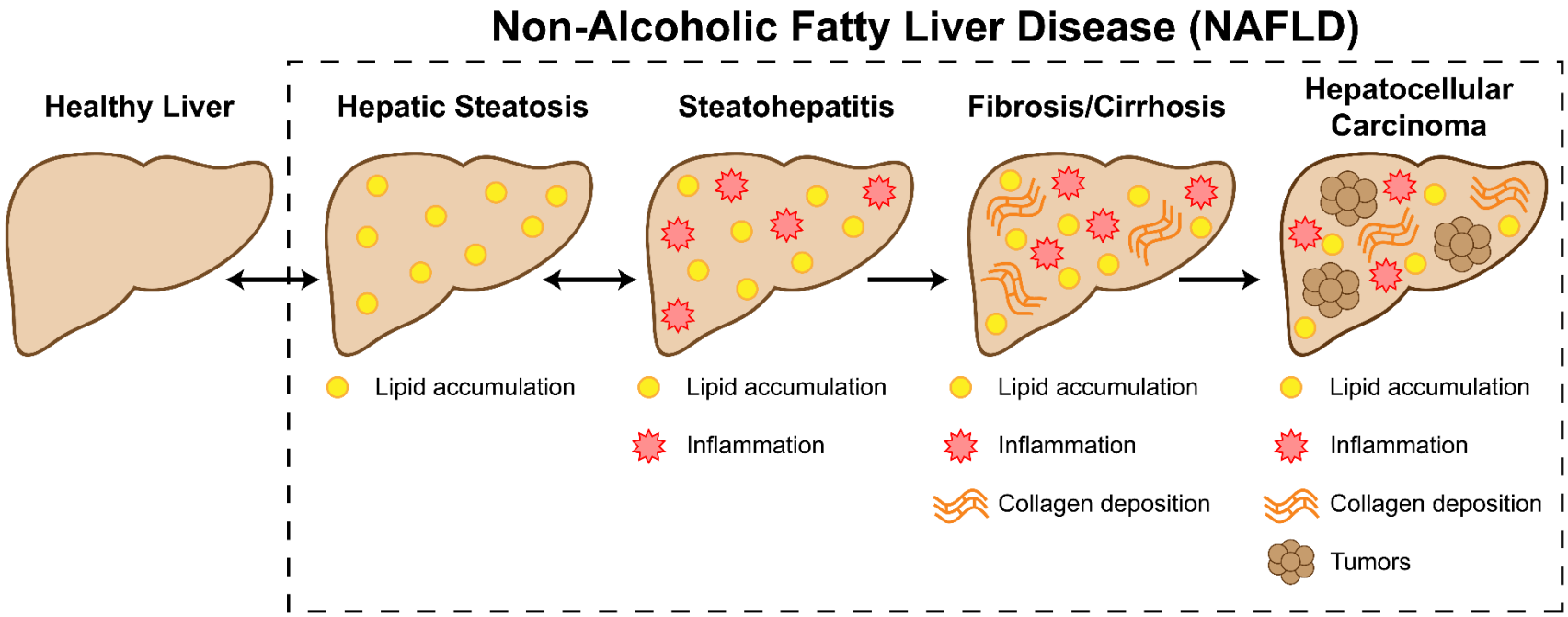

FIGURE 3. STAGES OF NON-ALCOHOLIC FATTY LIVER DISEASE PROGRESSION

Furthermore, accumulating evidence suggests that exposure to TCDD and other persistent AhR agonists plays an underappreciated role in the development of NAFLD and other complex metabolic disorders [6-9]. However, the extent to which circadian dysregulation and environmental contaminants contribute, and the underlying mechanisms involved, have not been fully elucidated.

ROLE OF TCDD IN FATTY LIVER DISEASE

TCDD and other AhR agonists have been shown to cause hepatotoxic features resembling NAFLD in several animal models. In mice, a single bolus dose of TCDD elicits AhR-dependent lipid accumulation in the liver, which is completely reversed 4 weeks later [10, 118, 119]. Progression to steatohepatitis with fibrosis has been observed following repeated TCDD exposure in mice [11]. AhR null (*Ahr-/-*) mice do not exhibit lipid accumulation or immune cell infiltration following TCDD treatment, demonstrating that TCDD-elicited NAFLD is AhR-dependent [119]. Similarly, dioxin-like PCB126 and 3MC are also reported to cause hepatic steatosis in mice [120, 121]. AhR-mediated hepatic lipid accumulation has also been observed in PCB-treated rats [57, 122] and BaP-treated killifish [123]. Furthermore, chronic TCDD exposure over a 2-year period increases the incidence of hepatocellular carcinoma in rodents, where male mice are more susceptible than female mice, and vice versa in rats [47, 124].

In rodent models, AhR-mediated NAFLD cannot be attributed to dysregulation of a single target gene or metabolic pathway, but rather is a collective response to the cumulative burden of multiple disrupted pathways and physiological processes [125]. TCDD-elicited hepatic lipid accumulation is largely attributed to induction of transporters/receptors involved in the hepatic uptake of fatty acids (e.g. *Cd36*) and chylomicron remnants (e.g. very low density lipoprotein receptor (*Vldlr*)) [10, 121, 126]. Impaired assembly of lipoproteins (e.g. repression of apolipoprotein B (*Apob*)), coupled with repression of enzymes involved in peroxisomal beta oxidation (e.g. acetyl-CoA acyltransferase 1B (*Acaa1b*) and acyl-CoA oxidase 1 (*Acox1*)), further

promote hepatic lipid accumulation by reducing the export and breakdown of fatty acids [126, 127]. These accumulating lipids are highly susceptible to peroxidation as a result of AhR-mediated oxidative stress. AhR activation stimulates reactive oxygen species (ROS) production through several processes including induction of cytochrome P450s (e.g. *Cyp1a1*) and oxidoreductases (e.g. xanthine dehydrogenase/xanthine oxidase (XDH/XO)), partial uncoupling of oxidative phosphorylation, peroxisome proliferation, and the inhibition of selenium-dependent glutathione (GSH) peroxidase [10, 127, 128]. Beyond lipid peroxidation, this oxidative stress can damage the proteins, DNA, and membrane integrity of hepatocytes, resulting in the release of damage-associated molecular patterns (DAMPs) and the activation of resident hepatic macrophages (Kupffer cells). Following activation, Kupffer cells release pro-inflammatory cytokines such as TNFα, IL-1β, and IL-6, which trigger the recruitment of immune cells (circulating monocytes, neutrophils) to the liver [10]. Warburg-like metabolic reprogramming driven by pyruvate kinase M2 (*Pkm2*)-induction helps to counteract oxidative stress by supporting nicotinamide adenine dinucleotide phosphate (NADPH) biosynthesis and GSH recycling [127]. Hepatic inflammation not only further propagates ROS production, but also stimulates profibrotic signaling (e.g. TGFβ2, TNFα) which promotes the differentiation of hepatic stellate cells and portal fibroblasts into collagen-producing myofibroblasts [11, 12]. Dysregulation of glycogen, ascorbic acid, and amino acid metabolism supports remodeling of the extracellular matrix, further promoting the development of hepatic fibrosis [12].

In humans, epidemiological studies have identified an association between accidental exposure to AhR agonists and an increased risk of NAFLD and other complex metabolic disorders [6-8]. For example, the Taiwanese “Yucheng” cohort which consumed PCB- and PCDF-contaminated cooking oil in 1979 exhibited an elevated mortality rate from chronic liver disease and cirrhosis compared to the general population [129]. Furthermore, a study involving Taiwanese residents living near a closed pentachlorophenol (PCP) factory reported that individuals with high serum levels of PCDDs/PCDFs and a high body mass index (BMI) exhibited a significantly

elevated risk of developing hepatic steatosis [130]. Analysis of the National Health and Nutrition Examination Survey (NHANES, 2003-2004) dataset identified a dose-dependent association between blood PCB levels and increased alanine amino transferase (ALT) levels, where elevated ALT in the absence of viral hepatitis, ethanol, or iron was used as a surrogate biomarker for NAFLD [9]. Additionally, Italian residents exposed to TCDD during the Seveso industrial accident and Vietnam War veterans exposed to Agent Orange exhibited an increased incidence of both diabetes and CVD [131, 132]. Beyond epidemiological studies, TCDD elicits *in vitro* lipid accumulation in human primary hepatocytes [133] and *in vitro* activation of human hepatic stellate cells [134]. Further studies are required to compare the mechanisms of AhR-mediated NAFLD between humans and rodent models.

SEGMENT-SPECIFIC FUNCTIONS OF THE INTESTINE

The intestine of monogastric mammals such as humans and rodents is divided into two primary sections – the small intestine and the large intestine. The small intestine is further subdivided into three segments: (i) the duodenum, the shortest region which connects to the stomach via the pyloric sphincter, (ii) the jejunum, and (iii) the ileum, which connects to the large intestine via the ileocecal sphincter. Similarly, the large intestine consists of: (i) the caecum and appendix, (ii) the colon, (iii) the rectum, and (iv) the anal canal. These intestinal sections differ in their cellular make-up, morphology, and gene expression profiles, allowing each segment to carry out specialized functions [135].

Following consumption of a meal, chyme from the stomach, digestive enzymes from the pancreas, and bile from the gallbladder are secreted into the lumen of the duodenum, which serves as an important site for the digestion of polysaccharides, proteins, and fats [136]. Additionally, the duodenum is the segment primarily responsible for the absorption of minerals including iron, calcium, magnesium, zinc, and phosphorus [137]. Most digestion products including monosaccharides, amino acids, and fatty acids are predominantly absorbed by the

jejunum, with compensatory uptake by the ileum as the nutrient load increases [136, 138]. After aiding in the emulsification and absorption of lipids within the proximal intestine, the majority of bile acids are reabsorbed across the ileal epithelium, facilitating enterohepatic circulation [139]. The ileum is also the main site of vitamin B12 absorption [140]. The epithelium of the small intestine is folded into finger-like projections known as villi, which extend into the intestinal lumen and increase the absorptive surface area. Although the colon is the primary site for water reabsorption, it contributes little to the absorption of nutrients and minerals and thus it lacks villi [136].

The intestinal lumen hosts the gut microbiome, the densest and most diverse microbial community of all body habitats. Chemical gradients (e.g. pH), nutrient availability, oxygen levels, host immune activity, and mucus structure create distinctive microenvironments along the length of the intestinal tract which determine the identity, diversity, and density of the bacterial populations present [141, 142]. The microbial biomass of the intestinal lumen increases from 10^2 colony forming units (cfu) per g in the duodenum to 10^{11} cfu/g in the colon and caecum. In the small intestine, bacterial growth is limited to lower densities by high concentrations of host-derived antimicrobial peptides and bile acids, a lower pH, more oxygen, and a faster transit time [141]. These conditions favor rapidly dividing facultative anaerobes including Proteobacteria (particularly Enterobacteriaceae), Lactobacillaceae, and *Clostridium* species [143, 144]. In contrast, the slower transit time, lower concentration of antimicrobials, and lack of a simple carbon source within the colon promote the growth of fermentative polysaccharide-degrading anaerobes such as Bacteroidaceae, Prevotellaceae, Ruminococcaceae, and Lachnospiraceae [141, 143]. Additionally, bacterial species capable of metabolizing primary bile acids into secondary bile acids reside within the colon, and thus this intestinal segment plays a key role in shaping the composition of the bile acid pool [145, 146]. Alterations in the segment-specific microenvironments of the intestinal lumen including changes in motility, pH, nutrient availability, and bile flow have been linked with dysbiosis of the normal gut microbiota [13].

The proximal small intestine (duodenum and jejunum) is continuously exposed to dietary antigens during digestion and nutrient absorption, while the ileum and colon are exposed to high levels of microbial antigens from the gut microbiome. In order to respond to these antigenic stimuli, the intestine is equipped with a complex network of segment-specific immunological features consisting of both organized lymphoid structures and individual immune effector cells. Organized structures including gut-associated lymphoid tissue (GALT; e.g. Peyer's Patches) and draining lymph nodes are the primary sites for adaptive responses including T cell priming and generation of IgA-producing plasma cells [147]. Peyer's Patches, which consist of large B cell follicles with smaller T cell regions, increase in size and density from the jejunum to the ileum and are particularly concentrated in the distal ileum [148, 149]. Additionally, individual effector cells including B cells, T cells, innate immune cells (e.g. dendritic cells, macrophages, eosinophils, mast cells), and innate lymphoid cells (ILCs) are distributed throughout the lamina propria beneath the epithelium, where the frequency of each cell type varies along the length of the intestinal tract [147]. Dendritic cells and macrophages within the lamina propria are key players in early innate responses, where they are primarily responsible for antigen uptake and presentation to naïve T cells [150].

Along the entire length of the intestinal tract, a single layer of epithelial cells forms a physical barrier to separate the carefully regulated internal environment of the body from the continuously changing contents of the intestinal lumen. The hydrophobic plasma membrane of the epithelial cells serves as an effective barrier to hydrophilic molecules, while the paracellular spaces are sealed by tight junctions. These tight junctions are selectively permeable, regulating the movement of fluids and solutes on the basis of size and charge [151]. Beyond this physical barrier, the intestinal epithelium exhibits segment-specific strategies to protect the absorptive epithelial cells against their microbial neighbors [147]. For example, Paneth cells, which are only present in the small intestine, secrete antimicrobial peptides such as defensins, lysozyme, and REGIIIγ [152, 153]. In contrast, the number of mucus-secreting Goblet cells increases down the

intestinal tract, accounting for at least 25% of the epithelial cells in the colon compared to only 10% in the proximal small intestine. As a result, the colon produces the thickest and densest mucus layer, which not only forms a charged physical barrier, but also contains toxic mucin glycoproteins which limit bacterial colonization within the intestinal mucosa [154].

DYSREGULATION OF THE INTESTINE-LIVER AXIS

Hepatic and intestinal homeostasis are interdependent, establishing the intestine-liver axis. During development, the liver buds directly from the endoderm of the foregut and thus these two organs are intrinsically linked in embryological terms [155]. More importantly, the intestine and liver are physiologically connected by bidirectional flow involving (i) portal circulation and (ii) enterohepatic circulation (Figure 4). Intestine-derived factors which cross the intestinal barrier are delivered directly to the liver via portal circulation, facilitating metabolism and/or detoxification [156]. Additionally, enterohepatic circulation involves the secretion of hepatically synthesized bile acids from the biliary tract into the duodenal lumen. After aiding in the emulsification and absorption of dietary lipids, most bile acids are reabsorbed by ileal enterocytes and delivered back to the liver through portal circulation [139]. It is well established that dysregulation of the intestine-liver axis promotes the development of several complex metabolic disorders including obesity, diabetes, and NAFLD [13, 14, 157, 158]. Multiple mechanisms along the intestine-liver axis have been implicated in NAFLD including alterations in: (i) intestinal absorption of nutrients and minerals, (ii) the gut microbiome, (iii) intestinal permeability, (iv) gut motility, and (v) enterohepatic circulation of bile acids.

Hepatic accumulation of certain diet-derived nutrients and minerals alters metabolic status and redox homeostasis, and therefore diet composition is an important factor in determining NAFLD susceptibility. Specifically, over-consumption of fatty acids (particularly saturated fatty acids), cholesterol, simple carbohydrates (e.g. sucrose and fructose), and iron greatly increases the risk of developing metabolic disorders such as NAFLD [159]. Moreover, factors which alter

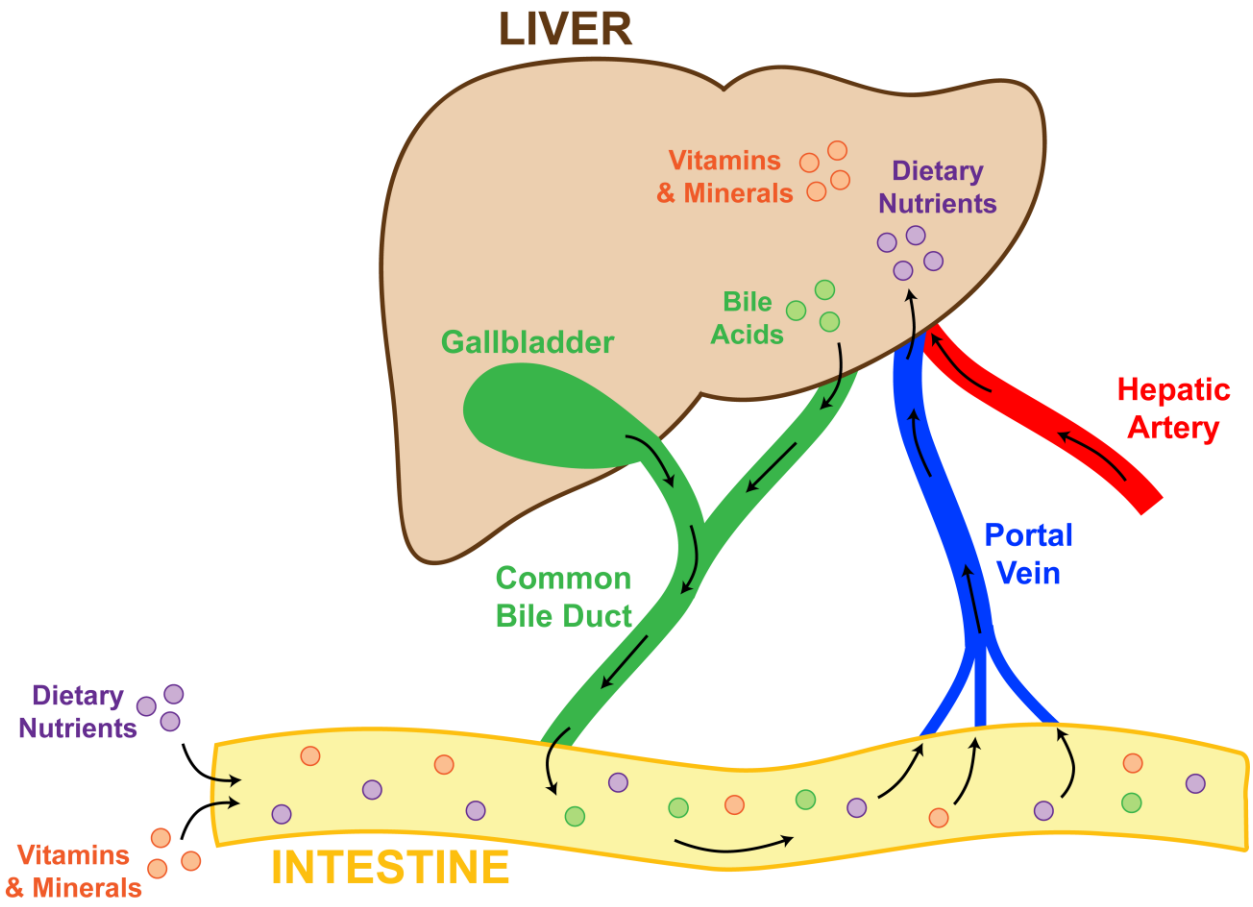

FIGURE 4. BIDIRECTIONAL FLOW ALONG THE INTESTINE-LIVER AXIS

the intestine's ability to absorb these nutrients and minerals also affect NAFLD susceptibility. For example, mutations in the gene responsible for hemochromatosis (*HFE*), a disorder characterized by iron overloading due to increased duodenal absorption, have been associated with an increased risk of NAFLD [160, 161]. Additionally, treatment with Ezetimibe, an NPC1L1 cholesterol transporter inhibitor which reduces intestinal absorption of dietary cholesterol, is reported to decrease serum ALT in human clinical trials and reduce hepatic lipid accumulation in mice [162, 163]. The absorption of cholesterol and triglycerides is also reduced by bile acid sequestration, leading to decreased weight gain and increased fecal lipid excretion [164].

Accumulating evidence demonstrates an association between NAFLD and dysbiosis of the gut microbiome, which may involve bacterial overgrowth, changes in the relative abundance of specific commensal taxa, and/or increased abundance of specific pathogenic microorganisms [13]. In general, the ratio of Bacteroidetes to Firmicutes is typically lower in obese vs. lean individuals, with further reductions in Bacteroidetes in NASH patients vs. obese individuals without NASH [165]. Metabolites produced by the microbiome including short chain fatty acids (SCFAs), trimethylamine (TMA), and non-dietary ethanol can affect the metabolic phenotype of the host. For example, anaerobic bacteria in the colon ferment complex polysaccharides to yield SCFAs such as acetate, propionate, and butyrate, which account for 30% of the liver's energy supply. Alterations in the gut microbiota are reported to increase colonic SCFA production, dysregulating the hepatic metabolism of fatty acids and cholesterol [166, 167]. Furthermore, increased bacterial conversion of choline to TMA not only depletes the host's choline supply, but also increases hepatic trimethylamine N-oxide (TMAO) production [168]. Given that choline is required for hepatic very low density lipoprotein (VLDL) synthesis and lipid export, choline deficiency is associated with hepatic steatosis [168], while TMAO promotes atherosclerosis and impairs glucose tolerance [169, 170]. Several factors have been shown to alter the gut microbiome including certain nutrients (e.g. dietary fat, sucrose, artificial sweeteners, caffeine), exercise, probiotics, and alterations in circadian rhythm [13].

Portal circulation exposes the liver to several antigenic and/or pro-inflammatory gut-derived substances including translocated bacteria, pathogen-associated molecular patterns (PAMPs; e.g. lipopolysaccharide (LPS), flagellin, lipoteichoic acid, peptidoglycan), and secreted cytokines. Under normal conditions, the resident immune cells within the liver rapidly eliminate small amounts of bacterial products. However, increases in intestinal permeability increase the translocation of bacteria and PAMPs which enter the body, overwhelming hepatic immunological tolerance. These PAMPs activate pattern recognition receptors such as toll-like receptor 4 (TLR4) on Kupffer cells and stellate cells, stimulating pro-inflammatory and pro-fibrotic pathways [171]. Not surprisingly, several rodent models and human epidemiological studies demonstrate that tight junction dysfunction, increased permeability, and elevated serum LPS levels are associated with NAFLD development and progression [15, 172-174]. Various factors have been found to impair intestinal barrier function including small intestine bacterial overgrowth [175], specific bacterial species (e.g. *Helicobacter pylori*) [176], both dietary and non-dietary bacterially-derived ethanol [177], and various dietary components (gliadin from wheat, capsianoside from peppers) [178]. Beyond barrier function, alterations in gut motility and intestinal transit may also contribute to the development of NAFLD. For example, a high-fat diet causes degeneration and loss of the enteric neurons which control gut motility, accompanying the development of hepatic steatosis and fibrosis [179]. Decreased gut motility is reported to facilitate small intestine bacterial overgrowth, promote growth of specific bacterial taxa leading to dysbiosis, and alter nutrient absorption [180, 181].

Enterohepatic circulation is an important aspect of the intestine-liver axis due largely to the reciprocal relationship between the gut microbiome and the composition of the bile acid pool [14]. Bile acids are toxic to specific bacterial taxa due to their detergent-like properties, and thus alterations in host bile acid metabolism and transport can shift the microbiota community structure [182, 183]. In turn, colonic bacteria which express bile salt hydrolase (*bsh*) and bile acid inducible operon (*baiCD*) metabolize bile acids, thereby altering the ratio of primary to secondary bile acid

species [146]. Changes in the size and composition of the bile acid pool affect the activation of nuclear receptors such as farnesoid X receptor (FXR) and G protein-coupled bile acid receptor 1 (GPBAR1), dysregulating bile, glucose, lipid, and energy homeostasis [184]. For example, increased levels of conjugated bile acids in antibiotic-treated mice inhibit intestinal FXR signaling, leading to decreased hepatic triglyceride accumulation [185]. As a result, targeting the bile acid-microbiome axis with pro- or anti-biotics has emerged as a potential therapeutic approach for decreasing the risk of NAFLD [186].

AHR MODULATES INTESTINAL HOMEOSTASIS

Accumulating evidence demonstrates that the AhR plays a role in establishing intestinal homeostasis, where it regulates immunological development, immunosurveillance, and the host-microbiota relationship. AhR knockout models exhibit increased susceptibility to bacterial infections and chemically-induced gastrointestinal diseases, while AhR activation is often protective [86, 187-189]. A key mechanism implicated in the anti-inflammatory properties of AhR involves promoting the differentiation of $CD4^+$ naïve T cells into Th17 cells and IL-22-expressing cells [190-193]. Upon IL-22 stimulation, intestinal epithelial cells release anti-microbials such as defensins and RegIII, which modulate the host-microbiota relationship [194]. Indeed, AhR is reported to regulate the community structure of the gut microbiota in mice. Specifically, AhR knockout mice exhibit increased species diversity and alterations in the relative abundance of certain bacterial taxa including increased ileal and caecal populations of segmented filamentous bacteria (SFB) and *Akkermansia muciniphila*, respectively [195]. Additionally, TCDD-elicited AhR activation decreases the Bacteroidetes to Firmicutes ratio of the gut microbiota [196], consistent with shifts detected in NAFLD patients [165]. Collectively, these studies demonstrate that AhR modulates both the intestinal inflammatory tone and the gut microbial composition, however the impact of these intestinal changes on hepatic homeostasis has not been elucidated.

Previous studies demonstrate that hepatic accumulation of intestine-derived factors contributes to the development of AhR-mediated NAFLD. For example, dietary fat rather than *de novo* synthesis is a primary source of lipids involved in TCDD-elicited hepatic steatosis [197]. TCDD-treated mice fed diets containing 5, 10, or 15% fat exhibited dose-dependent increases in total fatty acids, as well as the dietary essential fatty acids linoleic acid (18:2n6) and α-linolenic (18:3n3) acid [197]. Additionally, an iron-supplemented diet exacerbated hepatic lipid peroxidation and oxidative stress in TCDD-treated rats, while an iron-deficient diet was protective [198]. Moreover, the intestinal tract is the first site exposed to both synthetic (PCDDs, PCDFs, PCBs) and natural (I3C) AhR ligands consumed through the diet, as well as the AhR ligands produced in the intestinal lumen following acid condensation (ICZ) or microbial metabolism (indole-3-acetic acid, indole-3-aldehyde) [58]. However, AhR-mediated transcriptional and functional changes along the intestinal tract have not been thoroughly investigated. In particular, little is known about the effects of AhR activation on gut permeability and motility, nutrient and mineral absorption, and bile acid homeostasis.

HEPATIC CIRCADIAN CLOCK

The circadian clock allows an organism to achieve temporal homeostasis with its environment, whereby physiological activities such as sleeping and feeding are entrained to specific periods with an ~24h-cycle [199]. A master pacemaker in the suprachiasmatic nucleus (SCN) of the hypothalamus is the only level of the circadian hierarchy which is directly entrained by light [200]. In turn, the SCN clock generates oscillations in systemic cues (e.g. endocrine signals and neuronal connections) and behavioral cycles (e.g. feeding/fasting, activity/rest) that synchronize a network of tissue-specific cell-autonomous peripheral clocks [201, 202]. The circadian clock of the liver synchronizes hepatic metabolism with feeding/fasting cycles, allowing the liver to anticipate the timing of incoming nutrients and optimize metabolic efficiency. Specifically, the rate-limiting enzymes of several metabolic pathways are transcriptionally-

regulated by the hepatic clock including bile acid homeostasis, gluconeogenesis and glycogen synthesis, beta oxidation, and lipogenesis [203]. In turn, intestine-derived nutrients reset the phase of the hepatic circadian clock, allowing adaptation with altered feeding times [204]. For example, nutrient availability regulates expression of peroxisome proliferator-activated receptor γ coactivator 1-α (PPARGC1A, aka PGC-1α), which is responsible for activating transcription of aminolevulinate synthase 1 (*Alas1*), the rate-limiting step of heme biosynthesis [205]. Heme serves as a co-factor for several core clock regulators, allowing the hepatic clock to respond to changes in nutrient availability [206, 207]. Hepatic circadian rhythmicity is therefore an important mechanism for establishing cross-talk between the intestine and liver, and thus perturbations in circadian cycling dysregulate the intestine-liver axis.

At the cellular level, the mammalian circadian clock consists of autonomous, interdependent transcription-translation feedback loops (Figure 5) [208]. The primary feedback loop involves the core activators CLOCK, brain and muscle ARNT-like 1 (BMAL1, aka ARNTL), and neuronal PAS domain protein 2 (NPAS2, a CLOCK paralog), which are all members of the bHLH-PAS protein family. A heterodimer consisting of ARNTL and either CLOCK or NPAS2 binds to E-box response elements and induces cryptochrome (*Cry1*, *Cry2*) and period (*Per1*, *Per2*, *Per3*) transcription. As PER and CRY accumulate, they dimerize and interfere with ARNTL/CLOCK activity, leading to repression of their own transcription. A secondary feedback loop involves the transcriptional repressors REV-ERBα (encoded by *Nr1d1*) and REV-ERBβ (encoded by *Nr1d2*), which compete with the retinoic acid-related orphan receptor (ROR) α, β, and γ activators for ROR-response elements (ROREs). The ARNTL/CLOCK complex induces transcription of *Nr1d1* and *Nr1d2*, which then repress *Arntl* transcription as their protein levels accumulate. In turn, tissue-specific clock-controlled target genes (CCGs) are regulated by the cyclic activity of these core transcription factors, where the combination of E-boxes and ROREs within the promoter of each gene dictates the phase of expression [209].

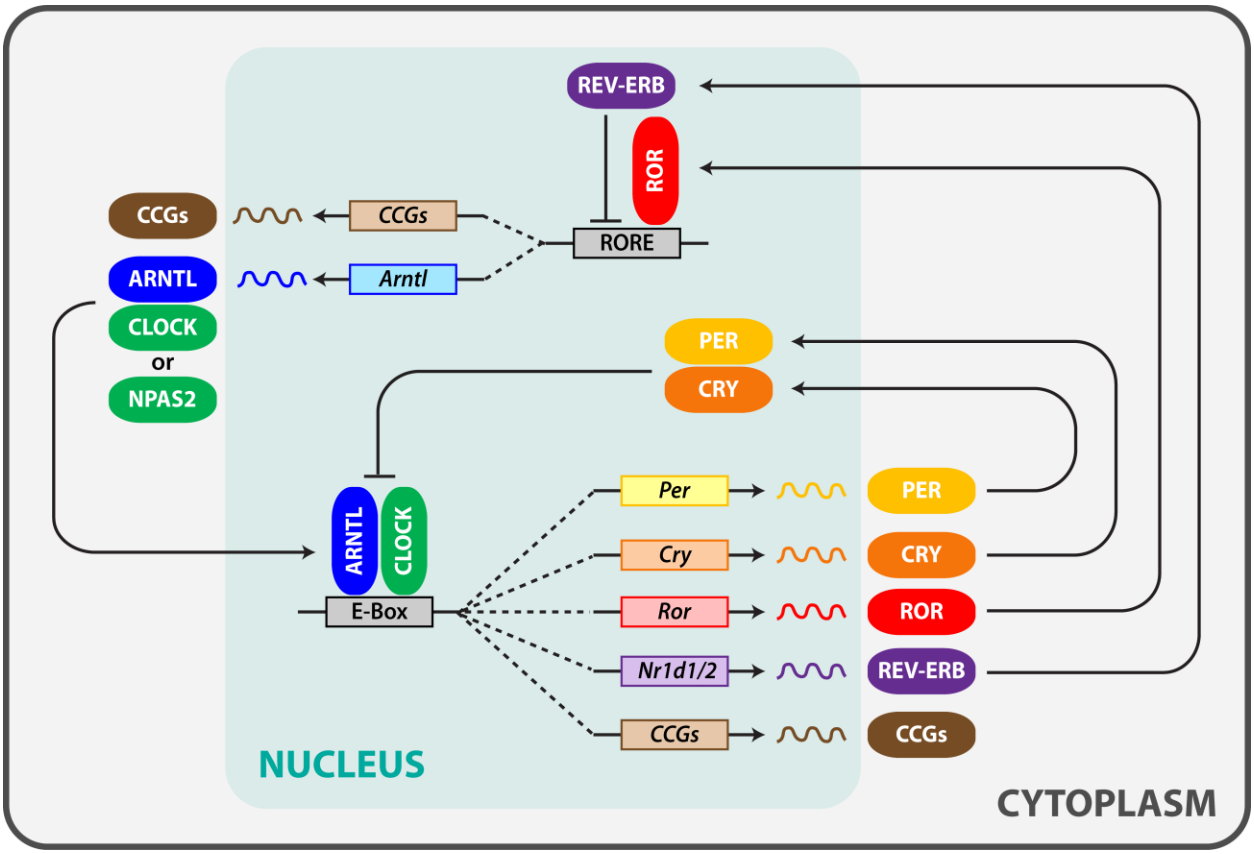

FIGURE 5. THE MOLECULAR MECHANISM OF THE CIRCADIAN CLOCK

Accumulating evidence from human epidemiological studies and rodent models demonstrates that disruptions in circadian behaviors such as shift work, jet lag, binge eating, and sleep restriction, promote the development of complex metabolic disorders including obesity, NAFLD, and cancer [18, 210-212]. Interestingly, AhR activation is reported to perturb the expression of core clock genes not only in the SCN master clock, but also in several peripheral tissues including the liver, ovaries, and bone marrow [213-216]. Accordingly, AhR may serve a physiological role in circadian regulation based on its homology with other core clock regulators (i.e. ARNTL and CLOCK), and given that photo-oxidation tryptophan metabolites (e.g. FICZ) are endogenous AhR ligands [97, 217]. However, the impact of AhR activation on the circadian rhythmicity of hepatic metabolism has not been thoroughly examined.

CONCLUSION

NAFLD is a complex multifactorial disease caused by interactions between genetic alleles, diet, lifestyle choices, and age [115-117]. Accumulating evidence demonstrates that disruptions in circadian behavior (e.g shift work, jet lag, binge eating) [16, 18, 203] and exposure to environmental contaminants (e.g. TCDD and other AhR agonists) [6, 8, 9] are also associated with NAFLD development. However, the extent to which these factors contribute, and the underlying mechanisms involved, have not been elucidated. Intestinal and hepatic homeostasis are closely linked by portal and enterohepatic circulation, creating bidirectional flow along the intestine-liver axis. Consequently, alterations in intestinal permeability and motility, nutrient absorption, bile acid homeostasis, the gut microbiome, and hepatic circadian rhythmicity affect the metabolic and inflammatory status of the liver [13-15, 203]. Rodent models demonstrate AhR-mediated NAFLD involves the hepatic accumulation of intestine-derived factors such as dietary lipids and iron [197, 198]. To date, the segment-specific effects of AhR activation on intestinal gene expression and function have not been examined in depth. Moreover, little is known about the impact of AhR activation on the circadian regulation of hepatic metabolism and its contribution

to TCDD-elicited hepatotoxicity. An improved understanding of the intestine's role in AhR-mediated NAFLD may lead to the development of novel preventative and therapeutic strategies, which would be of great benefit to public health with the increasing prevalence of metabolic disorders [4, 5].

REFERENCES

REFERENCES

1. Trauner, M., M. Arrese, and M. Wagner, *Fatty liver and lipotoxicity.* Biochim Biophys Acta, 2010. 1801(3): p. 299-310.

2. Moore, J.B., *Non-alcoholic fatty liver disease: the hepatic consequence of obesity and the metabolic syndrome.* Proc Nutr Soc, 2010. 69(2): p. 211-20.

3. Wong, R.J., M. Aguilar, R. Cheung, R.B. Perumpail, S.A. Harrison, Z.M. Younossi, and A. Ahmed, *Nonalcoholic steatohepatitis is the second leading etiology of liver disease among adults awaiting liver transplantation in the United States.* Gastroenterology, 2015. 148(3): p. 547-55.

4. Grundy, S.M., *Metabolic syndrome pandemic.* Arterioscler Thromb Vasc Biol, 2008. 28(4): p. 629-36.

5. Fazel, Y., A.B. Koenig, M. Sayiner, Z.D. Goodman, and Z.M. Younossi, *Epidemiology and natural history of non-alcoholic fatty liver disease.* Metabolism, 2016. 65(8): p. 1017-25.

6. Casals-Casas, C. and B. Desvergne, *Endocrine disruptors: from endocrine to metabolic disruption.* Annu Rev Physiol, 2011. 73: p. 135-62.

7. Chen, J.Q., T.R. Brown, and J. Russo, *Regulation of energy metabolism pathways by estrogens and estrogenic chemicals and potential implications in obesity associated with increased exposure to endocrine disruptors.* Biochim Biophys Acta, 2009. 1793(7): p. 1128-43.

8. Grun, F. and B. Blumberg, *Endocrine disrupters as obesogens.* Mol Cell Endocrinol, 2009. 304(1-2): p. 19-29.

9. Cave, M., S. Appana, M. Patel, K.C. Falkner, C.J. McClain, and G. Brock, *Polychlorinated biphenyls, lead, and mercury are associated with liver disease in American adults: NHANES 2003-2004.* Environ Health Perspect, 2010. 118(12): p. 1735-42.

10. Boverhof, D.R., L.D. Burgoon, C. Tashiro, B. Chittim, J.R. Harkema, D.B. Jump, and T.R. Zacharewski, *Temporal and dose-dependent hepatic gene expression patterns in mice provide new insights into TCDD-Mediated hepatotoxicity.* Toxicol Sci, 2005. 85(2): p. 1048-63.

11. Pierre, S., A. Chevallier, F. Teixeira-Clerc, A. Ambolet-Camoit, L.C. Bui, A.S. Bats, J.C. Fournet, P. Fernandez-Salguero, M. Aggerbeck, S. Lotersztajn, R. Barouki, and X. Coumoul, *Aryl hydrocarbon receptor-dependent induction of liver fibrosis by dioxin.* Toxicol Sci, 2014. 137(1): p. 114-24.

12. Nault, R., K.A. Fader, D.A. Ammendolia, P. Dornbos, D. Potter, B. Sharratt, K. Kumagai, J.R. Harkema, S.Y. Lunt, J. Matthews, and T. Zacharewski, *Dose-Dependent Metabolic Reprogramming and Differential Gene Expression in TCDD-Elicited Hepatic Fibrosis.* Toxicol Sci, 2016. 154(2): p. 253-266.

13. Leung, C., L. Rivera, J.B. Furness, and P.W. Angus, *The role of the gut microbiota in NAFLD.* Nat Rev Gastroenterol Hepatol, 2016. 13(7): p. 412-25.

14. Ridlon, J.M., J.M. Alves, P.B. Hylemon, and J.S. Bajaj, *Cirrhosis, bile acids and gut microbiota: unraveling a complex relationship.* Gut Microbes, 2013. 4(5): p. 382-7.

15. Miele, L., V. Valenza, G. La Torre, M. Montalto, G. Cammarota, R. Ricci, R. Masciana, A. Forgione, M.L. Gabrieli, G. Perotti, F.M. Vecchio, G. Rapaccini, G. Gasbarrini, C.P. Day, and A. Grieco, *Increased intestinal permeability and tight junction alterations in nonalcoholic fatty liver disease.* Hepatology, 2009. 49(6): p. 1877-87.

16. Tahara, Y. and S. Shibata, *Circadian rhythms of liver physiology and disease: experimental and clinical evidence.* Nat Rev Gastroenterol Hepatol, 2016. 13(4): p. 217-26.

17. Li, M.D., C.M. Li, and Z. Wang, *The role of circadian clocks in metabolic disease.* Yale J Biol Med, 2012. 85(3): p. 387-401.

18. Mazzoccoli, G., S. De Cosmo, and T. Mazza, *The Biological Clock: A Pivotal Hub in Non-alcoholic Fatty Liver Disease Pathogenesis.* Front Physiol, 2018. 9: p. 193.

19. Gu, Y.Z., J.B. Hogenesch, and C.A. Bradfield, *The PAS superfamily: sensors of environmental and developmental signals.* Annu Rev Pharmacol Toxicol, 2000. 40: p. 519-61.

20. Ramadoss, P., C. Marcus, and G.H. Perdew, *Role of the aryl hydrocarbon receptor in drug metabolism.* Expert Opin Drug Metab Toxicol, 2005. 1(1): p. 9-21.

21. Mulero-Navarro, S. and P.M. Fernandez-Salguero, *New Trends in Aryl Hydrocarbon Receptor Biology.* Front Cell Dev Biol, 2016. 4: p. 45.

22. Kung, T., K.A. Murphy, and L.A. White, *The aryl hydrocarbon receptor (AhR) pathway as a regulatory pathway for cell adhesion and matrix metabolism.* Biochem Pharmacol, 2009. 77(4): p. 536-46.

23. Lindsey, S. and E.T. Papoutsakis, *The evolving role of the aryl hydrocarbon receptor (AHR) in the normophysiology of hematopoiesis.* Stem Cell Rev, 2012. 8(4): p. 1223-35.

24. Barouki, R., X. Coumoul, and P.M. Fernandez-Salguero, *The aryl hydrocarbon receptor, more than a xenobiotic-interacting protein.* FEBS Lett, 2007. 581(19): p. 3608-15.

25. Denison, M.S., A. Pandini, S.R. Nagy, E.P. Baldwin, and L. Bonati, *Ligand binding and activation of the Ah receptor.* Chem Biol Interact, 2002. 141(1-2): p. 3-24.

26. Hankinson, O., *The aryl hydrocarbon receptor complex.* Annu Rev Pharmacol Toxicol, 1995. 35: p. 307-40.

27. Beischlag, T.V., J. Luis Morales, B.D. Hollingshead, and G.H. Perdew, *The aryl hydrocarbon receptor complex and the control of gene expression.* Crit Rev Eukaryot Gene Expr, 2008. 18(3): p. 207-50.

28. Dere, E., R. Lo, T. Celius, J. Matthews, and T.R. Zacharewski, *Integration of genome-wide computation DRE search, AhR ChIP-chip and gene expression analyses of TCDD-elicited responses in the mouse liver.* BMC Genomics, 2011. 12: p. 365.

29. Huang, G. and C.J. Elferink, *A novel nonconsensus xenobiotic response element capable of mediating aryl hydrocarbon receptor-dependent gene expression.* Mol Pharmacol, 2012. 81(3): p. 338-47.

30. Wilson, S.R., A.D. Joshi, and C.J. Elferink, *The tumor suppressor Kruppel-like factor 6 is a novel aryl hydrocarbon receptor DNA binding partner.* J Pharmacol Exp Ther, 2013. 345(3): p. 419-29.

31. Tijet, N., P.C. Boutros, I.D. Moffat, A.B. Okey, J. Tuomisto, and R. Pohjanvirta, *Aryl hydrocarbon receptor regulates distinct dioxin-dependent and dioxin-independent gene batteries.* Mol Pharmacol, 2006. 69(1): p. 140-53.

32. Swanson, H.I. and C.A. Bradfield, *The AH-receptor: genetics, structure and function.* Pharmacogenetics, 1993. 3(5): p. 213-30.

33. Ma, Q., *Overview of AHR Functional Domains and the Classical AHR Signaling Pathway: Induction of Drug Metabolizing Enzymes*, in *The AH Receptor in Biology and Toxicology*, R. Pohjanvirta, Editor. 2011.

34. Burbach, K.M., A. Poland, and C.A. Bradfield, *Cloning of the Ah-receptor cDNA reveals a distinctive ligand-activated transcription factor.* Proc Natl Acad Sci U S A, 1992. 89(17): p. 8185-9.

35. Fukunaga, B.N., M.R. Probst, S. Reisz-Porszasz, and O. Hankinson, *Identification of functional domains of the aryl hydrocarbon receptor.* J Biol Chem, 1995. 270(49): p. 29270-8.

36. Lindebro, M.C., L. Poellinger, and M.L. Whitelaw, *Protein-protein interaction via PAS domains: role of the PAS domain in positive and negative regulation of the bHLH/PAS dioxin receptor-Arnt transcription factor complex.* EMBO J, 1995. 14(14): p. 3528-39.

37. Ma, Q. and J.P. Whitlock, Jr., *A novel cytoplasmic protein that interacts with the Ah receptor, contains tetratricopeptide repeat motifs, and augments the transcriptional response to 2,3,7,8-tetrachlorodibenzo-p-dioxin.* J Biol Chem, 1997. 272(14): p. 8878-84.

38. Ma, Q., L. Dong, and J.P. Whitlock, Jr., *Transcriptional activation by the mouse Ah receptor. Interplay between multiple stimulatory and inhibitory functions.* J Biol Chem, 1995. 270(21): p. 12697-703.

39. Gronemeyer, H., J.A. Gustafsson, and V. Laudet, *Principles for modulation of the nuclear receptor superfamily.* Nat Rev Drug Discov, 2004. 3(11): p. 950-64.

40. Denison, M.S., A.A. Soshilov, G. He, D.E. DeGroot, and B. Zhao, *Exactly the same but different: promiscuity and diversity in the molecular mechanisms of action of the aryl hydrocarbon (dioxin) receptor.* Toxicol Sci, 2011. 124(1): p. 1-22.

41. Dere, E., A.W. Lee, L.D. Burgoon, and T.R. Zacharewski, *Differences in TCDD-elicited gene expression profiles in human HepG2, mouse Hepa1c1c7 and rat H4IIE hepatoma cells.* BMC Genomics, 2011. 12: p. 193.

42. North, C.M., R.B. Crawford, H. Lu, and N.E. Kaminski, *2,3,7,8-tetrachlorodibenzo-p-dioxin-mediated suppression of toll-like receptor stimulated B-lymphocyte activation and initiation of plasmacytic differentiation.* Toxicol Sci, 2010. 116(1): p. 99-112.

43. Kerkvliet, N.I., *TCDD, AHR, and Immune Regulation*, in *The AH Receptor in Biology and Toxicology*, R. Pohjanvirta, Editor. 2011.

44. Sulentic, C.E., M.P. Holsapple, and N.E. Kaminski, *Aryl hydrocarbon receptor-dependent suppression by 2,3,7, 8-tetrachlorodibenzo-p-dioxin of IgM secretion in activated B cells.* Mol Pharmacol, 1998. 53(4): p. 623-9.

45. De Heer, C., A.P. Verlaan, A.H. Penninks, J.G. Vos, H.J. Schuurman, and H. Van Loveren, *Time course of 2,3,7,8-tetrachlorodibenzo-p-dioxin (TCDD)-induced thymic atrophy in the Wistar rat.* Toxicol Appl Pharmacol, 1994. 128(1): p. 97-104.

46. Knerr, S. and D. Schrenk, *Carcinogenicity of 2,3,7,8-tetrachlorodibenzo-p-dioxin in experimental models.* Mol Nutr Food Res, 2006. 50(10): p. 897-907.

47. NTP, *Carcinogenesis Bioassay of 2,3,7,8-Tetrachlorodibenzo-p-dioxin (CAS No. 1746-01-6) in Osborne-Mendel Rats and B6C3F1 Mice (Gavage Study).* Natl Toxicol Program Tech Rep Ser, 1982. 209: p. 1-195.

48. Safe, S., S.O. Lee, and U.H. Jin, *Role of the aryl hydrocarbon receptor in carcinogenesis and potential as a drug target.* Toxicol Sci, 2013. 135(1): p. 1-16.

49. Whysner, J. and G.M. Williams, *2,3,7,8-Tetrachlorodibenzo-p-dioxin mechanistic data and risk assessment: gene regulation, cytotoxicity, enhanced cell proliferation, and tumor promotion.* Pharmacol Ther, 1996. 71(1-2): p. 193-223.

50. Ju, Q., C.C. Zouboulis, and L. Xia, *Environmental pollution and acne: Chloracne.* Dermatoendocrinol, 2009. 1(3): p. 125-8.

51. Hernandez-Ochoa, I., B.N. Karman, and J.A. Flaws, *The role of the aryl hydrocarbon receptor in the female reproductive system.* Biochem Pharmacol, 2009. 77(4): p. 547-59.

52. Pocar, P., B. Fischer, T. Klonisch, and S. Hombach-Klonisch, *Molecular interactions of the aryl hydrocarbon receptor and its biological and toxicological relevance for reproduction.* Reproduction, 2005. 129(4): p. 379-89.

53. Mimura, J., K. Yamashita, K. Nakamura, M. Morita, T.N. Takagi, K. Nakao, M. Ema, K. Sogawa, M. Yasuda, M. Katsuki, and Y. Fujii-Kuriyama, *Loss of teratogenic response to 2,3,7,8-tetrachlorodibenzo-p-dioxin (TCDD) in mice lacking the Ah (dioxin) receptor.* Genes Cells, 1997. 2(10): p. 645-54.

54. Abbott, B.D., *Teratogenic Impact of Dioxin Activated AHR in Laboratory Animals*, in *The AH Receptor in Biology and Toxicology*, R. Pohjanvirta, Editor. 2011.

55. Fader, K.A., R. Nault, S. Raehtz, L.R. McCabe, and T.R. Zacharewski, *2,3,7,8-Tetrachlorodibenzo-p-dioxin dose-dependently increases bone mass and decreases marrow adiposity in juvenile mice.* Toxicol Appl Pharmacol, 2018. 348: p. 85-98.

56. Viluksela, M., H.M. Miettinen, and M. Korkalainen, *Effects of Dioxins on Teeth and Bone: The Role of AHR*, in *The AH Receptor in Biology and Toxicology*, R. Pohjanvirta, Editor. 2011.

57. Yoshimura, H., S. Yoshihara, N. Ozawa, and M. Miki, *Possible correlation between induction modes of hepatic enzymes by PCBs and their toxicity in rats.* Ann N Y Acad Sci, 1979. 320: p. 179-92.

58. Denison, M.S. and S.R. Nagy, *Activation of the aryl hydrocarbon receptor by structurally diverse exogenous and endogenous chemicals.* Annu Rev Pharmacol Toxicol, 2003. 43: p. 309-34.

59. Soshilov, A.A. and M.S. Denison, *Ligand promiscuity of aryl hydrocarbon receptor agonists and antagonists revealed by site-directed mutagenesis.* Mol Cell Biol, 2014. 34(9): p. 1707-19.

60. Safe, S., *Polychlorinated biphenyls (PCBs), dibenzo-p-dioxins (PCDDs), dibenzofurans (PCDFs), and related compounds: environmental and mechanistic considerations which support the development of toxic equivalency factors (TEFs).* Crit Rev Toxicol, 1990. 21(1): p. 51-88.

61. Poland, A. and J.C. Knutson, *2,3,7,8-tetrachlorodibenzo-p-dioxin and related halogenated aromatic hydrocarbons: examination of the mechanism of toxicity.* Annu Rev Pharmacol Toxicol, 1982. 22: p. 517-54.

62. Van den Berg, M., L.S. Birnbaum, M. Denison, M. De Vito, W. Farland, M. Feeley, H. Fiedler, H. Hakansson, A. Hanberg, L. Haws, M. Rose, S. Safe, D. Schrenk, C. Tohyama, A. Tritscher, J. Tuomisto, M. Tysklind, N. Walker, and R.E. Peterson, *The 2005 World Health Organization reevaluation of human and Mammalian toxic equivalency factors for dioxins and dioxin-like compounds.* Toxicol Sci, 2006. 93(2): p. 223-41.

63. Kafafi, S.A., H.Y. Afeefy, H.K. Said, and A.G. Kafafi, *Relationship between aryl hydrocarbon receptor binding, induction of aryl hydrocarbon hydroxylase and 7-ethoxyresorufin O-deethylase enzymes, and toxic activities of aromatic xenobiotics in animals. A new model.* Chem Res Toxicol, 1993. 6(3): p. 328-34.

64. Denison, M.S. and S. Heath-Pagliuso, *The Ah receptor: a regulator of the biochemical and toxicological actions of structurally diverse chemicals.* Bull Environ Contam Toxicol, 1998. 61(5): p. 557-68.

65. Travis, C.C. and H.A. Hattemer-Frey, *Human exposure to dioxin.* Sci Total Environ, 1991. 104(1-2): p. 97-127.

66. Hutzinger, O., G.G. Choudhry, B.G. Chittim, and L.E. Johnston, *Formation of polychlorinated dibenzofurans and dioxins during combustion, electrical equipment fires and PCB incineration.* Environ Health Perspect, 1985. 60: p. 3-9.

67. Pirkle, J.L., W.H. Wolfe, D.G. Patterson, L.L. Needham, J.E. Michalek, J.C. Miner, M.R. Peterson, and D.L. Phillips, *Estimates of the half-life of 2,3,7,8-tetrachlorodibenzo-p-dioxin in Vietnam Veterans of Operation Ranch Hand.* J Toxicol Environ Health, 1989. 27(2): p. 165-71.

68. Manh, H.D., T. Kido, P.T. Tai, R. Okamoto, S. Honma, S.X. Liang, T. Anh le, S. Maruzeni, T.N. Nghi, M. Nishijo, H. Nakagawa, D.D. Nhu, D. Van Tung, N.N. Hung, and K. Son le, *Levels of polychlorinated dibenzodioxins and polychlorinated dibenzofurans in breast milk samples from three dioxin-contaminated hotspots of Vietnam.* Sci Total Environ, 2015. 511: p. 416-22.

69. Wolfe, W.H., J.E. Michalek, J.C. Miner, J.L. Pirkle, S.P. Caudill, D.G. Patterson, Jr., and L.L. Needham, *Determinants of TCDD half-life in veterans of operation ranch hand.* J Toxicol Environ Health, 1994. 41(4): p. 481-8.

70. Eskenazi, B., P. Mocarelli, M. Warner, S. Samuels, P. Vercellini, D. Olive, L.L. Needham, D.G. Patterson, Jr., P. Brambilla, N. Gavoni, S. Casalini, S. Panazza, W. Turner, and P.M. Gerthoux, *Serum dioxin concentrations and endometriosis: a cohort study in Seveso, Italy.* Environ Health Perspect, 2002. 110(7): p. 629-34.

71. Warner, M., P. Mocarelli, P. Brambilla, A. Wesselink, S. Samuels, S. Signorini, and B. Eskenazi, *Diabetes, Metabolic Syndrome, and Obesity in Relation to Serum Dioxin Concentrations: The Seveso Women's Health Study.* Environ Health Perspect, 2013. 121(8): p. 906-11.

72. Zober, A., M.G. Ott, and P. Messerer, *Morbidity follow up study of BASF employees exposed to 2,3,7, 8-tetrachlorodibenzo-p-dioxin (TCDD) after a 1953 chemical reactor incident.* Occup Environ Med, 1994. 51(7): p. 479-86.

73. Ott, M.G. and A. Zober, *Cause specific mortality and cancer incidence among employees exposed to 2,3,7,8-TCDD after a 1953 reactor accident.* Occup Environ Med, 1996. 53(9): p. 606-12.

74. Stehr, P.A., D. Forney, G. Stein, H.D. Donnell, H. Falk, R. Hotchkiss, W.A. Spratlin, E. Sampson, and S.J. Smith, *The public health response to 2,3,7,8-TCDD environmental contamination in Missouri.* Public Health Rep, 1985. 100(3): p. 289-93.

75. Hoffman, R.E., P.A. Stehr-Green, K.B. Webb, R.G. Evans, A.P. Knutsen, W.F. Schramm, J.L. Staake, B.B. Gibson, and K.K. Steinberg, *Health effects of long-term exposure to 2,3,7,8-tetrachlorodibenzo-p-dioxin.* JAMA, 1986. 255(15): p. 2031-8.

76. Collins, J.J., K. Bodner, L.L. Aylward, M. Wilken, and C.M. Bodnar, *Mortality rates among trichlorophenol workers with exposure to 2,3,7,8-tetrachlorodibenzo-p-dioxin.* Am J Epidemiol, 2009. 170(4): p. 501-6.

77. Fingerhut, M.A., W.E. Halperin, D.A. Marlow, L.A. Piacitelli, P.A. Honchar, M.H. Sweeney, A.L. Greife, P.A. Dill, K. Steenland, and A.J. Suruda, *Cancer mortality in workers exposed to 2,3,7,8-tetrachlorodibenzo-p-dioxin.* N Engl J Med, 1991. 324(4): p. 212-8.

78. Sorg, O., M. Zennegg, P. Schmid, R. Fedosyuk, R. Valikhnovskyi, O. Gaide, V. Kniazevych, and J.H. Saurat, *2,3,7,8-tetrachlorodibenzo-p-dioxin (TCDD) poisoning in Victor Yushchenko: identification and measurement of TCDD metabolites.* Lancet, 2009. 374(9696): p. 1179-85.

79. Frakes, R.A., C.Q. Zeeman, and B. Mower, *Bioaccumulation of 2,3,7,8-tetrachlorodibenzo-p-dioxin (TCDD) by fish downstream of pulp and paper mills in Maine.* Ecotoxicol Environ Saf, 1993. 25(2): p. 244-52.

80. Schecter, A., L. Birnbaum, J.J. Ryan, and J.D. Constable, *Dioxins: an overview.* Environ Res, 2006. 101(3): p. 419-28.

81. Tavakoly Sany, S.B., R. Hashim, A. Salleh, M. Rezayi, D.J. Karlen, B.B. Razavizadeh, and E. Abouzari-Lotf, *Dioxin risk assessment: mechanisms of action and possible toxicity in human health.* Environ Sci Pollut Res Int, 2015. 22(24): p. 19434-50.

82. Liem, A.K., P. Furst, and C. Rappe, *Exposure of populations to dioxins and related compounds.* Food Addit Contam, 2000. 17(4): p. 241-59.

83. Lim, J.S., D.H. Lee, and D.R. Jacobs, Jr., *Association of brominated flame retardants with diabetes and metabolic syndrome in the U.S. population, 2003-2004.* Diabetes Care, 2008. 31(9): p. 1802-7.

84. Wiseman, S.B., Y. Wan, H. Chang, X. Zhang, M. Hecker, P.D. Jones, and J.P. Giesy, *Polybrominated diphenyl ethers and their hydroxylated/methoxylated analogs: environmental sources, metabolic relationships, and relative toxicities.* Mar Pollut Bull, 2011. 63(5-12): p. 179-88.

85. van den Berg, M., M.S. Denison, L.S. Birnbaum, M.J. Devito, H. Fiedler, J. Falandysz, M. Rose, D. Schrenk, S. Safe, C. Tohyama, A. Tritscher, M. Tysklind, and R.E. Peterson, *Polybrominated dibenzo-p-dioxins, dibenzofurans, and biphenyls: inclusion in the toxicity equivalency factor concept for dioxin-like compounds.* Toxicol Sci, 2013. 133(2): p. 197-208.

86. Murray, I.A. and G.H. Perdew, *Ligand activation of the Ah receptor contributes to gastrointestinal homeostasis.* Curr Opin Toxicol, 2017. 2: p. 15-23.

87. Bjeldanes, L.F., J.Y. Kim, K.R. Grose, J.C. Bartholomew, and C.A. Bradfield, *Aromatic hydrocarbon responsiveness-receptor agonists generated from indole-3-carbinol in vitro and in vivo: comparisons with 2,3,7,8-tetrachlorodibenzo-p-dioxin.* Proc Natl Acad Sci U S A, 1991. 88(21): p. 9543-7.

88. Ciolino, H.P., P.J. Daschner, T.T. Wang, and G.C. Yeh, *Effect of curcumin on the aryl hydrocarbon receptor and cytochrome P450 1A1 in MCF-7 human breast carcinoma cells.* Biochem Pharmacol, 1998. 56(2): p. 197-206.

89. Gradelet, S., J. Leclerc, M.H. Siess, and P.O. Astorg, *beta-Apo-8'-carotenal, but not beta-carotene, is a strong inducer of liver cytochromes P4501A1 and 1A2 in rat.* Xenobiotica, 1996. 26(9): p. 909-19.

90. Ciolino, H.P., P.J. Daschner, and G.C. Yeh, *Dietary flavonols quercetin and kaempferol are ligands of the aryl hydrocarbon receptor that affect CYP1A1 transcription differentially.* Biochem J, 1999. 340 (Pt 3): p. 715-22.

91. Cheng, Y., U.H. Jin, C.D. Allred, A. Jayaraman, R.S. Chapkin, and S. Safe, *Aryl Hydrocarbon Receptor Activity of Tryptophan Metabolites in Young Adult Mouse Colonocytes.* Drug Metab Dispos, 2015. 43(10): p. 1536-43.

92. Zelante, T., R.G. Iannitti, C. Cunha, A. De Luca, G. Giovannini, G. Pieraccini, R. Zecchi, C. D'Angelo, C. Massi-Benedetti, F. Fallarino, A. Carvalho, P. Puccetti, and L. Romani, *Tryptophan catabolites from microbiota engage aryl hydrocarbon receptor and balance mucosal reactivity via interleukin-22.* Immunity, 2013. 39(2): p. 372-85.

93. Helferich, W.G. and M.S. Denison, *Ultraviolet photoproducts of tryptophan can act as dioxin agonists.* Mol Pharmacol, 1991. 40(5): p. 674-8.

94. Adachi, J., Y. Mori, S. Matsui, H. Takigami, J. Fujino, H. Kitagawa, C.A. Miller, 3rd, T. Kato, K. Saeki, and T. Matsuda, *Indirubin and indigo are potent aryl hydrocarbon receptor ligands present in human urine.* J Biol Chem, 2001. 276(34): p. 31475-8.

95. Heath-Pagliuso, S., W.J. Rogers, K. Tullis, S.D. Seidel, P.H. Cenijn, A. Brouwer, and M.S. Denison, *Activation of the Ah receptor by tryptophan and tryptophan metabolites.* Biochemistry, 1998. 37(33): p. 11508-15.

96. Mezrich, J.D., J.H. Fechner, X. Zhang, B.P. Johnson, W.J. Burlingham, and C.A. Bradfield, *An interaction between kynurenine and the aryl hydrocarbon receptor can generate regulatory T cells.* J Immunol, 2010. 185(6): p. 3190-8.

97. Wei, Y.D., U. Rannug, and A. Rannug, *UV-induced CYP1A1 gene expression in human cells is mediated by tryptophan.* Chem Biol Interact, 1999. 118(2): p. 127-40.

98. Jaeger, C. and S.A. Tischkau, *Role of Aryl Hydrocarbon Receptor in Circadian Clock Disruption and Metabolic Dysfunction.* Environ Health Insights, 2016. 10: p. 133-41.

99. Tischkau, S.A., *AHR and the Circadian Clock*, in *The AH Receptor in Biology and Toxicology*, R. Pohjanvirta, Editor. 2011.

100. Goldstein, J.A., P. Hickman, H. Bergman, and J.G. Vos, *Hepatic porphyria induced by 2,3,7,8-tetrachlorodibenzo-p-dioxin in the mouse.* Res Commun Chem Pathol Pharmacol, 1973. 6(3): p. 919-28.

101. Phelan, D., G.M. Winter, W.J. Rogers, J.C. Lam, and M.S. Denison, *Activation of the Ah receptor signal transduction pathway by bilirubin and biliverdin.* Arch Biochem Biophys, 1998. 357(1): p. 155-63.

102. Schaldach, C.M., J. Riby, and L.F. Bjeldanes, *Lipoxin A4: a new class of ligand for the Ah receptor.* Biochemistry, 1999. 38(23): p. 7594-600.

103. Seidel, S.D., G.M. Winters, W.J. Rogers, M.H. Ziccardi, V. Li, B. Keser, and M.S. Denison, *Activation of the Ah receptor signaling pathway by prostaglandins.* J Biochem Mol Toxicol, 2001. 15(4): p. 187-96.

104. Bui, P., P. Solaimani, X. Wu, and O. Hankinson, *2,3,7,8-Tetrachlorodibenzo-p-dioxin treatment alters eicosanoid levels in several organs of the mouse in an aryl hydrocarbon receptor-dependent fashion.* Toxicol Appl Pharmacol, 2012. 259(2): p. 143-51.

105. Yao, L., C. Wang, X. Zhang, L. Peng, W. Liu, Y. Liu, J. He, C. Jiang, D. Ai, and Y. Zhu, *Hyperhomocysteinemia activates the aryl hydrocarbon receptor/CD36 pathway to promote hepatic steatosis in mice.* Hepatology, 2016. 64(1): p. 92-105.

106. Nagy, S.R., G. Liu, K.S. Lam, and M.S. Denison, *Identification of novel Ah receptor agonists using a high-throughput green fluorescent protein-based recombinant cell bioassay.* Biochemistry, 2002. 41(3): p. 861-8.

107. Bisson, W.H., D.C. Koch, E.F. O'Donnell, S.M. Khalil, N.I. Kerkvliet, R.L. Tanguay, R. Abagyan, and S.K. Kolluri, *Modeling of the aryl hydrocarbon receptor (AhR) ligand binding domain and its utility in virtual ligand screening to predict new AhR ligands.* J Med Chem, 2009. 52(18): p. 5635-41.

108. Larsson, M., D. Fraccalvieri, C.D. Andersson, L. Bonati, A. Linusson, and P.L. Andersson, *Identification of potential aryl hydrocarbon receptor ligands by virtual screening of industrial chemicals.* Environ Sci Pollut Res Int, 2018. 25(3): p. 2436-2449.

109. Cheung, O. and A.J. Sanyal, *Recent advances in nonalcoholic fatty liver disease.* Curr Opin Gastroenterol, 2010. 26(3): p. 202-8.

110. Olufadi, R. and C.D. Byrne, *Clinical and laboratory diagnosis of the metabolic syndrome.* J Clin Pathol, 2008. 61(6): p. 697-706.

111. Sakhuja, P., *Pathology of alcoholic liver disease, can it be differentiated from nonalcoholic steatohepatitis?* World J Gastroenterol, 2014. 20(44): p. 16474-9.

112. Wong, R.J., R. Cheung, and A. Ahmed, *Nonalcoholic steatohepatitis is the most rapidly growing indication for liver transplantation in patients with hepatocellular carcinoma in the U.S.* Hepatology, 2014. 59(6): p. 2188-95.

113. Byrne, C.D. and G. Targher, *NAFLD: a multisystem disease.* J Hepatol, 2015. 62(1 Suppl): p. S47-64.

114. Ford, E.S., C. Li, and G. Zhao, *Prevalence and correlates of metabolic syndrome based on a harmonious definition among adults in the US.* J Diabetes, 2010. 2(3): p. 180-93.

115. Musso, G., R. Gambino, F. De Michieli, M. Cassader, M. Rizzetto, M. Durazzo, E. Faga, B. Silli, and G. Pagano, *Dietary habits and their relations to insulin resistance and postprandial lipemia in nonalcoholic steatohepatitis.* Hepatology, 2003. 37(4): p. 909-16.

116. Dongiovanni, P., Q.M. Anstee, and L. Valenti, *Genetic predisposition in NAFLD and NASH: impact on severity of liver disease and response to treatment.* Curr Pharm Des, 2013. 19(29): p. 5219-38.

117. Thoma, C., C.P. Day, and M.I. Trenell, *Lifestyle interventions for the treatment of non-alcoholic fatty liver disease in adults: a systematic review.* J Hepatol, 2012. 56(1): p. 255-66.

118. Kopec, A.K., D.R. Boverhof, R. Nault, J.R. Harkema, C. Tashiro, D. Potter, B. Sharratt, B. Chittim, and T.R. Zacharewski, *Toxicogenomic evaluation of long-term hepatic effects of TCDD in immature, ovariectomized C57BL/6 mice.* Toxicol Sci, 2013. 135(2): p. 465-75.

119. Fernandez-Salguero, P.M., D.M. Hilbert, S. Rudikoff, J.M. Ward, and F.J. Gonzalez, *Aryl-hydrocarbon receptor-deficient mice are resistant to 2,3,7,8-tetrachlorodibenzo-p-dioxin-induced toxicity.* Toxicol Appl Pharmacol, 1996. 140(1): p. 173-9.

120. Kopec, A.K., D.R. Boverhof, L.D. Burgoon, D. Ibrahim-Aibo, J.R. Harkema, C. Tashiro, B. Chittim, and T.R. Zacharewski, *Comparative toxicogenomic examination of the hepatic effects of PCB126 and TCDD in immature, ovariectomized C57BL/6 mice.* Toxicol Sci, 2008. 102(1): p. 61-75.

121. Kawano, Y., S. Nishiumi, S. Tanaka, K. Nobutani, A. Miki, Y. Yano, Y. Seo, H. Kutsumi, H. Ashida, T. Azuma, and M. Yoshida, *Activation of the aryl hydrocarbon receptor induces hepatic steatosis via the upregulation of fatty acid transport.* Arch Biochem Biophys, 2010. 504(2): p. 221-7.

122. Gadupudi, G.S., W.D. Klaren, A.K. Olivier, A.J. Klingelhutz, and L.W. Robertson, *PCB126-Induced Disruption in Gluconeogenesis and Fatty Acid Oxidation Precedes Fatty Liver in Male Rats.* Toxicol Sci, 2016. 149(1): p. 98-110.

123. Wills, L.P., D. Jung, K. Koehrn, S. Zhu, K.L. Willett, D.E. Hinton, and R.T. Di Giulio, *Comparative chronic liver toxicity of benzo[a]pyrene in two populations of the atlantic killifish (Fundulus heteroclitus) with different exposure histories.* Environ Health Perspect, 2010. 118(10): p. 1376-81.

124. Kociba, R.J., D.G. Keyes, J.E. Beyer, R.M. Carreon, C.E. Wade, D.A. Dittenber, R.P. Kalnins, L.E. Frauson, C.N. Park, S.D. Barnard, R.A. Hummel, and C.G. Humiston, *Results of a two-year chronic toxicity and oncogenicity study of 2,3,7,8-tetrachlorodibenzo-p-dioxin in rats.* Toxicol Appl Pharmacol, 1978. 46(2): p. 279-303.

125. Fader, K.A. and T.R. Zacharewski, *Beyond the Aryl Hydrocarbon Receptor: Pathway Interactions in the Hepatotoxicity of 2,3,7,8-Tetrachlorodibenzo-p-dioxin and Related Compounds.* Curr Opin Toxicol, 2017. 2: p. 36-41.

126. Nault, R., K.A. Fader, T.A. Lydic, and T.R. Zacharewski, *Lipidomic Evaluation of Aryl Hydrocarbon Receptor-Mediated Hepatic Steatosis in Male and Female Mice Elicited by 2,3,7,8-Tetrachlorodibenzo-p-dioxin.* Chem Res Toxicol, 2017. 30(4): p. 1060-1075.

127. Nault, R., K.A. Fader, M.P. Kirby, S. Ahmed, J. Matthews, A.D. Jones, S.Y. Lunt, and T.R. Zacharewski, *Pyruvate Kinase Isoform Switching and Hepatic Metabolic Reprogramming by the Environmental Contaminant 2,3,7,8-Tetrachlorodibenzo-p-Dioxin.* Toxicol Sci, 2016. 149(2): p. 358-71.

128. Stohs, S.J., *Oxidative stress induced by 2,3,7,8-tetrachlorodibenzo-p-dioxin (TCDD).* Free Radic Biol Med, 1990. 9(1): p. 79-90.

129. Yu, M.L., Y.L. Guo, C.C. Hsu, and W.J. Rogan, *Increased mortality from chronic liver disease and cirrhosis 13 years after the Taiwan "yucheng" ("oil disease") incident.* Am J Ind Med, 1997. 31(2): p. 172-5.

130. Lee, C.C., Y.J. Yao, H.L. Chen, Y.L. Guo, and H.J. Su, *Fatty liver and hepatic function for residents with markedly high serum PCDD/Fs levels in Taiwan.* J Toxicol Environ Health A, 2006. 69(5): p. 367-80.

131. Kern, P.A., S. Said, W.G. Jackson, Jr., and J.E. Michalek, *Insulin sensitivity following agent orange exposure in Vietnam veterans with high blood levels of 2,3,7,8-tetrachlorodibenzo-p-dioxin.* J Clin Endocrinol Metab, 2004. 89(9): p. 4665-72.

132. Pesatori, A.C., C. Zocchetti, S. Guercilena, D. Consonni, D. Turrini, and P.A. Bertazzi, *Dioxin exposure and non-malignant health effects: a mortality study.* Occup Environ Med, 1998. 55(2): p. 126-31.

133. Forgacs, A.L., E. Dere, M.M. Angrish, and T.R. Zacharewski, *Comparative analysis of temporal and dose-dependent TCDD-elicited gene expression in human, mouse, and rat primary hepatocytes.* Toxicol Sci, 2013. 133(1): p. 54-66.

134. Harvey, W.A., K. Jurgensen, X. Pu, C.L. Lamb, K.A. Cornell, R.J. Clark, C. Klocke, and K.A. Mitchell, *Exposure to 2,3,7,8-tetrachlorodibenzo-p-dioxin (TCDD) increases human hepatic stellate cell activation.* Toxicology, 2016. 344-346: p. 26-33.

135. Kararli, T.T., *Comparison of the gastrointestinal anatomy, physiology, and biochemistry of humans and commonly used laboratory animals.* Biopharm Drug Dispos, 1995. 16(5): p. 351-80.

136. Goodman, B.E., *Insights into digestion and absorption of major nutrients in humans.* Adv Physiol Educ, 2010. 34(2): p. 44-53.

137. Kiela, P.R. and F.K. Ghishan, *Physiology of Intestinal Absorption and Secretion.* Best Pract Res Clin Gastroenterol, 2016. 30(2): p. 145-59.

138. Booth, C.C., A.E. Read, and E. Jones, *Studies on the site of fat absorption: 1. The sites of absorption of increasing doses of I-labelled triolein in the rat.* Gut, 1961. 2(1): p. 23-31.

139. Hofmann, A.F., *The enterohepatic circulation of bile acids in mammals: form and functions.* Front Biosci (Landmark Ed), 2009. 14: p. 2584-98.

140. Schjonsby, H., *Vitamin B12 absorption and malabsorption.* Gut, 1989. 30(12): p. 1686-91.

141. Donaldson, G.P., S.M. Lee, and S.K. Mazmanian, *Gut biogeography of the bacterial microbiota.* Nat Rev Microbiol, 2016. 14(1): p. 20-32.

142. Tropini, C., K.A. Earle, K.C. Huang, and J.L. Sonnenburg, *The Gut Microbiome: Connecting Spatial Organization to Function.* Cell Host Microbe, 2017. 21(4): p. 433-442.

143. Gu, S., D. Chen, J.N. Zhang, X. Lv, K. Wang, L.P. Duan, Y. Nie, and X.L. Wu, *Bacterial community mapping of the mouse gastrointestinal tract.* PLoS One, 2013. 8(10): p. e74957.

144. Zoetendal, E.G., J. Raes, B. van den Bogert, M. Arumugam, C.C. Booijink, F.J. Troost, P. Bork, M. Wels, W.M. de Vos, and M. Kleerebezem, *The human small intestinal microbiota is driven by rapid uptake and conversion of simple carbohydrates.* ISME J, 2012. 6(7): p. 1415-26.

145. Ridlon, J.M., D.J. Kang, and P.B. Hylemon, *Bile salt biotransformations by human intestinal bacteria.* J Lipid Res, 2006. 47(2): p. 241-59.

146. Gérard, P., *Metabolism of Cholesterol and Bile Acids by the Gut Microbiota.* Pathogens, 2014. 3(1): p. 14-24.

147. Mowat, A.M. and W.W. Agace, *Regional specialization within the intestinal immune system.* Nat Rev Immunol, 2014. 14(10): p. 667-85.

148. Cornes, J.S., *Number, size, and distribution of Peyer's patches in the human small intestine: Part I The development of Peyer's patches.* Gut, 1965. 6(3): p. 225-9.

149. Van Kruiningen, H.J., A.B. West, B.J. Freda, and K.A. Holmes, *Distribution of Peyer's patches in the distal ileum.* Inflamm Bowel Dis, 2002. 8(3): p. 180-5.

150. Tomasello, E. and S. Bedoui, *Intestinal innate immune cells in gut homeostasis and immunosurveillance.* Immunol Cell Biol, 2013. 91(3): p. 201-3.

151. Zihni, C., C. Mills, K. Matter, and M.S. Balda, *Tight junctions: from simple barriers to multifunctional molecular gates.* Nat Rev Mol Cell Biol, 2016. 17(9): p. 564-80.

152. Ouellette, A.J., *Paneth cells and innate mucosal immunity.* Curr Opin Gastroenterol, 2010. 26(6): p. 547-53.

153. Bevins, C.L. and N.H. Salzman, *Paneth cells, antimicrobial peptides and maintenance of intestinal homeostasis.* Nat Rev Microbiol, 2011. 9(5): p. 356-68.

154. Hansson, G.C., *Role of mucus layers in gut infection and inflammation.* Curr Opin Microbiol, 2012. 15(1): p. 57-62.

155. Zorn, A.M. and J.M. Wells, *Vertebrate endoderm development and organ formation.* Annu Rev Cell Dev Biol, 2009. 25: p. 221-51.

156. Kan, Z. and D.C. Madoff, *Liver anatomy: microcirculation of the liver.* Semin Intervent Radiol, 2008. 25(2): p. 77-85.

157. Musso, G., R. Gambino, and M. Cassader, *Obesity, diabetes, and gut microbiota: the hygiene hypothesis expanded?* Diabetes Care, 2010. 33(10): p. 2277-84.

158. Kirpich, I.A., L.S. Marsano, and C.J. McClain, *Gut-liver axis, nutrition, and non-alcoholic fatty liver disease.* Clin Biochem, 2015. 48(13-14): p. 923-30.

159. Yasutake, K., M. Kohjima, K. Kotoh, M. Nakashima, M. Nakamuta, and M. Enjoji, *Dietary habits and behaviors associated with nonalcoholic fatty liver disease.* World J Gastroenterol, 2014. 20(7): p. 1756-67.

160. Lee, S.H., S.H. Jeong, D. Lee, J.H. Lee, S.H. Hwang, Y.A. Cho, Y.S. Park, J.H. Hwang, J.W. Kim, N. Kim, D.H. Lee, and W. Kang, *An epidemiologic study on the incidence and significance of HFE mutations in a Korean cohort with nonalcoholic fatty liver disease.* J Clin Gastroenterol, 2010. 44(7): p. e154-61.

161. Valenti, L., P. Dongiovanni, A.L. Fracanzani, G. Santorelli, E. Fatta, C. Bertelli, E. Taioli, G. Fiorelli, and S. Fargion, *Increased susceptibility to nonalcoholic fatty liver disease in heterozygotes for the mutation responsible for hereditary hemochromatosis.* Dig Liver Dis, 2003. 35(3): p. 172-8.

162. Enjoji, M., K. Machida, M. Kohjima, M. Kato, K. Kotoh, K. Matsunaga, M. Nakashima, and M. Nakamuta, *NPC1L1 inhibitor ezetimibe is a reliable therapeutic agent for non-obese patients with nonalcoholic fatty liver disease.* Lipids Health Dis, 2010. 9: p. 29.

163. Deushi, M., M. Nomura, A. Kawakami, M. Haraguchi, M. Ito, M. Okazaki, H. Ishii, and M. Yoshida, *Ezetimibe improves liver steatosis and insulin resistance in obese rat model of metabolic syndrome.* FEBS Lett, 2007. 581(29): p. 5664-70.

164. Sugimoto-Kawabata, K., H. Shimada, K. Sakai, K. Suzuki, T. Kelder, E.J. Pieterman, L.H. Cohen, L.M. Havekes, H.M. Princen, and A.M. van den Hoek, *Colestilan decreases weight gain by enhanced NEFA incorporation in biliary lipids and fecal lipid excretion.* J Lipid Res, 2013. 54(5): p. 1255-64.

165. Doulberis, M., G. Kotronis, D. Gialamprinou, J. Kountouras, and P. Katsinelos, *Non-alcoholic fatty liver disease: An update with special focus on the role of gut microbiota.* Metabolism, 2017. 71: p. 182-197.

166. Cho, I., S. Yamanishi, L. Cox, B.A. Methe, J. Zavadil, K. Li, Z. Gao, D. Mahana, K. Raju, I. Teitler, H. Li, A.V. Alekseyenko, and M.J. Blaser, *Antibiotics in early life alter the murine colonic microbiome and adiposity.* Nature, 2012. 488(7413): p. 621-6.

167. Turnbaugh, P.J., R.E. Ley, M.A. Mahowald, V. Magrini, E.R. Mardis, and J.I. Gordon, *An obesity-associated gut microbiome with increased capacity for energy harvest.* Nature, 2006. 444(7122): p. 1027-31.

168. Spencer, M.D., T.J. Hamp, R.W. Reid, L.M. Fischer, S.H. Zeisel, and A.A. Fodor, *Association between composition of the human gastrointestinal microbiome and development of fatty liver with choline deficiency.* Gastroenterology, 2011. 140(3): p. 976-86.

169. Randrianarisoa, E., A. Lehn-Stefan, X. Wang, M. Hoene, A. Peter, S.S. Heinzmann, X. Zhao, I. Konigsrainer, A. Konigsrainer, B. Balletshofer, J. Machann, F. Schick, A. Fritsche, H.U. Haring, G. Xu, R. Lehmann, and N. Stefan, *Relationship of Serum Trimethylamine N-Oxide (TMAO) Levels with early Atherosclerosis in Humans.* Sci Rep, 2016. 6: p. 26745.

170. Gao, X., X. Liu, J. Xu, C. Xue, Y. Xue, and Y. Wang, *Dietary trimethylamine N-oxide exacerbates impaired glucose tolerance in mice fed a high fat diet.* J Biosci Bioeng, 2014. 118(4): p. 476-81.

171. Schwabe, R.F., E. Seki, and D.A. Brenner, *Toll-like receptor signaling in the liver.* Gastroenterology, 2006. 130(6): p. 1886-900.

172. Mao, J.W., H.Y. Tang, T. Zhao, X.Y. Tan, J. Bi, B.Y. Wang, and Y.D. Wang, *Intestinal mucosal barrier dysfunction participates in the progress of nonalcoholic fatty liver disease.* Int J Clin Exp Pathol, 2015. 8(4): p. 3648-58.

173. Cani, P.D., J. Amar, M.A. Iglesias, M. Poggi, C. Knauf, D. Bastelica, A.M. Neyrinck, F. Fava, K.M. Tuohy, C. Chabo, A. Waget, E. Delmee, B. Cousin, T. Sulpice, B. Chamontin, J. Ferrieres, J.F. Tanti, G.R. Gibson, L. Casteilla, N.M. Delzenne, M.C. Alessi, and R. Burcelin, *Metabolic endotoxemia initiates obesity and insulin resistance.* Diabetes, 2007. 56(7): p. 1761-72.

174. Verdam, F.J., S.S. Rensen, A. Driessen, J.W. Greve, and W.A. Buurman, *Novel evidence for chronic exposure to endotoxin in human nonalcoholic steatohepatitis.* J Clin Gastroenterol, 2011. 45(2): p. 149-52.

175. Kapil, S., A. Duseja, B.K. Sharma, B. Singla, A. Chakraborti, A. Das, P. Ray, R.K. Dhiman, and Y. Chawla, *Small intestinal bacterial overgrowth and toll-like receptor signaling in patients with non-alcoholic fatty liver disease.* J Gastroenterol Hepatol, 2016. 31(1): p. 213-21.

176. Fedwick, J.P., T.K. Lapointe, J.B. Meddings, P.M. Sherman, and A.G. Buret, *Helicobacter pylori activates myosin light-chain kinase to disrupt claudin-4 and claudin-5 and increase epithelial permeability.* Infect Immun, 2005. 73(12): p. 7844-52.

177. Volynets, V., M.A. Kuper, S. Strahl, I.B. Maier, A. Spruss, S. Wagnerberger, A. Konigsrainer, S.C. Bischoff, and I. Bergheim, *Nutrition, intestinal permeability, and blood ethanol levels are altered in patients with nonalcoholic fatty liver disease (NAFLD).* Dig Dis Sci, 2012. 57(7): p. 1932-41.

178. Ulluwishewa, D., R.C. Anderson, W.C. McNabb, P.J. Moughan, J.M. Wells, and N.C. Roy, *Regulation of tight junction permeability by intestinal bacteria and dietary components.* J Nutr, 2011. 141(5): p. 769-76.

179. Rivera, L.R., C. Leung, R.V. Pustovit, B.L. Hunne, S. Andrikopoulos, C. Herath, A. Testro, P.W. Angus, and J.B. Furness, *Damage to enteric neurons occurs in mice that develop fatty liver disease but not diabetes in response to a high-fat diet.* Neurogastroenterol Motil, 2014. 26(8): p. 1188-99.

180. Quigley, E.M. and A. Abu-Shanab, *Small intestinal bacterial overgrowth.* Infect Dis Clin North Am, 2010. 24(4): p. 943-59, viii-ix.

181. Fu, X.Y., Z. Li, N. Zhang, H.T. Yu, S.R. Wang, and J.R. Liu, *Effects of gastrointestinal motility on obesity.* Nutr Metab (Lond), 2014. 11(1): p. 3.

182. Begley, M., C.G. Gahan, and C. Hill, *The interaction between bacteria and bile.* FEMS Microbiol Rev, 2005. 29(4): p. 625-51.

183. Kakiyama, G., W.M. Pandak, P.M. Gillevet, P.B. Hylemon, D.M. Heuman, K. Daita, H. Takei, A. Muto, H. Nittono, J.M. Ridlon, M.B. White, N.A. Noble, P. Monteith, M. Fuchs, L.R. Thacker, M. Sikaroodi, and J.S. Bajaj, *Modulation of the fecal bile acid profile by gut microbiota in cirrhosis.* J Hepatol, 2013. 58(5): p. 949-55.

184. Chiang, J.Y.L., *Bile acid metabolism and signaling in liver disease and therapy.* Liver Res, 2017. 1(1): p. 3-9.

185. Jiang, C., C. Xie, F. Li, L. Zhang, R.G. Nichols, K.W. Krausz, J. Cai, Y. Qi, Z.Z. Fang, S. Takahashi, N. Tanaka, D. Desai, S.G. Amin, I. Albert, A.D. Patterson, and F.J. Gonzalez, *Intestinal farnesoid X receptor signaling promotes nonalcoholic fatty liver disease.* J Clin Invest, 2015. 125(1): p. 386-402.

186. Arab, J.P., S.J. Karpen, P.A. Dawson, M. Arrese, and M. Trauner, *Bile acids and nonalcoholic fatty liver disease: Molecular insights and therapeutic perspectives.* Hepatology, 2017. 65(1): p. 350-362.

187. Shi, L.Z., N.G. Faith, Y. Nakayama, M. Suresh, H. Steinberg, and C.J. Czuprynski, *The aryl hydrocarbon receptor is required for optimal resistance to Listeria monocytogenes infection in mice.* J Immunol, 2007. 179(10): p. 6952-62.

188. Monteleone, I., A. Rizzo, M. Sarra, G. Sica, P. Sileri, L. Biancone, T.T. MacDonald, F. Pallone, and G. Monteleone, *Aryl hydrocarbon receptor-induced signals up-regulate IL-22 production and inhibit inflammation in the gastrointestinal tract.* Gastroenterology, 2011. 141(1): p. 237-48, 248 e1.

189. Ji, T., C. Xu, L. Sun, M. Yu, K. Peng, Y. Qiu, W. Xiao, and H. Yang, *Aryl Hydrocarbon Receptor Activation Down-Regulates IL-7 and Reduces Inflammation in a Mouse Model of DSS-Induced Colitis.* Dig Dis Sci, 2015. 60(7): p. 1958-66.

190. Brembilla, N.C., J.M. Ramirez, R. Chicheportiche, O. Sorg, J.H. Saurat, and C. Chizzolini, *In vivo dioxin favors interleukin-22 production by human CD4+ T cells in an aryl hydrocarbon receptor (AhR)-dependent manner.* PLoS One, 2011. 6(4): p. e18741.

191. Hayes, M.D., V. Ovcinnikovs, A.G. Smith, I. Kimber, and R.J. Dearman, *The aryl hydrocarbon receptor: differential contribution to T helper 17 and T cytotoxic 17 cell development.* PLoS One, 2014. 9(9): p. e106955.

192. Ramirez, J.M., N.C. Brembilla, O. Sorg, R. Chicheportiche, T. Matthes, J.M. Dayer, J.H. Saurat, E. Roosnek, and C. Chizzolini, *Activation of the aryl hydrocarbon receptor reveals distinct requirements for IL-22 and IL-17 production by human T helper cells.* Eur J Immunol, 2010. 40(9): p. 2450-9.

193. Veldhoen, M., K. Hirota, J. Christensen, A. O'Garra, and B. Stockinger, *Natural agonists for aryl hydrocarbon receptor in culture medium are essential for optimal differentiation of Th17 T cells.* J Exp Med, 2009. 206(1): p. 43-9.

194. Rubino, S.J., K. Geddes, and S.E. Girardin, *Innate IL-17 and IL-22 responses to enteric bacterial pathogens.* Trends Immunol, 2012. 33(3): p. 112-8.

195. Murray, I.A., R.G. Nichols, L. Zhang, A.D. Patterson, and G.H. Perdew, *Expression of the aryl hydrocarbon receptor contributes to the establishment of intestinal microbial community structure in mice.* Sci Rep, 2016. 6: p. 33969.

196. Lefever, D.E., J. Xu, Y. Chen, G. Huang, N. Tamas, and T.L. Guo, *TCDD modulation of gut microbiome correlated with liver and immune toxicity in streptozotocin (STZ)-induced hyperglycemic mice.* Toxicol Appl Pharmacol, 2016. 304: p. 48-58.

197. Angrish, M.M., B.D. Mets, A.D. Jones, and T.R. Zacharewski, *Dietary fat is a lipid source in 2,3,7,8-tetrachlorodibenzo-rho-dioxin (TCDD)-elicited hepatic steatosis in C57BL/6 mice.* Toxicol Sci, 2012. 128(2): p. 377-86.

198. al-Turk, W.A., M.A. Shara, H. Mohammadpour, and S.J. Stohs, *Dietary iron and 2,3,7,8-tetrachlorodibenzo-p-dioxin induced alterations in hepatic lipid peroxidation, glutathione content and body weight.* Drug Chem Toxicol, 1988. 11(1): p. 55-70.

199. Partch, C.L., C.B. Green, and J.S. Takahashi, *Molecular architecture of the mammalian circadian clock.* Trends Cell Biol, 2014. 24(2): p. 90-9.

200. Hastings, M.H., E.S. Maywood, and M. Brancaccio, *Generation of circadian rhythms in the suprachiasmatic nucleus.* Nat Rev Neurosci, 2018. 19(8): p. 453-469.

201. Dibner, C., U. Schibler, and U. Albrecht, *The mammalian circadian timing system: organization and coordination of central and peripheral clocks.* Annu Rev Physiol, 2010. 72: p. 517-49.

202. Buijs, R.M., F.A. Scheer, F. Kreier, C. Yi, N. Bos, V.D. Goncharuk, and A. Kalsbeek, *Organization of circadian functions: interaction with the body.* Prog Brain Res, 2006. 153: p. 341-60.

203. Tong, X. and L. Yin, *Circadian rhythms in liver physiology and liver diseases.* Compr Physiol, 2013. 3(2): p. 917-40.

204. Oike, H., K. Oishi, and M. Kobori, *Nutrients, Clock Genes, and Chrononutrition.* Curr Nutr Rep, 2014. 3: p. 204-212.

205. Handschin, C., J. Lin, J. Rhee, A.K. Peyer, S. Chin, P.H. Wu, U.A. Meyer, and B.M. Spiegelman, *Nutritional regulation of hepatic heme biosynthesis and porphyria through PGC-1alpha.* Cell, 2005. 122(4): p. 505-15.

206. Raghuram, S., K.R. Stayrook, P. Huang, P.M. Rogers, A.K. Nosie, D.B. McClure, L.L. Burris, S. Khorasanizadeh, T.P. Burris, and F. Rastinejad, *Identification of heme as the ligand for the orphan nuclear receptors REV-ERBalpha and REV-ERBbeta.* Nat Struct Mol Biol, 2007. 14(12): p. 1207-13.

207. Lukat-Rodgers, G.S., C. Correia, M.V. Botuyan, G. Mer, and K.R. Rodgers, *Heme-based sensing by the mammalian circadian protein CLOCK.* Inorg Chem, 2010. 49(14): p. 6349-65.

208. Takahashi, J.S., *Transcriptional architecture of the mammalian circadian clock.* Nat Rev Genet, 2017. 18(3): p. 164-179.

209. Fang, B., L.J. Everett, J. Jager, E. Briggs, S.M. Armour, D. Feng, A. Roy, Z. Gerhart-Hines, Z. Sun, and M.A. Lazar, *Circadian enhancers coordinate multiple phases of rhythmic gene transcription in vivo.* Cell, 2014. 159(5): p. 1140-52.

210. Roenneberg, T. and M. Merrow, *The Circadian Clock and Human Health.* Curr Biol, 2016. 26(10): p. R432-43.

211. Savvidis, C. and M. Koutsilieris, *Circadian rhythm disruption in cancer biology.* Mol Med, 2012. 18: p. 1249-60.

212. Shi, S.Q., T.S. Ansari, O.P. McGuinness, D.H. Wasserman, and C.H. Johnson, *Circadian disruption leads to insulin resistance and obesity.* Curr Biol, 2013. 23(5): p. 372-81.

213. Tischkau, S.A., C.D. Jaeger, and S.L. Krager, *Circadian clock disruption in the mouse ovary in response to 2,3,7,8-tetrachlorodibenzo-p-dioxin.* Toxicol Lett, 2011. 201(2): p. 116-22.

214. Sato, S., H. Shirakawa, S. Tomita, Y. Ohsaki, K. Haketa, O. Tooi, N. Santo, M. Tohkin, Y. Furukawa, F.J. Gonzalez, and M. Komai, *Low-dose dioxins alter gene expression related to cholesterol biosynthesis, lipogenesis, and glucose metabolism through the aryl hydrocarbon receptor-mediated pathway in mouse liver.* Toxicol Appl Pharmacol, 2008. 229(1): p. 10-9.

215. Garrett, R.W. and T.A. Gasiewicz, *The aryl hydrocarbon receptor agonist 2,3,7,8-tetrachlorodibenzo-p-dioxin alters the circadian rhythms, quiescence, and expression of clock genes in murine hematopoietic stem and progenitor cells.* Mol Pharmacol, 2006. 69(6): p. 2076-83.

216. Miller, J., D. Settachan, L. Frame, and R. Dickerson, *2,3,7,8-Tetrachlorodobenzo-p-dioxin phase advance the deer mouse (Peromyscus maniculatus) circadian rhythm by altering expression of clock proteins.* Organohalogen Compounds,, 1999. 42: p. 23-28.

217. Hogenesch, J.B., Y.Z. Gu, S. Jain, and C.A. Bradfield, *The basic-helix-loop-helix-PAS orphan MOP3 forms transcriptionally active complexes with circadian and hypoxia factors.* Proc Natl Acad Sci U S A, 1998. 95(10): p. 5474-9.

CHAPTER 2: RATIONALE, HYPOTHESIS, AND SPECIFIC AIMS

RATIONALE

Accumulating evidence demonstrates that exposure to environmental contaminants such as 2,3,7,8-tetrachlorodibenzo-*p*-dioxin (TCDD) and related aryl hydrocarbon receptor (AhR) agonists plays an underappreciated role in the development of several metabolic disorders including obesity, diabetes, and non-alcoholic fatty liver disease (NAFLD) [1-4]. In mice, a single bolus dose of TCDD causes hepatic lipid accumulation [5], which progresses to steatohepatitis and fibrosis following repeated treatment [6, 7]. Moreover, chronic AhR activation is reported to increase the incidence of hepatocellular carcinoma in both mice and rats [8, 9]. To date, the majority of studies investigating AhR-mediated hepatotoxicity, NAFLD, and hepatocellular carcinoma have focused on the liver in isolation. In doing so, these studies failed to consider the interdependence of hepatic and intestinal homeostasis, where portal and enterohepatic circulation create bidirectional flow between the organs. Circadian rhythmicity is an important means of communication between the intestine and liver, facilitating synchronization of hepatic metabolism with feeding/fasting cycles and nutrient availability [10, 11]. Alterations along the intestine-liver axis, including accumulation of gut-derived factors, dysbiosis of the gut microbiome, and perturbations in the hepatic circadian clock, have been shown to contribute to the development of NAFLD [12-14]. However, AhR-mediated changes in intestinal gene expression and function have not been thoroughly investigated, while little is currently known about the effects of AhR activation on circadian-regulated hepatic metabolism.

HYPOTHESIS

TCDD-elicited changes across the intestine-liver axis promote the development and progression of AhR-mediated NAFLD.

SPECIFIC AIMS

Specific Aim 1: Profile TCDD-elicited transcriptomic changes in the jejunal epithelium associated with the development of hepatic steatosis and progression to steatohepatitis with fibrosis.

Specific Aim 2: Examine TCDD-elicited alterations in the enterohepatic circulation and microbial metabolism of hepatotoxic bile acid species.

Specific Aim 3: Investigate TCDD-elicited disruptions in duodenal iron absorption and systemic iron homeostasis which promote hepatic oxidative stress.

Specific Aim 4: Analyze TCDD-elicited perturbations in the circadian rhythmicity of the hepatic transcriptome and metabolome, focusing on the metabolism of dietary nutrients, iron/heme, and bile acids.

REFERENCES

REFERENCES

1. Casals-Casas, C. and B. Desvergne, *Endocrine disruptors: from endocrine to metabolic disruption.* Annu Rev Physiol, 2011. 73: p. 135-62.

2. Cave, M., S. Appana, M. Patel, K.C. Falkner, C.J. McClain, and G. Brock, *Polychlorinated biphenyls, lead, and mercury are associated with liver disease in American adults: NHANES 2003-2004.* Environ Health Perspect, 2010. 118(12): p. 1735-42.

3. Chen, J.Q., T.R. Brown, and J. Russo, *Regulation of energy metabolism pathways by estrogens and estrogenic chemicals and potential implications in obesity associated with increased exposure to endocrine disruptors.* Biochim Biophys Acta, 2009. 1793(7): p. 1128-43.

4. Grun, F. and B. Blumberg, *Endocrine disrupters as obesogens.* Mol Cell Endocrinol, 2009. 304(1-2): p. 19-29.

5. Boverhof, D.R., L.D. Burgoon, C. Tashiro, B. Chittim, J.R. Harkema, D.B. Jump, and T.R. Zacharewski, *Temporal and dose-dependent hepatic gene expression patterns in mice provide new insights into TCDD-Mediated hepatotoxicity.* Toxicol Sci, 2005. 85(2): p. 1048-63.

6. Pierre, S., A. Chevallier, F. Teixeira-Clerc, A. Ambolet-Camoit, L.C. Bui, A.S. Bats, J.C. Fournet, P. Fernandez-Salguero, M. Aggerbeck, S. Lotersztajn, R. Barouki, and X. Coumoul, *Aryl hydrocarbon receptor-dependent induction of liver fibrosis by dioxin.* Toxicol Sci, 2014. 137(1): p. 114-24.

7. Nault, R., K.A. Fader, D.A. Ammendolia, P. Dornbos, D. Potter, B. Sharratt, K. Kumagai, J.R. Harkema, S.Y. Lunt, J. Matthews, and T. Zacharewski, *Dose-Dependent Metabolic Reprogramming and Differential Gene Expression in TCDD-Elicited Hepatic Fibrosis.* Toxicol Sci, 2016. 154(2): p. 253-266.

8. NTP, *Carcinogenesis Bioassay of 2,3,7,8-Tetrachlorodibenzo-p-dioxin (CAS No. 1746-01-6) in Osborne-Mendel Rats and B6C3F1 Mice (Gavage Study).* Natl Toxicol Program Tech Rep Ser, 1982. 209: p. 1-195.

9. Kociba, R.J., D.G. Keyes, J.E. Beyer, R.M. Carreon, C.E. Wade, D.A. Dittenber, R.P. Kalnins, L.E. Frauson, C.N. Park, S.D. Barnard, R.A. Hummel, and C.G. Humiston, *Results of a two-year chronic toxicity and oncogenicity study of 2,3,7,8-tetrachlorodibenzo-p-dioxin in rats.* Toxicol Appl Pharmacol, 1978. 46(2): p. 279-303.

10. Tong, X. and L. Yin, *Circadian rhythms in liver physiology and liver diseases.* Compr Physiol, 2013. 3(2): p. 917-40.

11. Oike, H., K. Oishi, and M. Kobori, *Nutrients, Clock Genes, and Chrononutrition.* Curr Nutr Rep, 2014. 3: p. 204-212.

12. Mazzoccoli, G., S. De Cosmo, and T. Mazza, *The Biological Clock: A Pivotal Hub in Non-alcoholic Fatty Liver Disease Pathogenesis.* Front Physiol, 2018. 9: p. 193.

13. Leung, C., L. Rivera, J.B. Furness, and P.W. Angus, *The role of the gut microbiota in NAFLD.* Nat Rev Gastroenterol Hepatol, 2016. 13(7): p. 412-25.

14. Miele, L., V. Valenza, G. La Torre, M. Montalto, G. Cammarota, R. Ricci, R. Masciana, A. Forgione, M.L. Gabrieli, G. Perotti, F.M. Vecchio, G. Rapaccini, G. Gasbarrini, C.P. Day, and A. Grieco, *Increased intestinal permeability and tight junction alterations in nonalcoholic fatty liver disease.* Hepatology, 2009. 49(6): p. 1877-87.

CHAPTER 3: 2,3,7,8-TETRACHLORODIBENZO-*P*-DIOXIN (TCDD) ALTERS LIPID METABOLISM AND DEPLETES IMMUNE CELL POPULATIONS IN THE JEJUNUM OF C57BL/6 MICE

Fader, K.A., R. Nault, D.A. Ammendolia, J.R. Harkema, K.J. Williams, R.B. Crawford, N.E. Kaminski, D. Potter, B. Sharratt, and T.R. Zacharewski, *2,3,7,8-Tetrachlorodibenzo-p-Dioxin Alters Lipid Metabolism and Depletes Immune Cell Populations in the Jejunum of C57BL/6 Mice.* Toxicol Sci, 2015. 148(2): p. 567-80.

ABSTRACT

2,3,7,8-Tetrachlorodibenzo-*p*-dioxin (TCDD) is a potent aryl hydrocarbon receptor (AhR) agonist that elicits dose-dependent hepatic fat accumulation and inflammation that can progress to steatohepatitis. To investigate intestine – liver interactions that contribute to TCDD-elicited steatohepatitis, we examined the dose-dependent effects of TCDD (0.01, 0.03, 0.1, 0.3, 1, 3, 10 or 30 µg/kg) on jejunal epithelial gene expression in C57BL/6 mice orally gavaged every 4 days for 28 days. Agilent 4x44K whole genome microarray analysis of the jejunal epithelium identified 439 differentially expressed genes (|fold change| ≥ 1.5, P1(t) ≥ 0.999) across one or more doses, many related to lipid metabolism and immune system processes. TCDD-elicited differentially expressed genes were associated with lipolysis, fatty acid/cholesterol absorption and transport, the Kennedy pathway, and retinol metabolism, consistent with increased hepatic fat accumulation. Moreover, transcript levels of several major histocompatibility complex (MHC) class II genes (*H2-Aa*, *H2-Ab1*, *H2-DMb1*, *Cd74*) were decreased, coincident with decreased macrophage and dendritic cell levels in the lamina propria, suggesting migration of antigen-presenting cells out of the intestine. In contrast, hepatic RNA-Seq analysis identified increased expression of MHC class II genes, as well as chemokines and chemokine receptors involved in macrophage recruitment (*Ccr1*, *Ccr5*, *Ccl5*, *Cx3cr1*), consistent with hepatic F4/80 labeling and macrophage infiltration into the liver. Collectively, these results suggest TCDD elicits changes that support hepatic lipid accumulation, macrophage migration, and the progression of hepatic steatosis to steatohepatitis.

INTRODUCTION

Metabolic syndrome (MetS), a constellation of disorders that includes obesity, insulin resistance, and dyslipidemia [1, 2], is approaching pandemic levels [3, 4]. In the liver, MetS can manifest itself as non-alcoholic fatty liver disease (NAFLD), in which benign and reversible hepatic fat accumulation (steatosis) progresses to chronic steatohepatitis (steatosis with inflammation)

and fibrosis (collagen deposition) [5-7]. Recent reports suggest the aryl hydrocarbon receptor (AhR) plays an underappreciated role in the development of MetS and NAFLD [8-12].

2,3,7,8-Tetrachlorodibenzo-*p*-dioxin (TCDD) is the prototypical ligand for a group of structurally diverse synthetic chemicals, natural products, and endogenous metabolites that activate the AhR [13]. Upon binding, the cytoplasmic AhR dissociates from AIP, p23 and HSP90 chaperone proteins, translocates to the nucleus, and heterodimerizes with the aryl hydrocarbon receptor nuclear translocator (ARNT). The AhR/ARNT complex acts as a transcription factor, altering levels of gene expression primarily through binding to dioxin response elements (DREs) [14, 15]; however, DRE-independent mechanisms of differential gene expression have also been reported [16-18].

In mice, a single bolus dose of TCDD induces hepatic steatosis and immune cell infiltration [19, 20], with progression to steatohepatitis and fibrosis following repeated treatment [21]. Our previous studies have shown that dietary fat rather than *de novo* synthesis is a primary source of lipids involved in TCDD-elicited hepatic steatosis. Dose-dependent hepatic increases in essential dietary fatty acids (i.e. 18:2n6 and 18:3n3) were reported in TCDD-treated mice fed a high-fat diet but not a high-carbohydrate diet [22]. Furthermore, TCDD increased hepatic levels of oleate (18:1) in *Scd1*-null mice incapable of desaturating stearate (18:0), while hepatic *de novo* fatty acid synthesis and beta oxidation gene expression were repressed [22-24]. Based on these studies, we hypothesize that TCDD-mediated changes in intestinal function support the development of hepatic steatosis and its progression to steatohepatitis.

The intestine is divided into the duodenum, jejunum, ileum and colon, with each segment differing in structure and absorptive function. Lipid absorption occurs predominantly in the jejunum, with compensatory uptake by the ileum as the fat load increases [25]. Dietary fats such as triglycerides (TAGs) are hydrolyzed in the lumen by lipases and the resulting free fatty acids are absorbed into intestinal epithelial cells (enterocytes) either by passive diffusion or active processes involving membrane transporters. Inside enterocytes, fatty acids are reassembled into

TAGs and packaged with cholesterol and apolipoproteins into chylomicrons for transport to the liver via the lymphatic system [26]. During digestion and nutrient absorption, the gastrointestinal tract is continuously exposed to foreign antigens and thus the intestine is equipped with organized lymphoid tissue such as Peyer's Patches, as well as individual innate immune cells including monocytes/macrophages, dendritic cells (DCs), and innate lymphoid cells (ILCs) scattered throughout the epithelium and lamina propria [27, 28].

In this report, jejunal epithelial global gene expression and intestinal lamina propria immune cell populations were examined to further investigate intestine – liver interactions that may contribute to TCDD-elicited steatohepatitis in mice. Our results demonstrate that TCDD-elicited differentially expressed genes (DEGs) were associated with lipolysis, fatty acid/cholesterol absorption and transport, the Kennedy pathway, and retinol metabolism, consistent with increased hepatic fat accumulation. Furthermore, several major histocompatibility complex (MHC) class II genes involved in immune cell activation and antigen presentation exhibited reduced transcript levels, coincident with decreased populations of macrophages and DCs in the intestinal lamina propria. In contrast, hepatic macrophage levels increased in TCDD-treated animals, and thus we speculate that immune cells may be migrating from the intestine to the liver. Collectively, these results are consistent with jejunum – liver interactions that contribute to TCDD-elicited steatohepatitis.

MATERIALS & METHODS

Animal husbandry and treatment

Female C57BL/6 mice weighing within 10% of each other were obtained from Charles River Laboratories (Portage, MI) on postnatal day 25 (PND25). Animals were housed in polycarbonate cages containing cellulose fiber chips (Aspen Chip Laboratory Bedding, Northeastern Products, Warrensberg, NY) in a 23°C environment with 30 – 40% humidity and a 12-hour light/dark cycle (0700 h – 1900 h). Mice were provided deionized water and Harlan Teklad

22/5 Rodent Diet 8940 (Madison, WI) *ad libitum*, and were acclimated for 4 days. Animals (N = 8) were orally gavaged with sesame oil vehicle (Sigma-Aldrich, St. Louis, MO), 0.001, 0.01, 0.03, 0.1, 0.3, 1, 3, 10, or 30 µg/kg TCDD (Dow Chemical Company, Midland, MI) every 4 days for a total of 28 days (7 exposures; Figure 6A). For the high-dose female and male study, C57BL/6 mice (PND25) obtained from Charles River Laboratories (Kingston, NY) were housed in Innovive Innocages® (San Diego, CA) with ALPHA-dri® bedding (Shepherd Specialty Papers, Chicago, IL). Animals were fed *ad libitum* Harlan Teklad Rodent Diet 8940 and Aquavive® water (Innovive). Beginning on PND28 – 31, animals (N = 8 – 16) were orally gavaged with either sesame oil vehicle (Sigma) or 30 µg/kg TCDD (Dow Chemical Company) every 4 days for a total of 28 days (7 exposures; Figure 6B). All animal handling procedures were performed with the approval of the Michigan State University All-University Committee on Animal Use and Care.

Tissue collection

On day 28, female mice from the dose-response study were weighed and blood was collected from the submandibular vein prior to cervical dislocation. Four intestinal sections were removed: duodenum (entire length up to the duodenojejunal flexure), jejunum (~6 cm section proximal to the duodenum), ileum (~6 cm section proximal to the caecum), and colon (entire length). Each section was flushed with Ca^{2+}/Mg^{2+}-free phosphate buffered saline (PBS; Sigma) and cut open longitudinally. An ~0.5 cm segment was removed from each of the four sections and fixed in 10% neutral buffered formalin (NBF; Sigma). Epithelium from the remaining sections were individually scraped into vials containing 1.3 mL TRIzol (Invitrogen, Carlsbad, CA), frozen in liquid nitrogen, and stored at -80°C. Liver, pancreas, and gonadal white adipose tissue (gWAT) were removed, weighed, frozen in liquid nitrogen, and stored at -80°C. The right lobe of the liver was sectioned and either fixed in 10% NBF (Sigma) for histological analyses or frozen in Tissue-Tek O.C.T. compound (Sakura, Torrance, CA) for Oil Red O (ORO) staining of neutral lipids.

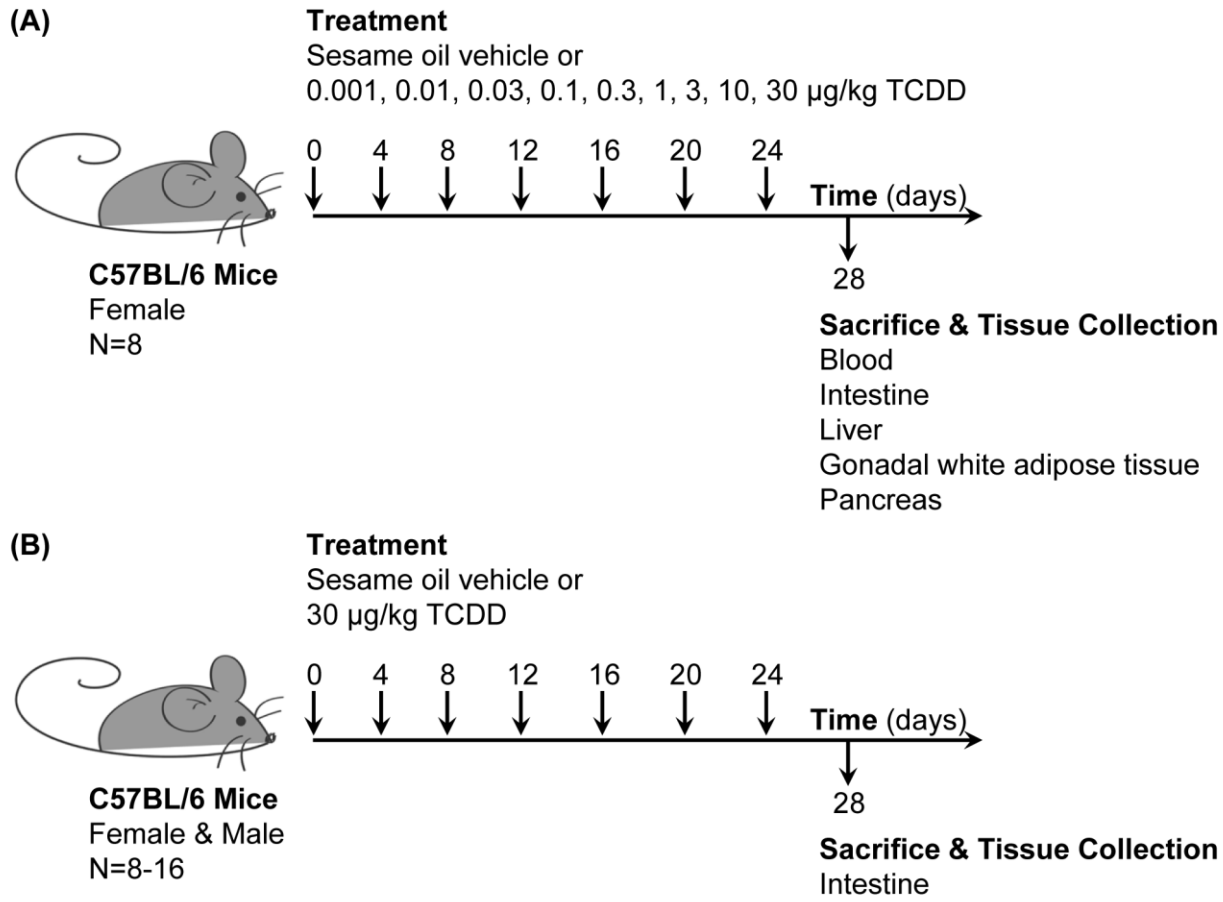

FIGURE 6. CHAPTER 3 STUDY DESIGN

(A) Female C57BL/6 mice (N = 8) were orally gavaged with sesame oil vehicle or 0.001 – 30 µg/kg TCDD every 4 days for 28 days. (B) Female and male C57BL/6 mice (N = 8 – 16) were orally gavaged with sesame oil vehicle or 30 µg/kg TCDD every 4 days for 28 days.

Flow cytometry

On day 28, female and male mice from the high-dose study were sacrificed by cervical dislocation and intestinal lamina propria cells were collected for flow cytometry analysis using a modified protocol [29]. Briefly, the small intestine was removed and cut into the proximal intestine consisting of the duodenum and jejunum, and the distal intestine consisting of the ileum. Each section was flushed with Ca^{2+}/Mg^{2+}-free PBS, opened longitudinally, and cut into ~1.5 cm pieces. The proximal and distal intestinal pieces were placed in separate conical tubes containing 10 mL of pre-warmed (37°C) Ca^{2+}/Mg^{2+}-free Hank's Balanced Salt Solution (HBSS; Sigma) with 5% heat-inactivated fetal bovine serum (HBSS/FBS) and 2 mM EDTA. Enterocytes were dissociated using two 20-minute rounds of horizontal shaking (~250 rpm) at 37°C, transferring the tissue to fresh HBSS/FBS with 2 mM EDTA after the first 20 minutes. The contents of each tube were strained, intestinal pieces minced, and tissue transferred to a conical tube containing 10 mL of pre-warmed HBSS/FBS with 1.5 mg/mL Collagenase Type IV from *Clostridium histolyticum* (Sigma) and 40 µg/mL Deoxyribonuclease I from bovine pancreas (Sigma). To digest the tissue, the proximal and distal samples were horizontally shaken (~250 rpm) at 37°C for 10 and 15 minutes, respectively, followed by 10 seconds of vortexing. Each tube was then filtered through a 70 µm cell strainer (Falcon, Tewksbury, MA) into a conical tube containing HBSS/FBS. The strained cells were pelleted at 1500 rpm for 5 minutes, washed twice in ice-cold HBSS/FBS and re-suspended in ice-cold FACS buffer (Ca^{2+}/Mg^{2+}-free HBSS with 1% bovine serum albumin (BSA; Sigma) and 0.1% sodium azide (Sigma), pH 7.6).

Proximal and distal intestinal suspensions were quantified using the TC20 Automated Cell Counter (Bio-Rad, Hercules, CA) with ≥ 90% viability confirmed by visual assessment of Trypan Blue (Life Technologies, Grand Island, NY) staining. Cells (10^6) were pelleted and surface Fc receptors blocked with anti-mouse CD16/CD32 antibody (2.4G2; BD Biosciences, San Jose, CA) for 10 minutes on ice. Cells were then labeled for 20 minutes on ice with an antibody cocktail. The immune cell panel cocktail consisted of fluorescently-labeled CD3e (145-2C11; BioLegend, San

Diego, CA), CD4 (GK1.5; BioLegend), CD8a (53-6.7; BioLegend), CD19 (6D5; BioLegend), F4/80 (BM8; eBioscience, San Diego, CA) and NK1.1 (PK136; BioLegend) anti-mouse antibodies. The DC cocktail consisted of fluorescently-labeled CD11b (M1/70), CD11c (N418) and CD103 (2E7) BioLegend anti-mouse antibodies. Following labeling, cells were washed with ice-cold FACS buffer, re-pelleted, fixed with Cytofix (BD Biosciences) for 15 minutes on ice, and re-suspended in ice-cold FACS buffer for subsequent analysis. Compensation and voltage settings of fluorescent parameters were performed using single color labeling controls. Fluorescent labeling of the cell suspensions was analyzed using a BD FACSCanto II flow cytometer (BD Biosciences).

TCDD tissue levels

Hepatic TCDD levels were quantified as previously described [30]. Briefly, tissues were weighed, spiked with $^{13}C_{12}$-2,3,7,8-TCDD, digested with hydrochloric acid, and subjected to extraction and clean-up procedures. Prior to injection, $^{13}C_{12}$-1,2,3,4-TCDD was added to the concentrated extracts. Calibration standards containing 2,3,7,8-TCDD, $^{13}C_{12}$-2,3,7,8-TCDD and $^{13}C_{12}$-1,2,3,4-TCDD were first analyzed by high-resolution gas chromatography/high-resolution mass spectrometry (HRGC/HRMS), followed by solvent blanks and then the extracts. The HRGC/HRMS system was a Hewlett Packard 6890N HRGC interfaced to a Waters Autospec Ultima HRMS. Chromatographic separations were carried out in constant flow mode (Helium, 1 mL/min) on a 60 m DB5 (0.25 mm ID, 0.25 µm film thickness) column. The HRMS was operated in EI+ selective ion recording mode (SIR) at a mass resolving power of 10,000 or greater.

Clinical chemistry

Total serum cholesterol, TAGs, and glucose were determined using commercially available kits (Pointe Scientific, Canton, MI) according to manufacturer's protocol. All assays were performed using an Infinite M200 plate reader (Tecan, Durham, NC).

Histological analysis

All tissue processing for histology was performed by the Michigan State University Investigative HistoPathology Laboratory (https://humanpathology.natsci.msu.edu). Formalin-fixed intestinal and hepatic tissues were processed and vacuum infiltrated with paraffin using a Tissue-Tek VIP 2000 tissue processor (Sakura) followed by embedding with the Thermo Fisher HistoCentre III embedding station (Thermo Fisher, Waltham, MA). Paraffin blocks were sectioned at 4 – 5 μm with a Reichert Jung 2030 rotary microtome (Reichert, Depew, NY) and dried for 2 – 24 hr at 56°C to ensure adherence to the slides. For lipid staining, liver sections frozen in O.C.T. compound were sectioned at 6 μm, fixed in 10% NBF for 5 min, rinsed with water, and immersed in 100% propylene glycol for 5 min.

Intestinal sections from vehicle and 30 μg/kg TCDD-treated female mice (N = 3) were stained with hematoxylin and eosin (H&E), and macrophages in the intestinal wall were labeled using a monoclonal anti-mouse F4/80 antibody (1:100 dilution; AbD Serotec, Raleigh, NC). Liver sections from female mice were stained with H&E for general assessment of histological features and identification of doses requiring further assessment using alternate staining or immunohistochemical analyses. Lipid staining was performed by ORO as previously described [20]. Macrophage infiltration was determined for vehicle, 3, 10, and 30 μg/kg TCDD-treated mice using the monoclonal anti-mouse F4/80 antibody as described above. Further characterization of the inflammatory response was achieved by labeling for eosinophils (vehicle, 3, 10, and 30 μg/kg TCDD) using a rat anti-mouse major basic protein (MBP) antibody (1:500; Mayo Clinic, Scottsdale, AZ) and the presence of alternatively activated macrophages (vehicle, 3, 10, and 30 μg/kg TCDD) was assessed using a goat polyclonal anti-mouse Chitinase 3-like 3/ECF-L antibody (Ym1; 1:1500 dilution; R&D Systems, Minneapolis, MN).

Quantitation of histological features was performed using the Quantitative Histological Analysis Tool (QuHAnT) [31]. Briefly, slides were digitized at 20x magnification using an Olympus Virtual Slide System VS110 (Olympus, PA). Digitized slides were then sampled at 100% coverage

using the Visiomorph Microimager (Visiopharm, Denmark). Each image was visually inspected for quality, and flawed images (e.g. debris, bubbles, false positives) were removed prior to analysis. Hue, Saturation, and Value (HSV) image segmentation values for feature extraction and background extraction were determined using ImageJ (http://rsb.info.nih.gov.ij/) and are provided in Table 1. Volume densities were estimated as the sum of positive hits ($P_{positive}$ staining) divided by the total number of tissue hits (P_{tissue}) for each section (V_v = ($P_{positive}$ staining/P_{tissue}) x 100). Assessment of micro- and macro-vesicular steatosis using ORO stained liver sections was determined using a cut-off of 176 μm^2 estimated based on a diameter of 15 µm previously reported to identify macro lipid vacuolization [32].

RNA isolation

Frozen intestinal epithelium scrapings stored in TRIzol were homogenized using a Mixer Mill 300 tissue homogenizer (Retsch, Germany). Total RNA was isolated according to the manufacturer's protocol with an additional acid phenol:chloroform (Sigma) extraction, and re-suspended in RNase-free RNA storage solution (Ambion Inc., Austin, TX). RNA was quantified using a Nano-drop spectrophotometer (Thermo Scientific, Wilmington, DE) at 260 nm and purity was assessed by calculating the A_{260}/A_{280} ratio. Quality of the RNA was visually evaluated by electrophoresis of 2 µg on a 1% denaturing formaldehyde-agarose gel.

Microarray analysis

Dose-dependent gene expression changes were examined using mouse 4×44K Agilent whole-genome oligonucleotide microarrays (version 1, Agilent Technologies, Inc., Santa Clara, CA). Hepatic RNA from treated and control samples were co-hybridized to individual arrays according to the manufacturer's protocol (Agilent Manual: G4140-90040 v. 5.7). All hybridizations were performed with three independent biological replicates (i.e. RNA samples were not pooled)

TABLE 1. HUE, SATURATION, AND VALUE (HSV) IMAGE SEGMENTATION VALUES FOR FEATURE EXTRACTION AND BACKGROUND EXTRACTION

Stain/ Antibody	Feature Extraction			Background Extraction		
	Hue	*Saturation*	*Value*	*Hue*	*Saturation*	*Value*
F4/80	222,255	45,255	0,255	0,255	12,255	0,255
ORO	0,50 & 225,255	125,255	0,255	0,255	20,255	0,255
Ym1	240,255	41,255	0,255	0,255	12,255	0,255
MBP	204,255	24,255	0,210	0,255	8,255	0,210

and two independent labelings (Cy3 and Cy5 dye swaps). Microarrays were scanned at 532 nm (Cy3) and 635 nm (Cy5) on a GenePix 4000B scanner (Molecular Devices, Union City, CA). Images were analyzed for feature and background intensities using GenePix Pro 6.0 software (Molecular Devices). All data passed our laboratory quality assurance protocol [33] and were managed in TIMS dbZach data management system [34]. The complete microarray data set has been deposited in the Gene Expression Omnibus (GEO; accession number GSE70379) database.

Data were normalized using a semi-parametric approach [35] in SAS v9.3 (SAS Institute Inc., Cary, NC). Posterior probability P1(*t*) values were calculated using an empirical Bayes method based on a per gene and dose basis using model-based t-values [36]. For TCDD-mediated differential gene expression, fold changes were calculated relative to vehicle controls. Genes were considered to be differentially expressed if |fold change| ≥ 1.5 and statistical P1(*t*) value ≥ 0.999 at one or more doses.

Dose-response modeling

Dose-response modeling was performed using the ToxResponse Modeler [34]. Median effective dose (ED_{50}) values for features exhibiting a sigmoidal response were reported if within the experimental dose range (0.01 – 30 µg/kg). Estimation of benchmark dose (BMD) and BMD lower confidence limit (BMDL) was performed using BMDExpress [37]. A benchmark response (BMR) factor of 1.349 was chosen to represent a 10% change in transcript levels compared to vehicle controls. Normalized linear microarray signal intensities for each feature were fit to Hill, linear (1° polynomial), 2° polynomial, or power dose-response models and the best globally-fitting model with the least complexity was selected following the criteria previously published by U.S. EPA [38].

Functional annotation

DEGs were analyzed for enriched functions using the Database for Annotation, Visualization, and Integrated Discovery (DAVID) v6.7. Only Gene Ontology (GO) Biological Processes were considered for the enrichment analysis. Functional groups with an enrichment score (ES) ≥ 1.3 were considered significantly enriched, representing the -log scale geometric mean *p*-value of 0.05.

Computational putative DRE identification

Putative dioxin response elements (pDREs) were previously identified [39]. Briefly, gene regulatory regions (10 kb upstream of the transcription start site (TSS) together with 5′- and 3'-untranslated regions (UTR)) and coding sequence obtained from the University of California, Santa Cruz (UCSC) Genome Browser for mouse (mm9, build 37) were computationally searched for the DRE core consensus sequences 5'-GCGTG-3'. Each identified core was extended by 7 bp upstream and downstream, and the resulting 19 bp sequences were scored using a position weight matrix (PWM) constructed from *bona fide* functional DREs. Matrix similarity scores (MSS) ≥ 0.8473 were considered to be pDREs.

Statistical analysis

All statistical analyses were performed in SAS 9.3 (SAS Institute Inc.). Unless otherwise stated, differences between groups were considered significant when $p < 0.05$.

RESULTS

Gross pathology and clinical chemistry

We have previously established that a single bolus dose of 30 µg/kg TCDD elicits hepatic fat accumulation that is almost completely reversed after 4 weeks following cessation of treatment [40], consistent with a half-life of 8.5 – 12 days in mice [40-42] compared to 1.3 – 11.3 years in

humans [43-46]. In order to approach steady-state TCDD levels, mice were gavaged every 4 days for 28 days to investigate the longer-term effects of TCDD exposure. Hepatic TCDD levels exhibited a dose-dependent increase (Table 2) that exceeded levels of a single bolus dose by ~4-fold [19].

In this study, TCDD did not affect terminal body weight, with the exception of a negligible increase at 0.03 µg/kg (Table 3). However, relative liver weights (RLW) displayed a 21 – 30% dose-dependent increase at 3, 10, and 30 µg/kg TCDD, while the relative gonadal white adipose tissue weight (RgWATW) decreased by 49% at 30 µg/kg TCDD (Table 3). No change in terminal pancreas weight was observed (results not shown).

Serum cholesterol levels decreased from 121.5 mg/dL to 88.3 mg/dL at 30 µg/kg TCDD, consistent with trends reported following a single bolus dose of 30 µg/kg TCDD [19, 47]. Although TAG levels exhibited a decrease, it did not achieve statistical significance. In contrast, serum TAG levels were elevated in fed mice following a single bolus dose of 30 µg/kg TCDD, but unchanged in fasted mice receiving the same dose, suggesting duration of exposure and access to chow affect the lipidemic profile [19, 47]. Glucose levels were unchanged in both the current study (Table 3) and in mice following a single bolus dose [19].

Jejunal differential gene expression

The jejunum is the segment of the small intestine predominantly responsible for dietary fat absorption. Dose-dependent differential gene expression in the jejunal epithelium of female mice was evaluated using Agilent 4X44K whole genome oligonucleotide microarrays containing 41,267 probes representing ~21,308 unique genes. Empirical Bayesian analysis identified 439 DEGs (|fold change| ≥ 1.5, P1(*t*) ≥ 0.999) across one or more doses (Figure 7A). The number of unique DEGs at each dose reveals a bimodal distribution with the largest number differentially expressed

TABLE 2. HEPATIC TCDD LEVELS

Dose (µg/kg)	Repeated (ppt)	Acute[a] (ppt)
0	61 ± 59	72 ± 98
0.001	48 ± 31	14 ± 9
0.01	122 ± 38	35 ± 12
0.03	297 ± 95*	*NM*
0.1	1,553 ± 368*	418 ± 84
0.3	5,600 ± 1,383*	*NM*
1	19,533 ± 5,008*	5,278 ± 2,087
3	57,200 ± 10,047*	*NM*
10	165,333 ± 34,818*	61,750 ± 10,546
30	653,666 ± 109,038*	*NM*

NM indicates not measured

[a]Single bolus dose after 24 hrs [19]

*Indicates $p \leq 0.05$ compared to vehicle control

TABLE 3. GROSS PATHOLOGY & SERUM CLINICAL CHEMISTRY

TCDD (ug/kg)	Gross Pathology			Serum Clinical Chemistry		
	Body Weight (g)	RLW (%)	RgWATW (%)	Cholesterol (mg/dL)	Glucose (mg/dL)	TAG (mg/dL)
0	17.1 ± 1.1	4.83 ± 0.12	1.36 ± 0.12	121.5 ± 3.0	103.2 ± 3.4	112.8 ± 8.2
0.001	17.5 ± 0.7	4.74 ± 0.26	1.13 ± 0.12	118.0 ± 4.4	107.1 ± 3.5	106.0 ± 8.4
0.01	17.7 ± 1.0	4.42 ± 0.58	0.97 ± 0.12	117.7 ± 4.6	104.1 ± 2.8	95.6 ± 6.1
0.03	18.2 ± 1.6*	5.07 ± 0.20	0.98 ± 0.11	119.2 ± 2.7	108.4 ± 4.3	101.8 ± 8.3
0.1	17.1 ± 0.7	5.10 ± 0.17	1.06 ± 0.07	116.8 ± 2.5	107.4 ± 2.7	94.1 ± 6.9
0.3	18.1 ± 1.2	5.54 ± 0.17	1.10 ± 0.09	119.4 ± 1.5	105.4 ± 2.1	102.0 ± 4.3
1	17.9 ± 1.5	5.57 ± 0.19	1.22 ± 0.11	114.2 ± 3.2	100.8 ± 3.4	100.4 ± 9.0
3	17.6 ± 1.2	5.86 ± 0.22*	1.13 ± 0.09	110.4 ± 2.5	102.6 ± 3.5	103.6 ± 9.7
10	17.6 ± 1.3	6.26 ± 0.22*	0.93 ± 0.17	95.8 ± 4.3	110.2 ± 4.6	98.3 ± 11.3
30	17.0 ± 1.0	6.22 ± 0.18*	0.69 ± 0.10*	88.3 ± 2.2*	102.2 ± 4.0	91.6 ± 6.4

*Indicates $p \leq 0.05$ compared to vehicle control

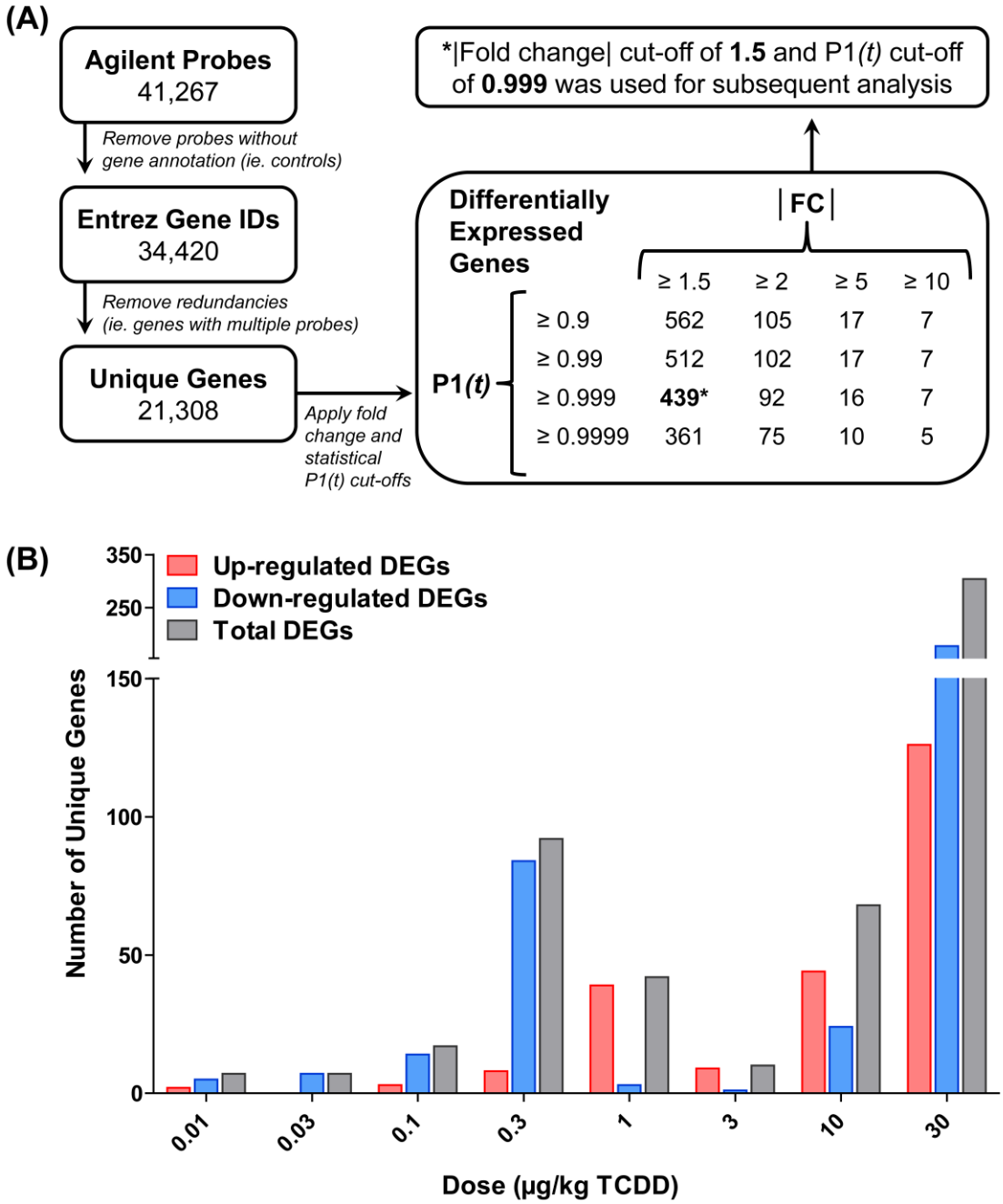

FIGURE 7. MICROARRAY ANALYSIS OF JEJUNAL DIFFERENTIAL GENE EXPRESSION

Female C57BL/6 mice were treated by oral gavage with sesame oil vehicle or 0.01 – 30 µg/kg TCDD every 4 days for 28 days. (A) Agilent 4X44K whole genome microarray data were filtered using |fold change| ≥ 1.5 and P1(*t*) ≥ 0.999 criteria, identifying 439 genes differentially expressed at one or more doses. (B) The number of up-regulated, down-regulated, and total differentially expressed unique genes at each dose.

at 30 µg/kg TCDD and a smaller peak at 0.3 µg/kg TCDD (Figure 7B). Similar anomalies have been observed in previous studies within the mid-dose range [48]. Salivary amylase 1 (*Amy1*) and pancreatic carboxypeptidase A2 (*Cpa2*) were among the most induced genes at 27.7- and 24.2-fold, respectively, while immunoglobulin joining chain (*Igj*) and cubilin (*Cubn)* were the most repressed at 3.9- and 3.1-fold, respectively. Several AhR battery genes including *Cyp1a1*, *Cyp1a2,* and TCDD-inducible poly(ADP-ribose) polymerase (*Tiparp*) were also induced 4.7-, 3.9- and 2.7-fold, respectively, at 30 µg/kg TCDD.

Dose-response modeling

ToxResponse Modeler [34] identified 264 sigmoidal, 28 Gaussian, and 47 exponential responses, with 123 features not fitting an appropriate model (Figure 8A). ED_{50} values for sigmoidal dose-responsive features ranged between 0.019 and 29.0 µg/kg TCDD. The frequency distribution for these ED_{50} values followed a step-wise pattern with peaks at 0.4, 1.1, and 3.2 µg/kg TCDD (Figure 8B).

BMDExpress [37] was also used to analyze the dose-response behavior of 368 unique DEGs, following removal of 71 genes containing a blank intensity value at one or more doses. Using EPA criteria [38], 10 hill, 53 linear, 24 second degree (2°) polynomial, and 37 power responses were identified. The remaining 291 features failed to meet modeling criteria defined by EPA (Figure 8A). The frequency distribution of BMDL values for all hill, linear, 2° polynomial, or power responses also exhibited peaks at 0.4, 1.1, and 3.2 µg/kg TCDD, consistent with the step-wise ED_{50} distribution pattern (Figure 8B).

Functional enrichment analysis

DAVID identified 11 significantly enriched functional clusters (ES ≥ 1.3), including 3 lipid-related processes: (i) lipid transport and metabolism (ES = 3.04), (ii) lipoprotein receptor activity and binding (ES = 1.62), and (iii) lipid homeostasis (ES = 1.60) (Figure 9A). A total of 38 lipid-

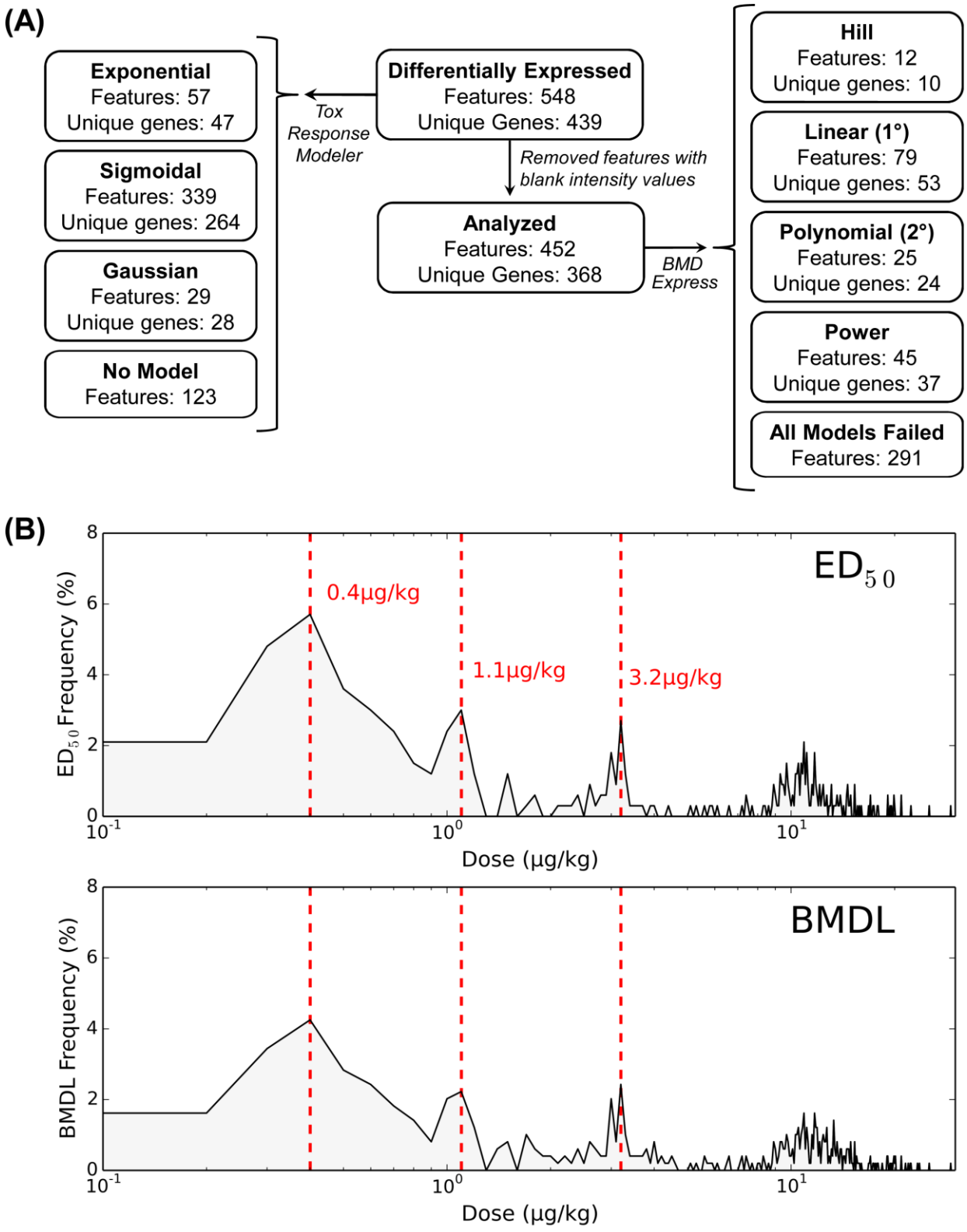

FIGURE 8. DOSE-RESPONSE MODELING OF JEJUNAL DIFFERENTIALLY EXPRESSED GENES

FIGURE 8 (cont'd)

Female C57BL/6 mice were treated by oral gavage with sesame oil vehicle or 0.01 – 30 µg/kg TCDD every 4 days for 28 days. (A) Summary of ToxResponse Modeler (left) and BMDExpress (right) dose-response modeling for jejunal epithelial differentially expressed genes. (B) Frequency distribution of ED_{50} values for 339 sigmoidal features (top) and bench mark dose lower confidence limit (BMDL) (bottom) values for 161 features exhibiting hill, linear, 2° polynomial, or power responses. The distributions reveal peaks at 0.4, 1.1, and 3.2 µg/kg TCDD, suggesting a dose-dependent step-wise response in differential gene expression.

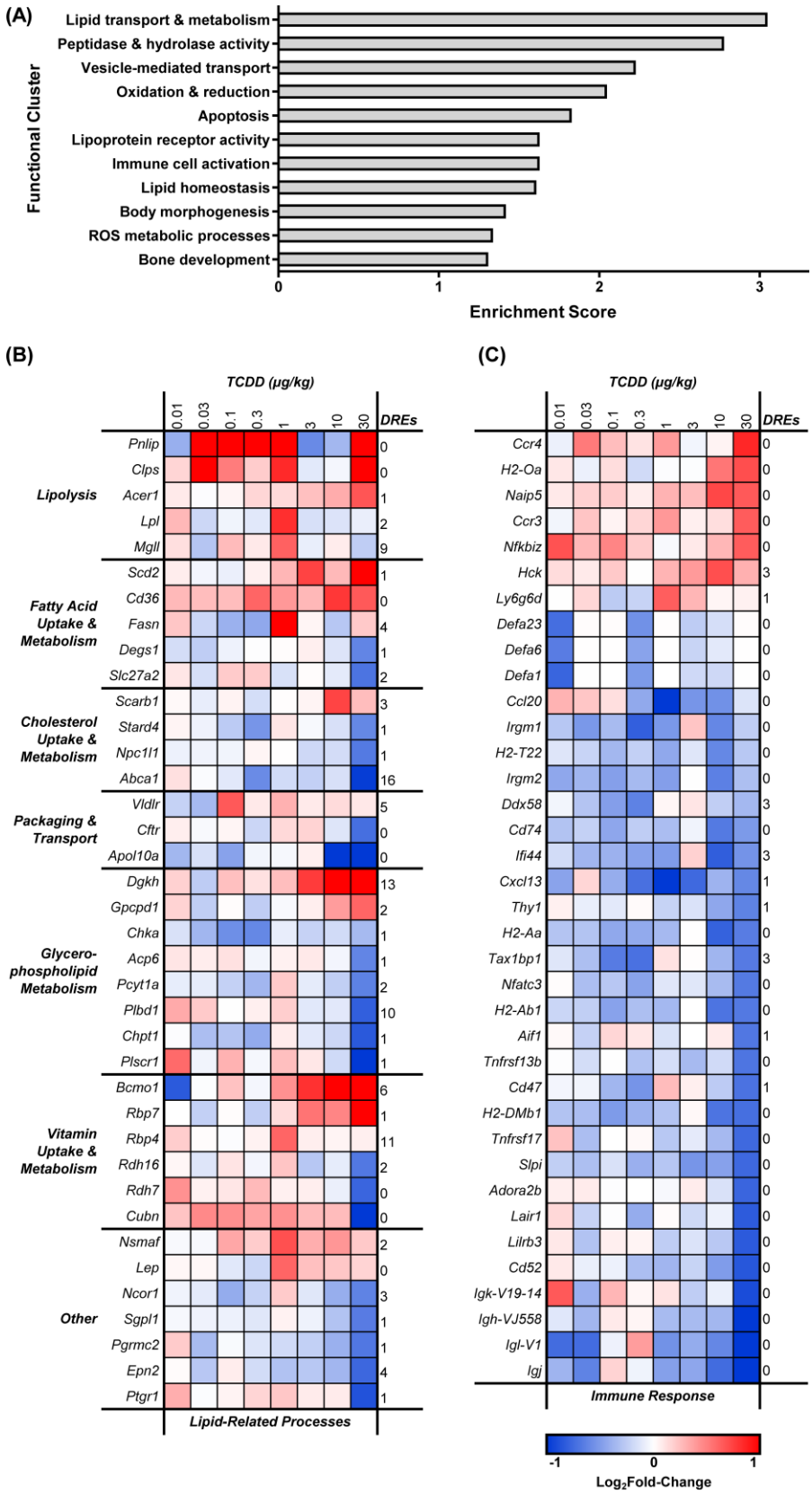

FIGURE 9. FUNCTIONAL ANALYSIS OF JEJUNAL DIFFERENTIALLY EXPRESSED GENES

FIGURE 9 (cont'd)

Female C57BL/6 mice were treated by oral gavage with sesame oil vehicle or 0.01 – 30 µg/kg TCDD every 4 days for 28 days. (A) Functional clusters identified using the Database for Annotation, Visualization and Integrated Discovery (DAVID). Scores ≥ 1.3 are considered significantly enriched. (B) Heat map of differentially expressed genes associated with lipid-related processes. (C) Heat map of differentially expressed genes associated with immune system processes. The number of pDREs (MS ≥ 0.8473) is indicated in the last column on the right of each heat map.

related DEGs were identified using representative GO terms (lipid metabolic process GO:0006629; lipid binding GO:0008289; lipid transport GO: 0006869), with manually curated additions (Figure 9B). pDREs were identified in 30 of 38 lipid-related DEGs, suggesting involvement of DRE-dependent and -independent mechanisms. Several lipases were up-regulated, including pancreatic lipase (*Pnlip*), primarily responsible for hydrolysis of dietary TAGs into free fatty acids, and its essential cofactor pancreatic colipase (*Clps*), induced 16.4- and 2.5-fold, respectively. Monoglyceride lipase (*Mgll*), alkaline ceramidase 1 (*Acer1*), and lipoprotein lipase (*Lpl*) were also upregulated 1.5- to 1.8-fold, suggesting TCDD enhances dietary fat hydrolysis. Various lipid transporters were also differentially expressed such as long-chain fatty acid transporter Cd36 antigen (*Cd36*; 1.7-fold), while cholesterol transporters, including NPC1-like 1 (*Npc1l1*) and ATP-binding cassette A1 (*Abca1*), were repressed 1.6- and 2.0-fold, respectively, and intracellular cholesterol binding protein StAR-related lipid transfer domain containing 4 (*Stard4*) was repressed 1.5-fold. This would suggest that absorption of dietary cholesterol is reduced by TCDD, consistent with lower serum cholesterol levels.

In addition, several genes involved in the metabolism of glycerophospholipids, specifically phosphatidylcholine (PC), were differentially expressed. Prior to absorption, dietary PC undergoes phospholipase A2 (PLA2)-mediated hydrolysis to yield free fatty acids and lysoPC, which are then taken up by enterocytes [49]. Phospholipase B domain containing 1 (*Plbd1*), which contains PLA2 activity, was repressed 1.7-fold, suggesting PC absorption may be impaired. Choline kinase α (*Chka*), phosphate cytidylyltransferase 1 choline α (*Pcyt1a*), and choline phosphotransferase 1 (*Chpt1*) were repressed 1.5-, 1.6-, and 1.8-fold, respectively. Interestingly, these enzymes catalyze the three consecutive steps of the PC branch of the Kennedy pathway, suggesting *de novo* synthesis of PC from choline and diacylglycerol (DAG) is repressed by TCDD. Diacylglycerol kinase η (*Dgkh*), which catalyzes the phosphorylation of DAG to diacylglycerol-3-phosphate, was induced 3.7-fold which could deplete DAG levels, further limiting the Kennedy pathway. Additionally, glycerophosphocholine phosphodiesterase GDE1 homolog (*Gpcpd1*),

responsible for the cleavage of choline from glycerol-3-phosphocholine, was induced 2.1-fold. This, with Kennedy pathway repression, could increase free choline in jejunal enterocytes.

Retinol (vitamin A) metabolism genes were also differentially expressed following TCDD treatment. For example, β-carotene 15,15'-monooxygenase (*Bcmo1*), responsible for converting β-carotene to retinal, was induced 6.7-fold. Interestingly, lipid transporters responsible for β-carotene uptake, including *Cd36* and scavenger receptor class B1 (*Scarb1*) [50], were also induced by TCDD. In contrast, retinol dehydrogenase 16 (*Rdh16*), which catalyzes the reduction of retinal to retinol, was repressed 1.6-fold, while *Rdh7* was repressed 1.7-fold. Moreover, cellular retinol binding protein 7 (*Rbp7*) and plasma retinol binding protein 4 (*Rbp4*), were induced 2.2- and 1.5-fold, respectively.

An immune cell activation and antigen presentation cluster was also enriched (ES = 1.62) (Figure 9A). A total of 37 immune-related DEGs were identified using a representative GO term (immune system process GO:0002376) followed by manual curation, of which 30 were down-regulated (Figure 9C). This includes several MHC class II genes (*H2-Aa*, *H2-Ab1*, *H2-DMb1*, *Cd74*) which exhibited 1.6- to 1.8-fold reductions in hepatic transcript levels. Additionally, several genes expressed predominantly by immune cells (*Cd52*, *Lair1*), macrophages (*Irgm1*, *Pirb*, *Ifi44*), T cells (*Thy1*), and B cells (*Tnfrsf13b, Tnfrsf17*) were repressed. The absence of DREs in 28 of 37 immune-related genes suggests that DRE-independent mechanisms are involved in TCDD-elicited intestinal immune cell effects.

Intestinal immune cell population changes

Previous studies have reported TCDD-elicited differential expression of genes associated with immune cell activation and antigen presentation in the mouse liver [19, 40]. As reported with the jejunal responses in this study, TCDD-elicited hepatic immune DEGs were predominantly independent of pDREs. Further investigation determined that the hepatic immune response was due to the dose-dependent infiltration of immune cells rather than DRE-dependent changes in

gene expression [19]. Therefore, histopathology and flow cytometry were used to examine the possibility that decreased transcript levels of immune-related genes were attributed to changes in intestinal immune cell populations.

No histological lesions were noted in the duodenum, jejunum, ileum, and colon of TCDD-treated mice. Moreover, visual assessment and quantitative analysis of F4/80 positive labeling using QuHAnT, an in-house developed, computational high throughput tool [31], detected no changes in macrophage populations (data not shown), although substantial inter-animal variability in the number of F4/80-positively labeled cells was observed.

The intestinal immune system includes effector lymphocytes interspersed in the epithelial lining, with the majority of scattered immune cells and lymphoid aggregates including Peyer's Patches located immediately below the epithelium in the lamina propria [28]. In order to focus on immune cell populations within the lamina propria, the epithelial layer was removed prior to labeling with a cocktail consisting of anti-mouse CD3, CD4, CD8, CD19, F4/80 and NK1.1 antibodies to investigate total T cell, T helper cell, cytotoxic T cell, B cell, mature macrophage, and natural killer cell populations, respectively (Figure 10A). $F4/80^+$ macrophages decreased 32% and 30% in the proximal and distal intestine, respectively, of female mice, and 29% in the proximal intestine of male mice, suggesting macrophage reductions in the lamina propria. There was also a 65% decrease in $NK1.1^+$ natural killer cells in male mice and a 68% decrease in $CD4^+$ lymphocytes in female mice in the proximal intestine, with a 28% decrease in $CD3^+$ T cells in male mice, and a 45% decrease in $CD19^+$ B cells in female mice in the distal intestine. These results are consistent with TCDD-elicited depletion of several populations of immune cells in the lamina propria, including natural killer cells, T helper cells, total T cells, and B cells.

A second antibody cocktail consisting of anti-mouse CD11b, CD11c, and CD103 antibodies examined three DC sub-populations including (i) $CD11c^+$ $CD11b^+$ $CD103^-$ DCs (herein referred to as $CD11b^+$ DCs), (ii) $CD11c^+$ $CD11b^-$ $CD103^+$ DCs (herein referred to as $CD103^+$ DCs), and (iii) $CD11c^+$ $CD11b^+$ $CD103^+$ DCs (herein referred to as double positive DCs) (Figure

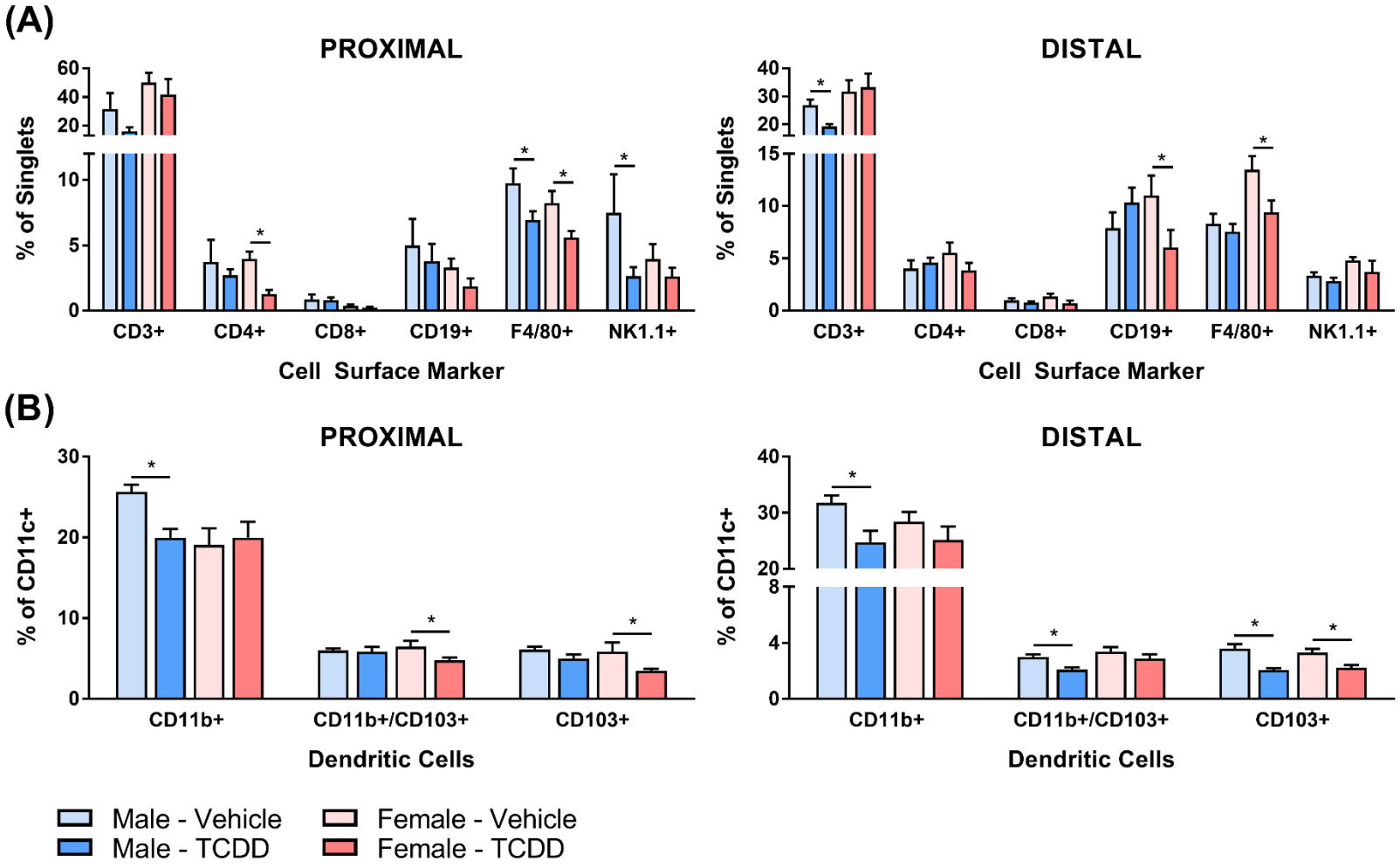

FIGURE 10. EFFECTS OF TCDD ON INTESTINAL IMMUNE CELL POPULATIONS

FIGURE 10 (cont'd)

Flow cytometry analysis of TCDD-mediated effects on immune cell populations within the intestinal lamina propria. Female (red) and male (blue) mice were treated by oral gavage with either sesame oil vehicle or 30 µg/kg TCDD every 4 days for 28 days. Single cell suspensions prepared from the lamina propria were labeled with either (A) immune cell panel or (B) dendritic cell sub-population antibodies. Immune cell panel results are expressed as the average percentage of singlets expressing various cell surface receptors ± standard error of the mean (SEM; $N \geq 3$), while dendritic cell sub-populations are expressed as the average percentage of CD11c+ cells co-expressing CD11b and/or CD103 ± SEM ($N \geq 12$). Asterisks (*) indicate a significant difference ($p < 0.05$) compared to vehicle control determined by standard t-test performed using SAS 9.3.

10B). Within the $CD11c^+$ population, $CD11b^+$ DCs decreased 22% in both the proximal and distal intestine of male mice. Furthermore, $CD103^+$ DCs decreased 41% and 32% in the proximal and distal intestine, respectively, of female mice, and decreased 43% in the distal intestine of male mice. In addition, double positive DCs decreased 26% in the proximal intestine of female mice, and 30% in the distal intestine of male mice. Therefore, TCDD-elicited intestinal immune cell population changes appear to exhibit some sex and intestinal region specificity. Collectively, TCDD reduced several immune cell populations consistent with decreased transcript levels of jejunal immune-related genes.

28-day TCDD-mediated liver effects

In order to examine jejunum – liver interactions, differential gene expression in the jejunal epithelium was compared to hepatic RNA-Seq data (GEO accession number GSE62903) from the same study [51] (Figure 11A). Empirical Bayes analysis identified 1172 hepatic DEGs (|fold change| ≥ 2.0, P1(*t*) ≥ 0.8) across one or more doses. Comparison with the 439 jejunal DEGs from the current study identified 53 DEGs common to both the jejunum and the liver, while 386 and 1119 DEGs were unique to the jejunum and liver, respectively. DAVID analysis of the common DEGs identified two enriched clusters functionally associated with antigen processing and presentation via MHC class II (ES = 3.99) and oxidative and reductive processes (ES = 2.75). Manual curation also revealed that several common DEGs were associated with lipid metabolism. Expression of common DEGs associated with these functions was compared across the two tissues (Figure 11B), revealing both consistent and divergent regulation. As expected, classical AhR battery genes *Cyp1a1* and *Cyp1a2* were induced in both tissues. Most lipid metabolism DEGs were also induced in both tissues. In contrast, fatty acid synthase (*Fasn*) and *Gpcpd1* were induced in the jejunum but repressed in the liver, indicating TCDD-mediated disruption of fatty acid synthesis and choline metabolism may involve tissue-specific responses. Notably, transcript levels of immune-related common DEGs including MHC class II genes (*H2-Aa*, *H2-Ab1*, *H2-DMb1*

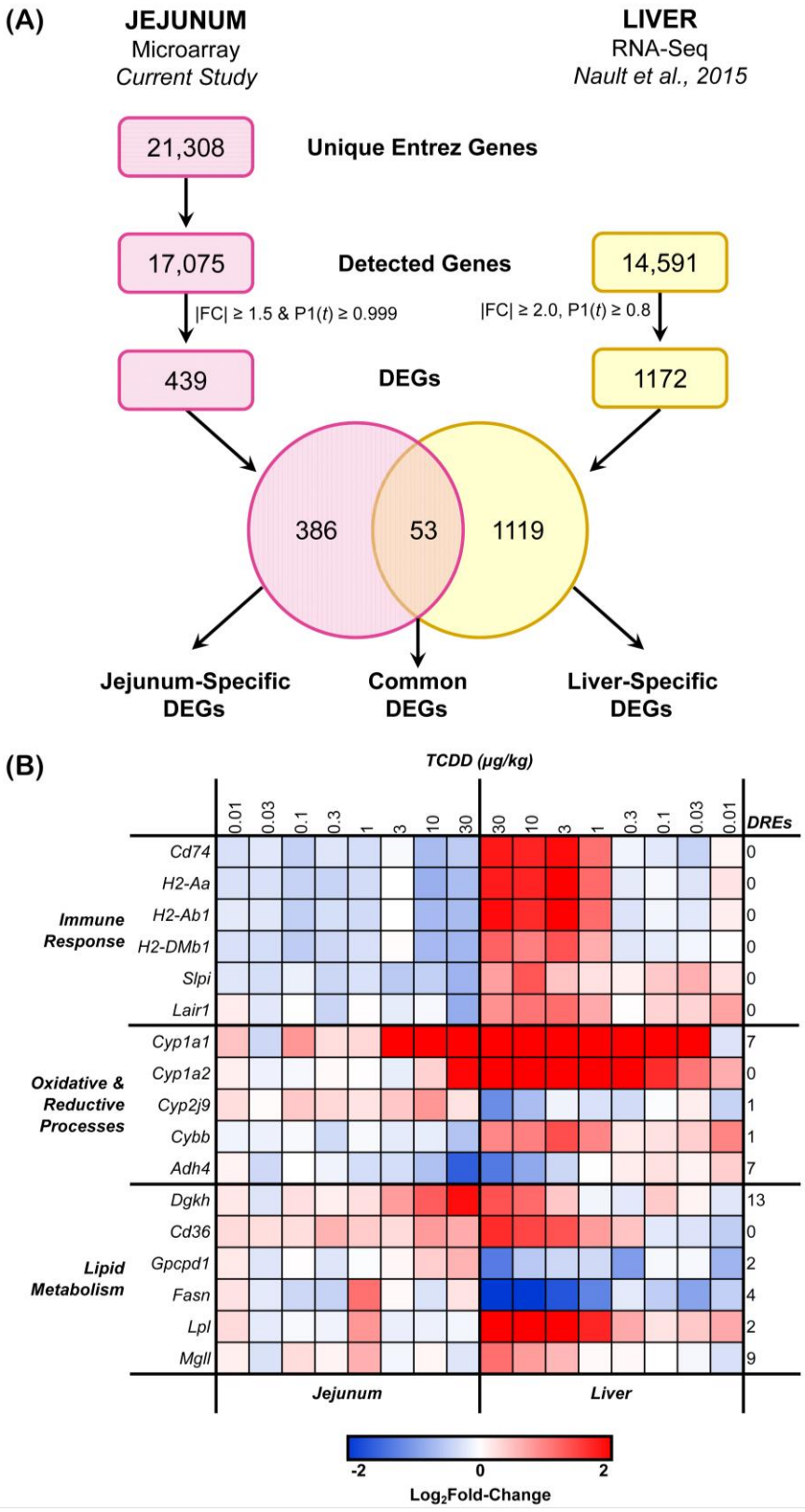

FIGURE 11. COMPARISON OF HEPATIC VS JEJUNAL GENE EXPRESSION

FIGURE 11 (cont'd)

Female C57BL/6 mice were treated by oral gavage with sesame oil vehicle or 0.01 – 30 µg/kg TCDD every 4 days for 28 days. (A) Venn diagram of jejunal and hepatic differentially expressed genes (DEGs), identifying 53 DEGs common to both tissues. (B) Heat map of common DEGs associated with immune response, oxidative and reductive processes, and lipid metabolism. The number of pDREs (MS ≥ 0.8473) is indicated in the last column on the right.

and *Cd74*) were exclusively decreased in the jejunum but increased in the liver. All 6 immune-related common DEGs lack pDREs, further supporting the notion that these changes in transcript levels were attributed to changes in immune cell populations.

Female mouse livers exhibited dose-dependent changes in fat accumulation and immune cell infiltration (Figure 12). H&E staining revealed minimal centriacinar micro-vesicular vacuolization at 3 µg/kg TCDD, characteristic of hepatic steatosis, while 10 µg/kg TCDD elicited mild to moderate micro-vesicular vacuolization and mild inflammation, indicating progression to steatohepatitis. At 30 µg/kg TCDD, substantial micro- and macro-vesicular vacuolization was observed in the centriacinar, mid-zonal, and periportal regions, accompanied by moderate inflammation and perivenular collagen deposition indicative of modest fibrosis.

ORO staining identified neutral lipid accumulation at 3, 10, and 30 µg/kg TCDD. QuHAnT analysis of digital ORO images confirmed dose-dependent lipid accumulation, with increases of 21- and 67-fold at 10 and 30 µg/kg, respectively. Although vacuole size exhibited a normal distribution, QuHAnT distinguished lipid vacuole size based on published criteria [32] with micro (< 176 μm^2) vacuole counts increasing 11- and 18-fold at 10 and 30 µg/kg TCDD, respectively, and macro (≥ 176 μm^2) vacuole counts increasing 580- and 5092-fold at 10 and 30 µg/kg TCDD, respectively, confirming a transition from micro- to macro-vesicular steatosis, consistent with H&E staining. F4/80 labeling indicated inflammatory foci consisted primarily of mature macrophages. Ym1 labeling increased 5.0-, 2.9- (not significant), and 3.0-fold at 3, 10, and 30 µg/kg, respectively, suggesting a polarized M2 macrophage phenotype. Increases in both F4/80 and Ym1 labeling suggest hepatic macrophage infiltration. In contrast, MBP labeling was not affected by TCDD, suggesting eosinophils are not a component of TCDD-mediated hepatic immune cell infiltration (data not shown).

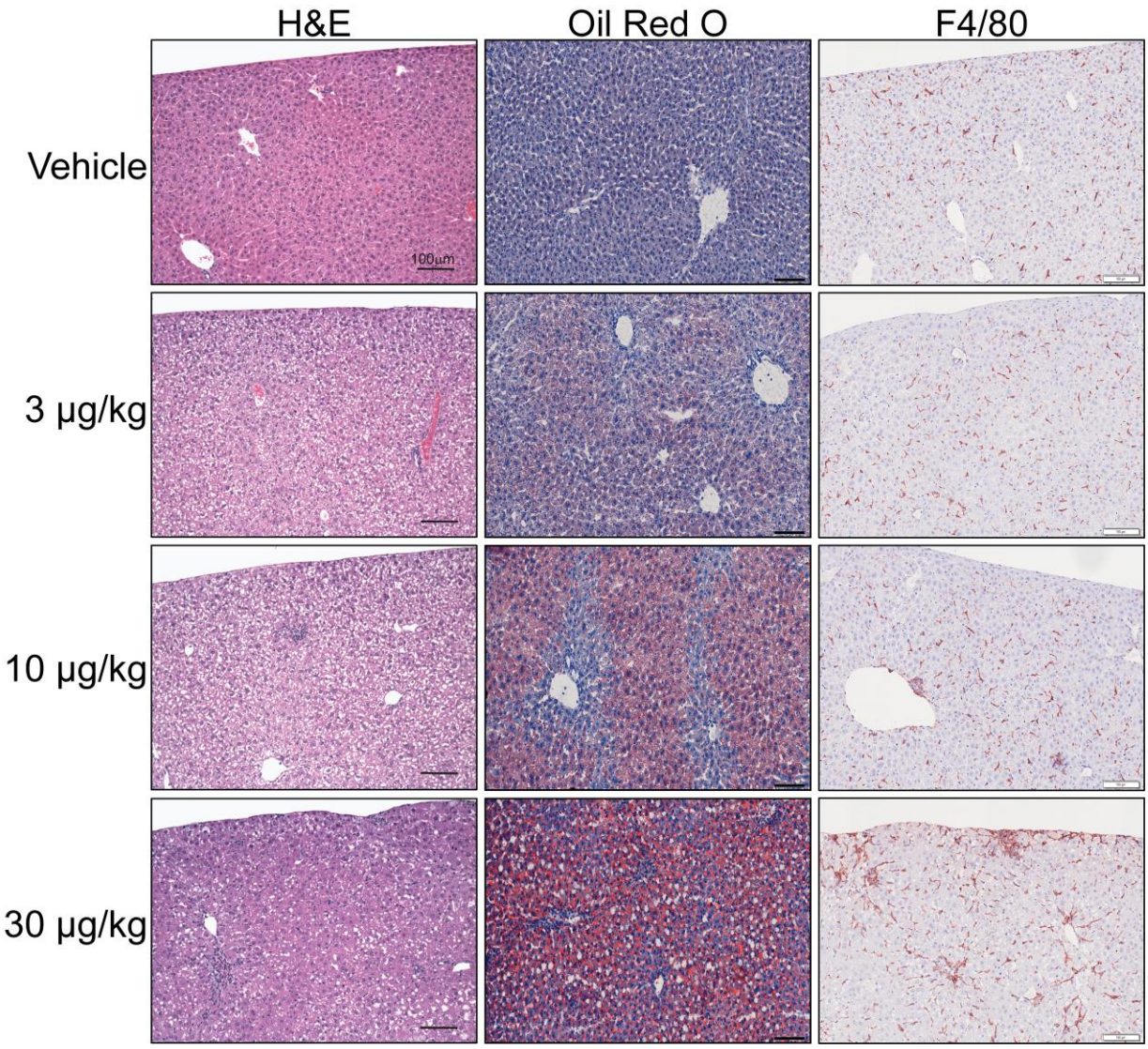

FIGURE 12. TCDD-ELICITED HEPATIC LESIONS IN FEMALE MICE

Representative images of hepatic lesions in female mice treated by oral gavage with sesame oil vehicle or 3 – 30 µg/kg TCDD every 4 days for 28 days. Livers were stained with hematoxylin and eosin (H&E) (left), Oil Red O (center), or anti-mouse F4/80 antibody (right). Scale bar represents 100 µm.

DISCUSSION

Hepatic homeostasis is directly affected by the composition of intestinal contents as the liver receives blood from the intestine through the portal vein, and therefore the gut – liver axis affects NAFLD development [52, 53]. Previous studies have shown that dietary fat rather than *de novo* synthesis is a primary lipid source for TCDD-elicited hepatic steatosis [22, 47]. We examined jejunal epithelial gene expression changes in order to investigate intestine – liver interactions in TCDD-elicited steatohepatitis, given the jejunum is the intestinal segment predominantly responsible for dietary lipid absorption [25]. Jejunal differential gene expression was associated with lipolysis, fatty acid/cholesterol absorption and transport, the Kennedy pathway, and retinol metabolism, suggesting TCDD-elicited alterations in lipid processing which are consistent with hepatic fat accumulation. Furthermore, transcript levels of several MHC class II genes exclusively expressed by professional antigen-presenting cells were decreased, coincident with macrophage and DC decreases in the intestinal lamina propria. The reciprocal increases in hepatic MHC class II transcript levels and infiltration of macrophages led us to speculate that immune cells may be migrating from the intestine to the liver.

Dose-dependent TCDD-mediated differential expression of lipid metabolism and transport genes in the jejunal epithelium is consistent with increased hepatic lipid accumulation. Genes involved in digestion of dietary fat and protein, including lipases (e.g. *Pnlip*, *Clps*, *Mgll*) and proteases (e.g. *Cpa2*, *Prss2*, *Cpb1*, *Ctrc*, *Cela1*), respectively, were among the most induced genes, suggesting that TCDD enhances dietary nutrient digestion. *Cd36* induction and cystic fibrosis transmembrane conductance regulator (*Cftr*) repression may promote fatty acid absorption, packaging, and clearance of intestinal lipoproteins as enterocytes from CD36-null mice exhibit reduced fatty acid uptake and chylomicron secretion [54, 55], while Caco-2/15 cells deficient in CFTR exhibit enhanced fatty acid uptake and transport [56, 57]. Furthermore, TCDD may alter the fatty acid composition of intestinal lipids through induction of stearoyl-CoA desaturase 2 (*Scd2*), consistent with an increase in the desaturation index (18:1n9/18:0) in TCDD-

treated mice [47]. Repression of cholesterol uptake (*Npc1l1*, *Abca1*) and trafficking (*Stard4*) genes suggests impaired absorption of dietary cholesterol, congruous with decreased serum cholesterol levels. Previous studies report increased cholesterol esters in the liver of TCDD-treated mice, likely due to increased hepatic uptake of high density lipoprotein (HDL) and low density lipoprotein (LDL) remnants, rather than *de novo* cholesterol biosynthesis [19, 47, 58], further depleting serum cholesterol levels.

Down-regulation of the PC branch of the Kennedy pathway suggests TCDD represses *de novo* synthesis using choline and DAG. Since PC is the predominant phospholipid in the chylomicron envelope, insufficient dietary or biliary PC reduces TAG clearance from the intestinal mucosa resulting in dietary fat retention in jejunal enterocytes [59]. However, jejunal epithelium H&E analysis did not reveal vacuolization within the enterocytes, suggesting dietary fat clearance was not affected by TCDD. Alternatively, negative feedback on the Kennedy pathway may have been initiated in response to sufficient PC stores from alternative sources such as phosphatidylethanolamine (PE) methylation.

TCDD is reported to elicit dose-dependent decreases in hepatic vitamin A levels. The induction of *Cd36* and *Scarb1*, the transporters primarily responsible for provitamin A carotenoid uptake [50], suggests hepatic vitamin A depletion is not due to insufficient dietary β-carotene absorption [60, 61]. Alternatively, retinol dehydrogenase (*Rdh7* and *Rdh16*) and alcohol dehydrogenase (*Adh4*) repression may decrease retinal to retinol conversion and thus retinyl ester synthesis, potentially impairing chylomicron packaging and hepatic delivery. Interestingly, previous studies have shown that CYP1B1 is involved in the oxidation of retinol to retinal [62], and thus TCDD-mediated induction of *Cyp1b1* (1.4-fold) may further impede the synthesis of retinyl esters. Furthermore, hepatic vitamin A deficiency in C57BL/6JF1 mice leads to fatty liver, likely as a result of PPARα-mediated repression of fatty acid beta oxidation [63]. Therefore, decreased hepatic vitamin A levels may also be a contributing factor in TCDD-mediated hepatic steatosis.

The intestinal lamina propria is well equipped with mononuclear phagocytes, including both DCs and macrophages, which are responsible for sampling potentially harmful antigens in the intestinal lumen. All subsets of intestinal lamina propria DCs are constitutively migratory in nature [64]. In contrast, intestinal resident macrophages have historically been reported to be non-migratory, although CX3CR1^{high} macrophages are capable of trafficking toward mesenteric lymph nodes under conditions of dysbiosis [65]. Interestingly, AhR activation modifies the gut microbiota of mice [66], potentially creating a dysbiotic state inducing migratory behavior in macrophages.

We demonstrate that TCDD decreases macrophages and DC subtypes in the intestinal lamina propria with concurrent increases in hepatic macrophages. Reciprocal changes in these immune cell populations may be driven by several underlying mechanisms. First, intestinal macrophages and DCs themselves may migrate from the intestine to the liver. The liver is continuously supplied with blood from the intestine through the portal vein, providing a direct link between the two tissues. During conditions of intestinal inflammation such as inflammatory bowel disease (IBD), blood monocytes are known to migrate from systemic circulation into the lamina propria [67], suggesting emigration of immune cells from the lamina propria into the portal vein is possible. Second, macrophages and DCs from the lamina propria may migrate into mesenteric lymph nodes following exposure to a foreign antigen such as lipopolysaccharide (LPS), which would initiate differentiation of naïve T cells into regulatory or effector cells. Activated T cells secrete various inflammatory chemokines that can be transferred to the liver and initiate macrophage infiltration. Pathogenic CD4 Th1 T cell clones are reported to recruit and activate macrophages through CCL1, CCL3 and CCL5 secretion [68]. Regardless of the mechanism, several chemokines and chemokine receptors involved in macrophage recruitment, including *Ccr1, Ccr5, Ccl5* and *Cx3cr1*, were induced 2.1- to 4.8-fold in the liver, suggesting involvement of chemokine signaling in hepatic macrophage infiltration. Other studies have also reported a link between the intestinal immune system and hepatic immune cell infiltration. For example, intestinal

inflammation is associated with infiltration of mononuclear cells into the liver, accompanied by emergence of macrophages and classical DCs, which predispose the liver to inflammation [69].

Collectively, we demonstrate that TCDD elicits transcriptome and immune cell population changes in the jejunum that would be expected to promote hepatic lipid accumulation, macrophage infiltration, and the progression to steatohepatitis. Although levels of TCDD and related dioxin-like compounds in the environment are decreasing, the accumulative exposure to all potential AhR ligands, such as polyaromatic hydrocarbons, flame retardants, and natural products, may be increasing and inducing conditions favorable to MetS and NAFLD development [70-72]. Furthermore, it is likely that TCDD-elicited changes in other intestinal segments also contribute to the development of hepatic steatosis and its progression to steatohepatitis.

REFERENCES

REFERENCES

1. Vanni, E., E. Bugianesi, A. Kotronen, S. De Minicis, H. Yki-Jarvinen, and G. Svegliati-Baroni, *From the metabolic syndrome to NAFLD or vice versa?* Dig Liver Dis, 2010. 42(5): p. 320-30.

2. Paschos, P. and K. Paletas, *Non alcoholic fatty liver disease and metabolic syndrome.* Hippokratia, 2009. 13(1): p. 9-19.

3. Ford, E.S., C. Li, and G. Zhao, *Prevalence and correlates of metabolic syndrome based on a harmonious definition among adults in the US.* J Diabetes, 2010. 2(3): p. 180-93.

4. Grundy, S.M., *Metabolic syndrome pandemic.* Arterioscler Thromb Vasc Biol, 2008. 28(4): p. 629-36.

5. Alberti, K.G., R.H. Eckel, S.M. Grundy, P.Z. Zimmet, J.I. Cleeman, K.A. Donato, J.C. Fruchart, W.P. James, C.M. Loria, and S.C. Smith, Jr., *Harmonizing the metabolic syndrome: a joint interim statement of the International Diabetes Federation Task Force on Epidemiology and Prevention; National Heart, Lung, and Blood Institute; American Heart Association; World Heart Federation; International Atherosclerosis Society; and International Association for the Study of Obesity.* Circulation, 2009. 120(16): p. 1640-5.

6. Olufadi, R. and C.D. Byrne, *Clinical and laboratory diagnosis of the metabolic syndrome.* J Clin Pathol, 2008. 61(6): p. 697-706.

7. Trauner, M., M. Arrese, and M. Wagner, *Fatty liver and lipotoxicity.* Biochim Biophys Acta, 2010. 1801(3): p. 299-310.

8. Casals-Casas, C. and B. Desvergne, *Endocrine disruptors: from endocrine to metabolic disruption.* Annu Rev Physiol, 2011. 73: p. 135-62.

9. Chen, J.Q., T.R. Brown, and J. Russo, *Regulation of energy metabolism pathways by estrogens and estrogenic chemicals and potential implications in obesity associated with increased exposure to endocrine disruptors.* Biochim Biophys Acta, 2009. 1793(7): p. 1128-43.

10. Cimafranca, M.A., P.R. Hanlon, and C.R. Jefcoate, *TCDD administration after the pro-adipogenic differentiation stimulus inhibits PPARgamma through a MEK-dependent process but less effectively suppresses adipogenesis.* Toxicol Appl Pharmacol, 2004. 196(1): p. 156-68.

11. Grun, F. and B. Blumberg, *Endocrine disrupters as obesogens.* Mol Cell Endocrinol, 2009. 304(1-2): p. 19-29.

12. Taylor, K.W., R.F. Novak, H.A. Anderson, L.S. Birnbaum, C. Blystone, M. Devito, D. Jacobs, J. Kohrle, D.H. Lee, L. Rylander, A. Rignell-Hydbom, R. Tornero-Velez, M.E. Turyk, A.L. Boyles, K.A. Thayer, and L. Lind, *Evaluation of the Association between Persistent Organic Pollutants (POPs) and Diabetes in Epidemiological Studies: A National Toxicology Program Workshop Review.* Environ Health Perspect, 2013. 121(7): p. 774-83.

13. Denison, M.S., A.A. Soshilov, G. He, D.E. DeGroot, and B. Zhao, *Exactly the same but different: promiscuity and diversity in the molecular mechanisms of action of the aryl hydrocarbon (dioxin) receptor.* Toxicol Sci, 2011. 124(1): p. 1-22.

14. Denison, M.S., A. Pandini, S.R. Nagy, E.P. Baldwin, and L. Bonati, *Ligand binding and activation of the Ah receptor.* Chem Biol Interact, 2002. 141(1-2): p. 3-24.

15. Hankinson, O., *The aryl hydrocarbon receptor complex.* Annu Rev Pharmacol Toxicol, 1995. 35: p. 307-40.

16. Beischlag, T.V., J. Luis Morales, B.D. Hollingshead, and G.H. Perdew, *The aryl hydrocarbon receptor complex and the control of gene expression.* Crit Rev Eukaryot Gene Expr, 2008. 18(3): p. 207-50.

17. Dere, E., R. Lo, T. Celius, J. Matthews, and T.R. Zacharewski, *Integration of genome-wide computation DRE search, AhR ChIP-chip and gene expression analyses of TCDD-elicited responses in the mouse liver.* BMC Genomics, 2011. 12: p. 365.

18. Huang, G. and C.J. Elferink, *A novel nonconsensus xenobiotic response element capable of mediating aryl hydrocarbon receptor-dependent gene expression.* Mol Pharmacol, 2012. 81(3): p. 338-47.

19. Boverhof, D.R., L.D. Burgoon, C. Tashiro, B. Chittim, J.R. Harkema, D.B. Jump, and T.R. Zacharewski, *Temporal and dose-dependent hepatic gene expression patterns in mice provide new insights into TCDD-Mediated hepatotoxicity.* Toxicol Sci, 2005. 85(2): p. 1048-63.

20. Kopec, A.K., L.D. Burgoon, D. Ibrahim-Aibo, B.D. Mets, C. Tashiro, D. Potter, B. Sharratt, J.R. Harkema, and T.R. Zacharewski, *PCB153-elicited hepatic responses in the immature, ovariectomized C57BL/6 mice: comparative toxicogenomic effects of dioxin and non-dioxin-like ligands.* Toxicol Appl Pharmacol, 2010. 243(3): p. 359-71.

21. Pierre, S., A. Chevallier, F. Teixeira-Clerc, A. Ambolet-Camoit, L.C. Bui, A.S. Bats, J.C. Fournet, P. Fernandez-Salguero, M. Aggerbeck, S. Lotersztajn, R. Barouki, and X. Coumoul, *Aryl hydrocarbon receptor-dependent induction of liver fibrosis by dioxin.* Toxicol Sci, 2014. 137(1): p. 114-24.

22. Angrish, M., B. Mets, A. Jones, and T. Zacharewski, *Dietary Fat is a Lipid Source in 2,3,7,8-Tetrachlorodibenzo-rho-dioxin (TCDD)-Elicited Hepatic Steatosis in C57BL/6 Mice.* Toxicol Sci, 2012.

23. Forgacs, A.L., M.N. Kent, M.K. Makley, B. Mets, N. DelRaso, G.L. Jahns, L.D. Burgoon, T.R. Zacharewski, and N.V. Reo, *Comparative metabolomic and genomic analyses of TCDD-elicited metabolic disruption in mouse and rat liver.* Toxicol Sci, 2012. 125(1): p. 41-55.

24. Lee, J.H., T. Wada, M. Febbraio, J. He, T. Matsubara, M.J. Lee, F.J. Gonzalez, and W. Xie, *A novel role for the dioxin receptor in fatty acid metabolism and hepatic steatosis.* Gastroenterology, 2010. 139(2): p. 653-63.

25. Booth, C.C., A.E. Read, and E. Jones, *Studies on the site of fat absorption: 1. The sites of absorption of increasing doses of I-labelled triolein in the rat.* Gut, 1961. 2(1): p. 23-31.

26. Hamilton, J.A., *Fatty acid transport: difficult or easy?* J Lipid Res, 1998. 39(3): p. 467-81.

27. Doe, W.F., *The intestinal immune system.* Gut, 1989. 30(12): p. 1679-85.

28. Tomasello, E. and S. Bedoui, *Intestinal innate immune cells in gut homeostasis and immunosurveillance.* Immunol Cell Biol, 2013. 91(3): p. 201-3.

29. Geem, D., O. Medina-Contreras, W. Kim, C.S. Huang, and T.L. Denning, *Isolation and characterization of dendritic cells and macrophages from the mouse intestine.* J Vis Exp, 2012(63): p. e4040.

30. Kopec, A.K., M.L. D'Souza, B.D. Mets, L.D. Burgoon, S.E. Reese, K.J. Archer, D. Potter, C. Tashiro, B. Sharratt, J.R. Harkema, and T.R. Zacharewski, *Non-additive hepatic gene expression elicited by 2,3,7,8-tetrachlorodibenzo-p-dioxin (TCDD) and 2,2',4,4',5,5'-hexachlorobiphenyl (PCB153) co-treatment in C57BL/6 mice.* Toxicol Appl Pharmacol, 2011. 256(2): p. 154-67.

31. Nault, R., D. Colbry, C. Brandenberger, J.R. Harkema, and T.R. Zacharewski, *Development of a computational high-throughput tool for the quantitative examination of dose-dependent histological features.* Toxicol Pathol, 2015. 43(3): p. 366-75.

32. Zaitoun, A.M., H. Al Mardini, S. Awad, S. Ukabam, S. Makadisi, and C.O. Record, *Quantitative assessment of fibrosis and steatosis in liver biopsies from patients with chronic hepatitis C.* J Clin Pathol, 2001. 54(6): p. 461-5.

33. Burgoon, L.D., J.E. Eckel-Passow, C. Gennings, D.R. Boverhof, J.W. Burt, C.J. Fong, and T.R. Zacharewski, *Protocols for the assurance of microarray data quality and process control.* Nucleic Acids Res, 2005. 33(19): p. e172.

34. Burgoon, L.D. and T.R. Zacharewski, *Automated quantitative dose-response modeling and point of departure determination for large toxicogenomic and high-throughput screening data sets.* Toxicol Sci, 2008. 104(2): p. 412-8.

35. Eckel, J.E., C. Gennings, T.M. Therneau, L.D. Burgoon, D.R. Boverhof, and T.R. Zacharewski, *Normalization of two-channel microarray experiments: a semiparametric approach.* Bioinformatics, 2005. 21(7): p. 1078-83.

36. Eckel, J.E., C. Gennings, V.M. Chinchilli, L.D. Burgoon, and T.R. Zacharewski, *Empirical bayes gene screening tool for time-course or dose-response microarray data.* J Biopharm Stat, 2004. 14(3): p. 647-70.

37. Yang, L., B.C. Allen, and R.S. Thomas, *BMDExpress: a software tool for the benchmark dose analyses of genomic data.* BMC Genomics, 2007. 8: p. 387.

38. Bhat, V.S., S.D. Hester, S. Nesnow, and D.A. Eastmond, *Concordance of transcriptional and apical benchmark dose levels for conazole-induced liver effects in mice.* Toxicol Sci, 2013. 136(1): p. 205-15.

39. Dere, E., A.L. Forgacs, T.R. Zacharewski, and L.D. Burgoon, *Genome-wide computational analysis of dioxin response element location and distribution in the human, mouse, and rat genomes.* Chem Res Toxicol, 2011. 24(4): p. 494-504.

40. Kopec, A.K., D.R. Boverhof, R. Nault, J.R. Harkema, C. Tashiro, D. Potter, B. Sharratt, B. Chittim, and T.R. Zacharewski, *Toxicogenomic evaluation of long-term hepatic effects of TCDD in immature, ovariectomized C57BL/6 mice.* Toxicol Sci, 2013. 135(2): p. 465-75.

41. Birnbaum, L.S., *Distribution and excretion of 2,3,7,8-tetrachlorodibenzo-p-dioxin in congenic strains of mice which differ at the Ah locus.* Drug Metab Dispos, 1986. 14(1): p. 34-40.

42. Gasiewicz, T.A., L.E. Geiger, G. Rucci, and R.A. Neal, *Distribution, excretion, and metabolism of 2,3,7,8-tetrachlorodibenzo-p-dioxin in C57BL/6J, DBA/2J, and B6D2F1/J mice.* Drug Metab Dispos, 1983. 11(5): p. 397-403.

43. Sorg, O., M. Zennegg, P. Schmid, R. Fedosyuk, R. Valikhnovskyi, O. Gaide, V. Kniazevych, and J.H. Saurat, *2,3,7,8-tetrachlorodibenzo-p-dioxin (TCDD) poisoning in Victor Yushchenko: identification and measurement of TCDD metabolites.* Lancet, 2009. 374(9696): p. 1179-85.

44. Michalek, J.E., J.L. Pirkle, S.P. Caudill, R.C. Tripathi, D.G. Patterson, Jr., and L.L. Needham, *Pharmacokinetics of TCDD in veterans of Operation Ranch Hand: 10-year follow-up.* J Toxicol Environ Health, 1996. 47(3): p. 209-20.

45. Pirkle, J.L., W.H. Wolfe, D.G. Patterson, L.L. Needham, J.E. Michalek, J.C. Miner, M.R. Peterson, and D.L. Phillips, *Estimates of the half-life of 2,3,7,8-tetrachlorodibenzo-p-dioxin in Vietnam Veterans of Operation Ranch Hand.* J Toxicol Environ Health, 1989. 27(2): p. 165-71.

46. Wolfe, W.H., J.E. Michalek, J.C. Miner, J.L. Pirkle, S.P. Caudill, D.G. Patterson, Jr., and L.L. Needham, *Determinants of TCDD half-life in veterans of operation ranch hand.* J Toxicol Environ Health, 1994. 41(4): p. 481-8.

47. Angrish, M.M., C.Y. Dominici, and T.R. Zacharewski, *TCDD-elicited effects on liver, serum, and adipose lipid composition in C57BL/6 mice.* Toxicol Sci, 2013. 131(1): p. 108-15.

48. Kopec, A.K., L.D. Burgoon, D. Ibrahim-Aibo, A.R. Burg, A.W. Lee, C. Tashiro, D. Potter, B. Sharratt, J.R. Harkema, J.C. Rowlands, R.A. Budinsky, and T.R. Zacharewski, *Automated dose-response analysis and comparative toxicogenomic evaluation of the hepatic effects elicited by TCDD, TCDF, and PCB126 in C57BL/6 mice.* Toxicol Sci, 2010. 118(1): p. 286-97.

49. Cohn, J.S., A. Kamili, E. Wat, R.W. Chung, and S. Tandy, *Dietary phospholipids and intestinal cholesterol absorption.* Nutrients, 2010. 2(2): p. 116-27.

50. Reboul, E., *Absorption of vitamin A and carotenoids by the enterocyte: focus on transport proteins.* Nutrients, 2013. 5(9): p. 3563-81.

51. Nault, R., K.A. Fader, and T. Zacharewski, *RNA-Seq versus oligonucleotide array assessment of dose-dependent TCDD-elicited hepatic gene expression in mice.* BMC Genomics, 2015. 16(1): p. 373.

52. Konrad, D. and S. Wueest, *The Gut-Adipose-Liver Axis in the Metabolic Syndrome.* Physiology (Bethesda), 2014. 29(5): p. 304-313.

53. Fukui, H., *Gut-liver axis in liver cirrhosis: How to manage leaky gut and endotoxemia.* World J Hepatol, 2015. 7(3): p. 425-42.

54. Nassir, F., B. Wilson, X. Han, R.W. Gross, and N.A. Abumrad, *CD36 is important for fatty acid and cholesterol uptake by the proximal but not distal intestine.* J Biol Chem, 2007. 282(27): p. 19493-501.

55. Drover, V.A., M. Ajmal, F. Nassir, N.O. Davidson, A.M. Nauli, D. Sahoo, P. Tso, and N.A. Abumrad, *CD36 deficiency impairs intestinal lipid secretion and clearance of chylomicrons from the blood.* J Clin Invest, 2005. 115(5): p. 1290-7.

56. Mailhot, G., R. Rabasa-Lhoret, A. Moreau, Y. Berthiaume, and E. Levy, *CFTR depletion results in changes in fatty acid composition and promotes lipogenesis in intestinal Caco 2/15 cells.* PLoS One, 2010. 5(5): p. e10446.

57. Mailhot, G., Z. Ravid, S. Barchi, A. Moreau, R. Rabasa-Lhoret, and E. Levy, *CFTR knockdown stimulates lipid synthesis and transport in intestinal Caco-2/15 cells.* Am J Physiol Gastrointest Liver Physiol, 2009. 297(6): p. G1239-49.

58. Tanos, R., R.D. Patel, I.A. Murray, P.B. Smith, A.D. Patterson, and G.H. Perdew, *Aryl hydrocarbon receptor regulates the cholesterol biosynthetic pathway in a dioxin response element-independent manner.* Hepatology, 2012. 55(6): p. 1994-2004.

59. O'Doherty, P.J., G. Kakis, and A. Kuksis, *Role of luminal lecithin in intestinal fat absorption.* Lipids, 1973. 8(5): p. 249-55.

60. Fletcher, N., A. Hanberg, and H. Hakansson, *Hepatic vitamin a depletion is a sensitive marker of 2,3,7,8-tetrachlorodibenzo-p-dioxin (TCDD) exposure in four rodent species.* Toxicol Sci, 2001. 62(1): p. 166-75.

61. Hakansson, H., L. Johansson, E. Manzoor, and U.G. Ahlborg, *Effects of 2,3,7,8-tetrachlorodibenzo-p-dioxin (TCDD) on the vitamin A status of Hartley guinea pigs, Sprague-Dawley rats, C57Bl/6 mice, DBA/2 mice, and Golden Syrian hamsters.* J Nutr Sci Vitaminol (Tokyo), 1991. 37(2): p. 117-38.

62. Choudhary, D., I. Jansson, I. Stoilov, M. Sarfarazi, and J.B. Schenkman, *Metabolism of retinoids and arachidonic acid by human and mouse cytochrome P450 1b1.* Drug Metab Dispos, 2004. 32(8): p. 840-7.

63. Kang, H.W., G.R. Bhimidi, D.P. Odom, P.J. Brun, M.L. Fernandez, and M.M. McGrane, *Altered lipid catabolism in the vitamin A deficient liver.* Mol Cell Endocrinol, 2007. 271(1-2): p. 18-27.

64. Cerovic, V., S.A. Houston, C.L. Scott, A. Aumeunier, U. Yrlid, A.M. Mowat, and S.W. Milling, *Intestinal CD103(-) dendritic cells migrate in lymph and prime effector T cells.* Mucosal Immunol, 2013. 6(1): p. 104-13.

65. Diehl, G.E., R.S. Longman, J.X. Zhang, B. Breart, C. Galan, A. Cuesta, S.R. Schwab, and D.R. Littman, *Microbiota restricts trafficking of bacteria to mesenteric lymph nodes by CX(3)CR1(hi) cells.* Nature, 2013. 494(7435): p. 116-20.

66. Zhang, L., R.G. Nichols, J. Correll, I.A. Murray, N. Tanaka, P.B. Smith, T.D. Hubbard, A. Sebastian, I. Albert, E. Hatzakis, F.J. Gonzalez, G.H. Perdew, and A.D. Patterson, *Persistent Organic Pollutants Modify Gut Microbiota-Host Metabolic Homeostasis in Mice Through Aryl Hydrocarbon Receptor Activation.* Environ Health Perspect, 2015. 123(7): p. 679-88.

67. Grimm, M.C., W.E. Pullman, G.M. Bennett, P.J. Sullivan, P. Pavli, and W.F. Doe, *Direct evidence of monocyte recruitment to inflammatory bowel disease mucosa.* J Gastroenterol Hepatol, 1995. 10(4): p. 387-95.

68. Cantor, J. and K. Haskins, *Recruitment and activation of macrophages by pathogenic CD4 T cells in type 1 diabetes: evidence for involvement of CCR8 and CCL1.* J Immunol, 2007. 179(9): p. 5760-7.

69. Mikami, Y., S. Mizuno, N. Nakamoto, A. Hayashi, T. Sujino, T. Sato, N. Kamada, K. Matsuoka, T. Hisamatsu, H. Ebinuma, T. Hibi, A. Yoshimura, and T. Kanai, *Macrophages and dendritic cells emerge in the liver during intestinal inflammation and predispose the liver to inflammation.* PLoS One, 2014. 9(1): p. e84619.

70. Lim, J.S., D.H. Lee, and D.R. Jacobs, Jr., *Association of brominated flame retardants with diabetes and metabolic syndrome in the U.S. population, 2003-2004.* Diabetes Care, 2008. 31(9): p. 1802-7.

71. Wiseman, S.B., Y. Wan, H. Chang, X. Zhang, M. Hecker, P.D. Jones, and J.P. Giesy, *Polybrominated diphenyl ethers and their hydroxylated/methoxylated analogs: environmental sources, metabolic relationships, and relative toxicities.* Mar Pollut Bull, 2011. 63(5-12): p. 179-88.

72. Denison, M.S. and S.R. Nagy, *Activation of the aryl hydrocarbon receptor by structurally diverse exogenous and endogenous chemicals.* Annu Rev Pharmacol Toxicol, 2003. 43: p. 309-34.

CHAPTER 4: 2,3,7,8-TETRACHLORODIBENZO-*P*-DIOXIN (TCDD)-ELICITED EFFECTS ON BILE ACID HOMEOSTASIS: ALTERATIONS IN BIOSYNTHESIS, ENTEROHEPATIC CIRCULATION, AND MICROBIAL METABOLISM

Fader, K.A., R. Nault, C. Zhang, K. Kumagai, J.R. Harkema, and T.R. Zacharewski, *2,3,7,8-Tetrachlorodibenzo-p-dioxin (TCDD)-elicited effects on bile acid homeostasis: Alterations in biosynthesis, enterohepatic circulation, and microbial metabolism.* Sci Rep, 2017. 7(1): p. 5921.

ABSTRACT

2,3,7,8-tetrachlorodibenzo-*p*-dioxin (TCDD) is a persistent environmental contaminant which elicits hepatotoxicity through activation of the aryl hydrocarbon receptor (AhR). Male C57BL/6 mice orally gavaged with TCDD (0.01-30 µg/kg) every 4 days for 28 days exhibited bile duct proliferation and pericholangitis. Untargeted mass spectrometry analysis detected a 4.6-fold increase in total hepatic bile acid levels, despite the coordinated repression of genes involved in cholesterol and primary bile acid biosynthesis including *Cyp7a1*. Specifically, TCDD elicited a >200-fold increase in taurolithocholic acid (TLCA), a potent G protein-coupled bile acid receptor 1 (GPBAR1) agonist associated with bile duct proliferation. Increased levels of microbial bile acid metabolism loci (*bsh, baiCD*) are consistent with accumulation of TLCA and other secondary bile acids. Fecal bile acids decreased 2.8-fold, suggesting enhanced intestinal reabsorption due to induction of ileal transporters (*Slc10a2*, *Slc51a*) and increases in whole gut transit time and intestinal permeability. Moreover, serum bile acids were increased 45.4-fold, consistent with blood-to-hepatocyte transporter repression (*Slco1a1*, *Slc10a1*, *Slco2b1*, *Slco1b2*, *Slco1a4*) and hepatocyte-to-blood transporter induction (*Abcc4*, *Abcc3*). These results suggest that systemic alterations in enterohepatic circulation, as well as host and microbiota bile acid metabolism, favor bile acid accumulation that contributes to AhR-mediated hepatotoxicity.

INTRODUCTION

Metabolic syndrome (MetS) is defined as a collection of cardiometabolic factors including obesity, dyslipidemia, hypertension, and hyperglycemia which increase the risk of developing cardiovascular disease, type II diabetes, and hepatocellular carcinoma [1]. The prevalence of MetS among adults in the United States is ~30%, representing an emerging epidemic of concern as the population ages [2]. In the liver, MetS can manifest as non-alcoholic fatty liver disease (NAFLD) where hepatic steatosis (lipid accumulation) progresses to steatohepatitis (steatosis with inflammation) with fibrosis (collagen deposition) [3]. High fat diet, sedentary behavior, and

various genetic loci are key risk factors for MetS and NAFLD development. However, accumulating evidence suggests that exposure to 2,3,7,8-tetrachlorodibenzo-*p*-dioxin (TCDD) and other environmental contaminants play an underappreciated role [4-6].

TCDD is the prototypical ligand for a structurally diverse group of synthetic chemicals, natural products, and endogenous metabolites that activate the aryl hydrocarbon receptor (AhR) [7]. Ligand binding initiates the dissociation of chaperone proteins, triggering translocation of the cytoplasmic AhR to the nucleus and heterodimerization with the aryl hydrocarbon receptor nuclear translocator (ARNT). In the canonical pathway, the liganded AhR-ARNT complex binds to dioxin response elements (DREs) within the promoter region of target genes, leading to recruitment of transcriptional co-regulators and altered gene expression [8]. However, an increasing number of studies report DRE-independent mechanisms of differential gene expression [9, 10]. AhR-mediated gene expression changes elicit a broad spectrum of toxic responses including wasting, tumor promotion, immunosuppression, dermal lesions, teratogenicity, and hepatotoxicity in a species-, sex-, age-, tissue-, and cell-specific manner [11, 12]. In mice, TCDD-elicits AhR-dependent lipid accumulation, immune cell infiltration, and bile duct proliferation [13-15], which progresses to steatohepatitis with fibrosis following repeated treatment [16, 17]. Beyond AhR activation, the specific target genes and altered biological processes that contribute to TCDD-elicited hepatotoxicity remain poorly understood.

Bile acids, the predominant organic solutes in bile, are synthesized from cholesterol in the liver, stored in the gallbladder, and secreted into the duodenal lumen following consumption of a meal. These amphipathic molecules promote the solubilization and absorption of dietary lipids and lipid-soluble vitamins, and provide an excretion mechanism for excess hepatic cholesterol. Additionally, specific bile acid species are endogenous ligands for a number of receptors including farnesoid X receptor (FXR), G protein-coupled bile acid receptor 1 (GPBAR1), pregnane X receptor (PXR), vitamin D receptor (VDR), liver X receptor α (LXRα), and sphingosine-1-phosphate receptor 2 (S1P2) [18, 19]. Consequently, they serve as important signaling molecules

that regulate not only bile and cholesterol homeostasis, but also glucose and energy metabolism. Moreover, bile acids can elicit hepatocyte and non-parenchymal cell injury by disrupting cell membranes through their detergent action and by contributing to oxidative stress through reactive oxygen species (ROS) generation [20]. Furthermore, they promote inflammation by inducing pro-inflammatory mediators such as cytokines (IL-1β, CSF1), chemokines (CXCL1, CXCL2, CCL2), and adhesion molecules (VCAM-1) [21]. The dysregulation of mitochondrial function, depletion of ATP, and activation of signaling cascades can trigger bile acid-induced necrosis [20]. Therefore, bile acid accumulation and/or disrupted biliary flow (cholestasis) can contribute to hepatotoxicity and impaired liver function, while promoting the development of fibrosis.

Previous studies have reported that TCDD and related AhR ligands increase bile acid levels in serum [22, 23], decrease biliary flow [24], and induce bile duct epithelial cell proliferation [25]. TCDD also alters hepatic expression of genes associated with cholesterol metabolism and bile acid biosynthesis [26], and exacerbates cholestatic liver disease induced by bile duct ligation (BDL) [27]. To further investigate AhR-mediated qualitative and quantitative changes in bile acid profiles, liquid chromatography mass spectrometry (LC-MS) was integrated with hepatic and ileal RNA-Seq analyses, along with complementary histopathological assessments. The effects of TCDD on intestinal permeability and motility, and gut microbiota bile acid metabolism were also examined. Despite the coordinated repression of genes involved in cholesterol and primary bile acid biosynthesis, total bile acid levels increased in the liver and serum, while fecal levels decreased. In particular, TCDD increased levels of hepatic taurolithocholic acid (TLCA), a potent GPBAR1 agonist associated with bile duct proliferation and cholestasis [28, 29]. Overall, TCDD-elicited differential expression of bile acid transporters, increased intestinal permeability, decreased gut motility, and alterations in the gut microbiome suggest disruption of enterohepatic circulation and bile acid metabolism. Collectively, the qualitative and quantitative changes in bile acid homeostasis are consistent with alterations in host and intestinal microbiota metabolism, yielding hepatotoxic species that contribute to the development of steatohepatitis with fibrosis.

MATERIALS & METHODS

Animal handling and treatment

Postnatal day 25 (PND25) male C57BL/6 mice weighing within 10% of each other were obtained from Charles River Laboratories (Kingston, NY) and housed in Innovive Innocages (San Diego, CA) containing ALPHA-dri bedding (Shepherd Specialty Papers, Chicago, IL) in a 23°C environment with 30-40% humidity and a 12-hour light/dark cycle (7am–7pm). Mice were provided Aquavive water (Innovive) and Harlan Teklad 22/5 Rodent Diet 8940 (Madison, WI) *ad libitum*, and were acclimated for 4 days (d) prior to treatment. Beginning on PND28, animals (n=8; co-housed 4 per cage) were orally gavaged with sesame oil vehicle (Sigma-Aldrich, St. Louis, MO), 0.01, 0.03, 0.1, 0.3, 1, 3, 10, or 30 µg/kg TCDD (AccuStandard, New Haven, CT) every 4d for a total of 28d (7 exposures; Figure 13). The doses used compensate for the relatively short study duration compared to lifelong cumulative human exposure from diverse AhR ligands, the bioaccumulative nature of halogenated AhR ligands, and differences in TCDD's metabolism and half-life (humans: 1-11 years [30, 31], mice: 8-12d [32]). TCDD doses between 0.01 and 30 µg/kg result in mouse hepatic tissue levels that span human background serum concentrations reported in the United States, Germany, Spain, and the United Kingdom as well as serum levels in Viktor Yushchenko 4-39 months following intentional poisoning [16]. For the histopathological comparison, female C57BL/6 mice were orally gavaged with sesame oil vehicle or 0.01-30 µg/kg TCDD every 4d for 28d, as previously described [33]. All animal handling procedures were performed with the approval of the Michigan State University (MSU) Institutional Animal Care and Use Committee, in accordance with the relevant ethical guidelines and regulations.

Sample collection

At 25d after the initial dose (PND53), fecal pellets from the previous 24 hours (h) were collected from each cage (4 mice per cage) and stored at -80°C. At 28d after the initial exposure (PND56), mice (fasted for 6h) were weighed and blood was collected from the submandibular

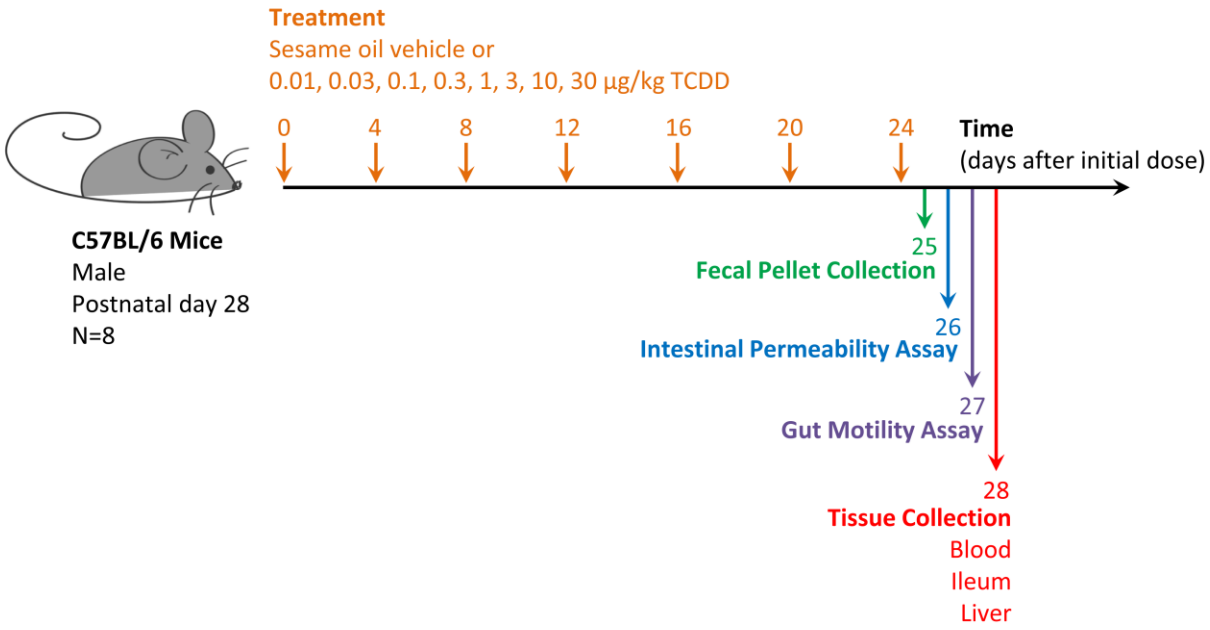

FIGURE 13. CHAPTER 4 STUDY DESIGN

Male C57BL/6 mice (n=8) were orally gavaged with sesame oil vehicle or 0.01-30 µg/kg TCDD every 4 days for 28 days.

vein prior to cervical dislocation. The gallbladder length, width, and depth were measured using a micro-caliper. Its volume was calculated assuming an ellipsoid shape: volume (µL) = length (mm) X width (mm) X depth (mm) X π/6 [34, 35]. The distal ileum (10 cm section extending from the caecum toward the jejunum) was removed, flushed with Ca^{2+}/Mg^{2+}-free phosphate buffered saline (PBS; Sigma), and opened longitudinally. The epithelial lining was scraped into a vial containing TRIzol (Invitrogen, Carlsbad, CA), frozen in liquid nitrogen, and stored at -80°C. Liver, gonadal white adipose tissue (gWAT), and brown adipose tissue were removed, weighed, frozen in liquid nitrogen, and stored at -80°C. Serum alkaline phosphatase (ALP) activity was determined using a commercial kit (Pointe Scientific, Canton, MI).

Histopathology

All processing was performed by the MSU Investigative Histopathology Laboratory (https://humanpathology.natsci.msu.edu/). Formalin-fixed hepatic tissues were vacuum infiltrated with paraffin using a Tissue-Tek VIP 2000 tissue processor (Sakura) and embedded with the Thermo Fisher HistoCentre III Embedding Center (Thermo Fisher, Waltham, Massachusetts). Paraffin blocks were sectioned at 4–5 µm with a Reichert Jung 2030 rotary microtome (Reichert, Depew, New York) and dried for 2–24 h at 56°C to ensure adherence to the slides. For lipid staining, liver sections frozen in O.C.T. compound were sectioned at 6 µm, fixed in 10% NBF for 5 min, rinsed with water, and immersed in 100% propylene glycol for 5 min. Liver sections were stained with hematoxylin and eosin (H&E) for general histological assessment. Lipids were stained using Oil Red O (ORO) as previously described [36]. Macrophages were labeled using a monoclonal anti-mouse F4/80 antibody (1:100 dilution; AbD Serotec, Raleigh, NC). Collagen was stained with 0.1% Picro-Sirius Red (PSR) dye, with Weigert's Hematoxylin nuclear dye. Histological assessment of hepatic tissue from female C57BL/6 mice was performed as previously described [16, 33].

Quantitation of ORO staining was performed using the Quantitative Histological Analysis Tool (QuHAnT) [37]. Briefly, slides were digitized at 20x magnification using an Olympus Virtual Slide System VS110 (Olympus, PA) and images were sampled at 100% coverage using the Visiomorph Microimager (Visiopharm, Denmark). Using ImageJ (http://rsb.info.nih.gov.ij/), optimal hue, saturation, and value (HSV) image segmentation thresholds for feature extraction were determined to be 0 to 50 and 225 to 255 (hue), 125 to 255 (saturation), and 0 to 255 (value), while optimal total tissue feature extraction thresholds were 0 to 255 (hue), 20 to 255 (saturation), and 0 to 255 (value). Volume densities were estimated as the sum of positive hits ($P_{positive}$ staining) divided by the total number of tissue hits (P_{tissue}) for each section: V_v = ($P_{positive}$ staining/P_{tissue}) x 100.

RNA-Seq

Frozen ileal epithelium scrapings and liver samples were homogenized in TRIzol (Ambion, Waltham, MA) using a Mixer Mill 300 tissue homogenizer (Retsch, Germany) and total RNA was isolated as previously described [13]. RNA was quantified using a Nano-drop spectrophotometer (Thermo Scientific, Wilmington, DE) at 260 nm, and purity was assessed using the A_{260}/A_{280} ratio and the Caliper LabChip GX (Perkin Elmer, Waltham, MA).

Dose-dependent gene expression was examined using RNA-Seq performed at the MSU Research Technology Support Facility (RTSF) Genomics Core (rtsf.natsci.msu.edu/genomics). Ileal libraries from three independent biological replicates (n=3) were prepared using the Ovation Mouse RNA-Seq System 1-16 sample preparation kit (NuGen, San Carlos, CA), with an additional DNase step. Libraries were quantified and sequenced as previously described, using a read depth of ~30M per sample [38, 39]. Quality was determined using FASTQC v0.11.3 and adaptor sequences were removed using Trimmomatic v0.33. Reads were mapped to the mouse reference genome (GRCm38 release 81) using Bowtie2 v2.2.6 and TopHat2 v2.1.0. Alignments were converted to SAM format using SAMTools v1.2.0. For TCDD-mediated differential gene

expression, fold changes were calculated relative to vehicle controls. Hepatic RNA-Seq analysis was previously published [39]. Genes were considered differentially expressed if |fold change| ≥ 1.5 and statistical P1(*t*) value ≥ 0.8 at one or more doses. RNA-Seq datasets for the ileal epithelium and liver were deposited in the Gene Expression Omnibus (GEO; accession number GSE89430 and GSE87519, respectively).

Putative DRE identification and hepatic AhR ChIP-Seq

Putative dioxin response elements (pDREs) with matrix similarity scores (MSS) ≥ 0.856 were previously identified [40]. ChIP-Seq was previously performed on liver samples from male C57BL/6 mice 2h after a single bolus oral gavage of 30 µg/kg TCDD [39, 41]. Briefly, cross-linked DNA was immunoprecipitated with either rabbit IgG or anti-AhR (H-211, sc-5579; Santa Cruz, CA). Libraries were prepared using the MicroPlex kit (Diagenode), pooled, and sequenced at a depth of a ~30M on an Illumina HiSeq 2500 at the MSU RTSF Genomics Core. Reads were mapped to the mouse reference genome (GRCm38 release 81) using Bowtie 2.0.0 and alignments converted to SAM format using SAMTools v0.1.2. Normalization and peak calling was performed using CisGenome [42], by comparing IgG control and AhR enriched samples (n = 5) using a bin size (−b) of 25 and boundary refinement resolution (−bw) of 1 with default parameters.

Hepatic quantitative real-time polymerase chain reaction (qRT-PCR)

Given the low (≤ 10) read counts for *Gpbar1* in the RNA-Seq dataset, differential expression was confirmed by qRT-PCR [13]. Total hepatic RNA was reverse transcribed by SuperScript II (Invitrogen) using oligo dT primer according to the manufacturer's protocol. PCR amplification was conducted on a Bio-Rad CFX Connect Real-Time PCR Detection System. Gene expression relative to vehicle control was calculated using the $2^{-\Delta\Delta CT}$ method, where each sample was normalized to the geometric mean of 3 housekeeping genes (*Actb*, *Gapdh*, and *Hprt*). Gene

expression data are plotted relative to vehicle control. Forward and reverse primer sequences are provided in Table 4.

LC-MS analysis of bile acids

Serum (10 µL) was added to 10 µL of a 20 ng/µL stock solution of deuterated (d4) glycochenodeoxycholic acid (GCDCA, from Steraloids, Inc.) in methanol, and extracted with ice-cold methanol as previously described [43]. Frozen liver samples (50 mg) or dried fecal pellets (50 mg) were combined with 10 µL of 20 ng/µL d4-GCDCA stock solution and 1.0 mL of ice-cold methanol [43], and homogenized with 0.5 mm zirconium oxide beads using an air-cooled Bullet Blender (NextAdvance). Extracts were dried under vacuum, reconstituted in 2.0 mL of 50% methanol, filtered through 0.2 µm nylon membranes (Pall Life Sciences), and stored at -80°C.

Bile acids were analyzed by high resolution/accurate mass (HRAM)-LC-MS using an Agilent 1260 capillary HPLC coupled to a Thermo Scientific LTQ-Orbitrap Velos mass spectrometer. Extracts (2 µL) were injected into water containing 0.1% formic acid, and loaded onto an inline peptide Opti-Trap (Optimize Technologies) for 3.0 min at 5 µL/min for desalting and concentration. Bile acids were then eluted by a 30 min water/acetonitrile gradient from 98% water containing 0.1% formic acid to 95% acetonitrile containing 0.1% formic acid (modified from [44]) and separated by a ProntoSil C18AQ 200 µm x 50mm, 3u column (nanoLCMS Solutions) at a flow rate of 2 µL/min. The column eluent was introduced to the LTQ-Orbitrap Velos mass spectrometer by an Advance nano-ESI source (Michrom BioResources) at a spray voltage of -1.7kV. High resolution (R=100,000 at 400 *m/z*) negative ion mass spectra were collected over 300-900 *m/z*. The ion transfer tube of the mass spectrometer was maintained at 250°C, and the S-lens was set to 50%. Appropriate sample dilution factors were determined empirically to ensure a linear range of detector response [45]. Chromatographic peak alignment, feature detection, quantitation and bile acid identification were performed using MAVEN [46] and SECD-LIMSA [47] software. All bile acids were identified by comparison of retention time and accurate mass data

TABLE 4. PRIMER SEQUENCES (5'-3') FOR GENES ANALYZED BY QRT-PCR

Target Organism	Gene ID	Gene Symbol	Ref Seq Accession	Forward Primer	Reverse Primer	Product Size
Mus musculus	11461	*Actb*	NM_007393	GCTACAGCTTCACCACCACA	TCTCCAGGGAGGAAGAGGAT	123
	14433	*Gapdh*	NM_008084	GTGGACCTCATGGCCTACAT	TGTGAGGGAGATGCTCAGTG	125
	15452	*Hprt*	NM_013556	AAGCCTAAGATGAGCGCAAG	TTACTAGGCAGATGGCCACA	104
	227289	*Gpbar1*	NM_174985	CAGCTGCCCAAAGGTGTCTA	CAAGTCCAGGTCAATGCTGC	110
Universal bacteria		16S rRNA		CCTACGGGAGGCAGCAG	ATTACCGCGGCTGCTGGC	193
Clostridium species		*baiCD*		CAGCCCRCAGATGTTCTTTG	GCATGGAATTCWACTGCYTC	145

against reference standards. Relative quantitation was performed against the deuterated GCDCA internal standard. TCDD-elicited changes in bile acid species are reported as fold changes relative to vehicle controls.

Intestinal function

At 26d after the initial dose (PND54), mice were fasted for 4h (without access to food or water) prior to oral gavage with 150 µL of a solution containing 100 mg sucrose, 12 mg lactulose, 8 mg mannitol, and 6 mg sucralose. Urine from each mouse was collected over a 5h period, flash frozen, and combined prior to analysis. Urine was diluted in 95% acetonitrile/5% water: 100-fold for mannitol detection, 200-fold for sucrose and lactulose detection, and 500-fold for sucralose detection. Sugar probe recovery was measured using ultra high performance liquid chromatography-tandem mass spectrometry (UPLC-MS/MS), performed at the MSU RTSF Mass Spectrometry and Metabolomics Core (https://rtsf.natsci.msu.edu/mass-spectrometry/). Diluted urine samples were injected onto an Acquity UPLC BEH Amide column (1.7 µm, 2.1 X 100mm) (Waters, Milford, MA) maintained at 50°C on a Waters ACQUITY UPLC systems (Waters). Mobile phase A was 50 mM ammonium acetate buffer (pH = 9.6) and mobile phase B was acetonitrile. Chromatographic separation was performed over 8 minutes (min) using a flow rate of 0.2 mL/min in the following gradient: time (t) = 0 min, 95% B; t = 1 min, 95% B; t = 2 min, 70% B; t = 5 min, 30% B; t = 5.01 min, 10% B; t = 6 min, 10% B; t = 6.01 min, 95% B; t = 8 min, 95% B. The autosampler was cooled to 10°C, with an injection volume of 5 µL. UPLC was coupled with negative-mode electrospray ionization to a Waters Quattro Premier XE Mass Spectrometer (Waters) operating in multiple reaction monitoring (MRM) mode. The capillary voltage was -2.5 kV, while desolvation gas flow rate was 600 L/h. Source temperature and desolvation temperature were 120°C and 450°C, respectively. MRM parameters including cone voltage, collision voltage, precursor ion, and product ion were optimized by flow injection of pure standard for each individual compound (Table 5).

Data analysis including peak integration was performed using MAVEN [46]. Waters raw data were converted to mzxml format using msconvert in the ProteoWizard Tools [48]. Fractional excretion of each probe was calculated using: (probe concentration from MS X total urine volume excreted)/probe input. Fractional sucrose excretion (%) was used to assess gastroduodenal permeability, the lactulose-to-mannitol ratio was used to assess small intestinal permeability, and fractional sucralose excretion (%) was used to assess colonic permeability [49, 50].

At 27d after the initial dose (PND55), whole gut transit time (WGTT) was determined using carmine red dye, which cannot be intestinally absorbed. At time 0 (t_0), mice were orally gavaged with 150 µL of carmine red solution (6% carmine red dye suspended in 0.5% methylcellulose). Fecal pellets were monitored continuously for the presence of carmine red. WGTT represents the time interval between t_0 and the first observance of carmine red dye in the fecal pellets.

Degenerate qRT-PCR of bacterial functional genes

The *bsh* Hidden Markov Model (HMM) constructed by the Ribosomal Database Project consisted of 12 vetted seed sequences from *Lactobacillus*, *Clostridium*, *Roseburia*, *Eubacterium*, *Butyrivibrio*, and *Streptococcus* species, while the *baiCD* HMM consisted of 10 vetted seed sequences from *Clostridium* and *Lachnospiraceae* species. Using these models, more inclusive sequence sets were created for *bsh* and *baiCD* within the 'FunGene functional gene pipeline & repository' [51] by extracting sequences from GenBank. Setting the HMM consensus percent identity cut-off to ≥ 40%, nucleotide sequences of *bsh* and *baiCD* were obtained from 2633 and 129 bacterial organisms, respectively. Given the diversity of bacterial organisms found to express *bsh*, the 2633 sequences from FunGene were separated into 4 groups based on nucleotide similarity determined through construction of a phylogenetic tree (Group 1: 423, Group 2: 330, Group 3: 955, Group 4: 925). In contrast, the 129 *baiCD* sequences exhibited sufficient similarity and were therefore kept as a single composite group. The Primer Design terminal program developed by the Ribosomal Database Project (https://github.com/rdpstaff/PrimerDesign) was

TABLE 5. MULTIPLE REACTION MONITORING (MRM) PARAMETERS USED FOR THE TANDEM MASS SPECTROMETRY (MS/MS) ANALYSIS OF FOUR SUGAR PROBES

Probe	Precursor Ion Q1	Product Ion Q3	Cone Voltage (V)	Collision Energy (V)
Mannitol	181.15	101.05	21	16
Lactulose	341.19	161.12	15	10
Sucrose	341.19	179.17	33	16
Sucralose	395.10	359.07	27	10

used to design degenerate primer sets which target conserved regions within *baiCD* and each phylogenetic group of *bsh* (http://dbzach.fst.msu.edu/index.php/primers/). To estimate the overall abundance of bile acid metabolism genes within the gut microbiome, primer sets were selected to target ≥75% of the *baiCD* sequences and the sequences within each *bsh* group. Fecal levels of *baiCD* were also quantified using a previously validated primer pair (Table 4) which targets a conserved region of the gene within *Clostridium scindens VPI 12708* and *Clostridium hiranonis TO931*, two strains known to exhibit bile acid 7α-dehydroxylation activity [52, 53].

Frozen fecal pellets were crushed into a powder and bacterial DNA was isolated using the QIAamp DNA Stool Mini Kit (Qiagen, Valencia, CA). To investigate bile acid metabolism loci, qRT-PCR was performed on a Bio-Rad CFX Connect Real-Time PCR Detection System as previously described [13]. Gene expression relative to vehicle control was calculated using the $2^{-\Delta\Delta CT}$ method, with each fecal sample extract normalized to total bacterial DNA levels using universal primers targeting the 16S ribosomal RNA gene [54]. Gene levels are plotted relative to vehicle control.

RESULTS

Histopathology

Previous studies report hepatic steatosis, immune cell infiltration, fibrosis, and bile duct proliferation in male mice following treatment with TCDD and related AhR agonists [14, 17, 25, 55, 56]. Comparable effects are reported in female C57BL/6 mice orally gavaged with TCDD every 4d for either 28 or 92d [16, 33]. Here, the histopathological features associated with TCDD-elicited hepatotoxicity in both female and male C57BL/6 mice orally gavaged with TCDD every 4d for 28d were compared. Histopathological scoring suggests the incidence and severity of vacuolization, inflammatory cell infiltration, bile duct proliferation, and periportal fibrosis were consistently greater in male mice compared to females (Table 6; Figure 14). More specifically, hepatocyte vacuolization (fatty change) was first observed in males at 0.3 μg/kg and in females at 10 μg/kg TCDD. Fat accumulation was more severe in males compared to females at ≥ 3 μg/kg

TABLE 6. COMPARISON OF TCDD-ELICITED HISTOPATHOLOGICAL CHANGES BETWEEN MALE AND FEMALE C57BL/6 MICE

TCDD (µg/kg)		**0.3**		**1**		**3**			**10**			**30**		
Sex		Male	Female	Male	Female	Male	Female		Male	Female		Male	Female	
Number of animals		8	8	8	6	8	6		8	4		8	4	
Vacuolation (centrilobular)	Mean Grade	0.1 ± 0.4	-	0.9 ± 0.8	-	1.0 ± 0.8	-	*	3.0 ± 0.5	0.5 ± 0.3	*	4.0 ± 0.0	2.0 ± 1.2	*
	Incidence	1/8	0/8	5/8	0/6	6/8	0/6		8/8	1/4		8/8	4/4	
Necrosis; Inflammatory cell foci	Mean Grade	-	-	-	-	0.3 ± 0.5	-		0.8 ± 0.5	-		1.3 ± 0.5	0.3 ± 0.5	*
	Incidence	0/8	0/8	0/8	0/6	2/8	0/6		6/8	0/4		8/8	1/4	
Bile duct proliferation	Mean Grade	-	-	-	-	-	-		-	-		0.9 ± 0.8	0.3 ± 0.5	
	Incidence	0/8	0/8	0/8	0/6	0/8	0/6		0/8	0/4		5/8	1/4	
Fibrosis (periportal)	Mean Grade	-	-	-	-	-	-		-	-		0.6 ± 0.5	0.3 ± 0.5	
	Incidence	0/8	0/8	0/8	0/6	0/8	0/6		0/8	0/4		5/8	1/4	

Histopathological grade: 0 = Within normal limits, 1 = Minimal, 2 = Slight, 3 = Moderate, 4 = Marked

No noteworthy hepatic changes were observed in mice treated with sesame oil vehicle or ≤ 0.1 µg/kg TCDD.

Mean Grade = Mean of histopathological grades ± SD. * $p \leq 0.05$ (compared between males and females at the same dose, Mann-Whitney rank sum test).

Incidence = Number of mice in which the histopathological feature was present.

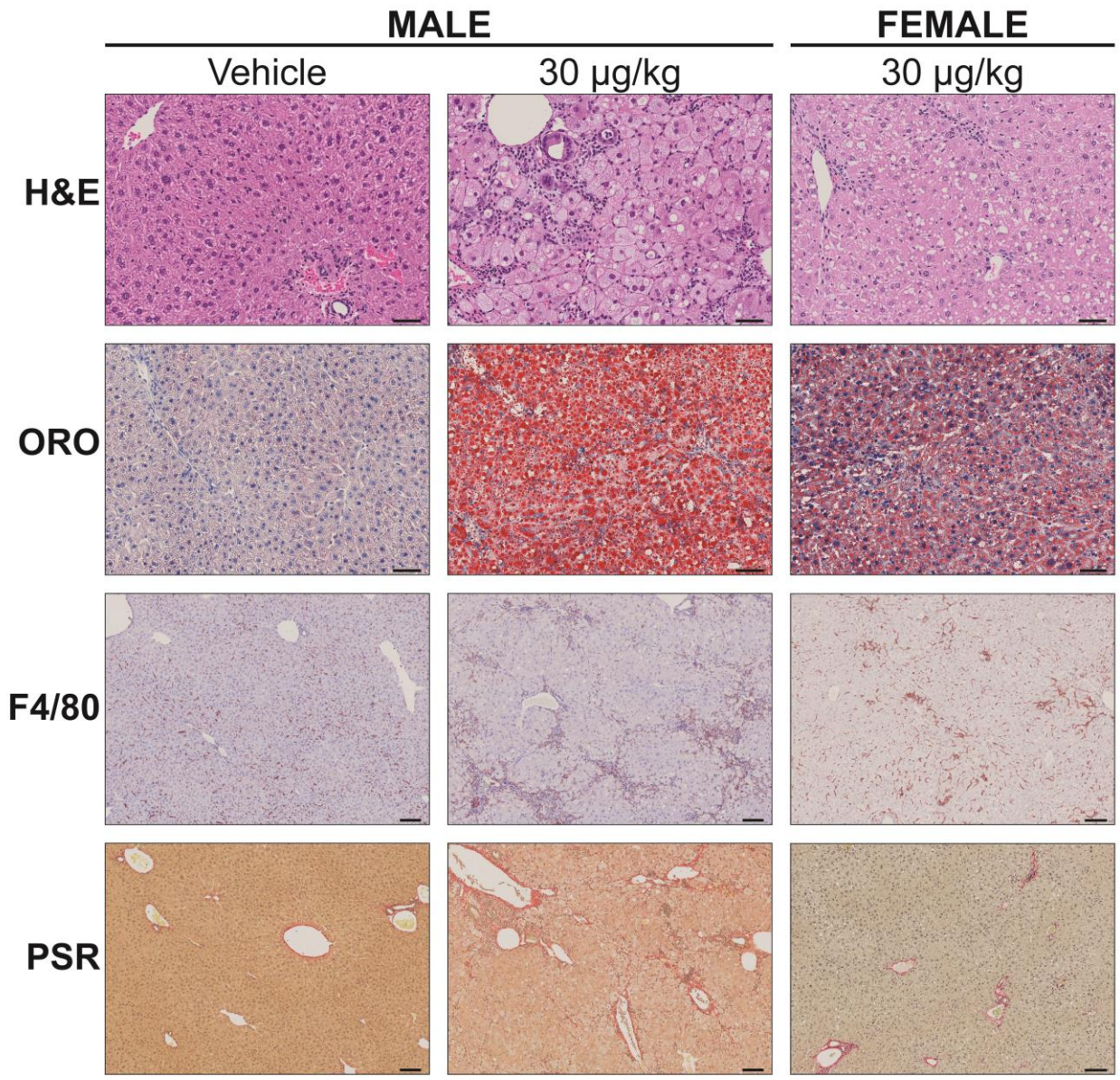

FIGURE 14. HISTOLOGICAL EVALUATION OF MALE AND FEMALE HEPATIC HISTOPATHOLOGY

Representative photomicrographs of livers from male and female C57BL/6 mice orally gavaged with sesame oil vehicle or 30 µg/kg TCDD every 4 days for 28 days. Livers were stained with hematoxylin and eosin (H&E) for general assessment, Oil Red O (ORO) for neutral lipids, F4/80 for macrophages, and Picrosirius Red (PSR) for collagen deposition. Scale bars represent 50 µm for H&E and ORO, and 100 µm for F4/80 and PSR.

TCDD (Table 6). QuHAnT analysis of ORO-stained sections indicated that hepatic fat accumulation at 30 µg/kg TCDD was 6.2-fold greater in males compared to females (Figure 14; Figure 15), consistent with the pathologist's assessment. Minimal to slight hepatocyte necrosis and inflammatory cell infiltration (e.g. neutrophils and lymphocytes) were present in males at ≥ 3 µg/kg and in females at 30 µg/kg. Both were more severe in males at 30 µg/kg compared to the females (Table 6). F4/80 labeling revealed that immune cell foci consisted primarily of macrophages, suggesting infiltration (Figure 14). Bile duct proliferation was observed in both sexes at 30 µg/kg, with a higher incidence in males, while inflammation surrounding the bile ducts (pericholangitis) was exclusive to males (Table 6; Figure 16A-B). Similarly, PSR-staining revealed that the incidence of periportal fibrosis at 30 µg/kg was higher in males compared to females (Table 6; Figure 14). In summary, male mice exhibited greater sensitivity to TCDD-elicited hepatotoxicity compared to females, and exhibited more severe histopathology at lower doses. Subsequent studies therefore focused on responses in male mice.

Gross morphology and clinical chemistry

Terminal body weights and tissue weights for the mice used in this study were previously reported [39]. Gallbladder volume increased 2.5-fold in mice treated with 30 µg/kg TCDD compared to controls (Figure 16C). The gallbladder distention is consistent with previous studies [56]. Serum alkaline phosphatase (ALP) activity was unchanged at 30 µg/kg, suggesting TCDD did not damage bile duct epithelial cells (cholangiocytes) (Figure 16D).

Cholesterol and primary bile acid biosynthesis

Cholesterol is not only essential for maintaining cell membrane fluidity, but it also serves as the precursor for steroid hormone and bile acid biosynthesis. In mammals, the liver is the primary site of acetyl-CoA conversion to cholesterol, while the intestine also exhibits *de novo* synthesis capabilities. Hepatic cholesterol (not confirmed by high resolution MS/MS) and

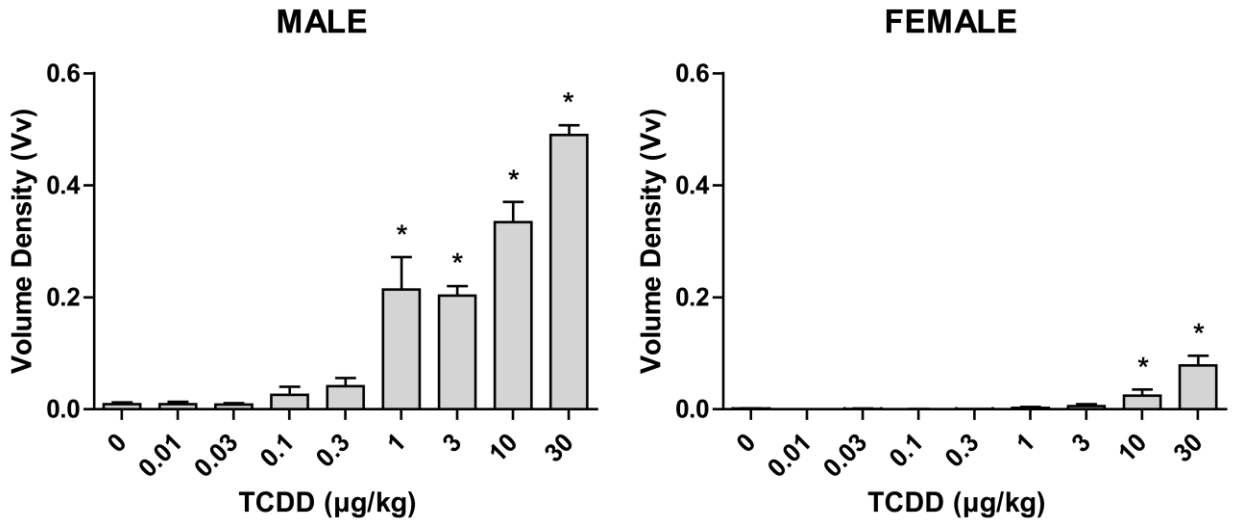

FIGURE 15. QUANTIFICATION OF HEPATIC LIPID ACCUMULATION

Male and female C57BL/6 mice orally gavaged with sesame oil vehicle or 0.01-30 µg/kg TCDD every 4 days for 28 days. Lipids were stained with Oil Red O and quantified using the Quantitative Histological Analysis Tool (QuHAnT). Bars represent the average ± standard error of the mean for at least 4 biological replicates. Statistical significance (* $p \leq 0.05$) was determined using one-way ANOVA analysis followed by Dunnett's post-doc test performed in SAS 9.3.

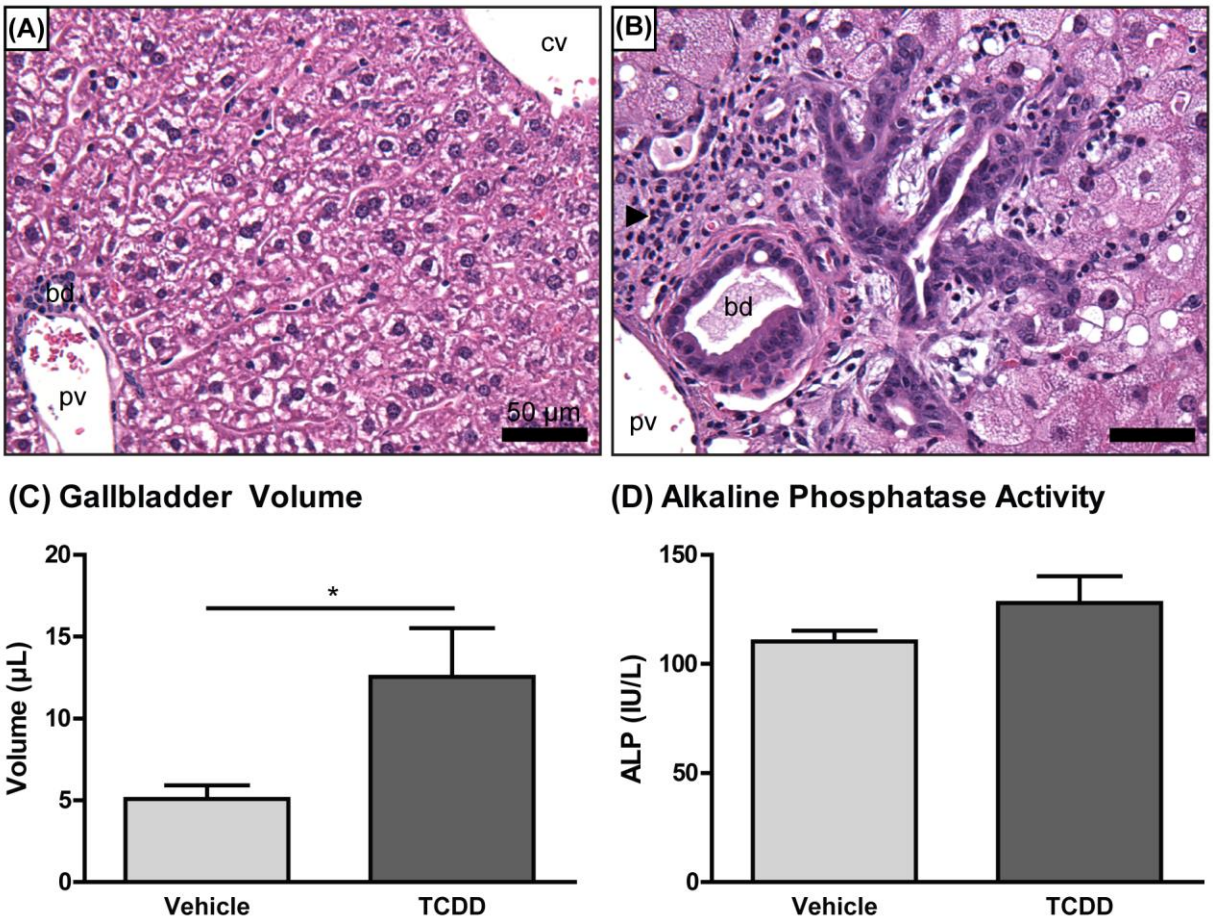

FIGURE 16. TCDD-ELICITED BILE DUCT TOXICITY

Representative photomicrographs of hematoxylin and eosin-stained livers from male C57BL/6 mice orally gavaged with (A) sesame oil vehicle or (B) 30 µg/kg TCDD every 4 days from 28 days. Bile duct proliferation and pericholangitis (arrow) were identified at 30 µg/kg TCDD. cv = central vein; pv = portal vein; bd = bile duct; bar = 50 µm. (C) Gallbladder volume and (D) serum alkaline phosphatase (ALP) activity of male C57BL/6 mice orally gavaged with sesame oil vehicle or 30 µg/kg TCDD every 4 days for 28 days. Bars represent the average ± standard error of the mean for at least 5 biological replicates. Statistical significance (* $p \leq 0.05$) was determined using a Student's t-test performed in SAS 9.3.

cholesterol ester levels increased 9.0- and 11.3-fold, respectively, in male C57BL/6 mice orally gavaged with 30 µg/kg TCDD every 4d for 28d [57]. The committed step of cholesterol biosynthesis involves the conversion of 3-hydroxy-3-methylglutaryl-CoA to mevalonate catalyzed by the rate-limiting enzyme 3-hydroxy-3-methylglutaryl-CoA reductase (HMGCR). Hepatic expression of *Hmgcr* was dose-dependently induced at 0.3-10 µg/kg TCDD (max 3.4-fold), with no significant induction at 30 µg/kg (Figure 17). Other enzymes involved in cholesterol biosynthesis including mevalonate kinase (*Mvk*), mevalonate diphosphate decarboxylase (*Mvd*), squalene epoxidase (*Sqle*), lanosterol synthase (*Lss*), methylsterol monoxygenase 1 (*Msmo1*), and 24-dehydrocholesterol reductase (*Dhcr24)* exhibited a comparable dose-dependent expression pattern (Figure 17). This suggests that at low doses, AhR activation induces cholesterol biosynthesis, consistent with a 10.3-fold increase in AhR genomic binding at the *Hmgcr* loci. However, negative feedback at 30 µg/kg TCDD may limit *de novo* biosynthesis.

Several genes involved in cholesterol biosynthesis, including 3-hydroxy-3-methylglutaryl-CoA synthase 1 (*Hmgcs1*), *Hmgcr*, farnesyl diphosphate synthetase (*Fdps*), and farnesyl diphosphate farnesyl transferase 1 (*Fdft1*), are transcriptionally regulated by sterol regulatory element-binding protein 2 (SREBP2) binding to sterol response elements (SREs). Elevated intracellular cholesterol levels prevent intramembrane SREBP2 proteolysis and subsequent nuclear translocation, thereby reducing SRE-regulated gene transcription. Consequently, higher hepatic cholesterol levels may repress SREBP2-mediated transcription. Furthermore, *Srebf2* (encodes SREBP2) was repressed 2.7-fold at 30 µg/kg TCDD, which may further compromise expression of cholesterol biosynthetic genes.

Approximately 90% of excess cholesterol is excreted from the body by hepatic conversion to bile acids. In humans, the two primary bile acids synthesized directly by the liver are cholic acid (CA) and chenodeoxycholic acid (CDCA). Rodent livers hydroxylate CDCA at the 6β-positon yielding α-muricholic acid (α-MCA), which can epimerize at the 7-OH position to form β-muricholic acid (β-MCA), and therefore α/β-MCA are also primary bile acids in mice [58]. In the classical bile

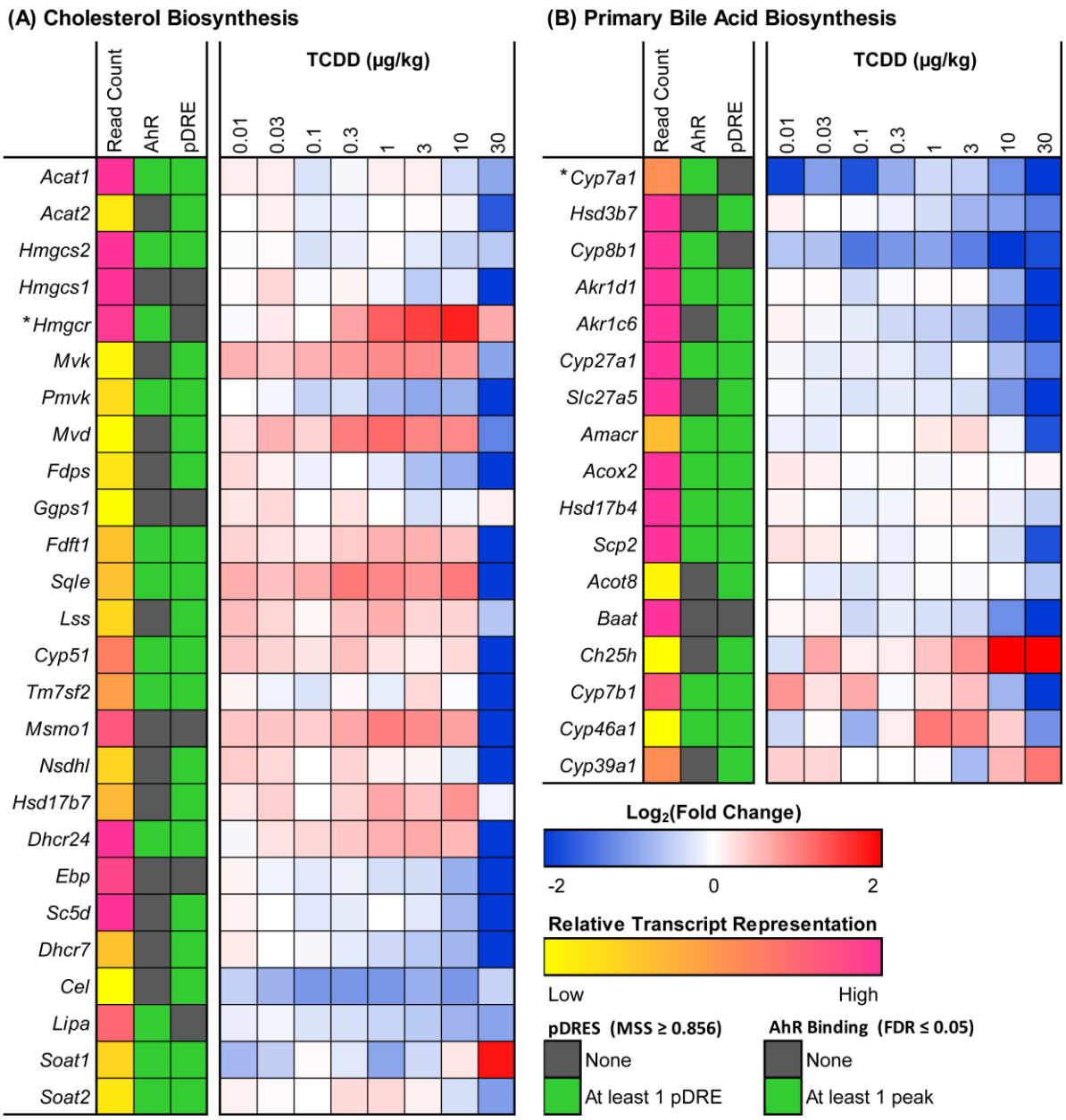

FIGURE 17. EFFECTS OF TCDD ON CHOLESTEROL AND BILE ACID BIOSYNTHESIS

TCDD-elicited hepatic differential expression of genes involved in (A) cholesterol and (B) primary bile acid biosynthesis in male C57BL/6 mice orally gavaged with sesame oil vehicle or TCDD (0.01-30 µg/kg TCDD) every 4 days for 28 days. Color scale represents the $\log_2$(fold change) for differential gene expression relative to vehicle controls, as determined through RNA-Seq analysis (n=3). The presence of pDREs (MSS ≥ 0.856) and AhR enrichment peaks (FDR ≤ 0.05) at 2h are shown as green boxes. Read count represents the raw number of aligned reads to each transcript indicating potential level of expression, where yellow represents a lower level of expression (≤ 500 reads) and pink represents a higher level of expression (≥ 10,000).

acid biosynthesis pathway, cholesterol is directly 7α-hydroxylated by CYP7A1, representing the rate-limiting step. Alternative pathways involve initial hydroxylation at C24, C25, or C27 catalyzed by CYP46A1, cholesterol 25-hydroxylase (CH25H), and CYP27A1, respectively, followed by 7α-hydroxylation. TCDD repressed *Cyp7a1* 39.7-fold with a 2.3-fold enrichment in AhR genomic binding (Figure 17). Furthermore, 9 of the 12 downstream enzymes involved in the classical pathway were also repressed, including hydroxy-delta-5-steroid dehydrogenase 3β7 (*Hsd3b7*; 2.5-fold), *Cyp8b1* (4.4-fold), aldo-keto reductase 1D1 (*Akr1d1*; 16.3-fold), aldo-keto reductase 1C6 (*Akr1c6*; 22.1-fold), *Cyp27a1* (2.4-fold), *Slc27a5* (16.0-fold), α-methylacyl-CoA racemase (*Amacr*; 3.3-fold), sterol carrier protein 2 (*Scp2*; 3.4-fold), and bile acid-Coenzyme A: amino acid N-acyltransferase (*Baat*; 12.0-fold) (Figure 17). With the exception of CYP8B1, which is unique to CA synthesis, these enzymes are required for synthesis of all murine primary bile acids. Interestingly, AhR binding was enriched 2.2-fold within *Cyp8b1*, suggesting AhR-mediated regulation of the CDCA to CA ratio. There are four genes unique to the alternative pathway of bile acid synthesis: *Cyp46a1* and *Cyp7b1*, which were repressed 2.1- and 7.6-fold, respectively, as well as *Cyp39a1* and *Ch25h*, which were induced 2.1- and 6.1-fold, respectively, by TCDD (Figure 17).

Bile acid biosynthesis is primarily regulated by two negative feedback loops that repress *Cyp7a1*, both involving bile acid-mediated activation of FXR. Hepatic FXR induces short heterodimer partner (*Shp*, aka *Nr0b2*), which then antagonizes liver receptor homolog 1(LRH-1)- and hepatocyte nuclear factor 4α (HNF4α)-mediated *Cyp7a1* expression. However, TCDD repressed hepatic *Nr0b2* 22.2-fold. Alternatively, activation of intestinal FXR induces ileal fibroblast growth factor 15 (*Fgf15*) expression. FGF15 binds its hepatic heterodimer receptor consisting of fibroblast growth factor receptor 4 (FGFR4) and klotho β (KLB), which causes *Cyp7a1* repression and regulates bile flow. Yet, hepatic *Fgfr4* and *Klb* were repressed 4.7- and 8.1-fold respectively, while ileal *Fgf15* was repressed 9.7-fold at 30 μg/kg TCDD. Therefore, it is unlikely that either feedback loop is responsible for *Cyp7a1* repression.

Hepatic, serum, and fecal bile acid profiles

HRAM-LC-MS analysis detected a dose-dependent increase in total hepatic bile acids, with 2.1- and 4.6-fold increases at 10 and 30 µg/kg TCDD, respectively (Figure 18). CA, the predominant primary hepatic bile acid in control samples, increased 4.7-fold following treatment with 30 µg/kg TCDD. α/β-MCA was the second most abundant primary bile acid in controls, while hepatic CDCA levels were negligible. TCDD had no effect on hepatic α/β-MCA or CDCA, but dose-dependently increased total hepatic conjugated primary bile acid levels (max 4.7-fold), including glycocholic acid (GCA; 3.9-fold), taurocholic acid (TCA; 9.7-fold), and tauro-α-muricholic acid (T-α-MCA; 3.7-fold) (Figure 18). Paradoxically, hepatic expression of *Baat*, which is responsible for hepatic taurine- and glycine-conjugation of bile acids, was repressed 12.0-fold (Figure 17). In female mice, TCDD increased hepatic taurine (max 1.4-fold; p=0.05) and glycine (max 20.3-fold; p=0.10) levels [40]. TCDD repressed hepatic expression of taurine biosynthesis genes including cysteine dioxygenase 1 (*Cdo1*; 2.7-fold) and cysteine sulfinic acid decarboxylase (*Csad*; 4.5-fold), while the taurine transporter *Slc6a6* (encoding TAUT) was induced 1.8-fold, suggesting hepatic taurine uptake rather than *de novo* synthesis. Furthermore, TCDD elicited a dose-dependent increase in total hepatic levels of conjugated secondary bile acids (max 77.7-fold), suggesting increased bacterial metabolism. More specifically, TLCA, the most induced hepatic bile acid, was dose-dependently increased 72.1- and 233.8-fold at 10 and 30 µg/kg TCDD, respectively (Figure 18).

Individual bile acids differ in their capacity to bind hepatic receptors. TLCA is the most potent endogenous activator of GPBAR1, a metabotrophic bile acid receptor located on non-parenchymal cells including Kupffer cells, sinusoidal epithelial cells, and bile duct epithelial cells (cholangiocytes) [28]. Using qRT-PCR, hepatic *Gpbar1* expression was induced 4.3-fold at 30 µg/kg TCDD (Figure 19). Increased hepatic TLCA levels combined with *Gpbar1* induction would promote activation of GPBAR1 following TCDD treatment. Likewise, CDCA is the most potent endogenous FXR agonist, while T-α-MCA and T-β-MCA are competitive antagonists [59]. At low

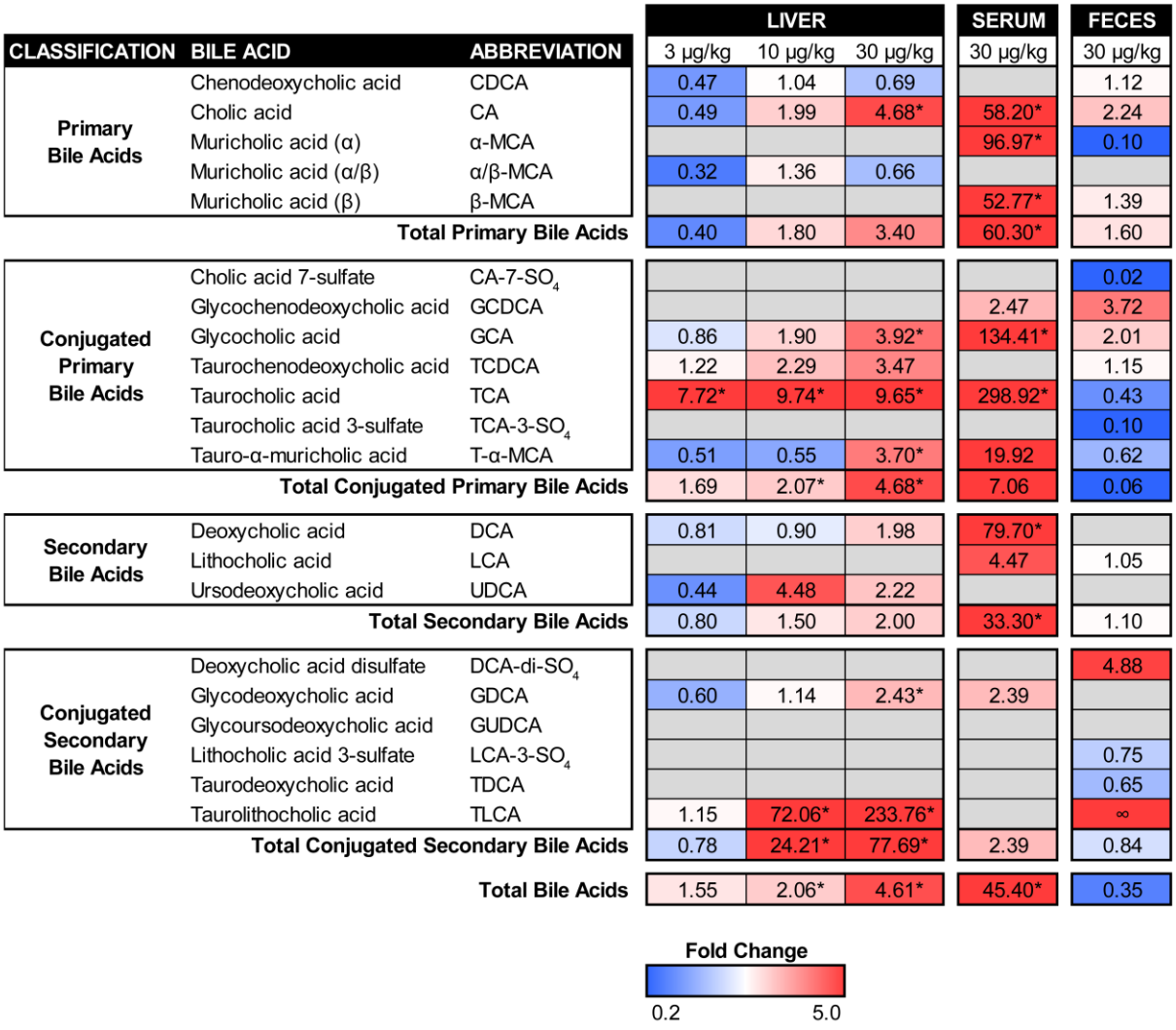

FIGURE 18. BILE ACID PROFILES FOR THE LIVER, SERUM, AND FECES

Male C57BL/6 mice were orally gavaged with sesame oil vehicle or TCDD (3-30 µg/kg) every 4 days for 28 days. Individual bile acid species were quantified using high resolution accurate mass liquid chromatography mass spectrometry and expressed as fold changes relative to vehicle controls. Red and blue indicate increased or decreased levels, respectively, while grey indicates 'not detected'. '∞' indicates an incalculable increase as the bile acid was detected in treated animals but not controls. Statistical significance (*$p \leq 0.05$) was determined using one-way ANOVA analysis followed by Dunnett's post-hoc test (liver) or a Student's t-test (serum) performed in SAS 9.3. Fecal pellets were collected from two cages of co-housed mice for each treatment group (n=2) and therefore statistical analysis was not performed.

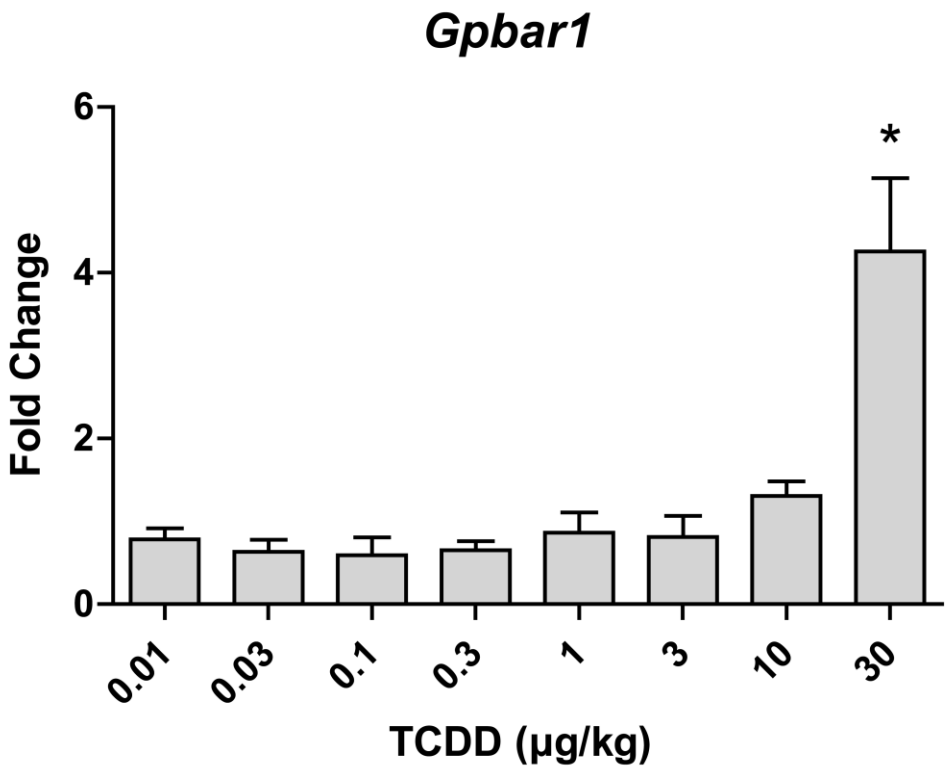

FIGURE 19. HEPATIC EXPRESSION OF G PROTEIN-COUPLED BILE ACID RECEPTOR 1

Quantitative real time polymerase chain reaction (qRT-PCR) analysis of G protein-coupled bile acid receptor 1 (*Gpbar1*) expression in the liver of male C57BL/6 mice orally gavaged with sesame oil vehicle or TCDD (0.01-30 µg/kg TCDD) every 4 days for 28 days. Bars represent the average fold change relative to vehicle ± standard error of the mean (SEM) for at least 3 independent biological replicates. Statistical significance (* $p \leq 0.05$) was determined using one-way ANOVA analysis followed by Dunnett's post-doc test performed in SAS 9.3.

hepatic CDCA levels due to conversion to α-MCA, TCDD-elicited increases in T-α-MCA levels may inhibit FXR activation. Moreover, TCDD repressed hepatic *Nr1h4* (encodes for FXR) 3.2-fold, further inhibiting the FXR signaling pathway.

Total bile acids in serum increased 45.4-fold at 30 µg/kg TCDD (Figure 18). Taurine- and glycine-conjugates of CA exhibited increases of 298.9- and 134.4-fold, respectively. CA, α-MCA, and β-MCA were the most abundant species present in treated serum samples with increases of 58.2-, 97.0-, and 52.8-fold, respectively. Additionally, the secondary bile acid deoxycholic acid (DCA) was increased 79.7-fold.

Total fecal bile acids decreased 2.8-fold at 30 µg/kg TCDD (Figure 18), suggesting decreased bile secretion from the gallbladder and/or increased intestinal reabsorption. Fecal levels of cholic acid 7-sulfate (CA-7-SO_4) and taurocholic acid 3-sulfate (TCA-3-SO_4) were decreased 55.2- and 10.3-fold, respectively, while deoxycholic acid disulfate (DCA-di-SO_4) levels increased 4.9-fold. The former is consistent with a 267.5-fold repression of *Sult2a8*, the predominant sulfotransferase in the male liver based on RNA-Seq read counts. TCDD also decreased α-MCA fecal levels 10.3-fold, while TLCA levels changed from undetectable in controls to detectable in treated mice.

Bile acid hydrophobicity

In general, bile acid toxicity increases with hydrophobicity [60, 61], which depends on ionization, hydroxylation, and conjugation (taurine, glycine, sulfate, glucoronate) [62]. The potential toxicity of a bile acid mixture can be estimated by calculating the hydrophilic-hydrophobic balance using the hydrophobicity index (HIx) of each bile acid species in the mixture, as described by Heuman [63]. The HIx of TCA was arbitrarily set to 0, with increasingly positive and negative values assigned to species exhibiting relatively greater hydrophobicity and hydrophilicity, respectively. TCDD (3-30 µg/kg) shifted the hepatic bile acid mixture HIx toward greater hydrophobicity (Figure 20), suggesting increased hepatotoxic potential. Each bile acid's

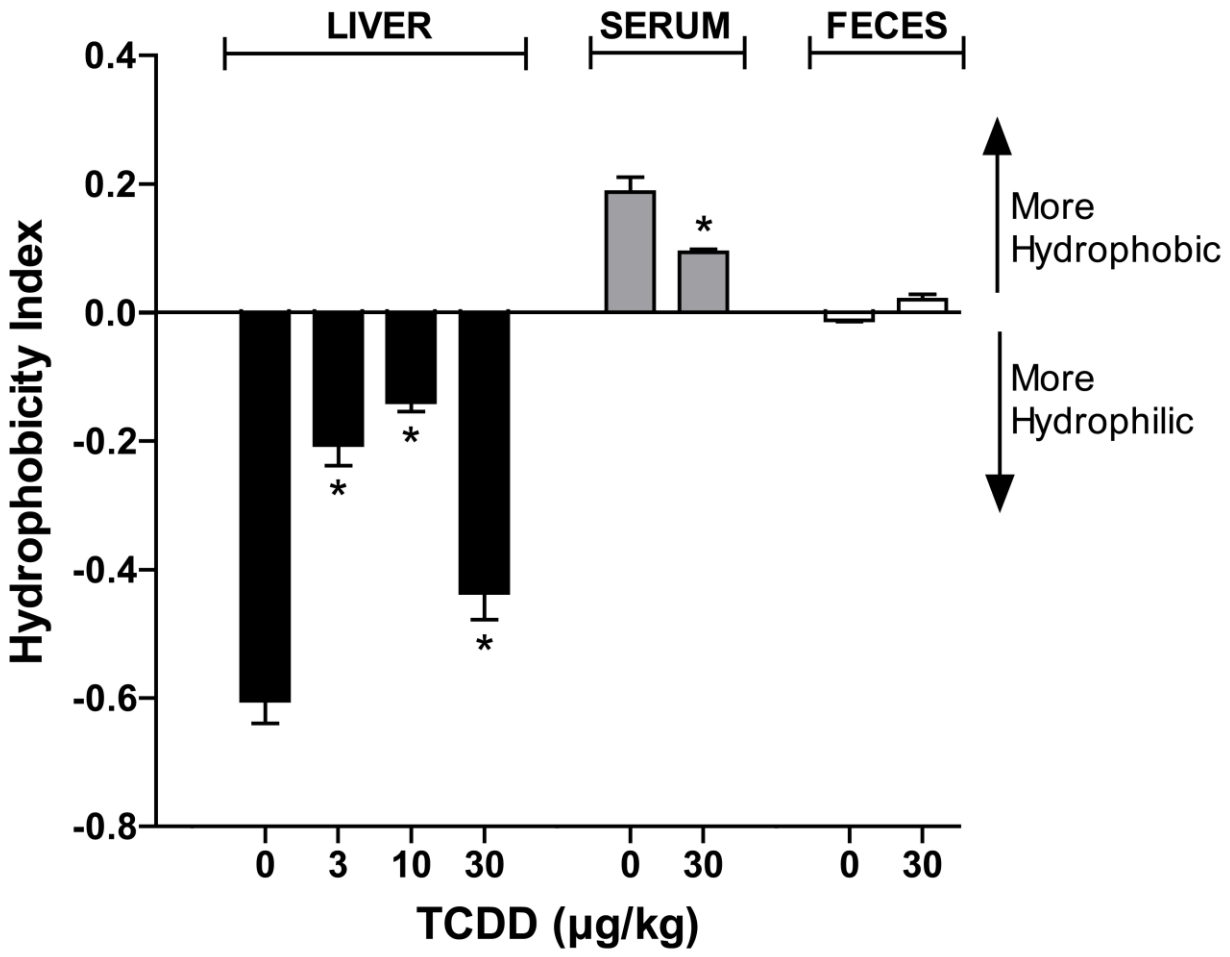

FIGURE 20. HYDROPHOBICITY INDICES (HIX) OF BILE ACID MIXTURES IN THE LIVER, SERUM, AND FECES

Male C57BL/6 mice were orally gavaged with sesame oil vehicle or TCDD (3-30 µg/kg TCDD) every 4 days for 28 days. Bile acid toxicity is positively associated with the degree of hydrophobicity, where increasingly positive and negative HIx values indicate greater hydrophobicity and hydrophilicity, respectively. Bars represent the average ± standard error of the mean for at least 4 biological replicates for liver and serum, or 2 pooled samples for feces. Statistical significance (* $p \leq 0.05$) was determined using one-way ANOVA analysis followed by Dunnett's post-hoc test (liver) or a Student's t-test (serum) performed in SAS 9.3. Fecal pellets were collected from two cages of co-housed mice for each treatment group (n=2) and therefore statistical analysis was not performed.

contribution to the overall HIx is dependent on its relative abundance within the mixture, and therefore low abundance species such as TLCA have lower impact. Consequently, the shift towards increased hydrophobicity is primarily driven by a decrease in the relative abundance of T-α-MCA, a highly hydrophilic species. In contrast, the serum bile acid mixture became more hydrophilic, while the fecal mixture exhibited a moderate increase in hydrophobicity (Figure 20).

CYP3A enzymes play a role in bile acid metabolism by catalyzing 6α-, 7α-, and 6β-hydroxylation [64, 65]. TCDD repressed all hepatic *Cyp3a* isoforms including *3a13*, *3a25*, *3a16*, *3a11*, *3a59*, *3a44*, and *3a57* (17.0-, 6.0-, 5.2-, 4.9-, 4.4-, 3.0-, 2.4-fold), as well as ileal *Cyp3a44* (2.2-fold). *Cyp3a* repression may decrease bile acid hydroxylation, thereby increasing the hydrophobicity of the bile acid pool.

Enterohepatic circulation

Following synthesis, conjugated primary bile acids are secreted into the bile canaliculi by canalicular bile salt export pump (BSEP; aka ABCB11) and ABCC2. TCDD repressed hepatic *Abcb11* 4.7-fold, while *Abcc2* was unchanged (Figure 21). Reduced hepatocyte-to-canaliculi export, combined with increased levels of hepatic conjugated primary bile acids likely caused spill-over into the sinusoidal blood and systemic circulation. Conjugated primary bile acids stored in the gallbladder are released into the duodenum in response to the intestinal hormone cholecystokinin following a meal, and progressively pass through the small intestine. Upon reaching the ileum, they are taken up into enterocytes by apical SLC10A2, and exported to the portal circulation by basal SLC51A and SLC51B. TCDD induced ileal expression of *Slc10a2* and *Slc51a* 1.6- and 1.5-fold, respectively, while ileal *Slc51b* was unchanged (Figure 21). Induction of these intestinal transporters likely promotes active reabsorption of bile acids across the ileum. Circulating bile acids are then transported into hepatocytes by *Slc10a1*, *Slco1a1*, *Slco1a4*, *Slco1b2*, and *Slco2b1*, which were repressed 17.9-, 1186.3-, 2.5-, 7.9-, and 12.9-fold, respectively, by TCDD (Figure 21). Specifically, SLC10A1 is primarily responsible for taurine- and

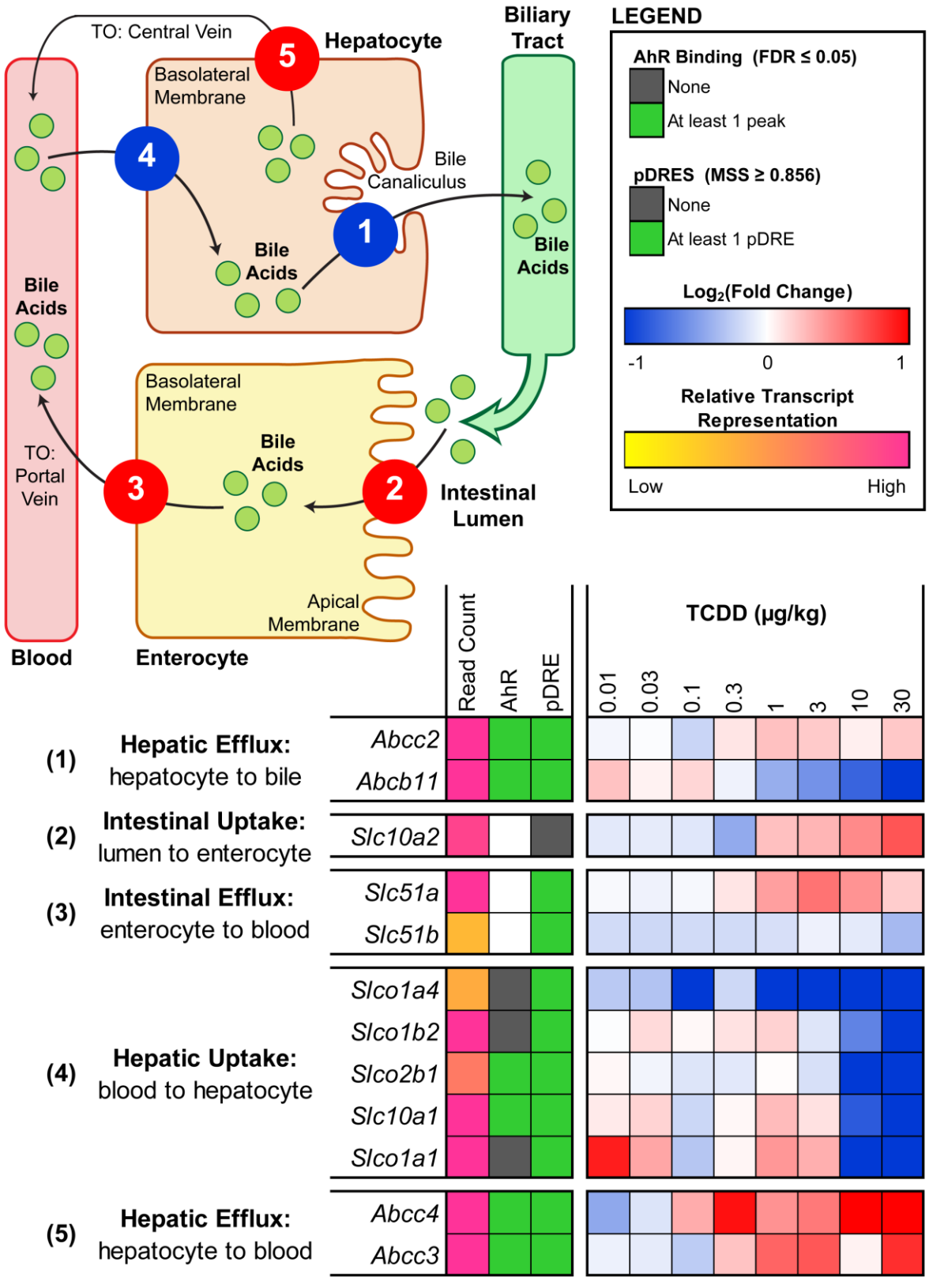

FIGURE 21. EFFECTS OF TCDD ON ENTEROHEPATIC CIRCULATION

FIGURE 21 (cont'd)

TCDD-elicited differential expression of bile acid transporters in the liver and ileum of male C57BL/6 mice orally gavaged with sesame oil vehicle or 0.01-30 µg/kg TCDD every 4 days for 28 days. Color scale represents the $\log_2$(fold change) for differential gene expression relative to vehicle controls, as determined through RNA-Seq analysis (n=3). The numeric labels to the left of the heat map correspond to the numbered transport functions in the pictorial representation, where the color of each function represents the overall direction of differential expression exhibited by the group of transporters involved (i.e. induced = red vs. repressed = blue). The presence of pDREs (MSS ≥ 0.856) and hepatic AhR enrichment peaks (FDR ≤ 0.05) at 2h are shown as green boxes. Read count represents the raw number of aligned reads to each transcript indicating potential level of expression, where yellow represents a lower level of expression (≤ 500 reads) and pink represents a higher level of expression (≥ 10,000).

glycine-conjugated bile acid uptake, while SLCO1B2 plays a key role in unconjugated bile acid uptake [66, 67]. *Abcc3* and *Abcc4*, which are responsible for bile acid efflux from hepatocytes into systemic circulation, were induced 1.8- and 58.1-fold at 30 µg/kg TCDD (Figure 21). Collectively, repression of hepatic importers combined with induction of hepatic exporters likely contributed to the 45.4-fold increase in total serum bile acids.

Approximately 95% of bile acids secreted into the intestinal lumen are reabsorbed with the remaining 5% lost via fecal excretion [18]. Highly efficient enterohepatic circulation allows the liver to maintain a low rate of *de novo* primary bile acid biosynthesis. At 30 µg/kg TCDD, sugar probe analysis revealed a 2.4- and 2.0-fold increase in gastroduodenal and colonic para-cellular (i.e. between enterocytes) permeability, respectively, while the permeability of the small intestine was unaffected (Figure 22A-C). Furthermore, whole gut transit time increased from 2.5h in controls to 4.1h in 30 µg/kg TCDD-treated mice, indicating a 1.6-fold reduction in gut motility (Figure 22D-E). Induction of active ileal transporters (*Slc10a2*, *Slc51a*), increased passive para-cellular duodenal and colonic transport, and decreased gut motility are in accordance with increased intestinal reabsorption and decreased fecal excretion of bile acids. These changes in intestinal function are also consistent with TCDD-elicited increases in total serum bile acids and decreases in total fecal bile acids.

Microbial bile acid metabolism

Bile acids not reabsorbed by ileal enterocytes are metabolized by microbiota in the colon, the intestinal segment with the densest and most diverse microbial population. Various bacterial genera metabolize primary and conjugated primary bile acids to yield “secondary” bile acids. Bacterial bile salt hydrolase (BSH) cleaves the C24 N-acyl amide bond of conjugated bile acids, removing the glycine or taurine moiety. Several gut bacterial genera express *bsh* including *Bacteroides*, *Bifidobacterium*, *Clostridium*, *Lactobacillus*, and *Listeria* [68]. The exposed 7-hydroxyl groups of unconjugated CA and CDCA are susceptible to bacterially-catalyzed 7α-

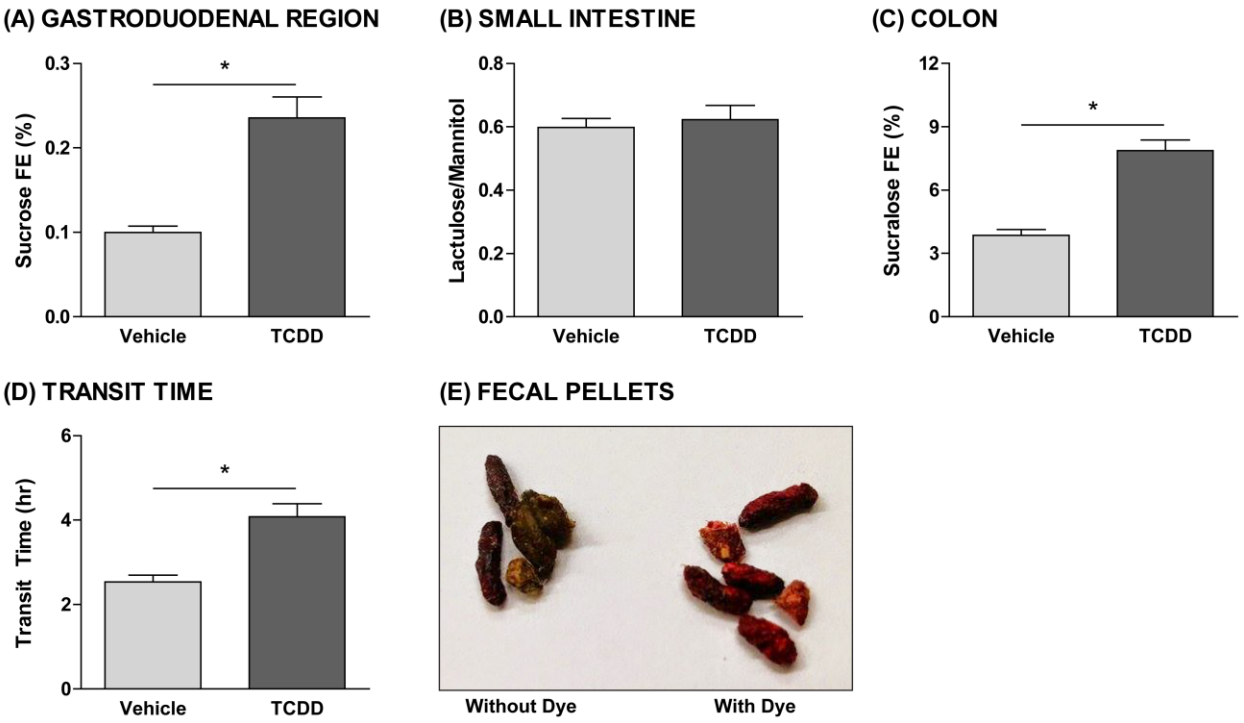

FIGURE 22. EFFECTS OF TCDD ON INTESTINAL PERMEABILITY AND MOTILITY

Para-cellular permeability of the (A) gastroduodenal region, (B) small intestine, and (C) colon in male C57BL/6 mice orally gavaged with sesame oil vehicle or 30 µg/kg TCDD every 4 days. At 26 days after the initial dose, mice were orally gavaged with sucrose, lactulose, mannitol, and sucralose to assess segment-specific intestinal permeability. Urine was collected over a 5-hour period, and fractional excretion (FE) of the probes was measured using ultra high performance liquid chromatography (UPLC) tandem mass spectrometry (MS/MS). (D) Whole gut transit time of male C57BL/6 mice orally gavaged with sesame oil vehicle or 30 µg/kg TCDD every 4 days. At 27 days after the initial dose, transit time was monitored by orally gavaging mice with Carmine Red and then measuring the interval between the gavage and the first observance of dye in the fecal pellets. (E) Fecal pellets collected from mice following oral gavage with Carmine Red dye (right) compared to pellets lacking the dye (left). Bars represent the average ± standard error of the mean for at least 6 biological replicates. Statistical significance (* $p \leq 0.05$) was determined using a Student's t-test performed in SAS 9.3.

dehydroxylation, yielding the secondary bile acids DCA and lithocholic acid (LCA), respectively. Bile acid 7α-dehydroxylation is a multi-step enzymatic process involving a set of genes encoded within the bile acid-inducible (*bai*) operon including *baiCD*, the oxidoreductase enzyme which catalyzes 3-dehydro-4-bile acid oxidation [69]. To date, 7α-dehydroxylation activity has only been identified in the *Clostridium* and *Eubacterium* genera [68].

As opposed to evaluating changes in the abundance of specific bacterial species associated with bile acid metabolism, we examined changes in the levels of *bsh* and *baiCD*, the loci responsible for bile acid deconjugation and dehydroxylation, respectively. Bacterial DNA extracted from fecal pellets was analyzed by qRT-PCR using computationally-designed degenerate primer sets. Overall, *bsh* gene levels within phylogenetic groups 1, 2, and 3 were increased, while levels within phylogenetic group 4 were unaffected by TCDD (Figure 23A). In particular, primer sets 7 and 8 within group 1 increased 21.8- and 7.3-fold, respectively, while primer sets 2 and 11 within group 2 increased 7.6- and 7.5-fold, respectively, and primer set 9 within group 3 increased 4.2-fold at 30 μg/kg TCDD. These primer sets primarily target *Lactobacillus* (Group1-Primer7; Group2-Primer2; Group2-Primer11), *Clostridium* (Group1-Primer8), *Streptococcus* (Group2-Primer11), and *Listeria* (Group3-Primer9) species, suggesting TCDD increased the relative abundance of several species within these genera. Primers targeting *Clostridium baiCD* [52, 53] identified a 2.1-fold increase at 30 μg/kg TCDD (Figure 23B), suggesting increased relative abundance of *Clostridium* strains known to exhibit 7α-dehydroxylation activity. Similarly, 7 of the 8 degenerate primer sets designed to target *baiCD* across the gut microbiome exhibited increased levels (1.5- to 2.5-fold). Consistent with these results, TCDD is reported to increase the abundance of several *Lactobacillus* and *Clostridium* species in the mouse gut microbiota [70]. Together, these results suggest that TCDD increased deconjugation and 7α-dehydroxylation activity within the gut microbiota, consistent with increased secondary bile acids such as DCA in the serum and increased conjugated secondary bile acids such as TLCA and GDCA in the liver (Figure 24).

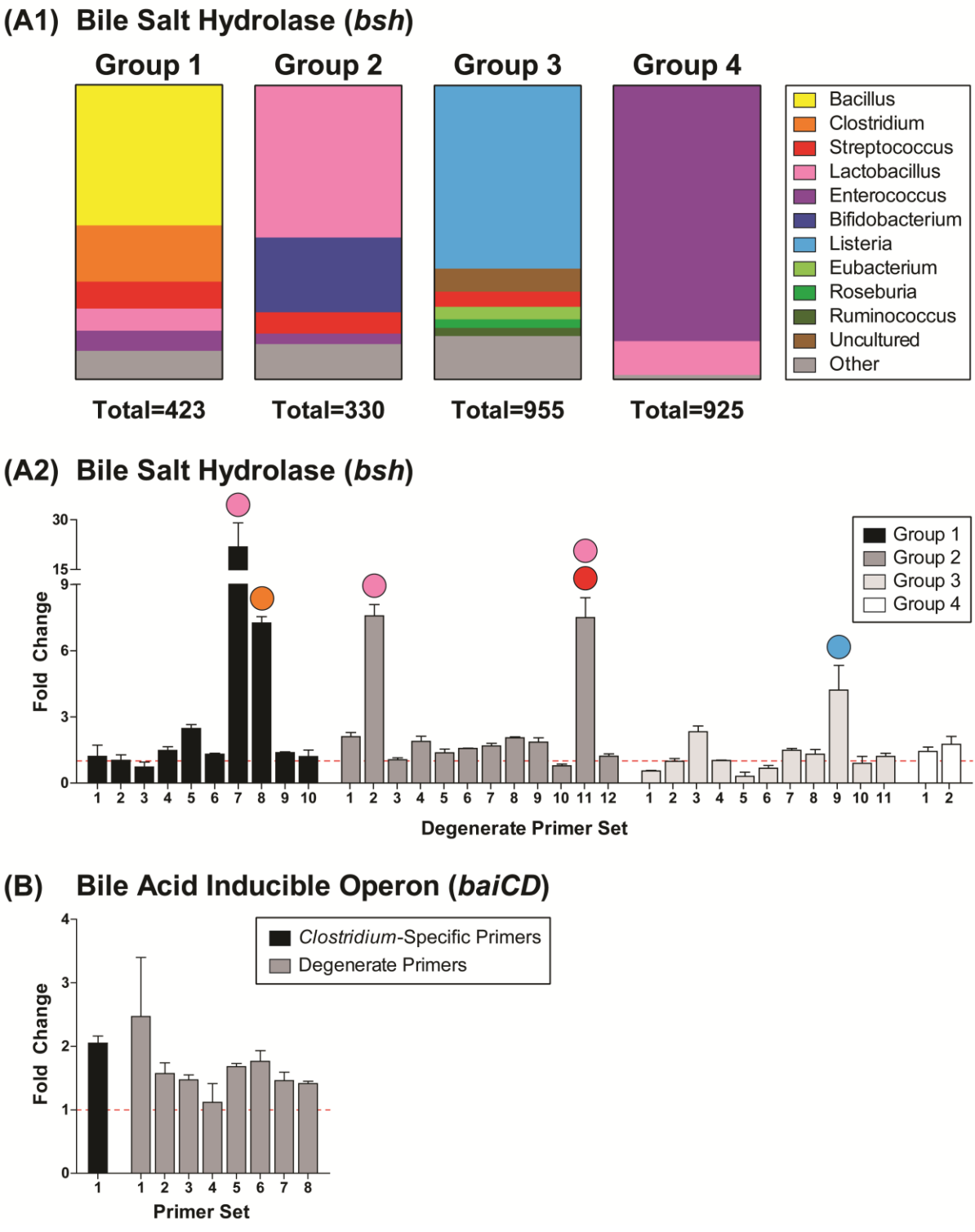

FIGURE 23. EFFECTS OF TCDD ON BACTERIAL GENES INVOLVED IN BILE ACID METABOLISM

FIGURE 23 (cont'd)

(A1) Bacterial classifications (genus level) of the *bsh* sequences in each phylogenetic group, which were separated based on nucleotide similarity. Degenerate qRT-PCR analysis of (A2) bile salt hydrolase (*bsh*) and (B) bile acid-inducible operon (*baiCD*) gene levels in the fecal pellets of male C57BL/6 mice orally gavaged with sesame oil vehicle or 30 µg/kg TCDD every 4 days for 28 days. Fecal levels of *baiCD* were also quantified using a primer set previously validated to target several *Clostridium* species which exhibit 7α-dehydroxylation activity (B: black bar). Colored circles above highly increased *bsh* primer sets indicate the bacterial genus which is primarily targeted. Values were normalized to levels of the 16S ribosomal RNA gene. Bars represent the average fold change relative to vehicle controls ± standard error of the mean. Fecal pellets were collected from two cages of co-housed mice for each treatment group (n=2) and therefore statistical analysis was not performed.

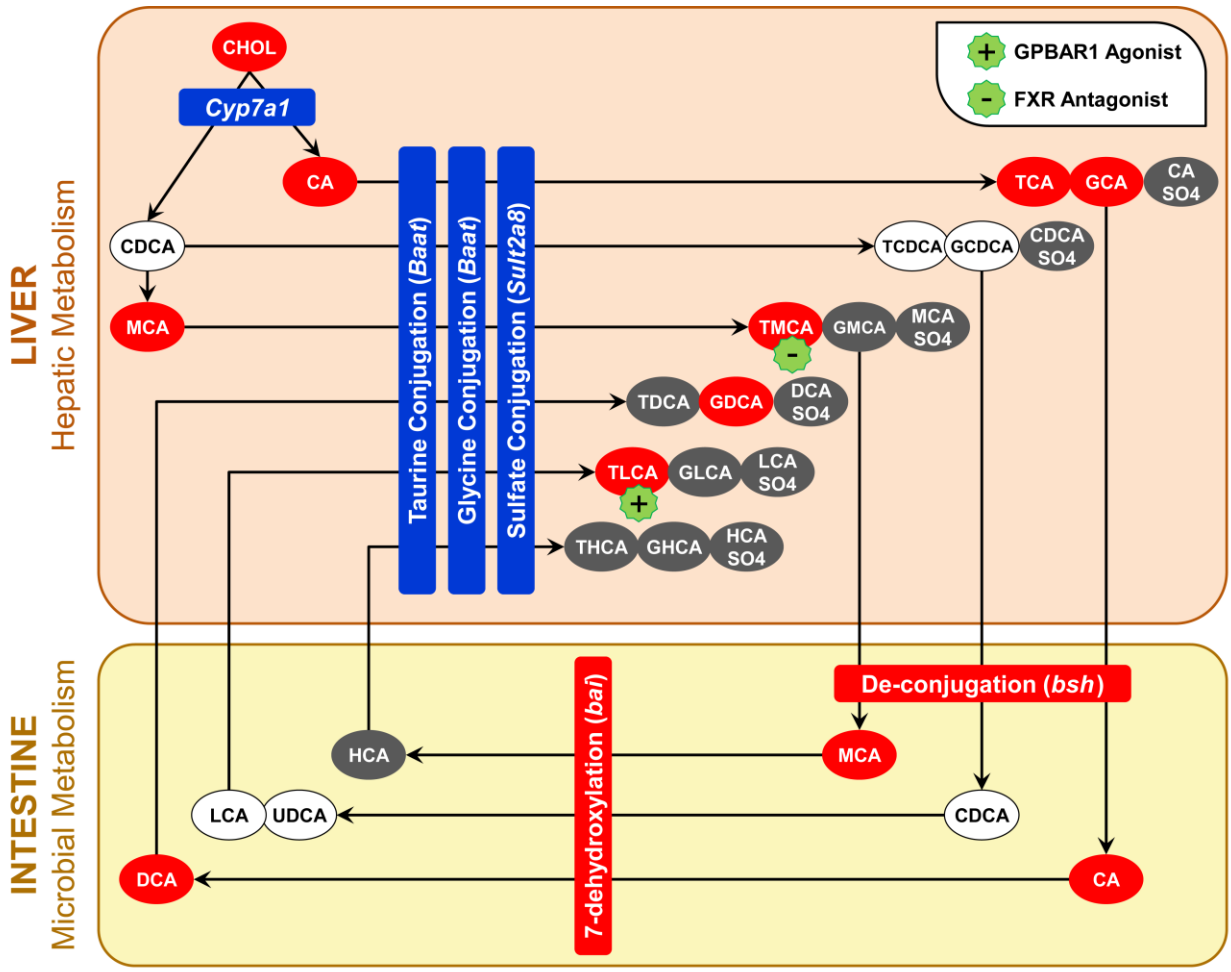

FIGURE 24. THE EFFECT OF TCDD ON THE HEPATIC AND MICROBIAL METABOLISM OF INDIVIDUAL BILE ACID SPECIES

Male C57BL/6 mice were orally gavaged with sesame oil vehicle or TCDD every 4 days for 28 days. Ovals represent bile acid species, while rectangles represent genes involved in bile acid metabolism. Placement of genes within the ‘liver’ and ‘intestine’ boxes represents the location of the metabolic reaction and the source of the enzyme involved. Red represents ‘increased levels’, blue represents ‘decreased levels’, white represents ‘no change’, and grey represents ‘not detected’. The color of each bile acid depicts the direction of change within the liver and/or serum relative to vehicle controls.

DISCUSSION

The effects of TCDD and related compounds on bile acid levels have been previously reported in a wide variety of rodent models using various treatment regimens [22, 23, 26, 55, 71, 72]. This study further elucidates AhR-mediated dysregulation of bile acid homeostasis in C57BL/6 mice by mapping complementary metabolomics, RNA-Seq, histopathology, and phenotypic data to bile acid biosynthesis, transport, and metabolism pathways. We demonstrate that TCDD altered primary and secondary bile acid profiles, consistent with changes in bile acid transport, gut microbiota metabolism, and intestinal permeability and motility.

In this study, TCDD dose-dependently increased total bile acid levels in the liver and serum, as previously reported in rodent studies involving AhR agonists [22, 23, 55, 71]. This is in accordance with the hepatic accumulation of cholesterol and cholesterol-esters, and may represent an adverse consequence of the liver's attempt to minimize potential lipotoxicity through the removal of excess cholesterol. Paradoxically, the majority of genes associated with bile acid biosynthesis exhibited dose-dependent repression including the rate-limiting enzyme *Cyp7a1*, *Cyp7b1* of the alternative pathway, and *Baat*, which catalyzes taurine/glycine-conjugation. AhR-mediated repression of *Cyp7a1* has been previously reported [13, 26, 27, 72], although TCDF is reported to induce *Cyp7a1* mRNA and increase CYP7A1 protein [71]. Interestingly, AhR binding was enriched upstream of the *Cyp7a1* transcription start site in both male and female mice, in the absence of a pDRE.

Bile acid biosynthesis is regulated by negative feedback involving FXR activation. Bile acid-activated FXR induces hepatic *Nr0b2* (encodes SHP), which interacts with LRH-1 and inhibits *Cyp7a1* expression [73]. Moreover, in the distal ileum, activated FXR induces *Fgf15* which binds to hepatic FGFR4/KLB to inhibit *Cyp7a1* expression. However, *Nr1h4* (encodes FXR), *Nr0b2*, *Fgfr4*, and *Klb* were all repressed by TCDD, while *Fgf15* exhibited no clear expression pattern. Related AhR agonists including TCDF and flutamide also repress *Nr1h4* and *Nr0b2* [71, 74]. Furthermore, hepatic CDCA levels, the most potent FXR agonist, were negligible, while

TCDD increased hepatic levels of T-α-MCA, a competitive FXR antagonist. Together, these results suggest that TCDD disrupts bile acid-induced feedback inhibition possibly by inhibiting the FXR signaling pathway.

In contrast to biosynthesis, TCDD-elicited differential expression of genes associated with enterohepatic circulation and transport is consistent with serum and hepatic bile acid accumulation. As previously reported [27, 75], TCDD repressed hepatic *Abcb11* (*Bsep*), which is responsible for transporting newly synthesized primary bile acids from hepatocytes to bile canaliculi. This would impair bile collection within the gallbladder, causing accumulation within hepatocytes and eventual spill over into sinusoidal blood. Inhibition of FXR signaling may be responsible for repression of *Abcb11*, a known FXR target gene. TCDD also repressed transporters involved in hepatic uptake from the blood (*Slco1a1*, *Slc10a1*, *Slco2b1*, *Slco1b2*, and *Slco1a4*) and induced hepatic efflux transporters (*Abcc4*, *Abcc3*). Accordingly, bile acid accumulation was greater in the serum compared to the liver. Serum bile acid accumulation may also be facilitated by enhanced enterocyte uptake (*Slc10a2*) and efflux (*Slc51a*), as well as passive reabsorption due to reduced gut motility and increased intestinal para-cellular permeability. As a result, TCDD reduced fecal bile acid levels, although impaired gallbladder emptying may also be a contributing factor. Overall, AhR-mediated differential expression of bile acid transporters is consistent with bile acid accumulation, as well as reduced bile flow and biliary excretion in TCDD-treated rodents [24].

Increased secondary bile acid levels provide indirect evidence of microbial bile acid metabolism and changes in the gut microbiota. qRT-PCR analysis of bacterial bile acid metabolism loci revealed that TCDD increased fecal levels of *bsh* and the *bai* operon, suggesting increased gut microbiota deconjugation and dehydroxylation activity. Accordingly, serum levels of secondary bile acids such as DCA and hepatic levels of conjugated secondary bile acids including TLCA and GDCA were increased by TCDD. Decreased gut motility may also facilitate bacterial metabolism and the passive reabsorption of hydrophobic secondary bile acids.

TCDD shifted the hepatic HIx towards increased hydrophobicity, which correlates with hepatotoxicity due to membrane disruption, ROS generation, induction of pro-inflammatory mediators, and the activation of necrotic signaling. Specifically, TLCA, a conjugated secondary bile acid species with a hydrophobicity index of 1.00, exhibited the greatest hepatic increase in response to TCDD. TLCA induces cholestasis by impairing hepatobiliary exocytosis, inhibiting the insertion of transport proteins into apical membranes, and disrupting bile flow [29, 76, 77]. It is also the most potent endogenous agonist of GPBAR1, a metabotrophic receptor highly expressed on bile duct cholangiocytes [28]. TLCA activation of GPBAR1 induces cholangiocyte proliferation through: (i) generation of ROS which activate Rous sarcoma oncogene (cSrc), epidermal growth factor receptor (EGFR), and ERK1/2, and (ii) inhibition of apoptosis through phosphorylation of the CD95 death receptor [29]. Therefore, increased levels of hepatic TLCA and other hydrophobic bile acids may contribute to TCDD-elicited hepatotoxicity by inducing bile duct proliferation and impairing bile flow.

Collectively, these results suggest that bile acid accumulation, enhanced enterohepatic circulation, and alterations in microbial metabolism contribute to TCDD-elicited hepatotoxicity and the progression of hepatic steatosis to steatohepatitis with fibrosis. Numerous studies involving whole-body AhR knockout mice have demonstrated that AhR activation is required for TCDD-elicited hepatotoxicity including bile duct proliferation [15, 78]. Other AhR ligands (TCDF, OCDD, PeCDF, and flutamide) also dysregulate bile acid homeostasis [22, 23, 71, 74]. Collectively, the presence of DREs, AhR enrichment, and dose-dependent induction/repression of key genes associated with bile acid homeostasis, provide compelling evidence that these effects are AhR mediated. However, hepatocyte-specific conditional AhR knockout studies would be required to unequivocally demonstrate the role of AhR activation in TCDD-elicited dysregulation of bile acid homeostasis.

In addition to effects on bile acid homeostasis, TCDD also disrupts other hepatic processes and metabolic pathways including lipid metabolism [13, 79], iron homeostasis and

heme metabolism [39], extracellular matrix deposition and remodeling [16], and antioxidant defenses [40]. Accumulating evidence suggests AhR-mediated hepatotoxicity is a cumulative response to the overall burden of multiple disrupted metabolic pathways, rather than a single event. Further studies are required to determine whether TCDD and related compounds elicit comparable metabolic effects in human models.

REFERENCES

REFERENCES

1. Vanni, E., E. Bugianesi, A. Kotronen, S. De Minicis, H. Yki-Jarvinen, and G. Svegliati-Baroni, *From the metabolic syndrome to NAFLD or vice versa?* Dig Liver Dis, 2010. 42(5): p. 320-30.

2. Ford, E.S., C. Li, and G. Zhao, *Prevalence and correlates of metabolic syndrome based on a harmonious definition among adults in the US.* J Diabetes, 2010. 2(3): p. 180-93.

3. Trauner, M., M. Arrese, and M. Wagner, *Fatty liver and lipotoxicity.* Biochim Biophys Acta, 2010. 1801(3): p. 299-310.

4. Taylor, K.W., R.F. Novak, H.A. Anderson, L.S. Birnbaum, C. Blystone, M. Devito, D. Jacobs, J. Kohrle, D.H. Lee, L. Rylander, A. Rignell-Hydbom, R. Tornero-Velez, M.E. Turyk, A.L. Boyles, K.A. Thayer, and L. Lind, *Evaluation of the Association between Persistent Organic Pollutants (POPs) and Diabetes in Epidemiological Studies: A National Toxicology Program Workshop Review.* Environ Health Perspect, 2013. 121(7): p. 774-83.

5. Casals-Casas, C. and B. Desvergne, *Endocrine disruptors: from endocrine to metabolic disruption.* Annu Rev Physiol, 2011. 73: p. 135-62.

6. Grun, F. and B. Blumberg, *Endocrine disrupters as obesogens.* Mol Cell Endocrinol, 2009. 304(1-2): p. 19-29.

7. Denison, M.S. and S.R. Nagy, *Activation of the aryl hydrocarbon receptor by structurally diverse exogenous and endogenous chemicals.* Annu Rev Pharmacol Toxicol, 2003. 43: p. 309-34.

8. Hankinson, O., *The aryl hydrocarbon receptor complex.* Annu Rev Pharmacol Toxicol, 1995. 35: p. 307-40.

9. Huang, G. and C.J. Elferink, *A novel nonconsensus xenobiotic response element capable of mediating aryl hydrocarbon receptor-dependent gene expression.* Mol Pharmacol, 2012. 81(3): p. 338-47.

10. Beischlag, T.V., J. Luis Morales, B.D. Hollingshead, and G.H. Perdew, *The aryl hydrocarbon receptor complex and the control of gene expression.* Crit Rev Eukaryot Gene Expr, 2008. 18(3): p. 207-50.

11. Safe, S., *Polychlorinated biphenyls (PCBs), dibenzo-p-dioxins (PCDDs), dibenzofurans (PCDFs), and related compounds: environmental and mechanistic considerations which support the development of toxic equivalency factors (TEFs).* Crit Rev Toxicol, 1990. 21(1): p. 51-88.

12. Denison, M.S., A.A. Soshilov, G. He, D.E. DeGroot, and B. Zhao, *Exactly the same but different: promiscuity and diversity in the molecular mechanisms of action of the aryl hydrocarbon (dioxin) receptor.* Toxicol Sci, 2011. 124(1): p. 1-22.

13. Boverhof, D.R., L.D. Burgoon, C. Tashiro, B. Chittim, J.R. Harkema, D.B. Jump, and T.R. Zacharewski, *Temporal and dose-dependent hepatic gene expression patterns in mice provide new insights into TCDD-Mediated hepatotoxicity.* Toxicol Sci, 2005. 85(2): p. 1048-63.

14. Jones, G. and J.B. Greig, *Pathological-Changes in Liver of Mice Given 2,3,7,8-Tetrachlorodibenzo-P-Dioxin.* Experientia, 1975. 31(11): p. 1315-1317.

15. Fernandez-Salguero, P.M., D.M. Hilbert, S. Rudikoff, J.M. Ward, and F.J. Gonzalez, *Aryl-hydrocarbon receptor-deficient mice are resistant to 2,3,7,8-tetrachlorodibenzo-p-dioxin-induced toxicity.* Toxicol Appl Pharmacol, 1996. 140(1): p. 173-9.

16. Nault, R., K.A. Fader, D.A. Ammendolia, P. Dornbos, D. Potter, B. Sharratt, K. Kumagai, J.R. Harkema, S.Y. Lunt, J. Matthews, and T. Zacharewski, *Dose-Dependent Metabolic Reprogramming and Differential Gene Expression in TCDD-Elicited Hepatic Fibrosis.* Toxicol Sci, 2016. 154(2): p. 253-266.

17. Pierre, S., A. Chevallier, F. Teixeira-Clerc, A. Ambolet-Camoit, L.C. Bui, A.S. Bats, J.C. Fournet, P. Fernandez-Salguero, M. Aggerbeck, S. Lotersztajn, R. Barouki, and X. Coumoul, *Aryl hydrocarbon receptor-dependent induction of liver fibrosis by dioxin.* Toxicol Sci, 2014. 137(1): p. 114-24.

18. Chiang, J.Y., *Bile acid metabolism and signaling.* Compr Physiol, 2013. 3(3): p. 1191-212.

19. Copple, B.L. and T. Li, *Pharmacology of bile acid receptors: Evolution of bile acids from simple detergents to complex signaling molecules.* Pharmacol Res, 2016. 104: p. 9-21.

20. Perez, M.J. and O. Briz, *Bile-acid-induced cell injury and protection.* World J Gastroenterol, 2009. 15(14): p. 1677-89.

21. Allen, K., H. Jaeschke, and B.L. Copple, *Bile acids induce inflammatory genes in hepatocytes: a novel mechanism of inflammation during obstructive cholestasis.* Am J Pathol, 2011. 178(1): p. 175-86.

22. Brewster, D.W., L.C. Uraih, and L.S. Birnbaum, *The acute toxicity of 2,3,4,7,8-pentachlorodibenzofuran (4PeCDF) in the male Fischer rat.* Fundam Appl Toxicol, 1988. 11(2): p. 236-49.

23. Couture, L.A., M.R. Elwell, and L.S. Birnbaum, *Dioxin-like effects observed in male rats following exposure to octachlorodibenzo-p-dioxin (OCDD) during a 13-week study.* Toxicol Appl Pharmacol, 1988. 93(1): p. 31-46.

24. Yang, K.H., W.A. Croft, and R.E. Peterson, *Effects of 2,3,7,8-tetrachlorodibenzo-p-dioxin on plasma disappearance and biliary excretion of foreign compounds in rats.* Toxicol Appl Pharmacol, 1977. 40(3): p. 485-96.

25. Vos, J.G., J.A. Moore, and J.G. Zinkl, *Toxicity of 2,3,7,8-tetrachlorodibenzo-p-dioxin (TCDD) in C57B1/6 mice.* Toxicol Appl Pharmacol, 1974. 29(2): p. 229-41.

26. Fletcher, N., D. Wahlstrom, R. Lundberg, C.B. Nilsson, K.C. Nilsson, K. Stockling, H. Hellmold, and H. Hakansson, *2,3,7,8-Tetrachlorodibenzo-p-dioxin (TCDD) alters the*

mRNA expression of critical genes associated with cholesterol metabolism, bile acid biosynthesis, and bile transport in rat liver: a microarray study. Toxicol Appl Pharmacol, 2005. 207(1): p. 1-24.

27. Ozeki, J., S. Uno, M. Ogura, M. Choi, T. Maeda, K. Sakurai, S. Matsuo, S. Amano, D.W. Nebert, and M. Makishima, *Aryl hydrocarbon receptor ligand 2,3,7,8-tetrachlorodibenzo-p-dioxin enhances liver damage in bile duct-ligated mice.* Toxicology, 2011. 280(1-2): p. 10-7.

28. Sato, H., A. Macchiarulo, C. Thomas, A. Gioiello, M. Une, A.F. Hofmann, R. Saladin, K. Schoonjans, R. Pellicciari, and J. Auwerx, *Novel potent and selective bile acid derivatives as TGR5 agonists: biological screening, structure-activity relationships, and molecular modeling studies.* J Med Chem, 2008. 51(6): p. 1831-41.

29. Reich, M., K. Deutschmann, A. Sommerfeld, C. Klindt, S. Kluge, R. Kubitz, C. Ullmer, W.T. Knoefel, D. Herebian, E. Mayatepek, D. Haussinger, and V. Keitel, *TGR5 is essential for bile acid-dependent cholangiocyte proliferation in vivo and in vitro.* Gut, 2016. 65(3): p. 487-501.

30. Sorg, O., M. Zennegg, P. Schmid, R. Fedosyuk, R. Valikhnovskyi, O. Gaide, V. Kniazevych, and J.H. Saurat, *2,3,7,8-tetrachlorodibenzo-p-dioxin (TCDD) poisoning in Victor Yushchenko: identification and measurement of TCDD metabolites.* Lancet, 2009. 374(9696): p. 1179-85.

31. Wolfe, W.H., J.E. Michalek, J.C. Miner, J.L. Pirkle, S.P. Caudill, D.G. Patterson, Jr., and L.L. Needham, *Determinants of TCDD half-life in veterans of operation ranch hand.* J Toxicol Environ Health, 1994. 41(4): p. 481-8.

32. Gasiewicz, T.A., L.E. Geiger, G. Rucci, and R.A. Neal, *Distribution, excretion, and metabolism of 2,3,7,8-tetrachlorodibenzo-p-dioxin in C57BL/6J, DBA/2J, and B6D2F1/J mice.* Drug Metab Dispos, 1983. 11(5): p. 397-403.

33. Fader, K.A., R. Nault, D.A. Ammendolia, J.R. Harkema, K.J. Williams, R.B. Crawford, N.E. Kaminski, D. Potter, B. Sharratt, and T.R. Zacharewski, *2,3,7,8-Tetrachlorodibenzo-p-Dioxin Alters Lipid Metabolism and Depletes Immune Cell Populations in the Jejunum of C57BL/6 Mice.* Toxicol Sci, 2015. 148(2): p. 567-80.

34. Everson, G.T., D.Z. Braverman, M.L. Johnson, and F. Kern, Jr., *A critical evaluation of real-time ultrasonography for the study of gallbladder volume and contraction.* Gastroenterology, 1980. 79(1): p. 40-6.

35. Wang, H.H., P. Portincasa, M. Liu, P. Tso, L.C. Samuelson, and D.Q. Wang, *Effect of gallbladder hypomotility on cholesterol crystallization and growth in CCK-deficient mice.* Biochim Biophys Acta, 2010. 1801(2): p. 138-46.

36. Kopec, A.K., L.D. Burgoon, D. Ibrahim-Aibo, B.D. Mets, C. Tashiro, D. Potter, B. Sharratt, J.R. Harkema, and T.R. Zacharewski, *PCB153-elicited hepatic responses in the immature, ovariectomized C57BL/6 mice: comparative toxicogenomic effects of dioxin and non-dioxin-like ligands.* Toxicol Appl Pharmacol, 2010. 243(3): p. 359-71.

37. Nault, R., D. Colbry, C. Brandenberger, J.R. Harkema, and T.R. Zacharewski, *Development of a computational high-throughput tool for the quantitative examination of dose-dependent histological features.* Toxicol Pathol, 2015. 43(3): p. 366-75.

38. Nault, R., K.A. Fader, and T. Zacharewski, *RNA-Seq versus oligonucleotide array assessment of dose-dependent TCDD-elicited hepatic gene expression in mice.* BMC Genomics, 2015. 16(1): p. 373.

39. Fader, K.A., R. Nault, M.P. Kirby, G. Markous, J. Matthews, and T.R. Zacharewski, *Convergence of hepcidin deficiency, systemic iron overloading, heme accumulation, and REV-ERBalpha/beta activation in aryl hydrocarbon receptor-elicited hepatotoxicity.* Toxicol Appl Pharmacol, 2017. 321: p. 1-17.

40. Nault, R., K.A. Fader, M.P. Kirby, S. Ahmed, J. Matthews, A.D. Jones, S.Y. Lunt, and T.R. Zacharewski, *Pyruvate Kinase Isoform Switching and Hepatic Metabolic Reprogramming by the Environmental Contaminant 2,3,7,8-Tetrachlorodibenzo-p-Dioxin.* Toxicol Sci, 2016. 149(2): p. 358-71.

41. Lo, R. and J. Matthews, *High-resolution genome-wide mapping of AHR and ARNT binding sites by ChIP-Seq.* Toxicol Sci, 2012. 130(2): p. 349-61.

42. Ji, H., H. Jiang, W. Ma, D.S. Johnson, R.M. Myers, and W.H. Wong, *An integrated software system for analyzing ChIP-chip and ChIP-seq data.* Nat Biotechnol, 2008. 26(11): p. 1293-300.

43. John, C., P. Werner, A. Worthmann, K. Wegner, K. Todter, L. Scheja, S. Rohn, J. Heeren, and M. Fischer, *A liquid chromatography-tandem mass spectrometry-based method for the simultaneous determination of hydroxy sterols and bile acids.* J Chromatogr A, 2014. 1371: p. 184-95.

44. Swann, J.R., E.J. Want, F.M. Geier, K. Spagou, I.D. Wilson, J.E. Sidaway, J.K. Nicholson, and E. Holmes, *Systemic gut microbial modulation of bile acid metabolism in host tissue compartments.* Proc Natl Acad Sci U S A, 2011. 108 Suppl 1: p. 4523-30.

45. Lydic, T.A., J.V. Busik, and G.E. Reid, *A monophasic extraction strategy for the simultaneous lipidome analysis of polar and nonpolar retina lipids.* J Lipid Res, 2014. 55(8): p. 1797-809.

46. Melamud, E., L. Vastag, and J.D. Rabinowitz, *Metabolomic analysis and visualization engine for LC-MS data.* Anal Chem, 2010. 82(23): p. 9818-26.

47. Haimi, P., A. Uphoff, M. Hermansson, and P. Somerharju, *Software tools for analysis of mass spectrometric lipidome data.* Anal Chem, 2006. 78(24): p. 8324-31.

48. Kessner, D., M. Chambers, R. Burke, D. Agus, and P. Mallick, *ProteoWizard: open source software for rapid proteomics tools development.* Bioinformatics, 2008. 24(21): p. 2534-6.

49. Arrieta, M.C., L. Bistritz, and J.B. Meddings, *Alterations in intestinal permeability.* Gut, 2006. 55(10): p. 1512-20.

50. Teshima, C.W. and J.B. Meddings, *The measurement and clinical significance of intestinal permeability.* Curr Gastroenterol Rep, 2008. 10(5): p. 443-9.

51. Fish, J.A., B. Chai, Q. Wang, Y. Sun, C.T. Brown, J.M. Tiedje, and J.R. Cole, *FunGene: the functional gene pipeline and repository.* Front Microbiol, 2013. 4: p. 291.

52. Wells, J.E., K.B. Williams, T.R. Whitehead, D.M. Heuman, and P.B. Hylemon, *Development and application of a polymerase chain reaction assay for the detection and enumeration of bile acid 7alpha-dehydroxylating bacteria in human feces.* Clin Chim Acta, 2003. 331(1-2): p. 127-34.

53. Ou, J., F. Carbonero, E.G. Zoetendal, J.P. DeLany, M. Wang, K. Newton, H.R. Gaskins, and S.J. O'Keefe, *Diet, microbiota, and microbial metabolites in colon cancer risk in rural Africans and African Americans.* Am J Clin Nutr, 2013. 98(1): p. 111-20.

54. Muyzer, G., E.C. de Waal, and A.G. Uitterlinden, *Profiling of complex microbial populations by denaturing gradient gel electrophoresis analysis of polymerase chain reaction-amplified genes coding for 16S rRNA.* Appl Environ Microbiol, 1993. 59(3): p. 695-700.

55. Birnbaum, L.S., M.M. McDonald, P.C. Blair, A.M. Clark, and M.W. Harris, *Differential toxicity of 2,3,7,8-tetrachlorodibenzo-p-dioxin (TCDD) in C57BL/6J mice congenic at the Ah Locus.* Fundam Appl Toxicol, 1990. 15(1): p. 186-200.

56. McConnell, E.E., J.A. Moore, J.K. Haseman, and M.W. Harris, *The comparative toxicity of chlorinated dibenzo-p-dioxins in mice and guinea pigs.* Toxicol Appl Pharmacol, 1978. 44(2): p. 335-56.

57. Nault, R., K.A. Fader, T.A. Lydic, and T.R. Zacharewski, *Lipidomic Evaluation of Aryl Hydrocarbon Receptor-Mediated Hepatic Steatosis in Male and Female Mice Elicited by 2,3,7,8-Tetrachlorodibenzo-p-dioxin.* Chem Res Toxicol, 2017. 30(4): p. 1060-1075.

58. Botham, K.M. and G.S. Boyd, *The metabolism of chenodeoxycholic acid to beta-muricholic acid in rat liver.* Eur J Biochem, 1983. 134(1): p. 191-6.

59. Sayin, S.I., A. Wahlstrom, J. Felin, S. Jantti, H.U. Marschall, K. Bamberg, B. Angelin, T. Hyotylainen, M. Oresic, and F. Backhed, *Gut microbiota regulates bile acid metabolism by reducing the levels of tauro-beta-muricholic acid, a naturally occurring FXR antagonist.* Cell Metab, 2013. 17(2): p. 225-35.

60. Billington, D., C.E. Evans, P.P. Godfrey, and R. Coleman, *Effects of bile salts on the plasma membranes of isolated rat hepatocytes.* Biochem J, 1980. 188(2): p. 321-7.

61. Palmer, R.H., *Bile acids, liver injury, and liver disease.* Arch Intern Med, 1972. 130(4): p. 606-17.

62. Hofmann, A.F. and A. Roda, *Physicochemical properties of bile acids and their relationship to biological properties: an overview of the problem.* J Lipid Res, 1984. 25(13): p. 1477-89.

63. Heuman, D.M., *Quantitative estimation of the hydrophilic-hydrophobic balance of mixed bile salt solutions.* J Lipid Res, 1989. 30(5): p. 719-30.

64. Araya, Z. and K. Wikvall, *6alpha-hydroxylation of taurochenodeoxycholic acid and lithocholic acid by CYP3A4 in human liver microsomes.* Biochim Biophys Acta, 1999. 1438(1): p. 47-54.

65. Xie, W., A. Radominska-Pandya, Y. Shi, C.M. Simon, M.C. Nelson, E.S. Ong, D.J. Waxman, and R.M. Evans, *An essential role for nuclear receptors SXR/PXR in detoxification of cholestatic bile acids.* Proc Natl Acad Sci U S A, 2001. 98(6): p. 3375-80.

66. Meier, P.J. and B. Stieger, *Bile salt transporters.* Annu Rev Physiol, 2002. 64: p. 635-61.

67. Csanaky, I.L., H. Lu, Y. Zhang, K. Ogura, S. Choudhuri, and C.D. Klaassen, *Organic anion-transporting polypeptide 1b2 (Oatp1b2) is important for the hepatic uptake of unconjugated bile acids: Studies in Oatp1b2-null mice.* Hepatology, 2011. 53(1): p. 272-81.

68. Gérard, P., *Metabolism of Cholesterol and Bile Acids by the Gut Microbiota.* Pathogens, 2014. 3(1): p. 14-24.

69. Ridlon, J.M. and P.B. Hylemon, *Identification and characterization of two bile acid coenzyme A transferases from Clostridium scindens, a bile acid 7alpha-dehydroxylating intestinal bacterium.* J Lipid Res, 2012. 53(1): p. 66-76.

70. Lefever, D.E., J. Xu, Y. Chen, G. Huang, N. Tamas, and T.L. Guo, *TCDD modulation of gut microbiome correlated with liver and immune toxicity in streptozotocin (STZ)-induced hyperglycemic mice.* Toxicol Appl Pharmacol, 2016. 304: p. 48-58.

71. Zhang, L., R.G. Nichols, J. Correll, I.A. Murray, N. Tanaka, P.B. Smith, T.D. Hubbard, A. Sebastian, I. Albert, E. Hatzakis, F.J. Gonzalez, G.H. Perdew, and A.D. Patterson, *Persistent Organic Pollutants Modify Gut Microbiota-Host Metabolic Homeostasis in Mice Through Aryl Hydrocarbon Receptor Activation.* Environ Health Perspect, 2015. 123(7): p. 679-88.

72. Kakizuka, S., T. Takeda, Y. Komiya, A. Koba, H. Uchi, M. Yamamoto, M. Furue, Y. Ishii, and H. Yamada, *Dioxin-Produced Alteration in the Profiles of Fecal and Urinary Metabolomes: A Change in Bile Acids and Its Relevance to Toxicity.* Biol Pharm Bull, 2015. 38(10): p. 1484-95.

73. Wahlstrom, A., S.I. Sayin, H.U. Marschall, and F. Backhed, *Intestinal Crosstalk between Bile Acids and Microbiota and Its Impact on Host Metabolism.* Cell Metab, 2016. 24(1): p. 41-50.

74. Gao, X., C. Xie, Y. Wang, Y. Luo, T. Yagai, D. Sun, X. Qin, K.W. Krausz, and F.J. Gonzalez, *The antiandrogen flutamide is a novel aryl hydrocarbon receptor ligand that disrupts bile acid homeostasis in mice through induction of Abcc4.* Biochem Pharmacol, 2016.

75. Iwanaga, T., M. Nakakariya, H. Yabuuchi, T. Maeda, and I. Tamai, *Involvement of bile salt export pump in flutamide-induced cholestatic hepatitis.* Biol Pharm Bull, 2007. 30(4): p. 739-44.

76. Javitt, N.B. and S. Emerman, *Effect of sodium taurolithocholate on bile flow and bile acid exeretion.* J Clin Invest, 1968. 47(5): p. 1002-14.

77. Beuers, U., G.U. Denk, C.J. Soroka, R. Wimmer, C. Rust, G. Paumgartner, and J.L. Boyer, *Taurolithocholic acid exerts cholestatic effects via phosphatidylinositol 3-kinase-dependent mechanisms in perfused rat livers and rat hepatocyte couplets.* J Biol Chem, 2003. 278(20): p. 17810-8.

78. Gonzalez, F.J. and P. Fernandez-Salguero, *The aryl hydrocarbon receptor: studies using the AHR-null mice.* Drug Metab Dispos, 1998. 26(12): p. 1194-8.

79. Angrish, M.M., C.Y. Dominici, and T.R. Zacharewski, *TCDD-elicited effects on liver, serum, and adipose lipid composition in C57BL/6 mice.* Toxicol Sci, 2013. 131(1): p. 108-15.

CHAPTER 5: CONVERGENCE OF HEPCIDIN DEFICIENCY, SYSTEMIC IRON OVERLOADING, HEME ACCUMULATION, AND REV-ERBα/β ACTIVATION IN ARYL HYDROCARBON RECEPTOR-ELICITED HEPATOTOXICITY

Fader, K.A., R. Nault, M.P. Kirby, G. Markous, J. Matthews, and T.R. Zacharewski, *Convergence of hepcidin deficiency, systemic iron overloading, heme accumulation, and REV-ERBalpha/beta activation in aryl hydrocarbon receptor-elicited hepatotoxicity.* Toxicol Appl Pharmacol, 2017. 321: p. 1-17.

ABSTRACT

Persistent aryl hydrocarbon receptor (AhR) agonists elicit dose-dependent hepatic lipid accumulation, oxidative stress, inflammation, and fibrosis in mice. Iron (Fe) promotes AhR-mediated oxidative stress by catalyzing reactive oxygen species (ROS) production. To further characterize the role of Fe in AhR-mediated hepatotoxicity, male C57BL/6 mice were orally gavaged with sesame oil vehicle or 0.01-30 µg/kg 2,3,7,8-tetrachlorodibenzo-*p*-dioxin (TCDD) every 4 days for 28 days. Duodenal epithelial and hepatic RNA-Seq data were integrated with hepatic AhR ChIP-Seq, capillary electrophoresis protein measurements, and clinical chemistry analyses. TCDD dose-dependently repressed hepatic expression of hepcidin (*Hamp* and *Hamp2*), the master regulator of systemic Fe homeostasis, resulting in a 2.6-fold increase in serum Fe with accumulating Fe spilling into urine. Total hepatic Fe levels were negligibly increased while transferrin saturation remained unchanged. Furthermore, TCDD elicited dose-dependent gene expression changes in heme biosynthesis including the induction of aminolevulinic acid synthase 1 (*Alas1*) and repression of uroporphyrinogen decarboxylase (*Urod*), leading to a 50% increase in hepatic hemin and a 13.2-fold increase in total urinary porphyrins. Consistent with this heme accumulation, differential gene expression suggests that heme activated BACH1 and REV-ERBα/β, causing induction of heme oxygenase 1 (*Hmox1*) and repression of fatty acid biosynthesis, respectively. Collectively, these results suggest that *Hamp* repression, Fe accumulation, and increased heme levels converge to promote oxidative stress and the progression of TCDD-elicited hepatotoxicity.

INTRODUCTION

Metabolic syndrome (MetS) is a multifactorial disease characterized by obesity, increased triacylglycerol (TAG) levels, decreased high density lipoprotein (HDL) cholesterol levels, hypertension, and hyperglycemia. In the liver, MetS is manifested as non-alcoholic fatty liver disease (NAFLD), where benign and reversible hepatic fat accumulation (steatosis) progresses

to chronic steatohepatitis (steatosis with inflammation) with fibrosis (collagen deposition) [1]. The worldwide prevalence of MetS and NAFLD is continuously increasing, currently affecting ~30% of adults in the United States [2]. Although genetics, high caloric diet, and sedentary lifestyle are major contributing factors, emerging evidence suggests exposure to environmental contaminants such as 2,3,7,8-tetrachlorodibenzo-*p*-dioxin (TCDD) and related compounds play an underappreciated role in the development of MetS and NAFLD [3].

TCDD is the prototypical ligand for a group of structurally diverse synthetic chemicals, natural products, and endogenous metabolites that activate the aryl hydrocarbon receptor (AhR) [4]. Upon ligand binding, the cytoplasmic AhR dissociates from chaperone proteins, followed by translocation to the nucleus and heterodimerization with the aryl hydrocarbon receptor nuclear translocator (ARNT). The AhR/ARNT complex acts as a transcription factor, altering gene expression through binding to dioxin response elements (DREs) [5], although DRE-independent mechanisms of differential gene expression have also been reported [6]. In mice, a single bolus dose of TCDD induces hepatic steatosis with immune cell infiltration [7, 8], which progresses to steatohepatitis with fibrosis following repeated dosing [9, 10]. TCDD-elicited hepatic inflammation and fibrosis are believed to be due, at least in part, to sustained oxidative stress mediated by AhR-dependent responses (reviewed in [11]).

Oxidative stress involves disruption of the balance between pro-oxidants and anti-oxidants, in which accumulating reactive oxygen species (ROS) overwhelm neutralizing defenses. In B6C3F1 mice, hepatic superoxide anion radical ($O_2^{\bullet-}$) production increased following a single acute dose of 10 µg/kg TCDD, while sub-chronic doses as low as 15 ng/kg/day TCDD also elevated ROS levels [12]. TCDD-elicited hepatic ROS production is stimulated via several processes including the infiltration of activated macrophages and other phagocytes, the induction of cytochrome P450s and oxidoreductases, increased number of mitochondria and the partial uncoupling of oxidative phosphorylation, peroxisome proliferation, xanthine dehydrogenase/xanthine oxidase (XDH/XO) induction, and the inhibition of selenium-dependent

glutathione (GSH) peroxidase. Increased production of hydrogen peroxide (H_2O_2), $O_2^{\bullet-}$, and hydroxyl radical ($^{\bullet}OH$) results in lipid peroxidation, DNA damage, decreased membrane fluidity, and altered levels of GSH and NADPH (reviewed in [11]).

Iron (Fe) is a micronutrient involved in several essential biological processes including oxygen transport, cellular respiration, and DNA synthesis. It is well established that Fe plays a fundamental role in TCDD-elicited hepatic oxidative stress. Cycling between the ferrous (Fe^{2+}) and ferric (Fe^{3+}) redox states allows Fe to catalyze the Haber-Weiss reaction, in which highly reactive $^{\bullet}OH$ is generated from H_2O_2 and $O_2^{\bullet-}$, leading to increased malondialdehyde (MDA) levels and other lipid peroxidation end products indicative of tissue damage and cell death. TCDD increased hepatic MDA levels in rats fed an Fe-supplemented diet, while Fe deficiency completely protected against MDA increases [13]. Similarly, *in vitro* lipid peroxidation in TCDD-treated rat hepatic microsomes was substantially reduced by desferrioxamine chelation [14], further demonstrating a role for Fe in TCDD-elicited hepatic lipid peroxidation. Additionally, Fe-catalyzed oxidative damage is considered to be a causal factor in the development of hepatic fibrosis and hepatocellular carcinoma [15, 16].

Previous studies report that AhR activation causes accumulation of Fe and heme precursors [17, 18], however the underlying mechanisms remain poorly understood. The objective of this study was to identify the altered biological processes and pathway interactions responsible for TCDD-elicited disruption of systemic Fe homeostasis and heme metabolism in mice. Using a systems biology approach, duodenal epithelial and hepatic RNA-Seq analyses were integrated with hepatic AhR ChIP-Seq data, capillary electrophoresis protein measurements, and clinical chemistry to investigate Fe absorption, transport, storage, and regulation. Our results demonstrate that TCDD repressed hepcidin, the master regulator of systemic iron homeostasis, leading to Fe accumulation in the serum and detection in urine. TCDD also altered hepatic heme biosynthesis and metabolism, leading to the activation of REV-ERBα/β, transcriptional repressors associated with the regulation of peripheral circadian rhythm and lipid metabolism. Taken

together, these results suggest that disruption of Fe homeostasis plays a key role in TCDD-elicited oxidative stress and the progression of steatosis to steatohepatitis with fibrosis in mice.

MATERIALS & METHODS

Animal handling and treatment

Postnatal day 25 (PND25) male C57BL/6 mice weighing within 10% of each other were obtained from Charles River Laboratories (Portage, MI) and housed in Innovive Innocages (San Diego, CA) containing ALPHA-dri bedding (Shepherd Specialty Papers, Chicago, IL) in a 23°C environment with 30-40% humidity and a 12-hour light/dark cycle (7am–7pm). Aquavive water (Innovive) and Harlan Teklad 22/5 Rodent Diet 8940 (Madison, WI) were provided *ad libitum*. Mice were acclimated for 4 days (d) prior to treatment. 4-week old mice were used because juveniles are more sensitive to TCDD compared to adults [19]. Animals (n=8) were orally gavaged with sesame oil vehicle (Sigma-Aldrich, St. Louis, MO), 0.01, 0.03, 0.1, 0.3, 1, 3, 10, or 30 μg/kg TCDD (AccuStandard, New Haven, CT) every 4d for a total of 28d (7 exposures; Figure 25). The doses used compensate for the relatively short duration of the study compared to lifelong cumulative human exposure from diverse AhR ligands, the bioaccumulative nature of halogenated AhR ligands, and differences in the metabolism and half-life of TCDD between humans (1-11 years [20, 21]) and mice (8-12d [22]). In addition, these doses result in hepatic tissue levels that span background serum concentrations reported in the United States, Germany, Spain, and the United Kingdom to serum levels reported in Viktor Yushchenko 4-39 months following poisoning [10]. Hepatic samples from female C57BL/6 mice treated with a single bolus dose of 3,3′,4,4′,5-pentachlorobiphenyl (PCB126; 3000 μg/kg), 2,3,7,8-tetrachlorodibenzofuran (TCDF; 3000 μg/kg), and 2,2′,4,4′,5,5′-hexachlorobiphenyl (PCB153; 300 mg/kg) were collected as previously described [8, 23]. All animal procedures were approved by the Michigan State University (MSU) All-University Committee on Animal Use and Care.

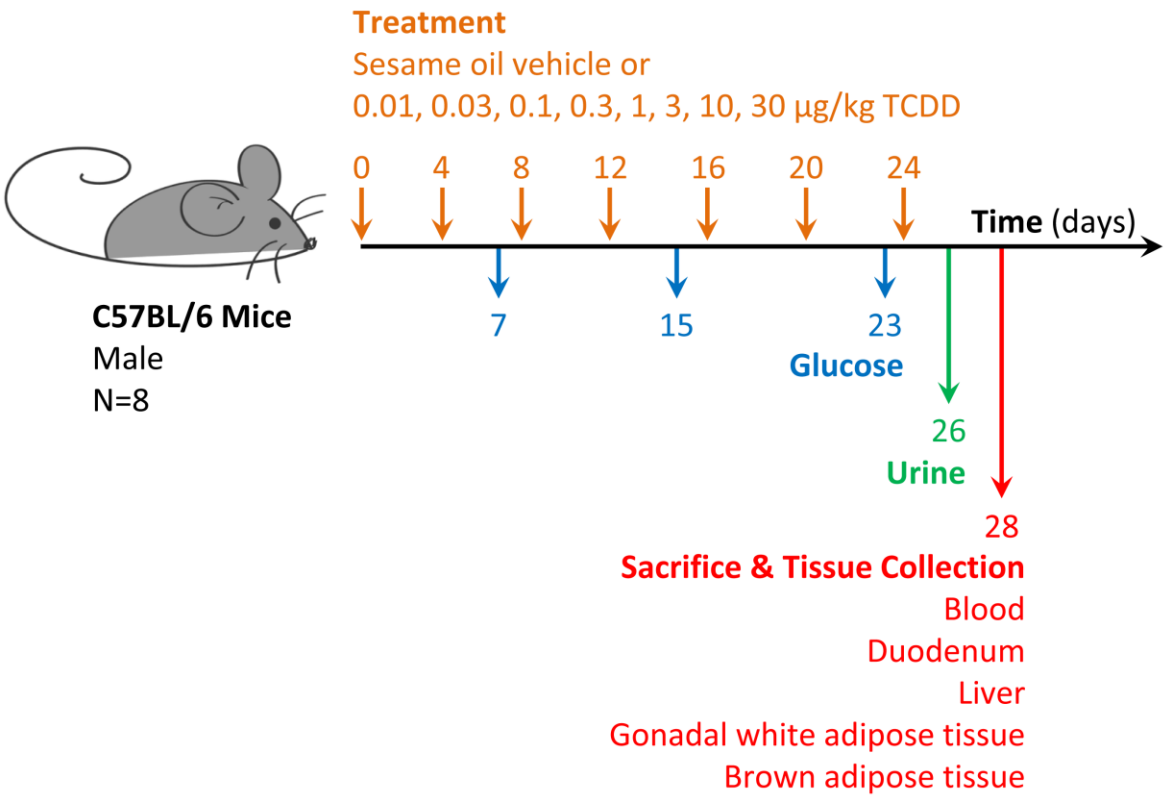

FIGURE 25. CHAPTER 5 STUDY DESIGN

Male C57BL/6 mice (n=8) were orally gavaged with sesame oil vehicle or 0.01-30 µg/kg TCDD every 4 days for 28 days.

Sample collection

At 7, 15, and 23d after the first dose, mice (vehicle and 30 µg/kg TCDD groups) were fasted for 6 hours (h) (access to water but not food) prior to tail blood glucose measurements using a FreeStyle Lite meter (Abbott Laboratories, IL). At 22d after the first dose, oral glucose tolerance tests (OGTT) were performed (vehicle and 30 µg/kg TCDD groups; fasted for 6h). Briefly, at time 0 minutes (min) animals were orally gavaged with 2 g/kg glucose in a 25% solution and tail blood glucose was measured at 0, 5, 15, 25, 30, 60, and 120 min. At 26d after the first dose, mice (vehicle and 30 µg/kg TCDD groups) were temporarily transferred to Innocages lacking bedding for 2h, with access to water but not food. Any urine expelled during this period was immediately collected, frozen in liquid nitrogen, and stored at -80°C. At 28d after the first dose, mice (all dose groups; fasted for 6h) were weighed and blood was collected from the submandibular vein prior to cervical dislocation. The duodenum (entire length from the stomach to the duodenojejunal flexure) was removed, flushed with Ca^{2+}/Mg^{2+}-free phosphate buffered saline (PBS; Sigma) and opened longitudinally. The epithelial lining was scraped into either an empty vial for protein analysis or a vial containing 1.3 mL TRIzol (Invitrogen, Carlsbad, CA) for RNA extraction, frozen in liquid nitrogen, and stored at -80°C. Liver, gonadal white adipose tissue (gWAT), and brown adipose tissue were removed, weighed, frozen in liquid nitrogen, and stored at -80°C.

Clinical chemistry

Total Fe levels (Fe^{2+} and Fe^{3+}, heme and non-heme) were measured in serum, urine, and liver (vehicle, 3-30 µg/kg TCDD groups) using inductively coupled plasma mass spectrometry (ICP-MS) at the MSU Diagnostic Center for Population and Animal Health (DCPAH). Free hemin (oxidized heme) was quantified in liver homogenates (vehicle and 30 µg/kg TCDD groups) using a commercial colorimetric assay (MAK036; Sigma). Total and direct (conjugated) bilirubin levels were measured in serum and urine (vehicle and 30 µg/kg TCDD groups) using commercial

colorimetric assays (B7576 and B7538, respectively; Pointe Scientific, Canton, MI). All colorimetric end products were measured using a Tecan (Männedorf, Switzerland) Infinite M200 plate reader. Indirect (unconjugated) bilirubin levels were calculated using indirect bilirubin = total bilirubin – direct bilirubin. Total iron binding capacity (TIBC) of serum (vehicle and 30 µg/kg TCDD groups) was measured through a direct ferric chloride colorimetric assay performed by MLabs (University of Michigan, Ann Arbor, MI). TIBC values were used to calculate transferrin saturation using transferrin saturation = serum Fe/TIBC X 100%. Total porphyrins in the urine (vehicle and 30 µg/kg TCDD groups) were quantified using a modified spectrophotometric method [24]. Uroporphyrin (8-carboxyporphyrin) accounts for 90% of mouse hepatic porphyrins in TCDD-elicited porphyria [18] and therefore the molar absorptivity of uroporphyrin (541,000 $M^{-1}cm^{-1}$) was used to calculate the concentration of total urinary porphyrins.

RNA extraction and RNA-sequencing

Frozen duodenal epithelium scrapings and liver samples (all doses) were homogenized in TRIzol (Ambion, Waltham, MA) using a Mixer Mill 300 tissue homogenizer (Retsch, Germany). Total RNA was isolated as previously described [7] and quantified using a Nano-drop spectrophotometer (Thermo Scientific, Wilmington, DE) at 260 nm. Purity was assessed by calculating the A_{260}/A_{280} ratio and RNA quality was analyzed using the Caliper LabChip GX (Perkin Elmer, Waltham, MA).

Duodenal and hepatic dose-dependent gene expression (all dose groups) was examined using RNA-Seq performed at the Research Technology Support Facility Genomics Core (rtsf.natsci.msu.edu/genomics). Duodenal libraries from three independent biological replicates (n=3) were prepared using the Ovation Mouse RNA-Seq System 1-16 sample preparation kit (NuGen, San Carlos, CA), with an additional DNase step. Hepatic libraries from three independent biological replicates (n=3) were prepared using the Illumina TruSeq RNA Sample Preparation Kit (Illumina, San Diego, CA). Libraries were quantified and sequenced using a read depth of ~30M

per sample, as previously described [25]. Quality was determined using FASTQC v0.11.2/v0.11.3 and adaptor sequences were removed using Trimmomatic v0.32/v0.33. Reads were mapped to the mouse reference genome (GRCm38 release 81) using Bowtie2 v2.2.3/v2.2.6 and TopHat2 v2.0.12/v2.1.0.

Following semi-parametric normalization, data were analyzed through an empirical Bayes method in which model-based *t* values were used to calculate posterior probability P1(*t*) values on a per gene and dose basis [26, 27]. Bayesian models take into account adjacent data points while considering trends within a dose-response dataset. In addition, P1(*t*) values can be used to rank and prioritize genes based on the probability of differential expression. For TCDD-mediated differential gene expression, fold changes were calculated relative to vehicle controls. Genes were considered differentially expressed if |fold change| ≥ 1.5 and statistical P1(*t*) value ≥ 0.8 at one or more doses. RNA-Seq datasets for the duodenal epithelium and liver were deposited in the Gene Expression Omnibus (GEO; accession number GSE87542 and GSE87519, respectively).

Putative DRE identification and hepatic AhR ChIP-Seq

Putative dioxin response elements (pDREs) with matrix similarity scores (MSS) ≥ 0.856 were previously identified [28]. ChIP-Seq was performed on liver samples from male C57BL/6 mice 2h following a single oral dose of 30 µg/kg TCDD as previously described [28]. Reads were mapped to the mouse reference genome (GRCm38 release 81) using Bowtie 2.0.0 and alignments were converted to SAM format using SAMTools v0.1.2.

Enrichment analyses and KEGG pathway integration

Differentially expressed genes (DEGs) in the duodenal epithelium were analyzed for enriched functions using the Database for Annotation, Visualization, and Integrated Discovery (DAVID) v6.7. Only Gene Ontology (GO) Biological Processes and Molecular Functions were

considered. Enrichment scores (ES) ≥ 1.3 were considered significantly enriched, representing the -log scale geometric mean *p*-value of 0.05.

CytoKEGG 0.0.5 within Cytoscape 3.2.0 was used to generate metabolism pathways with additional manual curation. Metabolite levels were obtained from clinical chemistry analyses or a published hepatic metabolomics dataset [28]. The largest |fold change| for differential gene expression and metabolite levels are represented regardless of dose. The fold change for AhR enrichment (upper left corner) and the number of pDREs (upper right corner) are also provided.

Quantitative real-time polymerase chain reaction (qRT-PCR)

qRT-PCR was performed for select genes as previously described [7]. Forward and reverse primer sequences and amplicon sizes are provided in Table 7. PCR amplification was conducted on a Bio-Rad CFX Connect Real-Time PCR Detection System. Gene expression relative to vehicle control was calculated using the $2^{-\Delta\Delta CT}$ method and the geometric mean of 3 housekeeping genes *ActB*, *Gapdh*, and *Hprt*. Gene expression data are plotted relative to vehicle control.

Protein measurements

Duodenal epithelial scrapings, liver (ground by mortar and pestle), and serum samples (vehicle and 30 µg/kg TCDD groups) were sonicated on ice in RIPA buffer supplemented with protease inhibitor cocktail (Sigma). Samples were centrifuged and total protein in the supernatant was measured using the bicinchoninic acid (BCA) assay (Sigma). The WES capillary electrophoresis system (ProteinSimple, San Jose, CA) was used with the following antibodies: ACO1 (1:65; ab126595; Abcam, Cambridge, MA), FTH1 (1:65; ab65080; Abcam), FTL1 (1:65; ab69090; Abcam), HAMP/HAMP2 (1:10; ab190775; Abcam), HAO1 (1:30; ab93137; Abcam), HP (1:650; ab131236; Abcam), HPX (1:10; ab90947; Abcam), SLC11A2 (DMT1; 1:10; ab123085; Abcam), SLC40A1 (1:30; NBP1-21502; Novus Biologicals, Littleton, CO), TFRC (1:30; ab84036;

TABLE 7. PRIMER SEQUENCES (5'-3') AND PRODUCT SIZES FOR GENES VERIFIED BY QRT-PCR

Gene ID	Gene Symbol	Ref Seq Accession	Forward Primer	Reverse Primer	Product Size
11461	*Actb*	NM_007393	GCTACAGCTTCACCACCACA	TCTCCAGGGAGGAAGAGGAT	123
14433	*Gapdh*	NM_008084	GTGGACCTCATGGCCTACAT	TGTGAGGGAGATGCTCAGTG	125
15452	*Hprt*	NM_013556	AAGCCTAAGATGAGCGCAAG	TTACTAGGCAGATGGCCACA	104
84506	*Hamp*	NM_032541	CCTGAGCAGCACCACCTATC	TGGGAATTGTTACAGCATTTACAGC	171
66438	*Hamp2*	NM_183257	CCAGCAACAGATGAGACAGACT	TGGCTCTAGGCTCTCTATTCTTCA	189

Abcam), and TRF (1:30; ab82411; Abcam). Primary antibodies were detected using a goat anti-rabbit secondary antibody conjugated to horseradish peroxidase. Chemiluminescence signals were analyzed with Compass software (ProteinSimple). Protein levels in the duodenum and liver were normalized to SDHA levels, while protein levels in the serum were normalized to sample volume.

RESULTS

Gross morphology and histopathology

Hepatic TCDD levels in female C57BL/6 mice gavaged every 4d for 28d approach steady state and are comparable to levels reported in human serum following accidental or intentional exposures [10]. In this study, 30 µg/kg TCDD decreased terminal body weight by 27% (Figure 26A), despite no significant change in daily food intake (data not shown). Absolute liver weights increased 18–30% at 1–10 µg/kg TCDD, while relative liver weight displayed an 18–57% dose-dependent increase at 0.3–30 µg/kg TCDD (Figure 26B). There was a 46% and 28% decrease in absolute and relative gonadal white adipose tissue weight, respectively, at 30 µg/kg TCDD (Figure 26C). No change in terminal brown adipose tissue was observed (not shown).

TCDD and related AhR agonists are reported to elicit hepatic lipid accumulation, immune cell infiltration, periportal fibrosis, and bile duct proliferation in mice [9, 29-32]. Similarly, we observe these same histopathological features in the livers of C57BL/6 mice orally gavaged with TCDD every 4d for 28d, where the incidence and severity are consistently greater in males compared to females [10, 33, 34]. Specifically, male mice exhibit hepatic lipid accumulation at ≥0.3 µg/kg determined through Oil Red O (ORO) staining and inflammatory cell infiltration (primarily macrophages) at ≥3 µg/kg determined through F4/80 labeling. Picrosirius red (PSR) and hematoxylin & eosin (H&E) staining reveal periportal fibrosis and bile duct proliferation, respectively, at 30 µg/kg [34]. Hepatic vacuolization indicative of lipid accumulation is first

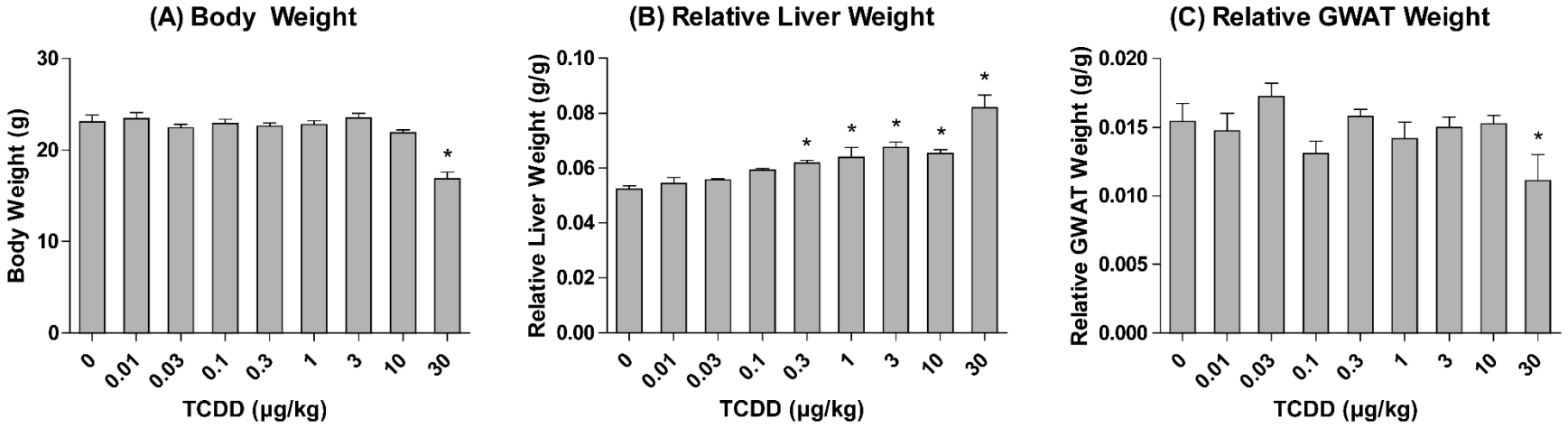

FIGURE 26. TERMINAL BODY AND TISSUE WEIGHTS OF MALE MICE

(A) Terminal body weight, (B) relative liver weight, and (C) relative gonadal white adipose tissue (GWAT) weight of male C57BL/6 mice orally gavaged with sesame oil vehicle or 0.01–30 µg/kg TCDD every 4 days for 28 days. Bars represent average ± standard error of the mean (SEM) for at least 7 biological replicates. Statistical significance (* $p \leq 0.05$) was determined using one-way ANOVA analysis followed by Dunnett's post-hoc test performed in SAS 9.3.

observed in mice 18h after a single oral dose of 30 µg/kg TCDD, while immune cell infiltration and individual cell apoptosis are evident at 168h [7].

Fe levels

Total Fe (Fe^{2+} and Fe^{3+}, heme and non-heme) levels were measured in serum, urine, and liver extracts. ICP-MS detected a dose-dependent increase in Fe from 314 µg/dL in controls to 816 µg/dL in serum at 30 µg/kg TCDD (Figure 27A). Fe was not detected in control urine but was present in the urine of all mice at 30 µg/kg TCDD, with an average level of 0.37 µg/mL (Figure 27B). A modest dose-dependent increase in total hepatic Fe levels was observed, although it was not statistically significant (p=0.086) due to inter-animal variability (Figure 27C). Previous studies report a 60% increase in hepatic Fe levels in mice receiving 4 weekly doses of 25 µg/kg TCDD [18]. Interestingly, the rate of Fe-catalyzed lipid peroxidation is dependent on the amount of free catalytically active Fe^{2+} rather than total Fe [35]. Intracellular Fe is normally sequestered in the ferric state by the storage protein ferritin. However, TCDD facilitates the mobilization of catalytically active Fe^{2+} through induction of cytochrome P450s [36] and XDH/XO which generate hepatic ROS [28]. Ascorbate, which also releases Fe^{2+} from ferritin [37], increased 1.3-fold in hepatic extracts and 124.4-fold in urine of TCDD-treated mice [10]. Consequently, TCDD can facilitate catalytically active Fe^{2+} mobilization through diverse mechanisms.

In blood, Fe is bound to transferrin (TRF), a plasma glycoprotein containing two high-affinity Fe^{3+}-binding sites. Serum TIBC increased from 236 µg/dL in controls to 534 µg/dL in TCDD-treated mice, indicating an increase in blood TRF levels, consistent with a 2.2-fold increase in TRF protein levels in the liver, the primary site of TRF synthesis (Figure 27D-E). This TIBC increase was proportional to increases in serum Fe, and therefore transferrin saturation (serum iron/TIBC X 100%) was unaffected by TCDD (Figure 27F).

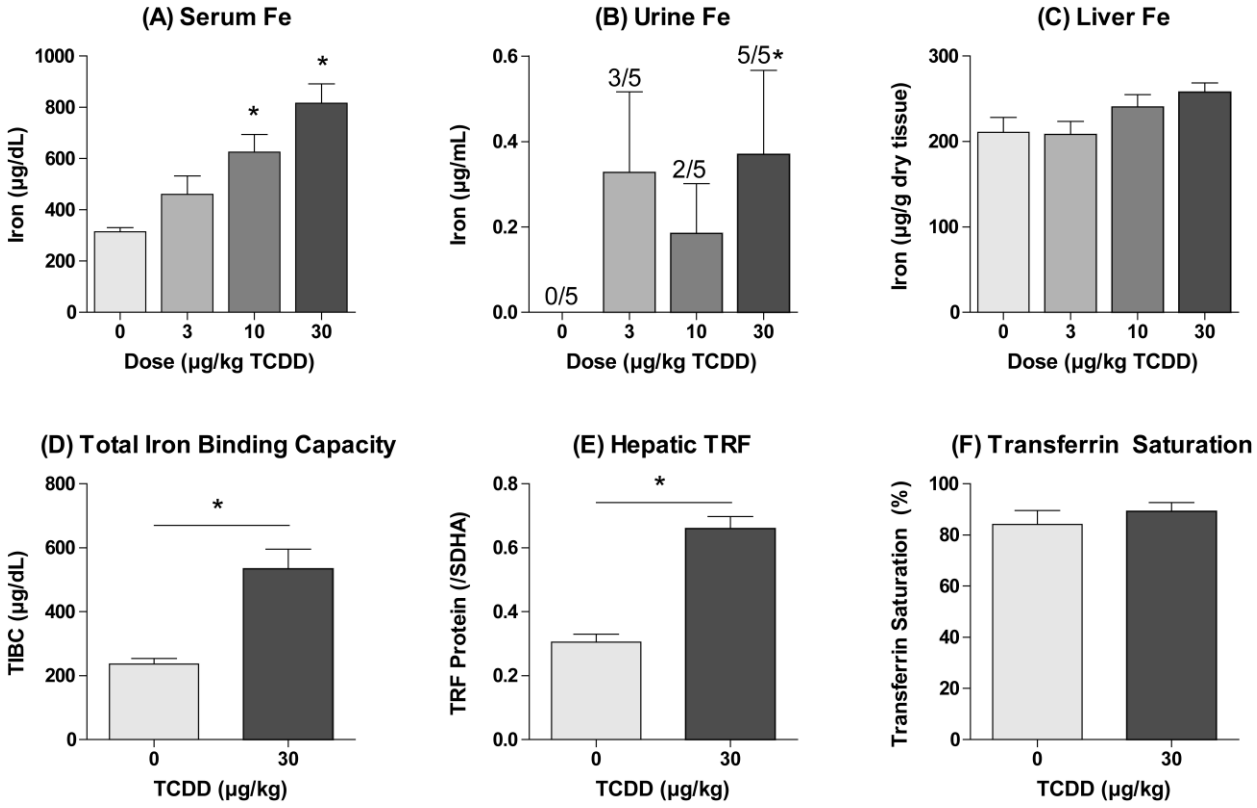

FIGURE 27. TCDD ELICITS SYSTEMIC IRON OVERLOADING

Total iron (Fe) levels in (A) serum, (B) urine, and (C) liver of male C57BL/6 mice orally gavaged with sesame oil vehicle or 3-30 µg/kg TCDD every 4 days for 28 days, as determined through inductively coupled plasma mass spectrometry (ICP-MS) analysis. For (B), the number of animals in which Fe was detected in the urine is indicated. (D) Serum total iron binding capacity (TIBC), (E) hepatic transferrin (TRF) protein levels, and (F) serum transferrin saturation of male C57BL/6 mice orally gavaged with sesame oil vehicle or 30 µg/kg TCDD every 4 days for 28 days. Bars represent the average ± standard error of the mean for at least 4 biological replicates. Statistical significance (* $p \leq 0.05$) was determined using one-way ANOVA analysis followed by Dunnett's post-hoc test (A,C) or a Student's t-test (D-F) performed in SAS 9.3, or Chi-Square analysis based on the presence or absence of Fe performed in R 3.3.1 (B).

Duodenal differential gene expression

The duodenum is the intestinal segment predominantly responsible for the absorption of dietary minerals including Fe. Analysis of duodenal epithelial differential gene expression detected 22,541 expressed genes, of which 969 were differentially expressed (|fold change| ≥ 1.5, P1(*t*) ≥ 0.8) at one or more doses. The majority of differentially expressed genes (DEGs) exhibited dose-dependent induction. AhR battery members including *Cyp1a1* (284.0-fold), *Cyp1a2* (117.1-fold), and *Cyp1b1* (51.0-fold) were among the most induced genes, while cubilin (*Cubn*; 4.2-fold), apolipoprotein L10A (*Apol10a*; 4.0-fold), and glutathione peroxidase 2 (*Gpx2*; 3.8-fold) were among the most repressed genes.

DAVID identified 25 enriched functional clusters (ES ≥ 1.3) within the 969 duodenal DEGs, including an Fe- and heme-binding cluster consisting of 17 cytochrome P450s and several Fe homeostasis genes. For example, ferritin heavy chain 1 (*Fth1*), lactotransferrin (*Ltf*), and solute carrier 40A1 (*Slc40a1*; aka ferroportin) were repressed 1.7-, 1.6-, and 2.1-fold, respectively. Functional analysis also identified clusters related to immune response and inflammation. Several MHC class II genes (*Cd74*, *H2-Oa*, *H2-Ob*, *H2-Aa*, *H2-Ab1*, *H2-Eb1*, *H2-DMa*, *H2-DMb1*) involved in antigen processing and presentation were repressed, consistent with TCDD-elicited depletion of antigen-presenting cells such as intestinal macrophages and dendritic cells [33]. Genes involved in T and B lymphocyte differentiation were also differentially expressed, including thymus cell antigen 1 (*Thy1* repressed 1.9-fold), interleukin-15 (*Il15* induced 1.5-fold), and interleukin-7 receptor (Il7r induced 1.5-fold), providing further evidence of duodenal lymphocyte population changes or disruption of lymphocyte activation. Clusters associated with lipid homeostasis and metabolism, including intestinal digestion and absorption, lipid transport, steroid biosynthesis, and vitamin A metabolism (e.g., *Adh1* induced 1.7-fold, *Rdh10* induced 1.7-fold, *Aldh1a1* repressed 1.9-fold, *Rdh16* repressed 1.9-fold) were also enriched. Various cholesterol transporters such as ATP-binding cassette A1 (*Abca1*), ATP-binding cassette G8 (*Abcg8*), scavenger receptor B1 (*Scarb1*), and NPC1-like 1 (*Npc1l1*) were repressed, while long chain fatty acid transporter Cd36

antigen (*Cd36)* was induced. Overall, these changes are consistent with reports that TCDD alters dietary fatty acid/cholesterol absorption and vitamin A metabolism in the jejunum [33].

Hepatic differential gene expression

Hepatic RNA-Seq analysis detected 19,935 expressed genes, of which 9,313 were differentially expressed (|fold change| ≥ 1.5, P1(*t*) ≥ 0.8) at one or more doses with the majority exhibiting dose-dependent induction. Highly induced AhR battery members included *Cyp1a1* (1,771-fold), flavin containing monooxygenase 3 (*Fmo3*; 1,491-fold), and *Cyp1b1* (1,436-fold). Carboxylesterase 3A (*Ces3a*), carbonic anhydrase 3 (*Car3*), and major urinary protein 7 (*Mup7*) were repressed at 3,062-, 2,198-, and 1,800-fold, respectively. Overall, the number of male liver DEGs (9,313) exceeded the previously reported number of female hepatic DEGs (3,677) [25]. In general, genes exhibited greater differential expression in males compared to that in females.

A previously published functional analysis of the hepatic transcriptome after repeated TCDD dosing identified dysregulation of lipid biosynthesis and metabolism, central carbon metabolism, and oxidative stress defense pathways [28]. The current study focuses specifically on hepatic genes related to iron and heme homeostasis. A list of 119 mouse genes involved in Fe homeostasis was compiled by searching the literature and the Gene Ontology (GO) database for: (i) Fe ion homeostasis GO:0055072, (ii) Fe ion transport GO:0006826, (iii) regulation of Fe ion transport GO:0034756, (iv) heme metabolic process GO:0042168, (v) heme biosynthetic process GO:0006783, and (vi) heme transport GO:0015886. Approximately 114 of these 119 Fe-related genes were expressed in the liver, of which 73 exhibited differential expression following TCDD treatment (Figure 28). The observed gene expression changes were consistent with Fe accumulation and disrupted Fe homeostasis, which are discussed below.

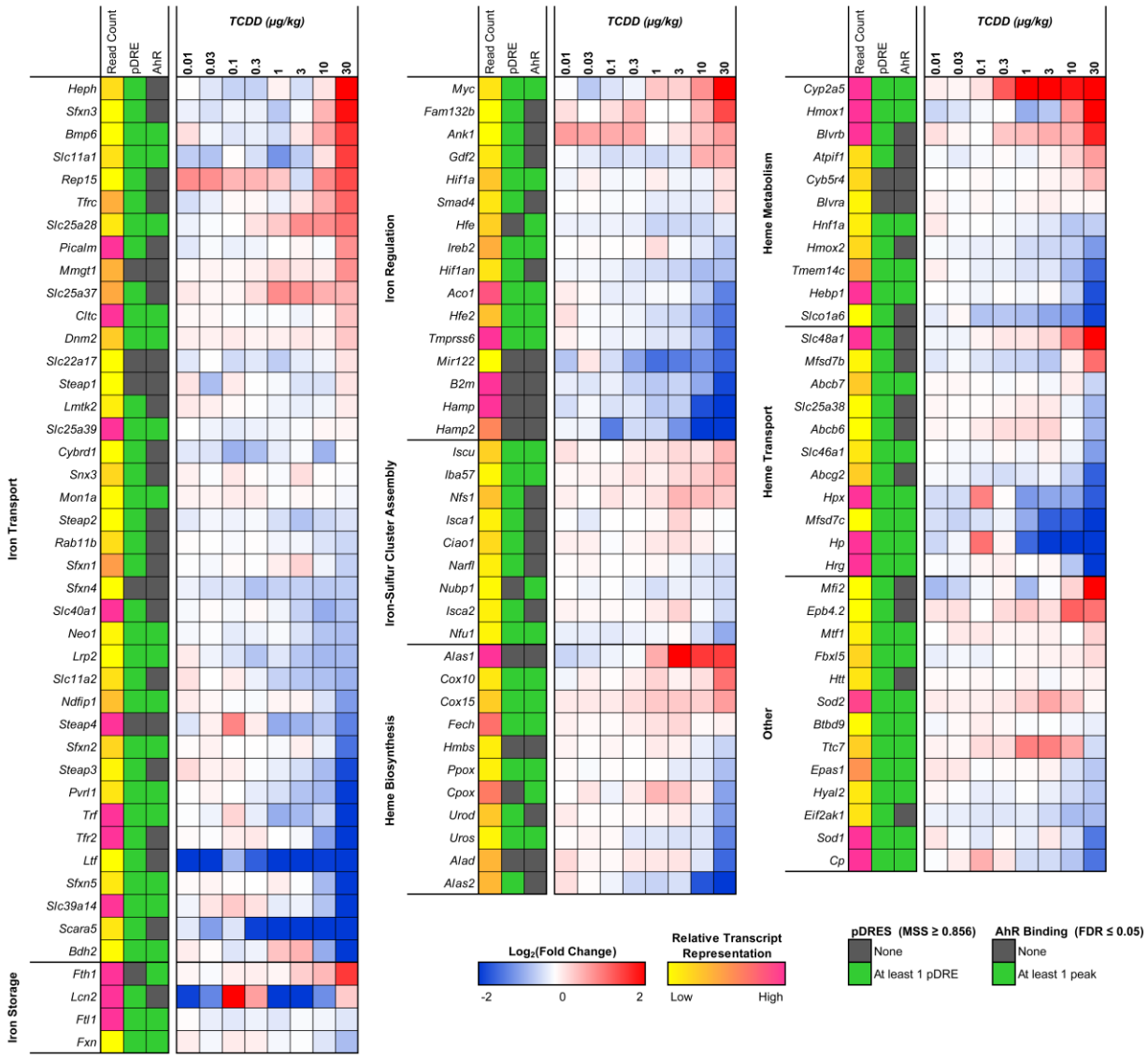

FIGURE 28. TCDD-ELICITED HEPATIC DIFFERENTIAL EXPRESSION OF GENES INVOLVED IN IRON HOMEOSTASIS

Male C57BL/6 mice were orally gavaged with sesame oil vehicle or TCDD (0.01-30 µg/kg) every 4 days for 28 days. Color scale represents the $\log_2$(fold change) for differential gene expression, as determined through RNA-Seq analysis (n=3). The presence of pDREs (MSS ≥ 0.856) and AhR enrichment peaks (FDR ≤ 0.05) at 2h are shown as green boxes. Relative gene expression level indicating the number of reads aligned to each transcript is also shown, where yellow represents lower expression (≤ 500 reads) and pink represents higher expression (≥ 10,000).

Systemic Fe regulation

Hepcidin is the master regulator of systemic Fe homeostasis. It limits serum levels by inhibiting duodenal absorption of dietary Fe, release of recycled heme Fe from macrophages, and efflux of Fe stores from hepatocytes [38]. While the human and rat genomes contain a single hepcidin (*Hamp*) gene, the mouse locus has undergone a duplication event, leading to two closely related isoforms, *Hamp* and *Hamp2* [39]. Homozygous *Hamp* knockout mice exhibit Fe accumulation in several tissues, and increased serum Fe and ferritin levels, similar to hereditary hemochromatosis in humans [40]. Transgenic mice overexpressing hepatic *Hamp* develop severe Fe-deficiency anemia [41], while *Hamp2* overexpression in the liver has no effect on Fe regulation, suggesting HAMP and HAMP2 are not redundant [42].

RNA-Seq analysis identified dose-dependent repression of *Hamp* (max 5.9-fold) and *Hamp2* (max 37.0-fold) at 10-30 µg/kg TCDD, which was confirmed by qRT-PCR (Figure 29A-B). Total HAMP (HAMP and HAMP2) protein was reduced 4.8-fold in the liver, consistent with the transcriptional repression (Figure 29C). No AhR binding occurred within ±10 kb of the *Hamp* or *Hamp2* transcription start sites. Other AhR agonists including PCB126 and TCDF also repressed *Hamp* expression 1.7- (not significant) and 2.8-fold, respectively, while non-dioxin-like PCB153 had no effect, suggesting *Hamp* repression involves the AhR (Figure 29D). *Hamp2* was repressed by PCB126 (6.3-fold), TCDF (19.7-fold), and PCB153 (2.2-fold), suggesting it may be regulated by both AhR and non-AhR mechanisms (Figure 29E).

Hepcidin reduces serum Fe levels via the internalization and degradation of SLC40A1 (aka ferroportin), a transmembrane Fe exporter expressed on macrophages, hepatocytes, and the basal membrane of duodenal enterocytes. Consistent with reductions in HAMP, SLC40A1 protein was increased 1.6-fold in the liver (Figure 29F). This would facilitate Fe efflux from hepatocytes and Kupffer cells into the blood, consistent with Fe accumulation in the serum and negligible hepatic increases. However, TCDD-elicited macrophage infiltration may also contribute to hepatic increases in SLC40A1. In the duodenal epithelium, SLC40A1 protein levels remained

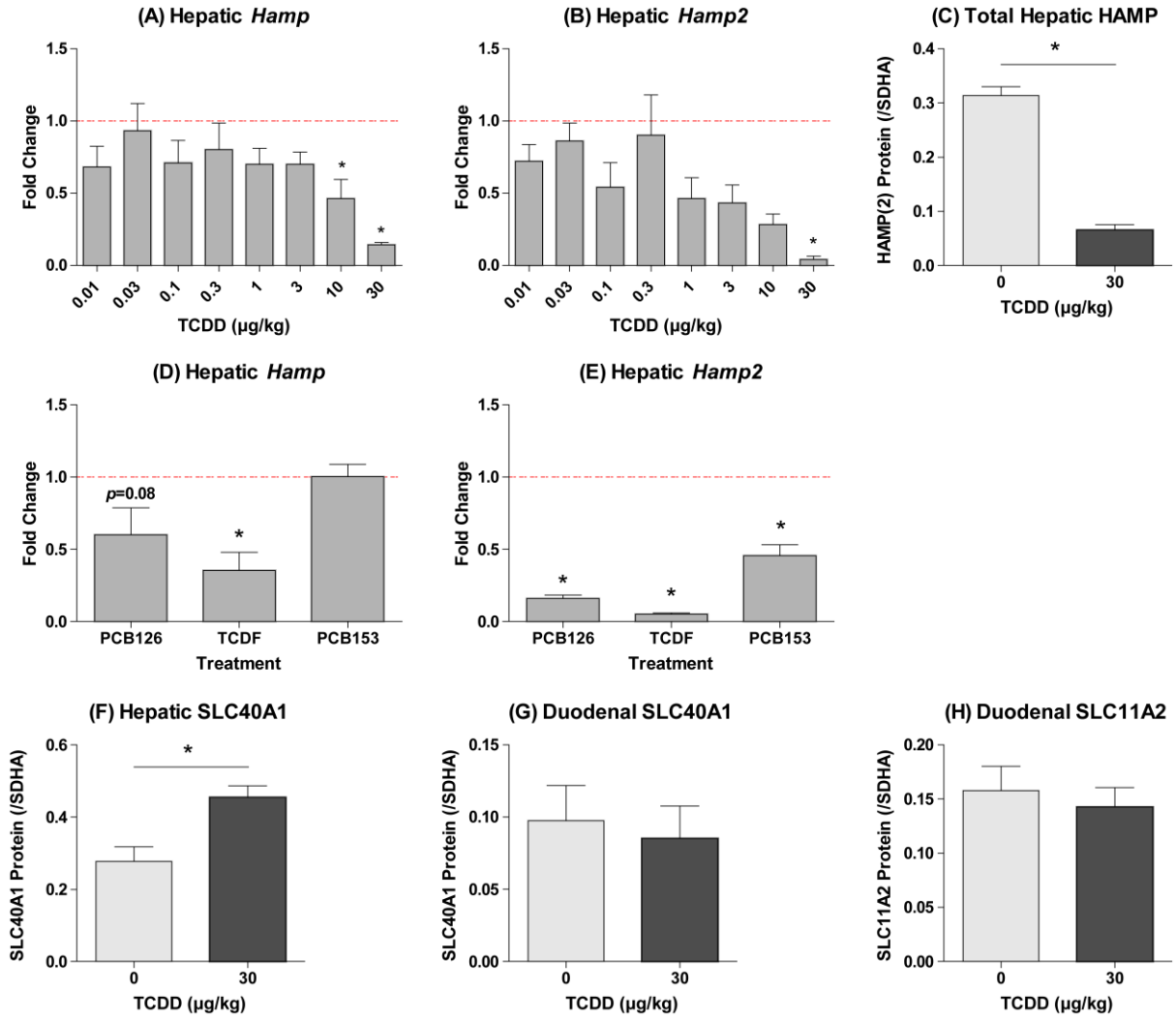

FIGURE 29. TCDD REPRESSES HEPATIC HEPCIDIN EXPRESSION

qRT-PCR analysis of hepatic dose-dependent differential gene expression of (A) hepcidin (*Hamp*) and (B) hepcidin 2 (*Hamp2*) in male C57BL/6 mice orally gavaged with sesame oil vehicle or 0.01-30 µg/kg TCDD every 4 days for 28 days. (C) Total hepatic HAMP (HAMP and HAMP2) protein levels in male C57BL/6 mice orally gavaged with sesame oil vehicle or 30 µg/kg TCDD every 4 days for 28 days. Ligand-dependent repression of (D) *Hamp* and (E) *Hamp2* 24h after a single oral gavage with AhR agonists (3000 µg/kg PCB126 and 3000 µg/kg TCDF) and a non-AhR agonist (300 mg/kg PCB153) [8, 23]. Protein levels of (F) hepatic SLC40A1 (ferroportin), (G) duodenal epithelial SLC40A1, and (H) duodenal epithelial SLC11A2 in male C57BL/6 mice orally gavaged with sesame oil vehicle or 30 µg/kg TCDD every 4 days for 28 days. Bars represent the average ± standard error of the mean for at least 3 biological replicates. Red dashed line indicates a fold change of 1. Statistical significance (* $p \leq 0.05$) was determined using one-way ANOVA analysis followed by Dunnett's test (A-B) or a Student's t-test (C-H) performed in SAS 9.3.

unchanged by TCDD (Figure 29G), despite 2.1-fold repression of *Slc40a1* mRNA. Thus, under conditions of TCDD-elicited HAMP deficiency, duodenal SLC40A1 protein levels were maintained, enabling continuous dietary Fe uptake across the basal duodenal membrane despite increasing serum Fe levels. Hepcidin is also reported to regulate dietary Fe absorption through proteasomal degradation of the apical solute carrier 11A2 (SLC11A2, aka DMT1) [43], however duodenal SLC11A2 protein levels were unaffected by treatment (Figure 29H). Studies using rat duodenal loops have shown that TCDD increases dietary Fe absorption, where enterocyte-to-blood transfer mediated by SLC40A1 was substantially more affected than SLC11A2-mediated lumen-to-enterocyte transfer [44].

Intracellular Fe regulation

Intracellular Fe homeostasis is also regulated by two iron response element (IRE)-binding proteins, aconitase 1 (ACO1, aka IREB1) and IRE-binding protein 2 (IREB2). During Fe deficiency, ACO1 and IREB2 bind to IREs within the 5' UTR or 3' UTR of target genes, leading to translational repression or mRNA stabilization, respectively. In contrast, abundant Fe lowers ACO1 and IREB2 binding affinity for IREs. TCDD repressed *Aco1* and *Ireb2* 2.4- and 1.5-fold, respectively, while ACO1 hepatic protein levels were reduced 3.2-fold (Figure 30A), suggesting transcriptional and/or translational repression due to Fe accumulation. Lower ACO1 levels may increase translation of 5' UTR IRE-containing transcripts and reduce mRNA stabilization of transcripts containing 3' UTR IREs. For example, hydroxyacid oxidase 1 (*Hao1*) mRNA, which contains a 3' UTR IRE, was repressed 856.2-fold possibly due to reduced ACO1 levels, although AhR enrichment was also observed. The corresponding protein was undetectable in liver extracts from TCDD-treated animals (Figure 30B). In contrast, TCDD had no effect on hepatic protein levels of ferritin heavy (FTH1) and light (FTL1) chains, despite 5' UTR IREs within both genes (Figure 30C-D).

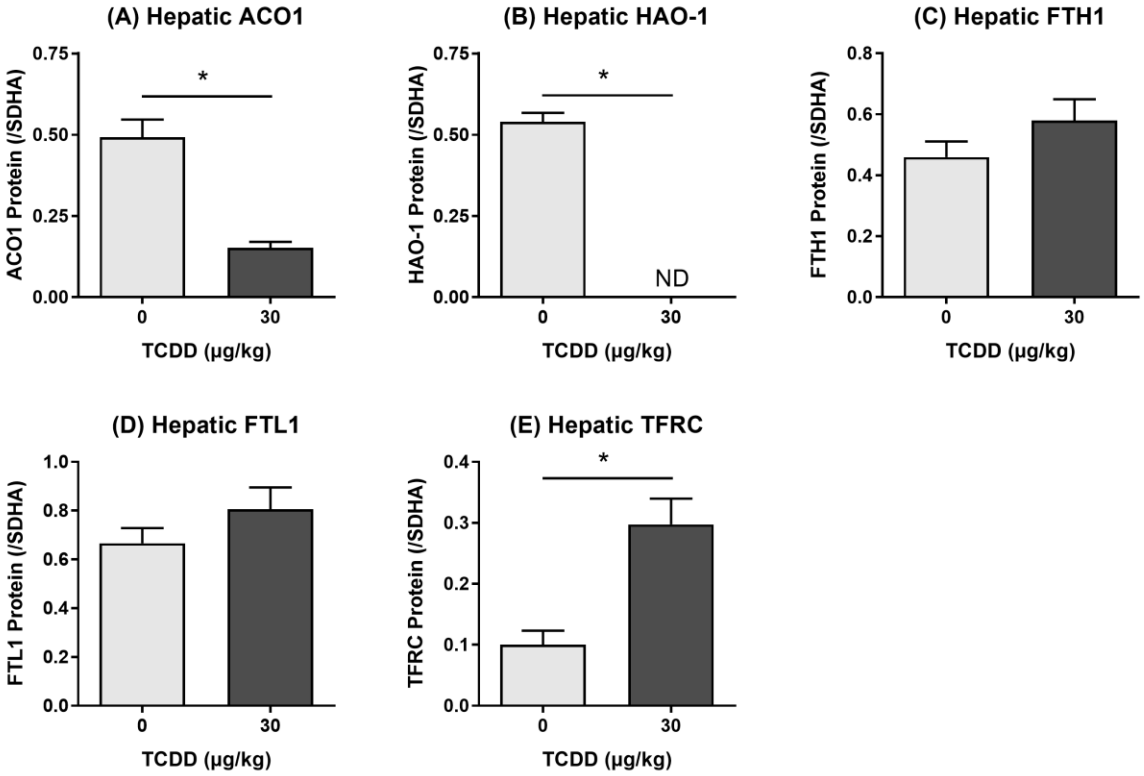

FIGURE 30. TCDD DYSREGULATES INTRACELLULAR IRON HOMEOSTASIS

Hepatic (A) aconitase 1 (ACO1), (B) hydroxyacid oxidase 1 (HAO1), (C) ferritin heavy chain 1 (FTH1), (D) ferritin light chain 1 (FTL1), and (E) transferrin receptor (TFRC) protein levels in male C57BL/6 mice orally gavaged with sesame oil vehicle or 30 µg/kg TCDD every 4 days for 28 days. Bars represent the average ± standard error of the mean (SEM) for at least 3 biological replicates. ND indicates 'not detected'. Statistical significance (* $p \leq 0.05$) was determined using a Student's t-test performed in SAS 9.3.

The transferrin receptor (TFRC), which is regulated by intracellular Fe levels, mediates cellular uptake of TRF-bound Fe via receptor-mediated endocytosis. Under low Fe conditions, *Tfrc* mRNA is stabilized by the presence of 5 IREs within the 3' UTR. Despite negligible increases in hepatic Fe levels, TCDD induced hepatic *Tfrc* mRNA and protein 2.3- and 3.0-fold, respectively, in the absence of AhR enrichment (Figure 30E). Hemochromatosis (HFE) is a membrane protein which competes with Fe^{3+}-TRF for overlapping binding sites on TFRC. With serum Fe accumulation, TRF saturation increases and TRF dislodges HFE from its overlapping binding sites on TFRC [45]. HFE then forms an iron-sensing complex with juvenile hemochromatosis type 2 (HFE2), transferrin receptor 2 (TFR2), and bone morphogenetic protein 6 (BMP6), using the cell surface receptor neogenin (NEO1) as a scaffold protein [45, 46]. Complex assembly initiates the canonical BMP signaling pathway, in which SMAD transcription factors induce *Hamp* transcription. The importance of HFE2, TFR2, and NEO1 in *Hamp* expression has been confirmed in human genetic disorders, human liver transplant studies, null mouse models, and mutation analysis studies. Hepatic *Hfe2*, *Tfr2,* and *Neo1* were repressed 2.6-, 6.1, and 1.6-fold, respectively, by TCDD, which may compromise HFE-HFE2-TFR2-BMP6 complex assembly thereby limiting *Hamp* and *Hamp2* transcription (Figure 31). AhR enrichment within *Hfe2* and *Neo1* was increased 6.2- and 3.2-fold, respectively, suggesting AhR involvement in *Hamp* and *Hamp2* repression. Alternatively, Qian *et al* propose that PCB126 and PCB153 repress hepatic *Hamp* in female mice in an estrogen response element (ERE)-dependent manner by mimicking estrogen activity [47].

Heme biosynthesis and metabolism

Heme, a cyclic tetrapyrrole cofactor containing Fe^{2+}, is essential for multiple biological functions including the capacity to bind gases and facilitate electron transfer in redox reactions. However, due to its ability to oxidize biological macromolecules and activate apoptotic enzymes, free heme must be incorporated into hemoproteins to minimize its toxicity. In our study, hepatic

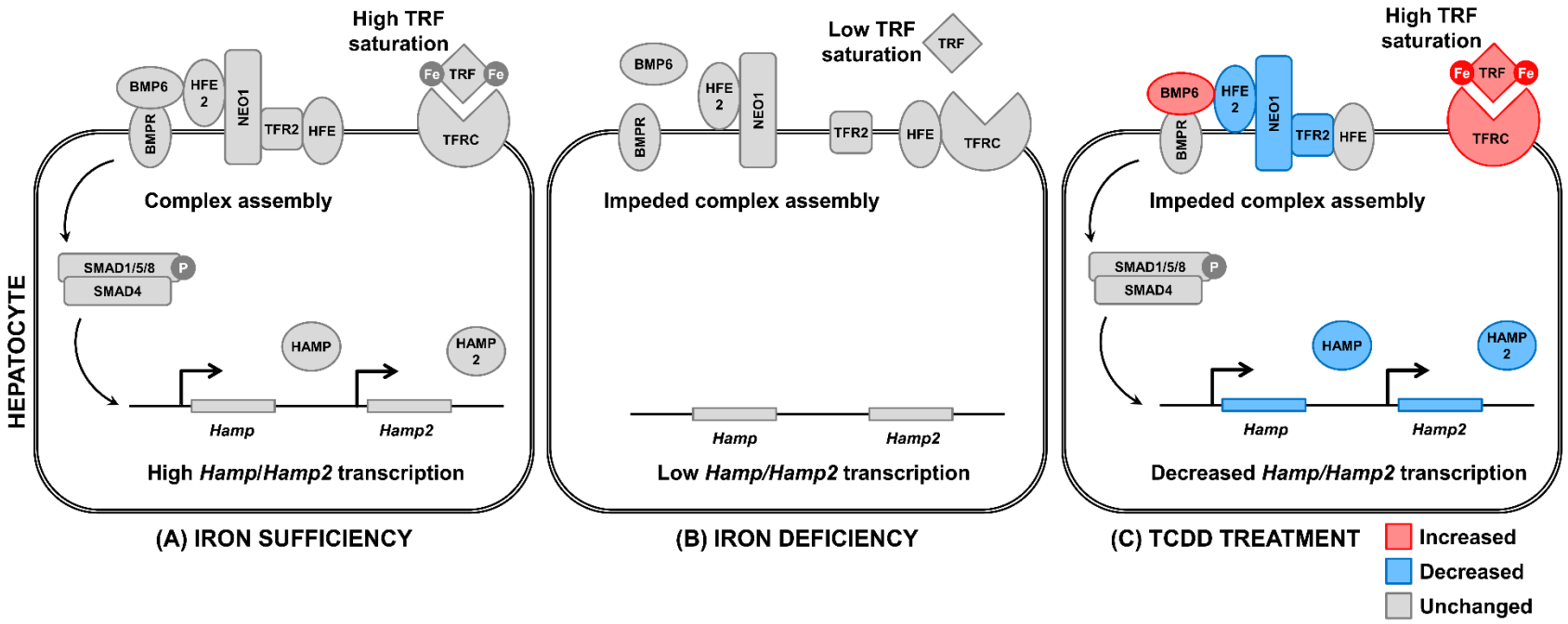

FIGURE 31. PROPOSED MECHANISM OF HEPCIDIN REPRESSION BY TCDD

(A) When Fe levels are sufficient, saturated Fe^{3+}-TRF binds to TFRC, dislodging HFE from its overlapping binding site on TFRC. HFE is then available to form a complex containing TFR2, NEO1, HFE2, BMP6, and BMPR, leading to SMAD-induced transcription of *Hamp* and *Hamp2*. Hepcidin controls systemic Fe levels by initiating internalization and eventual degradation of SLC40A1. (B) Under low Fe conditions, TRF does not interfere with TRFC-HFE binding, the complex required for SMAD signaling is not assembled, and *Hamp*/*Hamp2* are not transcribed (modified from [38]). Consequently, SLC40A1 continues to transport dietary Fe into the systemic circulation. (C) Despite sufficient Fe levels and the binding of Fe^{3+}-TRF to TRFC, TCDD compromises HFE-HFE2-TFR2-BMP6 complex assembly through repression of *Tfr2*, *Neo1*, and/or *Hfe2*, limiting *Hamp* and *Hamp2* transcription. Low hepcidin levels allow duodenal SLC40A1 to continue exporting dietary Fe into portal circulation, while hepatic SLC40A1 effluxes intracellular Fe into the blood thereby limiting hepatic Fe accumulation. Unregulated intestinal Fe absorption and hepatic efflux increases serum Fe levels, resulting in ROS production, oxidative stress, and hepatotoxicity. Red and blue indicate increased and decreased levels, respectively.

levels of free hemin (oxidized heme) increased from 510 pmole/mg in controls to 782 pmole/mg in TCDD-treated samples (Figure 32A).

Mammals are equipped with soluble scavengers to prevent heme and hemoprotein toxicity. Free hemoglobin in blood is captured by haptoglobin (HP) and removed by interaction with scavenger receptor CD163. TCDD repressed hepatic expression of *Hp* 7.5-fold and reduced serum protein levels 1.6-fold (Figure 32B), possibly through AhR-dependent transcriptional repression given the 2.1-fold increase in AhR enrichment. This would reduce HP buffering capacity while increasing hemoglobin oxidation to methemoglobin and the release of free heme. Free heme is bound by hemopexin (HPX), a high affinity plasma glycoprotein that is primarily expressed by the liver. HPX delivers heme to hepatocytes where it is endocytosed through LDL receptor-related protein 1 (LRP1). Hepatic *Hpx* was repressed 3.1-fold by TCDD, consistent with a 1.4-fold decrease in serum protein levels (Figure 32C), while AhR enrichment was increased 6.6-fold. Similarly, TCDD repressed *Lrp1* 1.8-fold, with a 7.0-fold increase in AhR genomic binding. In addition, a truncated form of α_1-microgloblulin (A1M, encoded by *Ambp*) binds and degrades extracellular heme but was dose-dependently repressed 9.0-fold, thereby further compromising antioxidant defenses against free heme.

Hepatic heme oxygenase 1 (*Hmox1*), an inducible enzyme which catabolizes heme to Fe^{2+}, biliverdin, and CO, was induced 6.5-fold (Figure 33). Heme is the most potent physiological inducer of *Hmox1* following binding to BACH1, a cap'n'collar basic region leucine zipper transcription factor, although oxidative stress and cytokines are also known inducers [48]. BACH1 forms heterodimers with small Maf proteins including MafF, MafG, and MafK, which bind Maf recognition elements (MAREs) within the promoter region of target genes to repress transcription. As heme accumulates, it binds to the heme regulatory motif (HRM) within BACH1, reducing DNA-binding activity and inducing nuclear export [48]. Maf proteins then form heterodimers with transcriptional activators such as NRF1 (*Nfe2l1*, repressed 1.6-fold) and NRF2 (*Nfe2l2*, induced 5.1-fold), to induce MARE-driven expression of target genes including *Hmox1*. Hepatic expression

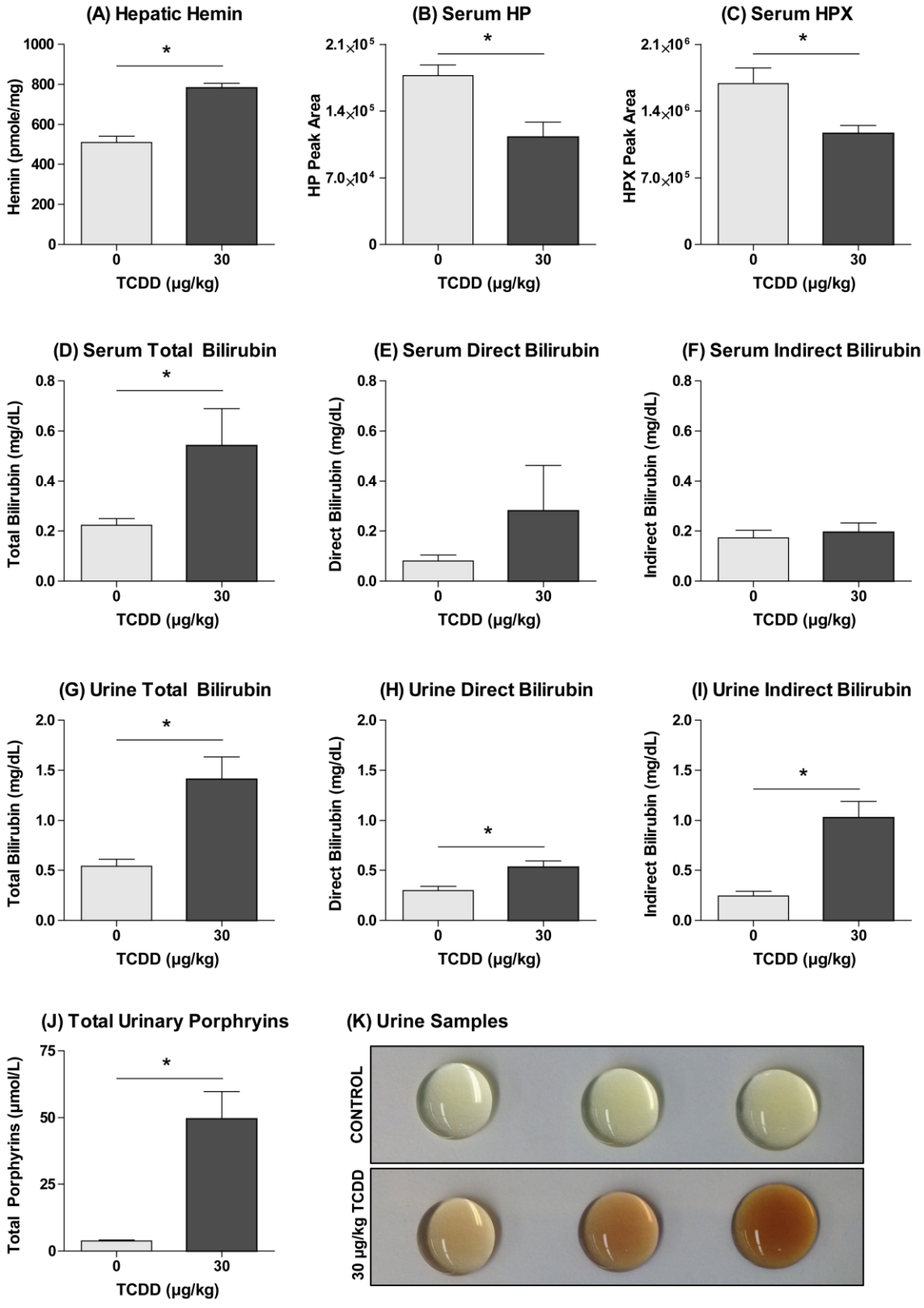

FIGURE 32. TCDD-ELICITED ALTERATIONS IN HEME METABOLITES

FIGURE 32 (cont'd)

(A) Hepatic hemin levels in the liver, and (B) serum haptoglobin (HP) and (C) serum hemopexin (HPX) levels in male C57BL/6 mice orally gavaged with sesame oil vehicle or 30 µg/kg TCDD every 4 days for 28 days. Total, direct, and indirect levels of bilirubin in the serum (D-F) and urine (G-I) of male C57BL/6 mice orally gavaged with sesame oil vehicle or 30 µg/kg TCDD every 4 days for 28 days. (J) Total porphyrins in urine samples collected on day 26 from male C57BL/6 mice orally gavaged with sesame oil control or 30 µg/kg TCDD every 4 days. (K) Urine samples collected from 3 mice treated with 30 µg/kg TCDD exhibit a dark tea color, compared to urine samples from 3 sesame oil controls. Bars represent the average ± standard error of the mean (SEM) for at least 4 biological replicates. Statistical significance (* $p \leq 0.05$) was determined using a Student's t-test performed in SAS 9.3.

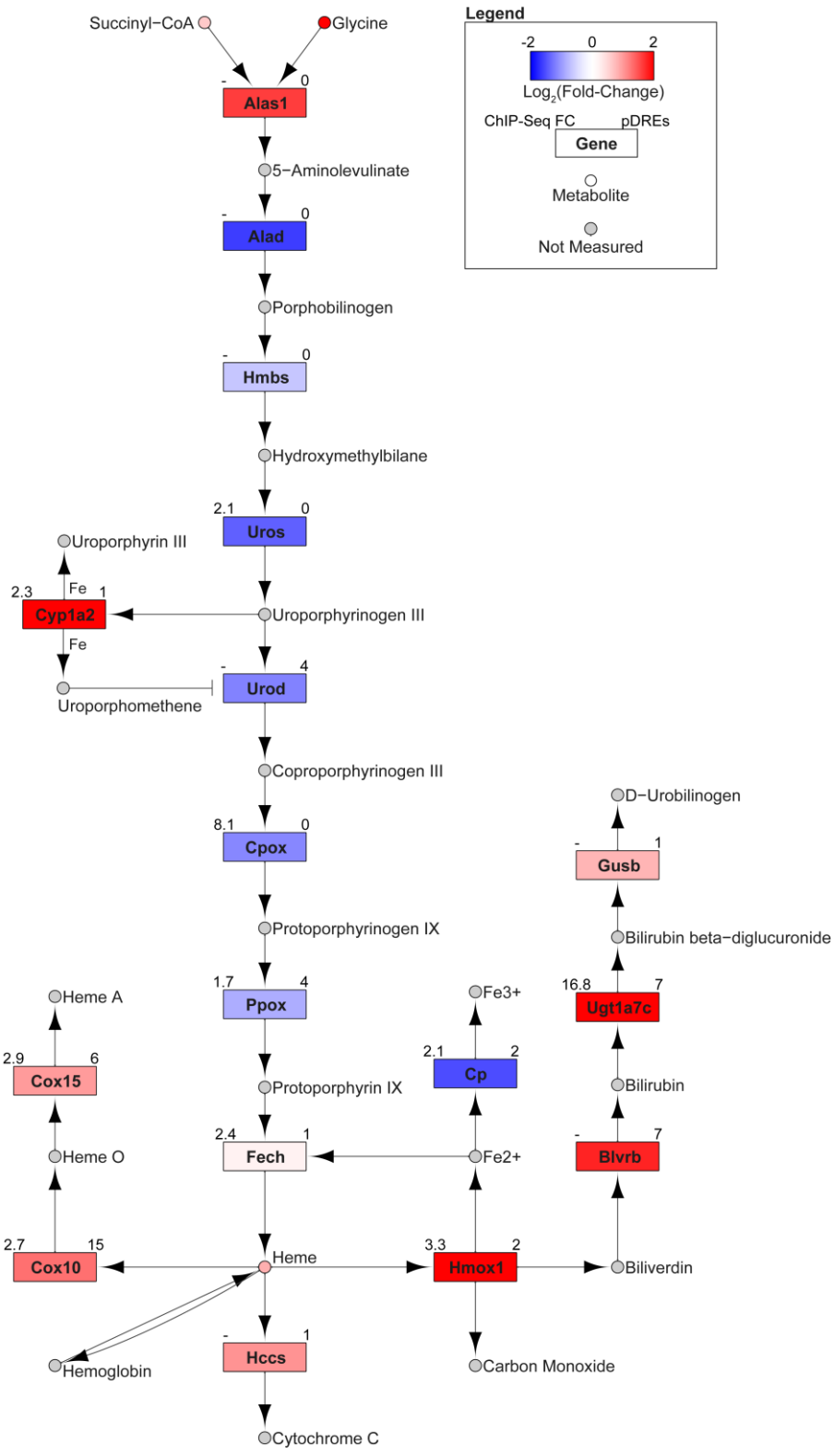

FIGURE 33. TCDD-ELICITED DYSREGULATION OF HEME BIOSYNTHESIS AND METABOLISM

FIGURE 33 (cont'd)

Genes are identified as rectangles and metabolites as circles. Color scale represents the $\log_2$(fold change) for differential gene expression and altered metabolite levels. Grey symbols indicate that the metabolite was not measured. The upper left corner of genes indicates maximum AhR enrichment fold change where '-' indicates no AhR enrichment, and the upper right corner indicates the number of pDREs (MSS ≥ 0.856).

of *Bach1* was induced 1.9-fold by TCDD, while *Maf*, *Maff*, and *Mafk* were induced 1.6-, 34.7-, and 3.0-fold, respectively. AhR enrichment was identified at several Maf-related gene loci, including 8.3-, 2.5-, 3.3, and 1.9-fold enrichment within *Maf*, *Mafb*, *Maff*, and *Mafk*, respectively. *Hmox1* induction is likely in response to TCDD-elicited heme accumulation; however, the 3.3-fold increase in AhR genomic enrichment within the *Hmox1* promoter may also be a contributing factor.

In addition, TCDD elicited a 3.3-fold induction of biliverdin reductase B (*Blvrb*) which metabolizes biliverdin to bilirubin, the latter being an effective peroxyl radical scavenger that inhibits heme-induced lipid peroxidation. Several UDP-glucuronosyltransferases involved in bilirubin conjugation were also induced including *Ugt1a1*, *Ugt1a7c, Ugt1a8,* and *Ugt1a9* (2.2-, 51.2-, 4.8-, and 4.8-fold, respectively) (Figure 33). In the serum, total bilirubin was increased 2.4-fold at 30 µg/kg TCDD, while conjugated (direct) and unconjugated (indirect) bilirubin levels exhibited no clear treatment effect (Figure 32D-F). Similarly, TCDD increased total, direct, and indirect bilirubin levels in the urine 2.6-, 1.8-, and 4.2-fold, respectively (Figure 32G-I). Conjugated-bilirubin in the blood is transported into hepatocytes by solute carrier organic anion transporter 1A1 (*Slco1a1*) and 1B2 (*Slco1b2*), and then exported to the biliary tract by ATP-binding cassette C2 (*Abcc2*) and ATP-binding cassette G2 (*Abcg2*). Hepatic *Slco1a1*, *Slco1b2*, and *Abcg2* were repressed 1,186-, 7.9-, and 3.0-fold, respectively, by TCDD, consistent with increased serum and urine bilirubin levels. Unconjugated bilirubin in the blood binds to albumin (ALB) to limit tissue uptake and toxicity, however TCDD repressed hepatic *Alb* 3.7-fold. In humans, reducing the bilirubin-binding capacity of ALB increases the risk of bilirubin toxicity in the brain (kernicterus) and skin (jaundice). Furthermore, bilirubin can be oxidized back to biliverdin by ROS, creating a redox cycle that draws NADPH away from other reactions including ROS defense responses [28]. Interestingly, bilirubin activates the AhR and induces *Cyp1a1* mRNA levels, likely to enhance bilirubin elimination [49].

Cyp1a1, *1a2,* and *1b1* induction was accompanied by an equally dramatic repression of several highly expressed cytochrome P450 subfamilies such as *2c* (*2c29*, *2c44*, *2c50*, 2c70, and *2c54* repressed 8.7-, 62.3-, 41.6-, 68.6-, and 550.5-fold, respectively), *2d* (*2d9*, *2d26*, *2d34,* and *2d40* repressed 5.8-, 32.4-, 14.8-, and 75.4-fold, respectively), *2e1* (repressed 7.6-fold), *2j* (*2j5*, and *2j9* repressed 32.1, and 17.5-fold, respectively), and *3a* (*3a13*, *3a16*, and *3a25* repressed 17.0-, 5.2-, and 6.0-fold, respectively) (Figure 34). Other hemoproteins were also repressed, including indoleamine 2,3-dioxygenase 2 (*Ido2*; 11.9-fold) and sulfite oxidase (*Suox*; 7.5-fold) (Figure 34). Heme released from degradation is not recycled, but catabolized by *Hmox1*. Therefore, hemoprotein degradation likely also contributes to transient increases in free heme, biliverdin, bilirubin, CO, and Fe^{2+}.

After erythroid progenitors, hepatocytes have the highest rate of heme biosynthesis, with 50% of hepatic heme committed to cytochrome P450 synthesis [50]. The first and rate limiting step of heme biosynthesis, which involves the condensation of glycine with succinyl-CoA to produce delta-aminolevulinic acid (ALA), is catalyzed by mitochondrial delta-aminolevulinate synthase 1 (*Alas1*). TCDD induced hepatic *Alas1* 4.1-fold in the absence of AhR enrichment, consistent with the TCDD-elicited hepatic hemin increases. However, 6 of the other 7 heme biosynthesis enzymes were repressed, including aminolevulinic acid dehydrase (*Alad*), hydroxymethylbilane synthase (*Hmbs*), uroporphyrinogen III synthase (*Uros*), uroporphyrinogen decarboxylase (*Urod*), coproporphyrinogen oxidase (*Cpox*), and protoporphyrinogen oxidase (*Ppox*) (2.9-, 1.3-, 2.4-, 2.0-, 1.9-, and 1.6-fold, respectively) (Figure 33). Furthermore, hepatic expression of *Alas2*, which is typically specific to erythroid-derived cells, was repressed 65.6-fold.

Porphyria cutanea tarda (PCT), the most common human porphyria, is a photosensitive skin disease caused by over-production of hepatic porphyrins, resulting in high urinary concentrations. Biochemically, PCT is characterized by a UROD deficiency that causes uroporphyrinogen III accumulation, although nutritional and/or environmental interactions, such as exposure to AhR agonists, are typically required for disease expression [17]. In the presence

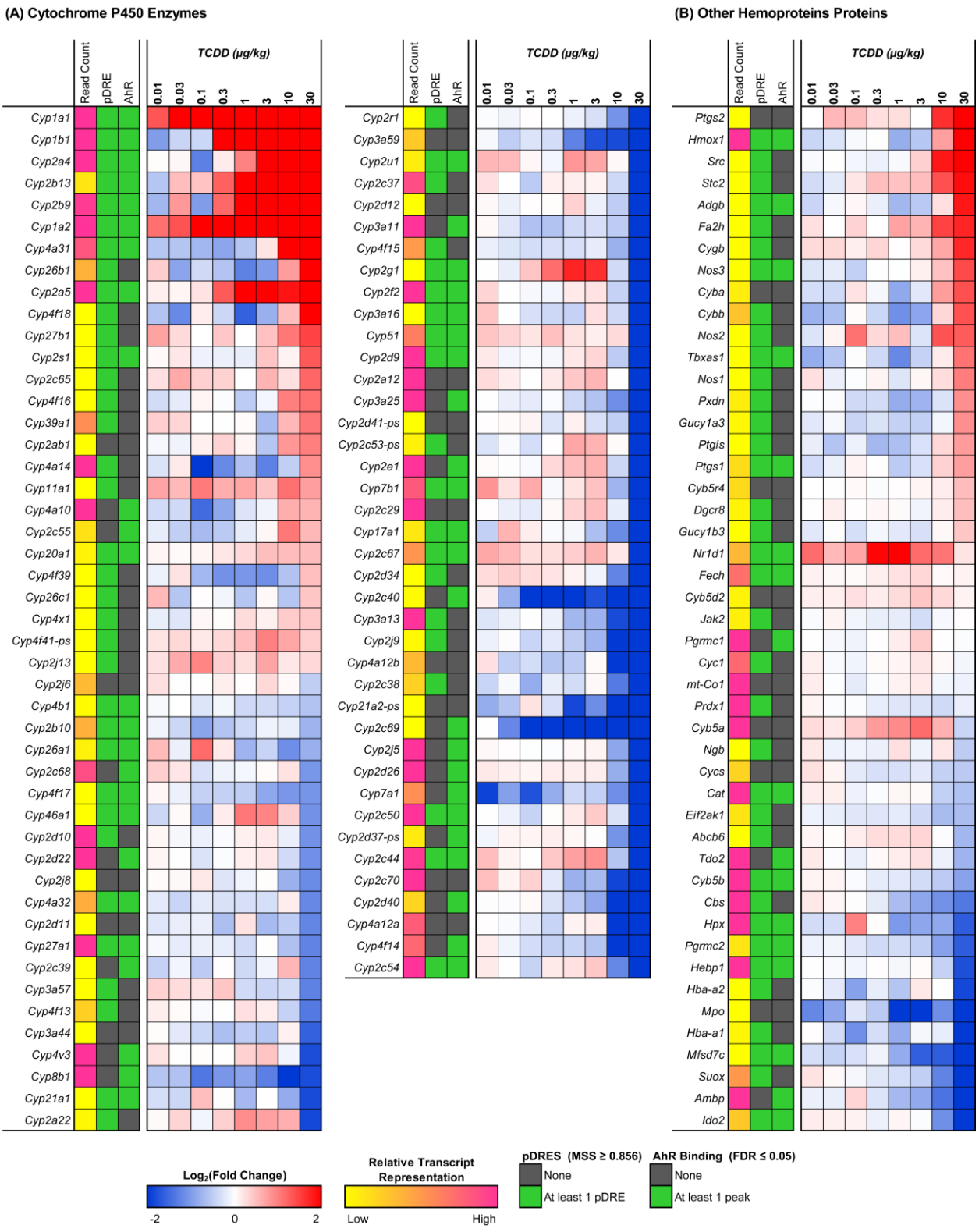

FIGURE 34. TCDD-ELICITED DIFFERENTIAL EXPRESSION OF HEMOPROTEINS

FIGURE 34 (cont'd)

TCDD-elicited hepatic differential expression of genes encoding (A) cytochrome P450 enzymes and (B) other hemoproteins. Male C57BL/6 mice were orally gavaged with sesame oil vehicle or TCDD (0.01-30 µg/kg) every 4 days for 28 days. Color scale represents the $\log_2$(fold change) for differential gene expression, as determined through RNA-Seq analysis (n=3). The presence of pDREs (MSS ≥ 0.856) and AhR enrichment peaks (FDR ≤ 0.05) at 2h are shown as green boxes. Relative gene expression level indicating the number of reads aligned to each transcript is also shown, where yellow represent lower expression (≤ 500 reads) and pink represents higher expression (≥ 10,000).

of Fe and CYP1A2, uroporphyrinogen III is oxidized to uroporphomethene, a UROD inhibitor, and finally, uroporphyrin III, a urinary metabolite identified in rodent porphyria models and PCT patients. Uroporphyrin III is not a substrate for heme synthesis and thus it accumulates in the liver, skin, and urine [17]. While TCDD induces hepatic uroporphyria in rodent models, CYP1A2 null mice are completely protected against uroporphyrin accumulation [17].

At 30 µg/kg TCDD, total urinary porphyrin levels increased 13.2-fold (Figure 32J), consistent with the dark tea color of the collected urine (Figure 32K). This is in agreement with the 2.0-fold repression of *Urod*, mirroring the genetic deficiency in human PCT, and the 4.1-fold induction of *Alas1* which initiates heme biosynthesis and increases precursor levels, as previously reported [18]. Transport of glycine, ALA, and coproporphyrinogen III between the cytosol and mitochondria may also be impaired by the 1.6-, 2.9- and 1.7-fold repression of *Slc25a38*, *Abcb10,* and *Abcb6*, respectively. Furthermore, TCDD induced *Cyp1a2* 20.0-fold, leading to uroporphyrinogen III oxidation and porphyrin accumulation. Lastly, TCDD-elicited mobilization of hepatic Fe^{2+} likely contributes to the development of porphyria as Fe exacerbates TCDD-elicited porphyria in mice [51] while Fe deficiency is completely protective [52].

REV-ERBα/β-regulated hepatic metabolism

In addition to serving as a prosthetic group for BACH1, heme also activates the transcriptional repressors REV-ERBα (*Nr1d1)* and REV-ERBβ (*Nr1d2*). TCDD-elicited hepatic heme accumulation would therefore favor the repressive activity of REV-ERBα and β. Heme-activated REV-ERBα/β compete with retinoic acid receptor-related orphan receptors α and ϒ (*Rora* and *Rorc* were repressed 1.3- and 5.2-fold, respectively) for binding to ROR response elements (RORE). Once bound, REV-ERBα/β recruit the nuclear receptor corepressor–histone deacetylase 3 (NCoR-HDAC3), resulting in the transcriptional repression of RORE-regulated genes.

Comparing hepatic DEGs from TCDD treated mice to RORα/RORɣ double knockout mice [53] revealed that 64 out of 111 genes exhibit the same profile, suggesting TCDD treatment mimics RORα/RORɣ knockout due to heme-mediated REV-ERBα/β activation (Figure 35). Furthermore, a REV-ERBα and HDAC3 co-localization study identified ~100 hepatic genes associated with lipid biosynthesis and metabolism [54], of which 66 were repressed by TCDD (Figure 36). REV-ERBα/β-mediated coordinated repression is consistent with the inhibition of *de novo* fatty acid synthesis and β-oxidation, and in line with TCDD-elicited disruption of lipid metabolism and hepatic steatosis [7, 28].

REV-ERBα/β transcriptional repressors serve as links between the positive and negative loops that regulate peripheral circadian expression. The positive loop consists of aryl hydrocarbon receptor nuclear translocator-like (ARNTL) and circadian locomotor output cycles kaput (CLOCK), which form a heterodimer and induce circadian output mediators. Accordingly, several circadian-regulated genes were repressed by TCDD, including *Arntl* (aka *Bmal1*; 23.9-fold), *Clock* (2.6-fold), neuronal PAS domain protein 2 (*Npas2*, 36.3-fold), elongation of very long chain fatty acids-like 3 (*Elovl3*, 736.3-fold), apolipoprotein A-I (*Apoa1*, 43.7-fold), and apolipoprotein C-III (*Apoc3*, 9.3-fold). There is also a connection between disruption of the hepatic peripheral clock and MetS/NAFLD development (reviewed in [55]). In mice, loss-of-function of *Clock* causes hyperlipidemia, hepatic steatosis, and obesity [56], while liver-specific *Arntl* knockout leads to exaggerated glucose clearance and hypoglycemia in the fasted state [57]. In our study, fasting blood glucose decreased 1.7- and 2.1-fold at 15 and 23 days, respectively, after the initial TCDD dose (Figure 37A). TCDD also increased glucose tolerance 22 days after the initial dose (Figure 37B-C), comparable to results in TCDD-treated female mice [10]. Although this suggests that TCDD disrupted the peripheral clock regulating hepatic metabolism, further studies which specifically consider time of day of dosing and tissue harvesting are required.

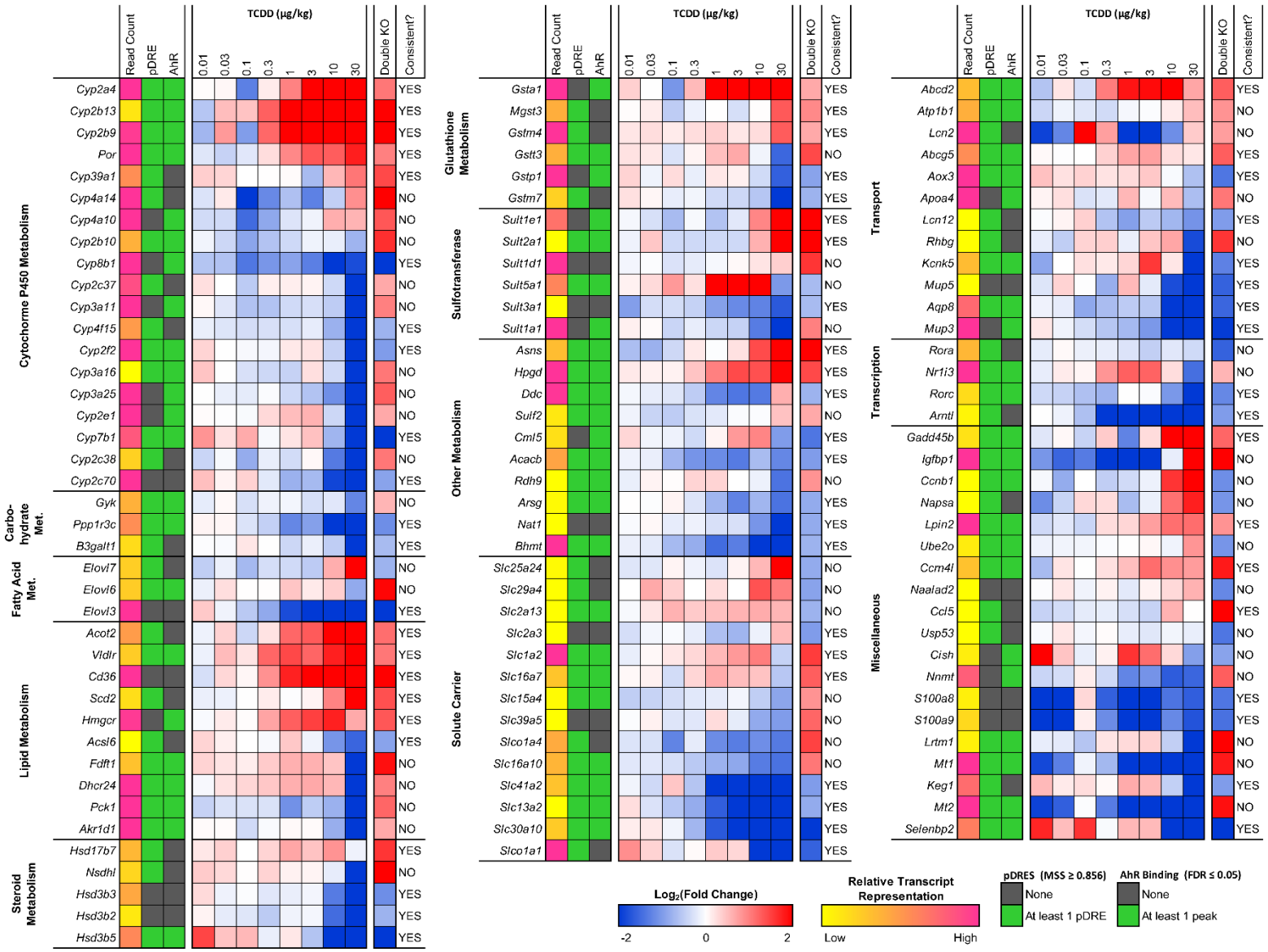

FIGURE 35. THE EFFECTS OF TCDD ON RORα/RORγ-REGULATED GENES

FIGURE 35 (cont'd)

Heat map comparing hepatic TCDD-elicited differential gene expression to RORα/RORϒ double knockout (KO) mice [53]. Color scale represents the $\log_2$(fold change) for differential gene expression, where fold change (FC) was determined relative to sesame oil vehicle for TCDD-treated mice and relative to wild type for RORα/RORϒ KO mice. For each gene, the maximal TCDD-elicited response (|FC| ≥ 1.5) was classified as consistent (yes vs. no) with the RORα/RORϒ double KO based on the direction of differential expression. The presence of pDREs (MSS ≥ 0.856) and AhR enrichment peaks (FDR ≤ 0.05) at 2h are shown as green boxes. Relative gene expression level indicating the number of reads aligned to each transcript is also shown, where yellow represents lower expression (≤ 500 reads) and pink represents higher expression (≥ 10,000).

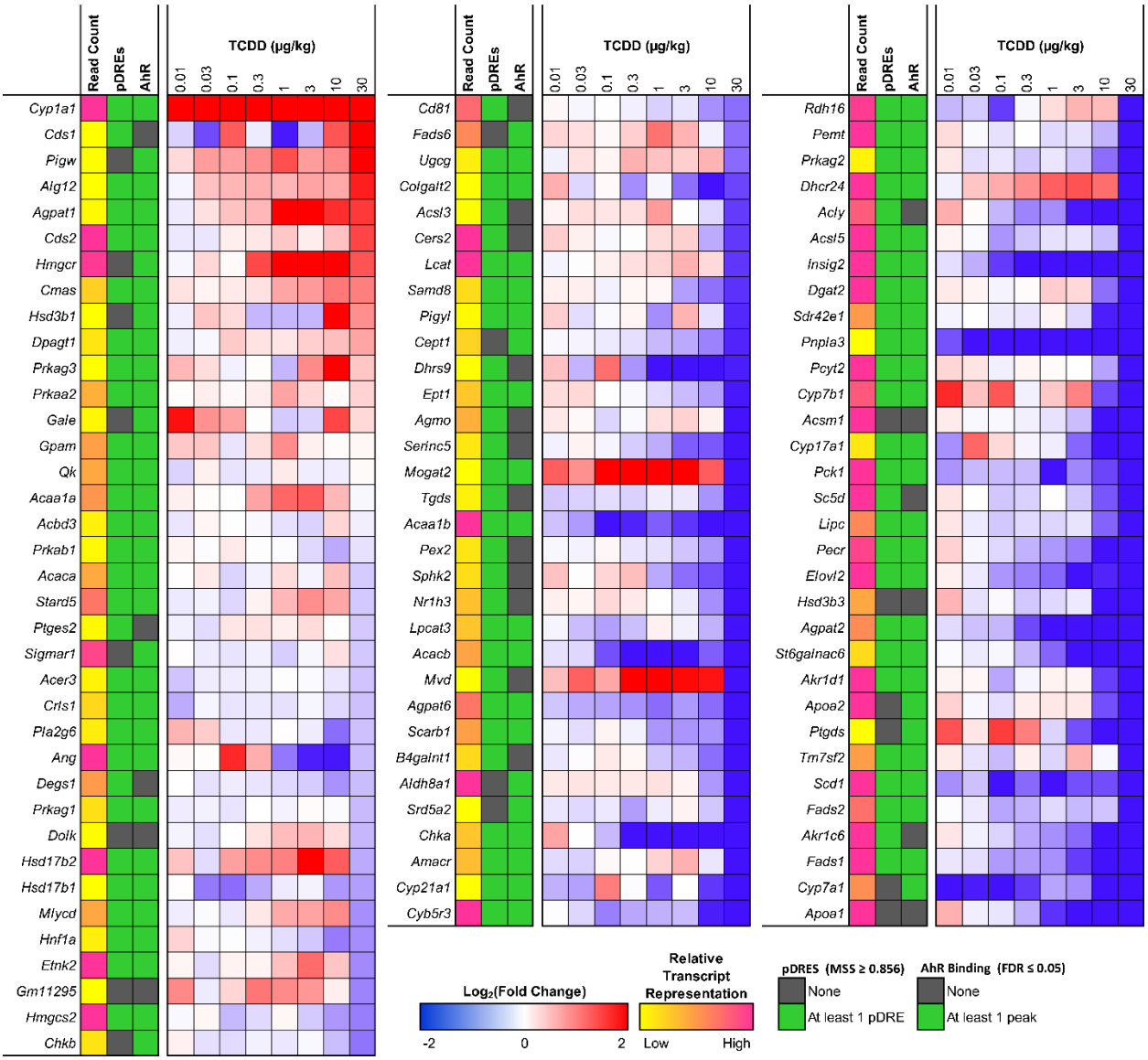

FIGURE 36. THE EFFECTS OF TCDD ON REV-ERBα-REGULATED GENES

TCDD-elicited hepatic differential expression of REV-ERBα target genes associated with lipid biosynthesis and metabolism identified by Feng et al [54]. Male C57BL/6 mice were orally gavaged with sesame oil vehicle or TCDD (0.01-30 µg/kg) every 4 days for 28 days. Color scale represents the $\log_2$(fold change) for differential gene expression, as determined through RNA-Seq analysis (n=3). The presence of pDREs (MSS ≥ 0.856) and AhR enrichment peaks (FDR ≤ 0.05) at 2h are shown as green boxes. Relative gene expression level indicating the number of reads aligned to each transcript is also shown, where yellow represents lower expression (≤ 500 reads) and pink represents higher expression (≥ 10,000).

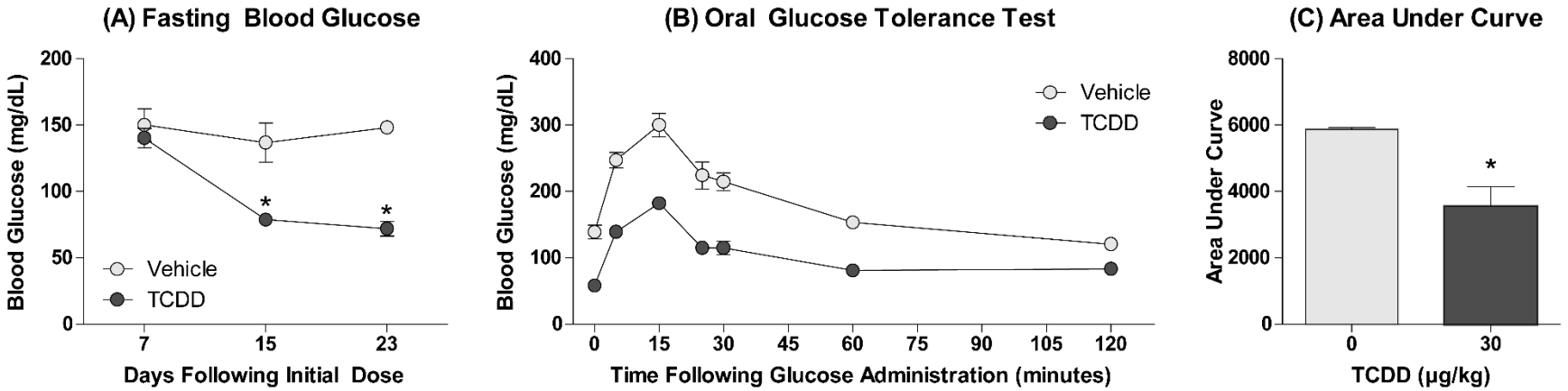

FIGURE 37. EFFECTS OF TCDD ON BLOOD GLUCOSE LEVELS

(A) Fasting blood glucose levels on days 7, 15, and 23 in male C57BL/6 mice orally gavaged with sesame oil vehicle or 30 µg/kg TCDD every 4 days. (B) Oral glucose tolerance test at 22d in male C57BL/6 mice receiving an oral gavage of sesame oil vehicle or 30 µg/kg TCDD every 4 days, and (C) the corresponding area under the curve. Data points represent the average ± standard error of the mean (SEM) for at least 3 biological replicates. Statistical significance (* $p \leq 0.05$) was determined using two-way ANOVA analysis followed by Tukey's test (A) or a Student's t-test (C) performed in SAS 9.3.

DISCUSSION

Dysregulation of Fe homeostasis plays an important role in NAFLD and MetS development (reviewed in [58]). Although there is no evidence that Fe significantly affects hepatic lipid accumulation, increased levels are associated with increased risk of steatohepatitis, fibrosis, and HCC, suggesting that Fe promotes the progression of steatosis to more severe liver pathologies [15, 16, 59]. NAFLD patients often exhibit 'dysmetabolic iron overload syndrome' (DIOS), characterized by moderate hepatic Fe accumulation, normal transferrin saturation, and elevated hepatic and serum HAMP levels [58]. In DIOS, elevated inflammatory cytokines (IL-6, TNF-α), LPS, and excess Fe trigger HAMP synthesis, thereby reducing Fe export from hepatocytes and macrophages.

In contrast to NAFLD and DIOS in humans, TCDD repressed *Hamp* expression, mimicking the underlying genetic cause of human hereditary hemochromatosis (HH), in which excessive dietary absorption leads to systemic Fe overloading. HAMP deficiency is the unifying mechanism responsible for both classic HH caused by a *Hfe* mutation, as well as juvenile HH caused by mutations in *Hfe2* or *Hamp* [60]. Our results suggest that TCDD decreased *Hamp* transcription by repressing expression of components of the HFE-HFE2-TFR2-BMP6 'iron sensing' complex, which is required for SMAD-mediated expression of *Hamp* and *Hamp2*. Consequently, HAMP is unavailable to initiate the endocytosis and eventual degradation of SLC40A1, leading to continuous absorption of dietary Fe and accumulation in the serum and urine.

On average, HH patients exhibit hepatic Fe concentrations ~12-fold higher compared to patients with other chronic liver diseases, along with transferrin saturation values >80% (normal range = 15-55%) and serum Fe levels reaching ~160-200 µg/dL (normal range = 50-170 µg/dL) [61, 62]. In 2-month-old *Hamp* knockout mice, hepatic Fe levels increased 5-fold, which worsened to 15-fold at 8 months of age. Serum Fe levels also increased ~1.25-fold at 2 months, but remained constant across time [40]. Unlike HH patients and *Hamp* null mice, TCDD caused greater Fe accumulation in the serum compared to the liver, while transferrin saturation was

unchanged due to corresponding increases in serum transferrin. However, our mice were only ~2 months old and hepatic Fe accumulation may have increased with age if the study had been prolonged. Additionally, substantial strain differences are reported in *Hfe* knockout models of HH. *Hfe* null mice on a C57BL/6 background exhibit more modest hepatic Fe accumulation and smaller increases in transferrin saturation compared to C3H or AKR nulls [63], suggesting other genetic factors influence Fe dysregulation and that C57BL/6 mice are comparatively resistant to hepatic Fe accumulation. Nevertheless, even moderate hepatic Fe accumulation has been associated with the progression of liver disease in combination with other underlying liver injuries (i.e., chronic HCV infection, oxidative stress) [64].

Although total Fe levels are often used as a biomarker for HH, oxidative stress is dependent on the redox state of Fe present [35]. TCDD accelerates the release of catalytically active Fe^{2+} from ferritin thereby increasing the pool of free Fe and ROS production through the Haber-Weiss reaction [36]. The induction of cytochrome P450s and XDH/XO, as well as accumulating heme levels from *de novo* synthesis and net repression of hepatic hemoproteins, further contribute to oxidative stress fueled by hepatic fat accumulation and lipid peroxidation. Free heme is not only a source of redox-active Fe, but it also promotes inflammation through activation of endothelial cells and neutrophils, leading to chemotaxis, leukocyte recruitment, and pro-inflammatory cytokine expression [65]. In addition, TCDD repressed several scavenging proteins (i.e., HP and HPX), compromising anti-oxidant cellular defense. As defense systems become overwhelmed, accumulating tissue damage leads to cell death and hepatotoxicity. Increased porphyrin biosynthesis through induction of *Alas1* draws succinyl-CoA away from the TCA cycle, reducing ATP production and putting further pressure on strained cellular bioenergetics. However, only a fraction of synthesized porphyrins is converted to heme due to repression of *Urod* and induction of *Cyp1a2*, leading to porphyrin accumulation.

Heme also serves as the biological ligand for several transcription factors including BACH1 and REV-ERBα/β, which regulate heme catabolism and peripheral circadian clocks,

respectively [48, 66]. In the liver, circadian oscillations are controlled by environmental cues (i.e., zeitgebers) that entrain or synchronize the biological rhythm to a 24h light/dark cycle. For example, feeding-fasting cycles regulate the core clock, as well as output regulators such as the REV-ERBs and RORs that subsequently coordinate the oscillatory expression patterns of downstream genes. Accumulating evidence suggests that AhR activation regulates peripheral circadian clocks [67]. TCDD-elicited differential gene expression and AhR enrichment suggest that interactions with circadian regulators may modulate the phase, period and/or amplitude of oscillating gene expression associated with fatty acid biosynthesis/metabolism, contributing to the progression of TCDD-elicited hepatotoxicity. Peripheral clock disruption has been associated with hepatic lipid accumulation, dysregulated glucose homeostasis, and the progression of NAFLD pathologies [55].

In summary, TCDD-elicited hepatotoxicity involves the convergence of primary AhR-mediated effects (e.g., *Cyp1a1/1a2* induction, hepatic fat accumulation) and elicited tertiary responses (e.g., *Hamp* repression, Fe^{2+} overloading, heme accumulation, oxidative stress) across the liver-intestine axis (Figure 38). This suggests that AhR-mediated toxicity is a cumulative response to the overall burden of multiple disrupted pathways, as opposed to a single adverse effect. It is consistent with the multiple “hit” paradigm proposed in numerous liver injury models where multiple factors contribute to disease progression and severity. Consequently, each response and the resulting interactions contribute to the overall pathological burden of toxicity. Additional comparative studies are required to identify which perturbations exert the greatest influence and are most relevant to the population of interest.

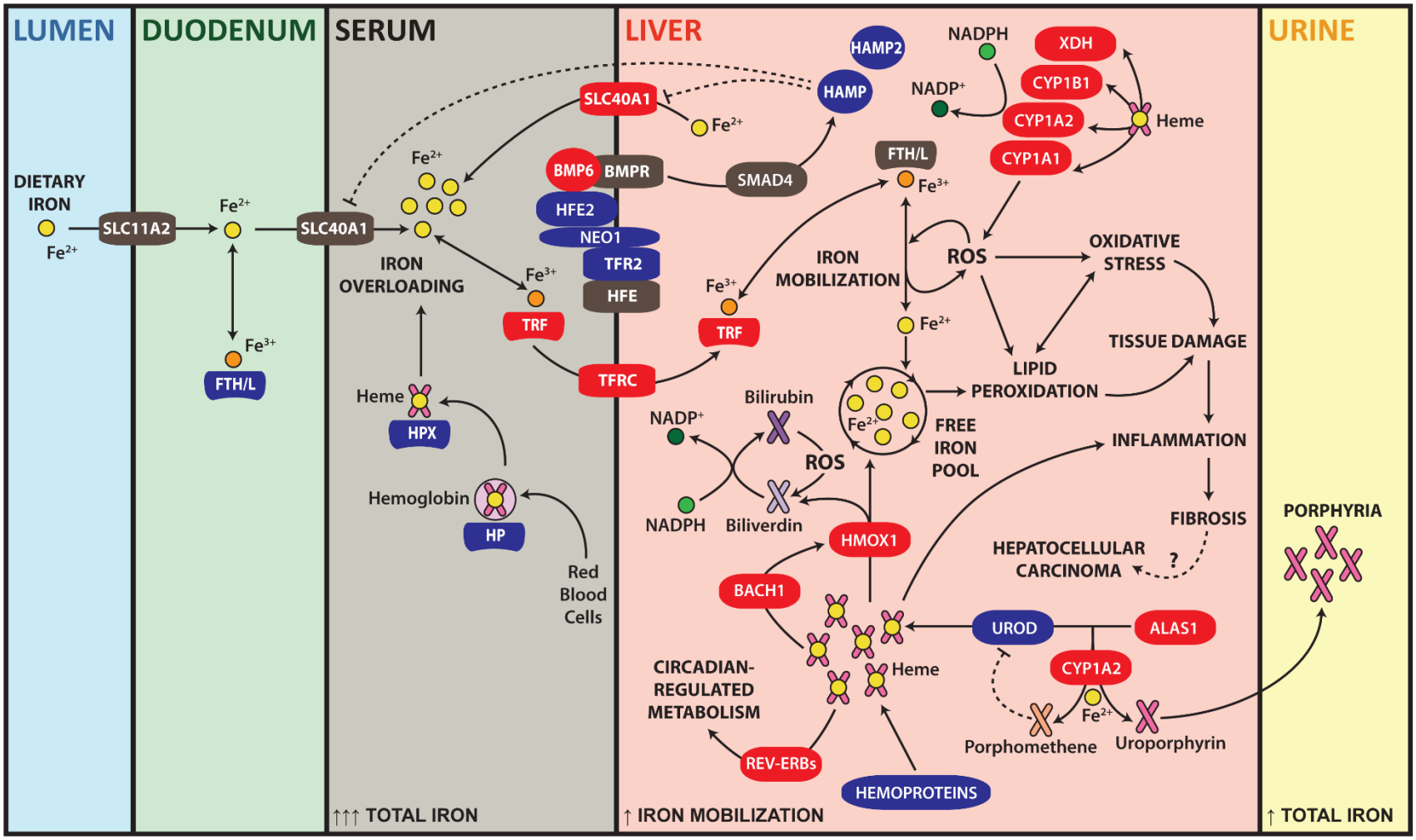

FIGURE 38. SUMMARY OF TCDD-ELICITED EFFECTS ON IRON AND HEME HOMEOSTASIS

Convergence of AhR-mediated disruption of systemic Fe homeostasis and heme metabolism involving interactions between the intestine, serum, liver, and urine. Red, blue, or grey indicate increased, decreased, or unchanged levels, respectively.

REFERENCES

REFERENCES

1. Trauner, M., M. Arrese, and M. Wagner, *Fatty liver and lipotoxicity.* Biochim Biophys Acta, 2010. 1801(3): p. 299-310.

2. Ford, E.S., C. Li, and G. Zhao, *Prevalence and correlates of metabolic syndrome based on a harmonious definition among adults in the US.* J Diabetes, 2010. 2(3): p. 180-93.

3. Casals-Casas, C. and B. Desvergne, *Endocrine disruptors: from endocrine to metabolic disruption.* Annu Rev Physiol, 2011. 73: p. 135-62.

4. Denison, M.S., A.A. Soshilov, G. He, D.E. DeGroot, and B. Zhao, *Exactly the same but different: promiscuity and diversity in the molecular mechanisms of action of the aryl hydrocarbon (dioxin) receptor.* Toxicol Sci, 2011. 124(1): p. 1-22.

5. Hankinson, O., *The aryl hydrocarbon receptor complex.* Annu Rev Pharmacol Toxicol, 1995. 35: p. 307-40.

6. Huang, G. and C.J. Elferink, *A novel nonconsensus xenobiotic response element capable of mediating aryl hydrocarbon receptor-dependent gene expression.* Mol Pharmacol, 2012. 81(3): p. 338-47.

7. Boverhof, D.R., L.D. Burgoon, C. Tashiro, B. Chittim, J.R. Harkema, D.B. Jump, and T.R. Zacharewski, *Temporal and dose-dependent hepatic gene expression patterns in mice provide new insights into TCDD-Mediated hepatotoxicity.* Toxicol Sci, 2005. 85(2): p. 1048-63.

8. Kopec, A.K., L.D. Burgoon, D. Ibrahim-Aibo, B.D. Mets, C. Tashiro, D. Potter, B. Sharratt, J.R. Harkema, and T.R. Zacharewski, *PCB153-elicited hepatic responses in the immature, ovariectomized C57BL/6 mice: comparative toxicogenomic effects of dioxin and non-dioxin-like ligands.* Toxicol Appl Pharmacol, 2010. 243(3): p. 359-71.

9. Pierre, S., A. Chevallier, F. Teixeira-Clerc, A. Ambolet-Camoit, L.C. Bui, A.S. Bats, J.C. Fournet, P. Fernandez-Salguero, M. Aggerbeck, S. Lotersztajn, R. Barouki, and X. Coumoul, *Aryl hydrocarbon receptor-dependent induction of liver fibrosis by dioxin.* Toxicol Sci, 2014. 137(1): p. 114-24.

10. Nault, R., K.A. Fader, D.A. Ammendolia, P. Dornbos, D. Potter, B. Sharratt, K. Kumagai, J.R. Harkema, S.Y. Lunt, J. Matthews, and T. Zacharewski, *Dose-Dependent Metabolic Reprogramming and Differential Gene Expression in TCDD-Elicited Hepatic Fibrosis.* Toxicol Sci, 2016. 154(2): p. 253-266.

11. Stohs, S.J., *Oxidative stress induced by 2,3,7,8-tetrachlorodibenzo-p-dioxin (TCDD).* Free Radic Biol Med, 1990. 9(1): p. 79-90.

12. Slezak, B.P., G.E. Hatch, M.J. DeVito, J.J. Diliberto, R. Slade, K. Crissman, E. Hassoun, and L.S. Birnbaum, *Oxidative stress in female B6C3F1 mice following acute and subchronic exposure to 2,3,7,8-tetrachlorodibenzo-p-dioxin (TCDD).* Toxicol Sci, 2000. 54(2): p. 390-8.

13. al-Turk, W.A., M.A. Shara, H. Mohammadpour, and S.J. Stohs, *Dietary iron and 2,3,7,8-tetrachlorodibenzo-p-dioxin induced alterations in hepatic lipid peroxidation, glutathione content and body weight.* Drug Chem Toxicol, 1988. 11(1): p. 55-70.

14. Al-Bayati, Z.A. and S.J. Stohs, *The role of iron in 2,3,7,8-tetrachlorodibenzo-p-dioxin-induced lipid peroxidation by rat liver microsomes.* Toxicol Lett, 1987. 38(1-2): p. 115-21.

15. Kew, M.C., *Hepatic iron overload and hepatocellular carcinoma.* Liver Cancer, 2014. 3(1): p. 31-40.

16. George, D.K., S. Goldwurm, G.A. MacDonald, L.L. Cowley, N.I. Walker, P.J. Ward, E.C. Jazwinska, and L.W. Powell, *Increased hepatic iron concentration in nonalcoholic steatohepatitis is associated with increased fibrosis.* Gastroenterology, 1998. 114(2): p. 311-8.

17. Smith, A.G., B. Clothier, P. Carthew, N.L. Childs, P.R. Sinclair, D.W. Nebert, and T.P. Dalton, *Protection of the Cyp1a2(-/-) null mouse against uroporphyria and hepatic injury following exposure to 2,3,7,8-tetrachlorodibenzo-p-dioxin.* Toxicol Appl Pharmacol, 2001. 173(2): p. 89-98.

18. Goldstein, J.A., P. Hickman, H. Bergman, and J.G. Vos, *Hepatic porphyria induced by 2,3,7,8-tetrachlorodibenzo-p-dioxin in the mouse.* Res Commun Chem Pathol Pharmacol, 1973. 6(3): p. 919-28.

19. Vos, J.G. and A.H. Penninks, *Dioxin and Organotin Compounds as Model Immunotoxic Chemicals* in *Selectivity and Molecular Mechanisms of Toxicity*, F. De Matteis and E.A. Lock, Editors. 1987, Palgrave Macmillan UK. p. 85-102.

20. Sorg, O., M. Zennegg, P. Schmid, R. Fedosyuk, R. Valikhnovskyi, O. Gaide, V. Kniazevych, and J.H. Saurat, *2,3,7,8-tetrachlorodibenzo-p-dioxin (TCDD) poisoning in Victor Yushchenko: identification and measurement of TCDD metabolites.* Lancet, 2009. 374(9696): p. 1179-85.

21. Wolfe, W.H., J.E. Michalek, J.C. Miner, J.L. Pirkle, S.P. Caudill, D.G. Patterson, Jr., and L.L. Needham, *Determinants of TCDD half-life in veterans of operation ranch hand.* J Toxicol Environ Health, 1994. 41(4): p. 481-8.

22. Gasiewicz, T.A., L.E. Geiger, G. Rucci, and R.A. Neal, *Distribution, excretion, and metabolism of 2,3,7,8-tetrachlorodibenzo-p-dioxin in C57BL/6J, DBA/2J, and B6D2F1/J mice.* Drug Metab Dispos, 1983. 11(5): p. 397-403.

23. Kopec, A.K., L.D. Burgoon, D. Ibrahim-Aibo, A.R. Burg, A.W. Lee, C. Tashiro, D. Potter, B. Sharratt, J.R. Harkema, J.C. Rowlands, R.A. Budinsky, and T.R. Zacharewski, *Automated dose-response analysis and comparative toxicogenomic evaluation of the hepatic effects elicited by TCDD, TCDF, and PCB126 in C57BL/6 mice.* Toxicol Sci, 2010. 118(1): p. 286-97.

24. Wolff, F., B. Gulbis, and F. Cotton, *Spectrophotometric quantification of total urinary porphyrins as a screening test for porphyrias: threshold value revisited.* Clin Biochem, 2013. 46(18): p. 1825-9.

25. Nault, R., K.A. Fader, and T. Zacharewski, *RNA-Seq versus oligonucleotide array assessment of dose-dependent TCDD-elicited hepatic gene expression in mice.* BMC Genomics, 2015. 16(1): p. 373.

26. Eckel, J.E., C. Gennings, V.M. Chinchilli, L.D. Burgoon, and T.R. Zacharewski, *Empirical bayes gene screening tool for time-course or dose-response microarray data.* J Biopharm Stat, 2004. 14(3): p. 647-70.

27. Eckel, J.E., C. Gennings, T.M. Therneau, L.D. Burgoon, D.R. Boverhof, and T.R. Zacharewski, *Normalization of two-channel microarray experiments: a semiparametric approach.* Bioinformatics, 2005. 21(7): p. 1078-83.

28. Nault, R., K.A. Fader, M.P. Kirby, S. Ahmed, J. Matthews, A.D. Jones, S.Y. Lunt, and T.R. Zacharewski, *Pyruvate Kinase Isoform Switching and Hepatic Metabolic Reprogramming by the Environmental Contaminant 2,3,7,8-Tetrachlorodibenzo-p-Dioxin.* Toxicol Sci, 2016. 149(2): p. 358-71.

29. Vos, J.G., J.A. Moore, and J.G. Zinkl, *Toxicity of 2,3,7,8-tetrachlorodibenzo-p-dioxin (TCDD) in C57B1/6 mice.* Toxicol Appl Pharmacol, 1974. 29(2): p. 229-41.

30. Birnbaum, L.S., M.M. McDonald, P.C. Blair, A.M. Clark, and M.W. Harris, *Differential toxicity of 2,3,7,8-tetrachlorodibenzo-p-dioxin (TCDD) in C57BL/6J mice congenic at the Ah Locus.* Fundam Appl Toxicol, 1990. 15(1): p. 186-200.

31. McConnell, E.E., J.A. Moore, J.K. Haseman, and M.W. Harris, *The comparative toxicity of chlorinated dibenzo-p-dioxins in mice and guinea pigs.* Toxicol Appl Pharmacol, 1978. 44(2): p. 335-56.

32. Jones, G. and J.B. Greig, *Pathological-Changes in Liver of Mice Given 2,3,7,8-Tetrachlorodibenzo-P-Dioxin.* Experientia, 1975. 31(11): p. 1315-1317.

33. Fader, K.A., R. Nault, D.A. Ammendolia, J.R. Harkema, K.J. Williams, R.B. Crawford, N.E. Kaminski, D. Potter, B. Sharratt, and T.R. Zacharewski, *2,3,7,8-Tetrachlorodibenzo-p-Dioxin Alters Lipid Metabolism and Depletes Immune Cell Populations in the Jejunum of C57BL/6 Mice.* Toxicol Sci, 2015. 148(2): p. 567-80.

34. Fader, K.A., R. Nault, C. Zhang, K. Kumagai, J.R. Harkema, and T.R. Zacharewski, *2,3,7,8-Tetrachlorodibenzo-p-dioxin (TCDD)-elicited effects on bile acid homeostasis: Alterations in biosynthesis, enterohepatic circulation, and microbial metabolism.* Sci Rep, 2017. 7(1): p. 5921.

35. Gruger, E.H., Jr. and A.L. Tappel, *Reactions of biological antioxidants. I. Fe(3)-catalyzed reactions of lipid hydroperoxides with alpha-tocopherol.* Lipids, 1970. 5(3): p. 326-31.

36. Rowley, B. and G.D. Sweeney, *Release of ferrous iron from ferritin by liver microsomes: a possible role in the toxicity of 2,3,7,8-tetrachlorodibenzo-p-dioxin.* Can J Biochem Cell Biol, 1984. 62(12): p. 1293-300.

37. Mazur, A., S. Baez, and E. Shorr, *The mechanism of iron release from ferritin as related to its biological properties.* J Biol Chem, 1955. 213(1): p. 147-60.

38. Zhao, N., A.S. Zhang, and C.A. Enns, *Iron regulation by hepcidin.* J Clin Invest, 2013. 123(6): p. 2337-43.

39. Ilyin, G., B. Courselaud, M.B. Troadec, C. Pigeon, M. Alizadeh, P. Leroyer, P. Brissot, and O. Loreal, *Comparative analysis of mouse hepcidin 1 and 2 genes: evidence for different patterns of expression and co-inducibility during iron overload.* FEBS Lett, 2003. 542(1-3): p. 22-6.

40. Lesbordes-Brion, J.C., L. Viatte, M. Bennoun, D.Q. Lou, G. Ramey, C. Houbron, G. Hamard, A. Kahn, and S. Vaulont, *Targeted disruption of the hepcidin 1 gene results in severe hemochromatosis.* Blood, 2006. 108(4): p. 1402-5.

41. Nicolas, G., M. Bennoun, A. Porteu, S. Mativet, C. Beaumont, B. Grandchamp, M. Sirito, M. Sawadogo, A. Kahn, and S. Vaulont, *Severe iron deficiency anemia in transgenic mice expressing liver hepcidin.* Proc Natl Acad Sci U S A, 2002. 99(7): p. 4596-601.

42. Lou, D.Q., G. Nicolas, J.C. Lesbordes, L. Viatte, G. Grimber, M.F. Szajnert, A. Kahn, and S. Vaulont, *Functional differences between hepcidin 1 and 2 in transgenic mice.* Blood, 2004. 103(7): p. 2816-21.

43. Brasse-Lagnel, C., Z. Karim, P. Letteron, S. Bekri, A. Bado, and C. Beaumont, *Intestinal DMT1 cotransporter is down-regulated by hepcidin via proteasome internalization and degradation.* Gastroenterology, 2011. 140(4): p. 1261-1271 e1.

44. Manis, J. and G. Kim, *Stimulation of iron absorption by polychlorinated aromatic hydrocarbons.* Am J Physiol, 1979. 236(6): p. E763-8.

45. D'Alessio, F., M.W. Hentze, and M.U. Muckenthaler, *The hemochromatosis proteins HFE, TfR2, and HJV form a membrane-associated protein complex for hepcidin regulation.* J Hepatol, 2012. 57(5): p. 1052-60.

46. Zhao, N., J.E. Maxson, R.H. Zhang, M. Wahedi, C.A. Enns, and A.S. Zhang, *Neogenin Facilitates the Induction of Hepcidin Expression by Hemojuvelin in the Liver.* J Biol Chem, 2016. 291(23): p. 12322-35.

47. Qian, Y., S. Zhang, W. Guo, J. Ma, Y. Chen, L. Wang, M. Zhao, and S. Liu, *Polychlorinated biphenyls (PCBs) inhibit hepcidin expression through an estrogen-like effect associated with disordered systemic iron homeostasis.* Chem Res Toxicol, 2015. 28(4): p. 629-40.

48. Sun, J., H. Hoshino, K. Takaku, O. Nakajima, A. Muto, H. Suzuki, S. Tashiro, S. Takahashi, S. Shibahara, J. Alam, M.M. Taketo, M. Yamamoto, and K. Igarashi, *Hemoprotein Bach1 regulates enhancer availability of heme oxygenase-1 gene.* EMBO J, 2002. 21(19): p. 5216-24.

49. Sinal, C.J. and J.R. Bend, *Aryl hydrocarbon receptor-dependent induction of cyp1a1 by bilirubin in mouse hepatoma hepa 1c1c7 cells.* Mol Pharmacol, 1997. 52(4): p. 590-9.

50. Chiabrando, D., F. Vinchi, V. Fiorito, S. Mercurio, and E. Tolosano, *Heme in pathophysiology: a matter of scavenging, metabolism and trafficking across cell membranes.* Front Pharmacol, 2014. 5: p. 61.

51. Smith, A.G., B. Clothier, S. Robinson, M.J. Scullion, P. Carthew, R. Edwards, J. Luo, C.K. Lim, and M. Toledano, *Interaction between iron metabolism and 2,3,7,8-tetrachlorodibenzo-p-dioxin in mice with variants of the Ahr gene: a hepatic oxidative mechanism.* Mol Pharmacol, 1998. 53(1): p. 52-61.

52. Sweeny, G.D., K.G. Jones, F.M. Cole, D. Basford, and F. Krestynski, *Iron deficiency prevents liver toxicity of 2,3,7,8-tetrachlorodibenzo-p-dioxin.* Science, 1979. 204(4390): p. 332-5.

53. Kang, H.S., M. Angers, J.Y. Beak, X. Wu, J.M. Gimble, T. Wada, W. Xie, J.B. Collins, S.F. Grissom, and A.M. Jetten, *Gene expression profiling reveals a regulatory role for ROR alpha and ROR gamma in phase I and phase II metabolism.* Physiol Genomics, 2007. 31(2): p. 281-94.

54. Feng, D., T. Liu, Z. Sun, A. Bugge, S.E. Mullican, T. Alenghat, X.S. Liu, and M.A. Lazar, *A circadian rhythm orchestrated by histone deacetylase 3 controls hepatic lipid metabolism.* Science, 2011. 331(6022): p. 1315-9.

55. Li, M.D., C.M. Li, and Z. Wang, *The role of circadian clocks in metabolic disease.* Yale J Biol Med, 2012. 85(3): p. 387-401.

56. Turek, F.W., C. Joshu, A. Kohsaka, E. Lin, G. Ivanova, E. McDearmon, A. Laposky, S. Losee-Olson, A. Easton, D.R. Jensen, R.H. Eckel, J.S. Takahashi, and J. Bass, *Obesity and metabolic syndrome in circadian Clock mutant mice.* Science, 2005. 308(5724): p. 1043-5.

57. Lamia, K.A., K.F. Storch, and C.J. Weitz, *Physiological significance of a peripheral tissue circadian clock.* Proc Natl Acad Sci U S A, 2008. 105(39): p. 15172-7.

58. Aigner, E., G. Weiss, and C. Datz, *Dysregulation of iron and copper homeostasis in nonalcoholic fatty liver.* World J Hepatol, 2015. 7(2): p. 177-88.

59. Fargion, S., M. Mattioli, A.L. Fracanzani, M. Sampietro, D. Tavazzi, P. Fociani, E. Taioli, L. Valenti, and G. Fiorelli, *Hyperferritinemia, iron overload, and multiple metabolic alterations identify patients at risk for nonalcoholic steatohepatitis.* Am J Gastroenterol, 2001. 96(8): p. 2448-55.

60. Roetto, A. and C. Camaschella, *New insights into iron homeostasis through the study of non-HFE hereditary haemochromatosis.* Best Pract Res Clin Haematol, 2005. 18(2): p. 235-50.

61. Kowdley, K.V., T.D. Trainer, J.R. Saltzman, M. Pedrosa, E.L. Krawitt, T.A. Knox, K. Susskind, D. Pratt, H.L. Bonkovsky, N.D. Grace, and M.M. Kaplan, *Utility of hepatic iron index in American patients with hereditary hemochromatosis: a multicenter study.* Gastroenterology, 1997. 113(4): p. 1270-7.

62. Parkash, O. and M. Akram, *Hereditary Hemochromatosis.* J Coll Physicians Surg Pak, 2015. 25(9): p. 644-7.

63. Fleming, R.E., C.C. Holden, S. Tomatsu, A. Waheed, E.M. Brunt, R.S. Britton, B.R. Bacon, D.C. Roopenian, and W.S. Sly, *Mouse strain differences determine severity of iron*

accumulation in Hfe knockout model of hereditary hemochromatosis. Proc Natl Acad Sci U S A, 2001. 98(5): p. 2707-11.

64. Isom, H.C., E.I. McDevitt, and M.S. Moon, *Elevated hepatic iron: a confounding factor in chronic hepatitis C.* Biochim Biophys Acta, 2009. 1790(7): p. 650-62.

65. Kumar, S. and U. Bandyopadhyay, *Free heme toxicity and its detoxification systems in human.* Toxicol Lett, 2005. 157(3): p. 175-88.

66. Raghuram, S., K.R. Stayrook, P. Huang, P.M. Rogers, A.K. Nosie, D.B. McClure, L.L. Burris, S. Khorasanizadeh, T.P. Burris, and F. Rastinejad, *Identification of heme as the ligand for the orphan nuclear receptors REV-ERBalpha and REV-ERBbeta.* Nat Struct Mol Biol, 2007. 14(12): p. 1207-13.

67. Wang, C., C.X. Xu, S.L. Krager, K.M. Bottum, D.F. Liao, and S.A. Tischkau, *Aryl hydrocarbon receptor deficiency enhances insulin sensitivity and reduces PPAR-alpha pathway activity in mice.* Environ Health Perspect, 2011. 119(12): p. 1739-44.

CHAPTER 6: PERSISTENT ARYL HYDROCARBON RECEPTOR ACTIVATION ABOLISHES CIRCADIAN REGULATION OF HEPATIC METABOLIC ACTIVITY IN MICE

ABSTRACT

Dysregulation of hepatic circadian rhythmicity is associated with the development of metabolic disorders such as non-alcoholic fatty liver disease (NAFLD). It is also reported that aryl hydrocarbon receptor (AhR) activation alters the hepatic expression of core clock regulators, however the global impact on circadian-controlled metabolism has not been investigated. This study examines the effects of AhR activation on hepatic transcriptome and metabolome rhythmicity in male C57BL/6 mice orally gavaged with 30 µg/kg 2,3,7,8-tetrachlorodibenzo-*p*-dioxin (TCDD) every 4 days for 28 days. Treatment not only increased relative liver weight (RLW), but also abolished the oscillation of RLW observed in control mice. Hepatic RNA-Seq analysis detected diminished rhythmicity in 15 core clock regulators (e.g. *Arntl, Clock, Nr1d1, Per1, Cry1, Nfil3*), involving either a ≥ 3.3-fold suppression in amplitude or complete loss of oscillation. Accordingly, protein levels (ARNTL, REV-ERBα, NFIL3) and genomic binding (ARNTL) of select regulators were reduced and arrhythmic following treatment. As a result, the oscillating expression of 99.6% of 5,636 clock-controlled hepatic genes was abolished including genes associated with lipid metabolism, glucose/glycogen metabolism, bile acid homeostasis, heme biosynthesis, and redox homeostasis. For example, TCDD flattened expression of the rate-limiting enzymes in both gluconeogenesis (*Pck1*) and glycogenesis (*Gys2*), consistent with the depletion and loss of rhythmicity in hepatic glycogen levels. Examination of polar hepatic extracts by untargeted mass spectrometry revealed that virtually all oscillating metabolites lost rhythmicity following treatment. Collectively, these results suggest TCDD decoupled hepatic metabolism from feeding/fasting cycles, consistent with the progression of AhR-mediated hepatic steatosis to steatohepatitis with fibrosis.

INTRODUCTION

In response to the rotation of the earth and the ensuing light-dark cycles, animals have evolved a ~24-hour (h) circadian clock that entrains physiological activities such as sleep and

feeding to specific times of the day. Circadian oscillations enable cells to anticipate upcoming functional needs, imparting the organism with competitive advantages associated with fitness and survival including enhanced growth and longevity, improved reproductive success, and effective predator/prey relationships [1]. Maintaining rhythmicity of circadian behaviors is critical for good health, while disruptions such as shift work, jet lag, binge eating, and sleep restriction are associated with a broad spectrum of pathogenic states in humans and rodent models including metabolic diseases (e.g. non-alcoholic fatty liver disease (NAFLD)), mental health disorders, cancer, and accelerated aging [2-6].

The circadian system consists of a hierarchical network of tissue-specific peripheral clocks coordinated by a master pacemaker in the suprachiasmatic nucleus (SCN) of the hypothalamus. The SCN master clock is the only level of the circadian network directly entrained by light detected at the retina [7]. In turn, this master clock generates oscillations in systemic cues (e.g. endocrine signals and neuronal connections) and behavioral cycles (e.g. feeding/fasting, activity/rest) that synchronize cell-autonomous peripheral clocks [8, 9]. For example, the hepatic peripheral clock ensures that genes associated with nutrient transport, metabolism, and detoxification are coordinated with feeding/fasting cycles [3]. Temporal separation of incompatible or opposing metabolic processes also minimizes futile cycles while optimizing metabolic efficiency, energy use/storage, and cellular function. Approximately 40% of all genes in the mouse genome are circadian-regulated in at least one tissue, while the liver expresses the largest number of rhythmic genes (~11-16% of all detected transcripts), with ~50% of hepatic metabolites exhibiting oscillating levels [10-12].

At the cellular level, circadian clocks comprise autonomous, interlocking transcription-translation feedback loops [13]. The positive limb involves the core activators circadian locomotor output cycles kaput (CLOCK), brain and muscle ARNT-like 1 (BMAL1, aka ARNTL), and neuronal PAS domain protein 2 (NPAS2, a CLOCK paralog), which are all members of the basic helix-loop-helix (bHLH) Per-Arnt-Sim (PAS) protein family. ARNTL forms a heterodimer with either CLOCK

or NPAS2, which binds to E-box-containing response elements and induces cryptochrome (*Cry1*, *Cry2*) and period (*Per1, Per2, Per3*) transcription. Accumulating CRY and PER dimerize and interfere with ARNTL/CLOCK activity, thereby repressing their own transcription to create the negative limb of the loop. The ARNTL/CLOCK complex also induces the transcription of the *Nr1d1* (encodes REV-ERBα) and *Nr1d2* (encodes REV-ERBβ) repressors, which compete with the retinoic acid-related orphan receptor (ROR) α, β and γ activators for ROR-response elements (ROREs). REV-ERBα and β rhythmically repress *Arntl* transcription, creating a second feedback loop within the core clock. Several D-box-binding transcription factors are also regulated by ARNTL/CLOCK including D-site albumin promoter binding protein (DBP), thyrotroph embryonic factor (TEF), hepatic leukemia factor (HLF), and interleukin-3 regulated nuclear factor (NFIL3, aka E4BP4). Interactions between these loops generate transcriptional oscillation patterns in circadian-controlled target genes, where the expression phase is determined by the combination of E-boxes, ROREs, and D-boxes within each gene's regulatory region.

The aryl hydrocarbon receptor (AhR) and its binding partner the aryl hydrocarbon receptor nuclear translocator (ARNT) are also members of the bHLH-PAS family and exhibit significant sequence homology with CLOCK and ARNTL, respectively [14-16]. Interestingly, several endogenous ligands of the AhR are photo-oxidation products of tryptophan (e.g. 6-formylindolo[3,2-b]carbazole (FICZ)), suggesting the AhR regulates biological rhythms in response to light-derived chemical messengers [17, 18]. Additionally, AhR-deficient mice exhibit exacerbated behavioral responses to shifts in light cycles, increased amplitudes in core clock gene expression, and alterations in circadian-controlled metabolites (e.g. glucose, insulin, triglycerides), further demonstrating a role for AhR in circadian regulation [19].

2,3,7,8-tetrachlorodibenzo-*p*-dioxin (TCDD) is the prototypical ligand for a structurally diverse group of synthetic chemicals, natural products, and endogenous metabolites that activate the AhR [20]. Following ligand binding, the cytoplasmic AhR dissociates from chaperone proteins, translocates to the nucleus, and heterodimerizes with ARNT. The ligand-bound AhR/ARNT

complex then binds to dioxin response elements (DREs) within the promoter region of target genes, leading to recruitment of transcriptional co-regulators and differential gene expression [21]. In mice, TCDD-elicited activation of the AhR affects the master clock, altering oscillations in circadian locomotor activity and expression patterns of core clock genes (*Arntl*, *Per1*) within the SCN [22, 23]. Furthermore, AhR activation alters the rhythmic expression of core circadian regulators within the peripheral clocks of the liver, ovaries, and hematopoietic stem cells [24-26].

Previous studies conducted by our group detected TCDD-elicited differential expression of several core clock regulators and clock-controlled target genes [27]. In addition to the expected sigmoidal, exponential, and linear dose-response curves, a surprising number of genes also exhibited U- or inverted U-shaped curves, potentially reflecting rhythmic expression patterns [28, 29]. TCDD also dysregulated porphyrin biosynthesis and increased hepatic levels of heme [27], a cofactor for several core clock regulators including REV-ERBα/β, NPAS2, CLOCK, and PER2 [30-33]. However, due to the large number of animals used to assess dose-response relationships, tissues were harvested over several hours across the day, and thus the confounding effects of circadian rhythm on gene expression were not adequately controlled. The current study was specifically designed to investigate the effects of AhR activation on the circadian rhythmicity of the hepatic transcriptome and metabolome in mice. We report TCDD abolished or dampened the rhythmicity of the core clock regulators at the mRNA, protein, and functional levels, collapsing the oscillation of virtually all circadian-controlled hepatic genes and metabolites. This loss of rhythmicity indicates hepatic metabolism was decoupled from feeding/fasting cycles, altering metabolic efficiency, energy storage, enterohepatic circulation, and redox homeostasis.

MATERIALS & METHODS

Animal husbandry and treatment

Postnatal day 25 (PND25) male and female C57BL/6 mice weighing within 10% of each other were obtained from Charles River Laboratories (Kingston, NY) and housed in Innovive Innocages (San Diego, CA) containing ALPHA-dri bedding (Shepherd Specialty Papers, Chicago, IL) in a 23°C environment with 30-40% humidity. Mice were provided Aquavive water (Innovive) and Harlan Teklad 22/5 Rodent Diet 8940 (Madison, WI) *ad libitum.* Mice were entrained to a 12h/12h light/dark cycle for ~2 weeks prior to treatment and were maintained on this schedule throughout the treatment period. Mice (PND36-41) were orally gavaged at zeitgeber time (ZT) 0 with sesame oil vehicle (Sigma-Aldrich, St. Louis, MO) or 30 µg/kg TCDD (AccuStandard, New Haven, CT) every 4 days (d) for a total of 28d (7 exposures; Figure 39). This TCDD dose was chosen to compensate for the relatively short study duration compared to lifelong cumulative human exposure from diverse AhR ligands, the bioaccumulative nature of halogenated AhR ligands, and differences in TCDD's metabolism and half-life (humans: 1-11 years [34, 35], mice: 8-12d [36, 37]). Food consumption was monitored in a separate cohort of male and female C57BL/6 mice exposed to the same treatment regimen of sesame oil vehicle or 30 µg/kg TCDD. Four cages of co-housed mice were included per treatment group. The food trough containing the rodent chow for each cage was weighed daily at ZT0 and food consumption was calculated based on the number of mice in the cage. Additionally, a separate cohort of male C57BL/6 mice was orally gavaged (between ZT2 and ZT4) with a single bolus dose of sesame oil vehicle or 30 µg/kg TCDD for chromatin immunoprecipitation (ChIP) analysis at 2h. All animal handling procedures were performed with the approval of the Michigan State University (MSU) Institutional Animal Care and Use Committee, in accordance with ethical guidelines and regulations.

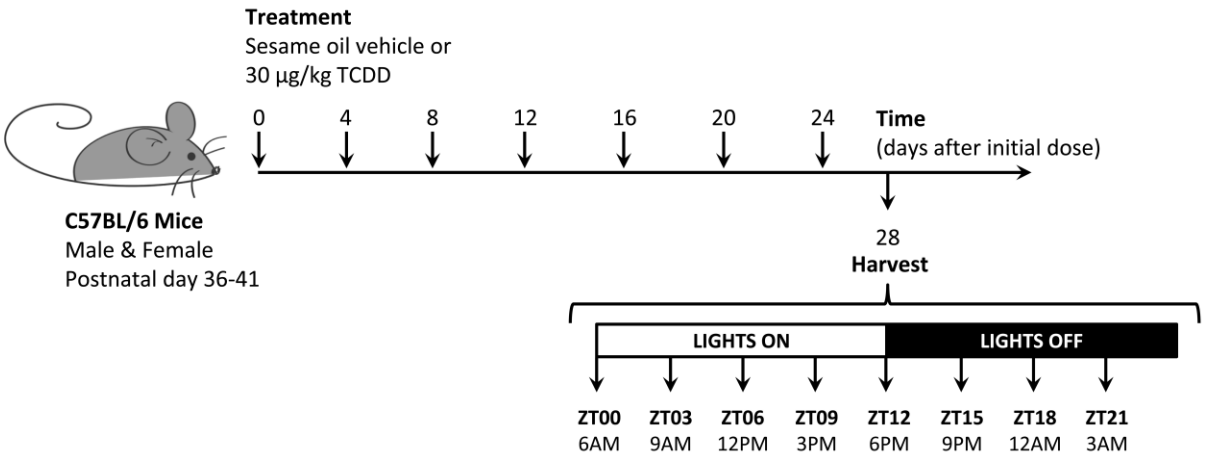

FIGURE 39. CHAPTER 6 STUDY DESIGN

Male and female C57BL/6 mice were orally gavaged with sesame oil vehicle or 30 µg/kg TCDD every 4 days for 28 days. Beginning at ZT00 on day 28, mice were euthanized every 3h for 24h (8 timepoints).

Sample collection

Beginning at ZT0 on the 28th day after the initial gavage, vehicle- and TCDD-treated mice were weighed and euthanized every 3h (±15 min) for 24h (8 timepoints). Mice at the ZT0, 3, 6, and 9 timepoints were euthanized with the lights on, while mice at the ZT12, 15, 18, and 21 timepoints were euthanized in the dark. Livers were removed, weighed, flash frozen in liquid nitrogen, and stored at -80°C. Liver samples for ChIP analysis were collected from a separate cohort of male mice 2h after treatment (between ZT4 and ZT6).

RNA-Seq analysis

Frozen liver samples were homogenized in TRIzol using a Mixer Mill 300 tissue homogenizer (Retsch, Germany) and total RNA was isolated as previously described [38]. RNA was quantified using a Nano-drop spectrophotometer (Thermo Scientific, Wilmington, DE) at 260 nm. Purity was assessed using the A_{260}/A_{280} ratio and quality was analyzed using the Caliper LabChip GX (Perkin Elmer, Waltham, MA).

Hepatic gene expression was examined using RNA-Seq performed at the MSU Research Technology Support Facility (RTSF) Genomics Core (rtsf.natsci.msu.edu/genomics). Hepatic libraries from three independent biological replicates (n=3) were prepared using the Illumina TruSeq RNA Sample Preparation Kit (Illumina, San Diego, CA). Libraries were quantified and sequenced as previously described, at a read depth of ~30M per sample [27, 29]. Reads were assessed for quality using FASTQC v0.11.3 and then mapped to the mouse reference genome (GRCm38 release 81) using Bowtie2 v2.2.6 and TopHat2 v2.1.0. The RNA-Seq dataset was deposited in the Gene Expression Omnibus (GEO; accession number GSE119780). For TCDD-mediated differential gene expression, fold changes were calculated relative to vehicle controls at each ZT. Genes were considered differentially expressed if |fold change| ≥ 1.5 and statistical P1(t) value ≥ 0.8 at one or more timepoints.

Protein quantification – capillary electrophoresis

Liver samples were homogenized in RIPA buffer supplemented with protease inhibitor cocktail (Sigma) using a Polytron PT2100 homogenizer (Kinematica, Lucerne, Switzerland) and sonicated on ice. Samples were centrifuged and total protein in the supernatant was measured using the bicinchoninic acid (BCA) assay (Sigma). The WES capillary electrophoresis system (ProteinSimple, San Jose, CA) was used with the following antibodies from Cell Signaling (Danvers, MA): ARNTL (#14020), REV-ERBα (#13418), NFIL3 (#14312). Primary antibodies were detected using a goat anti-rabbit secondary antibody conjugated to horseradish peroxidase. Chemiluminescence signals were analyzed with Compass software (ProteinSimple). Target protein levels were normalized to total protein.

ChIP and putative DRE identification

ChIP-PCR was used to: (i) investigate hepatic genomic ARNTL binding in male mice orally gavaged with sesame oil vehicle or 30 µg/kg TCDD every 4d for 28d, and (ii) compare genomic binding of AhR, ARNTL, and CLOCK in male mice 2h after treatment with sesame oil vehicle or 30 µg/kg TCDD. Hepatic chromatin was prepared using the *tru*ChIP Tissue Chromatin Shearing Kit (Covaris, Woburn, MA) according to the manufacturer's instructions with minor modifications. Briefly, frozen liver samples (~120mg) were homogenized using a Polytron PT2100 homogenizer (Kinematica) in cold PBS. Protein-DNA complexes were cross-linked in 1% formaldehyde for 10 min and chromatin was sheared for 10 min in a 1mL AFA Fiber milliTUBE using the M220 Focused-Ultrasonicator (Covaris). Size distributions of dsDNA fragments were assessed by running a DNA 1200 chip on the Agilent 2100 Bioanalyzer (Santa Clara, CA), to verify that ≥70% of fragments were within 150-700 bp. Triton X-100 (10%) was added to chromatin to achieve a final concentration of 1%. Cross-linked DNA was immunoprecipitated with rabbit antibodies as previously described [39]: IgG (#2729, Cell Signaling), ARNTL (#14020, Cell Signaling), CLOCK

(ab3517, Abcam, Cambridge, MA), or AhR (BML-SA210, Enzo, Farmingdale, NY). ChIP DNA was purified using a QIAquick PCR purification kit (QIAGEN, Hilden, Germany) and eluted in 40 µL water. ChIP DNA and input DNA (diluted 100-fold) was quantified using real-time PCR (qRT-PCR) conducted on a Bio-Rad CFX Connect Real-Time PCR Detection System (Hercules, CA) as previously described [38]. Previously identified binding sites were targeted using the forward and reverse primer sequences listed in Table 8 [27, 40, 41]. A negative control region on chromosome 6 was identified using our group's AhR [27] and ARNTL (unpublished) ChIP-Seq datasets. Percent input was calculated using $100\% * 2^{((Ct\ Input - 6.644) - Ct\ IP)}$.

Hepatic AhR ChIP-Seq was previously performed on samples from male C57BL/6 mice 2h following a single oral dose of 30 µg/kg TCDD [27]. The full ChIP-Seq dataset for the male liver is available on GEO (GSE97634).

Putative DREs (pDREs) were previously identified [42]. Briefly, the regulatory region (10 kb upstream of the transcription start site together with 5′- and 3′-untranslated regions) and coding sequence of each gene was obtained from the University of California, Santa Cruz (UCSC) Genome Browser for mouse (mm10 GRCm38 build) and computationally searched for the DRE core consensus sequence 5′-GCGTG-3′. Each identified core was extended by 7 bp upstream and downstream. The resulting 19 bp sequences were scored using a position weight matrix constructed from bona fide functional DREs. Matrix similarity scores (MSS) ≥ 0.856 were considered to be pDREs. UCSC genome browser tracks indicating pDRE locations within the mouse genome are available at http://dbzach.fst.msu.edu/index.php/supplementarydata.html.

Glucose and glycogen assay

Liver samples (~50 mg) were homogenized in 6% perchloric acid (250 µl) using a Polytron PT2100 homogenizer (Kinematica). To hydrolyze the glycogen, 25 µl of 1M $NaHCO_3$ and 125 µl of 2 mg/ml amyloglucosidase (Sigma-Aldrich) was added to 50 µl of the homogenate. Samples

TABLE 8. PRIMER SEQUENCES (5'-3') FOR GENOMIC REGIONS ANALYZED BY CHIP-PCR

Gene	Amplicon Coordinates	Amplicon Location	Forward Primer	Reverse Primer	Amplicon Size (bp)	pDRE?	E-box?
Per1	chr11:69,098,654-69,098,858	Promoter (Site 1)	ATCCTCCCTGAAAAGGGGTA	GGATCTCTTCCTGGCATCTG	205	No	Yes, within amplicon
Per1	chr11:69,094,904-69,094,974	Promoter (Site 2)	AGCCCTCTCAGCCTATGAGAAAGT	CCCGCCCTGCCTAAATCA	71	Yes, near amplicon	Yes, near amplicon
Per2	chr1:91,459,371-91,459,448	Promoter	TCATTTGCATACTGGCGGGG	TATGTAAAGAGAGCGACGGGC	78	No	Yes, near amplicon
Per2	chr1:91,446,265-91,446,397	Within intron 4	TCCGCCTTCACAGACTGGTA	ACCCTCCAGGGACTATTGGT	133	Yes, within amplicon	No
Dbp	chr7:45,707,643-45,707,707	Within intron 2	TGGGACGCCTGGGTACAC	GGGAATGTGCAGCACTGGTT	65	Yes, near amplicon	Yes, near amplicon
Nr1d1	chr11:98,783,446-98,783,535	Promoter	TGCAGCCTGCTCCATTTCTA	CCCCTCACTTGCACATGTCT	90	No	Yes, near amplicon
Cyp1a1	chr9:57,696,696-57,696,767	Promoter	GAGGATGGAGCAGGCTTACG	GGGCTACAAAGGGTGATGCTT	72	Yes, near amplicon	No
Negative Control	chr6:120,257,680-120,257,772	N/A	CTGGGGTCACCTACATCAGC	GAGCGAGATGATTCCTGCCA	93	No	No

were incubated and shaken (not stirred) for 2h at 37°C and then centrifuged to remove debris. Glycogen and glucose were quantified using the glucose assay kit (Pointe Scientific, Canton, MI) with a M200 plate reader (Tecan, Durham, NC). Total hepatic glycogen levels were corrected using hepatic glucose levels and expressed as glucose units.

Untargeted metabolomics analysis of hepatic extracts

Polar metabolites were extracted from liver samples using methanol:water:chloroform as previously described [43]. Briefly, flash frozen liver samples (~25 mg) were homogenized (Polytron PT2100, Kinematica) in a mixture of HPLC-grade methanol and water (5:3 ratio) containing all 20 ^{13}C-,^{15}N-labelled amino acids (Sigma; 767964) as internal standards. HPLC-grade chloroform (methanol:water:chloroform ratio 5:3:5) was added, vortexed, shaken for 15 min at 4°C, and centrifuged at maximum speed (3000×g) to achieve phase separation. The methanol:water phase containing the polar metabolites was transferred, dried under nitrogen gas at room temperature, and stored at -80°C. Prior to analysis, the dried metabolite extracts were resuspended in 300 µL HPLC-grade water. For analysis in negative mode, 3 parts of the resuspended polar extract was diluted with 1 part 4X mobile phase (40 mM tributylamine + 60 mM acetic acid in 88/12 H_2O/MeOH). For analysis in positive mode, 3 parts of the resuspended polar extract was diluted with 7 parts acetonitrile. Diluted samples were centrifuged at 15,000g for 10 minutes to remove any remaining protein and the supernatant was transferred to autosampler vials.

Extracts were examined by untargeted liquid chromatography mass spectrometry (LCMS) using an Acquity UPLC System (Waters, Milford, MA) coupled with an Xevo G2-XS Quadrupole Time of Flight (QTof) mass spectrometer (Waters) run in MS^E continuum mode. For negative mode analysis, ion-pairing reverse phase chromatography was performed on an Ascentis Express column (C18, 5 cm × 2.1 mm, 2.7 µm, Sigma) using a modified version of a previously described method [43] with the following LC parameters: injection volume, 10 µl; column

temperature, 30°C; and flow rate, 400 µl/min. The LC solvents were solvent A: 10 mM tributylamine and 15 mM acetic acid in 97:3 water:methanol (pH 4.95) and solvent B: methanol. Elution from the column was performed over 11 min with the following gradient: t = 0, 0% solvent B, flow rate 0.4 ml/min; t = 1, 0% solvent B, flow rate 0.4 ml/min; t = 2, 20% solvent B, flow rate 0.3 ml/min; t = 3, 20% solvent B, flow rate 0.25 ml/min; t = 5, 55% solvent B, flow rate 0.15 ml/min; t = 8, 95% solvent B, flow rate 0.15 ml/min; t = 8.5, 95% solvent B, flow rate 0.15 ml/min; t = 9, 0% solvent B, flow rate 0.4 ml/min; t = 11, 0% solvent B, flow rate 0.4 ml/min. Mass spectra were acquired using negative-mode electrospray ionization run in MS^E continuum mode. The capillary voltage was 2,500 V and cone voltage was 40 V. Nitrogen was used as cone gas and desolvation gas, with flow rates of 50 and 600 L/h, respectively. The source temperature was 100°C, and desolvation temperature was 300°C. Argon was used as collision gas.

For positive mode analysis, normal phase chromatography was performed using an Acquity UPLC Ethylene Bridged Hybrid (BEH) Amide column (10 cm × 2.1 mm, 2.7 µm, Waters) with the following LC parameters: injection volume, 10 µl; column temperature, 40°C; and flow rate, 300 µl/min. The LC solvents were solvent A: 10 mM ammonium formate and 0.1% formic acid in water (pH 3.26) and solvent B: acetonitrile. Elution from the column was performed over 10 min with the following gradient: t = 0, 99% solvent B, flow rate 0.3 ml/min; t = 7, 50% solvent B, flow rate 0.3 ml/min; t = 8, 50% solvent B, flow rate 0.3 ml/min; t = 8.01, 99% solvent B, flow rate 0.3 ml/min; t = 10, 99% solvent B, flow rate 0.3 ml/min. Mass spectra were acquired using positive-mode electrospray ionization run in MS^E continuum mode. The capillary voltage was 3,000 V and cone voltage was 35 V. Nitrogen was used as cone gas and desolvation gas, with flow rates of 25 and 600 L/h, respectively. The source temperature was 100°C, and desolvation temperature was 350°C. Argon was used as collision gas.

Progenesis QI software (Waters) was used for peak processing. Metabolites were identified using the Human Metabolome Database (HMDB). Data for each sample was normalized

to both liver weight and ^{13}C-,^{15}N-labelled amino acid standards: tryptophan and leucine for negative mode; phenylalanine and tyrosine for positive mode.

Data analysis

The JTK_CYCLE package (v3) for R (v3.2.4) was used to assess rhythmic oscillations in transcriptomic data, metabolite data, tissue weights, protein levels, and ChIP-PCR results [44]. Endpoints were considered to exhibit circadian rhythmicity if BH q-value ≤ 0.1 for a period range of 21-24 hr.

The Database for Annotation, Visualization, and Integrated Discovery (DAVID) v6.8 was used to identify enriched functional clusters within hepatic genes (i) exhibiting rhythmicity in controls but not TCDD-treated mice, and (ii) differentially expressed (fold change ≥ 1.5; P1(t) ≥ 0.8) by TCDD at three or more timepoints [45]. Only Gene Ontology (GO) Biological Processes were considered. The *mummichog* algorithm within MetaboAnalyst v4.0 (MS Peaks to Pathways module) was used to identify enriched KEGG pathways within mass spectrometry peaks that lost their rhythmicity following TCDD treatment [46]. Enrichment scores (ES; -log(p-value)) ≥ 1.3 were considered significant. Compound identifications determined by the *mummichog* analysis were used in select cases where the Progenesis QI software failed to identify a peak (e.g. heme).

RESULTS

TCDD abolished circadian oscillations in relative liver weight

The effects of TCDD on the circadian regulation of liver weight were examined in male and female mice orally gavaged with sesame oil vehicle or 30 µg/kg TCDD every 4d for 28d. On day 28, relative liver weights (RLWs) were assessed at 3h intervals over a 24h period beginning at ZT0. JTK_CYCLE analysis determined that the RLW of control males and females oscillated in a circadian manner, peaking at ZT0. In both sexes, RLW at ZT0 was 1.3-fold greater than that at ZT12 (Figure 40). This is consistent with previous mouse and rat studies in which both RLW

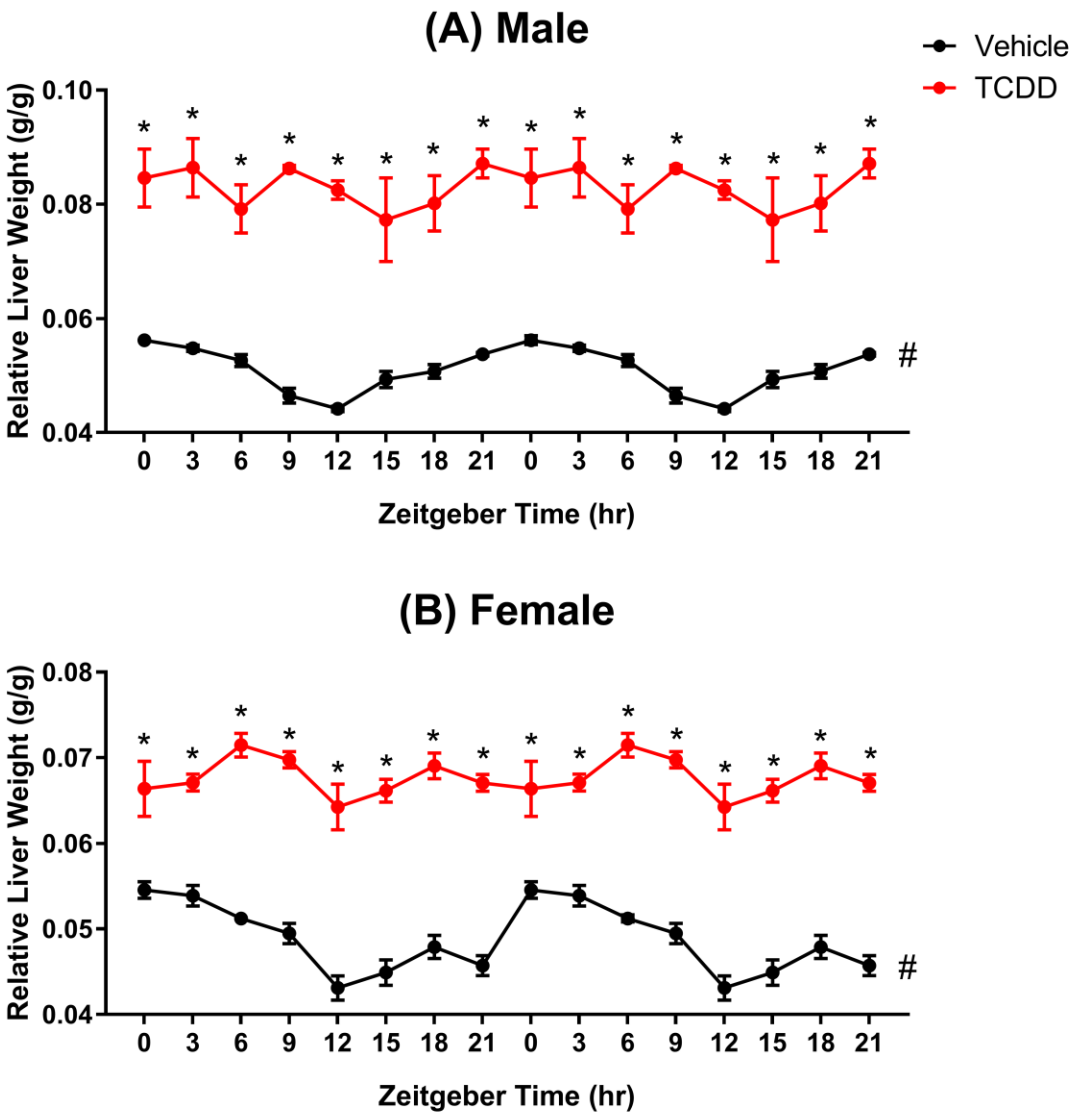

FIGURE 40. LOSS OF RHYTHMICITY IN RELATIVE LIVER WEIGHT

Relative liver weight (RLW) of (A) male and (B) female C57BL/6 mice orally gavaged with sesame oil vehicle or 30 µg/kg TCDD every 4 days for 28 days. Data points represent the average of at least 3 biological replicates ± standard error of the mean. Statistical significance (* $p \leq 0.05$) between vehicle and TCDD was determined using a two-way ANOVA analysis followed by Sidak's multiple comparison test. JTK_CYCLE determined RLW in control animals exhibited circadian oscillation (# BH $q \leq 0.1$), while RLW rhythmicity was not detected in TCDD-treated mice. Data is plotted twice to more easily visualize effects on rhythmicity.

and hepatocyte size were found to oscillate in a circadian manner, reaching maximal size and weight at the end of the feeding phase (ZT0) [47, 48]. These oscillations are reported to be driven by fluctuations in ribosomal protein mRNA translation and thus ribosome number. TCDD increased RLW in both males and females at each timepoint, with maximum increases of 1.9- and 1.5-fold, respectively, at ZT12, comparable to RLW increases reported in previous studies [27, 49]. Notably, the circadian rhythmicity in RLW was lost in both sexes following TCDD treatment (Figure 40). TCDD had no effect on daily food consumption in either sex over the 28d treatment regimen (Figure 41), consistent with previous studies [50]. Therefore, TCDD-elicited alterations in RLW and hepatic circadian rhythmicity are not driven by changes in feeding.

Loss of hepatic rhythmic gene expression following AhR activation

Using RNA-Seq, TCDD-elicited hepatic transcriptomic changes were assessed in male mice at 3h intervals over a 24h period. JTK_CYCLE analysis of the RNA-Seq data detected 5,636 hepatic genes exhibiting circadian rhythmic expression (BH q-value ≤ 0.1; period = 21-24 h) in control mice (Figure 42A), equivalent to 25.7% of the 21,896 genes expressed in the liver. This is higher than the ~11 to 16% of hepatic genes reported to exhibit circadian oscillations in other studies [10, 11], but less than a recent 37% estimate [12]. These discrepancies are likely due to differences in the BH q-value cut-off, transcriptomic platforms, sampling intervals, and statistical power. Specifically, 15 core hepatic clock regulators exhibited oscillating expression including (i) the E-box binding transcription factors *Arntl* (aka *Bmal1*), *Clock*, and *Npas2*, (ii) the PER/CRY genes *Per1*, *Per2*, *Per3*, *Cry1*, and *Cry2*, (iii) the RORE-binding transcription factors *Nr1d1* (encodes REV-ERBα), *Nr1d2* (encodes REV-ERBβ), and *Rorc* (encodes RORϒ), and (iv) the D-box binding transcription factors *Dbp*, *Tef*, *Hlf*, and *Nfil3*. Hepatic expression of the RORE-binding transcription factor *Rora* did not exhibit rhythmicity, consistent with previous reports that it lacks circadian oscillation in peripheral tissues [51]. Collectively, these results confirmed that our study

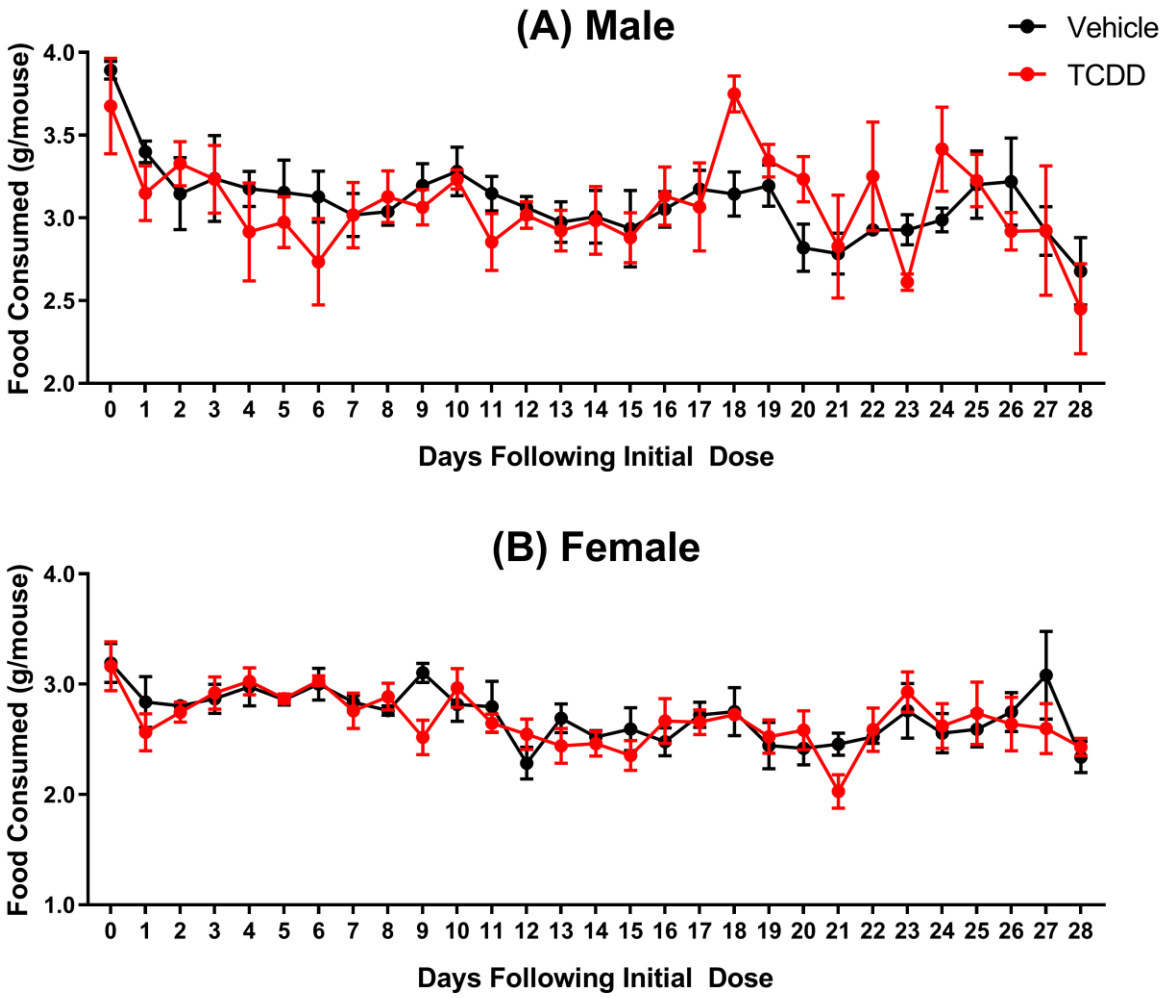

FIGURE 41. TCDD HAD NO EFFECT ON THE DAILY FOOD CONSUMPTION OF MICE

(A) Male and (B) female C57BL/6 mice were orally gavaged with sesame oil vehicle or 30 µg/kg TCDD every 4 days for 28 days. The food trough for each cage of co-housed mice was weighed daily and food consumption was calculated based on the number of mice in the cage. Data points represent the average of 4 cages per treatment group ± standard error of the mean. Statistical significance ($p \leq 0.05$) was evaluated through a 2-way ANOVA analysis followed by Sidak's multiple comparison test.

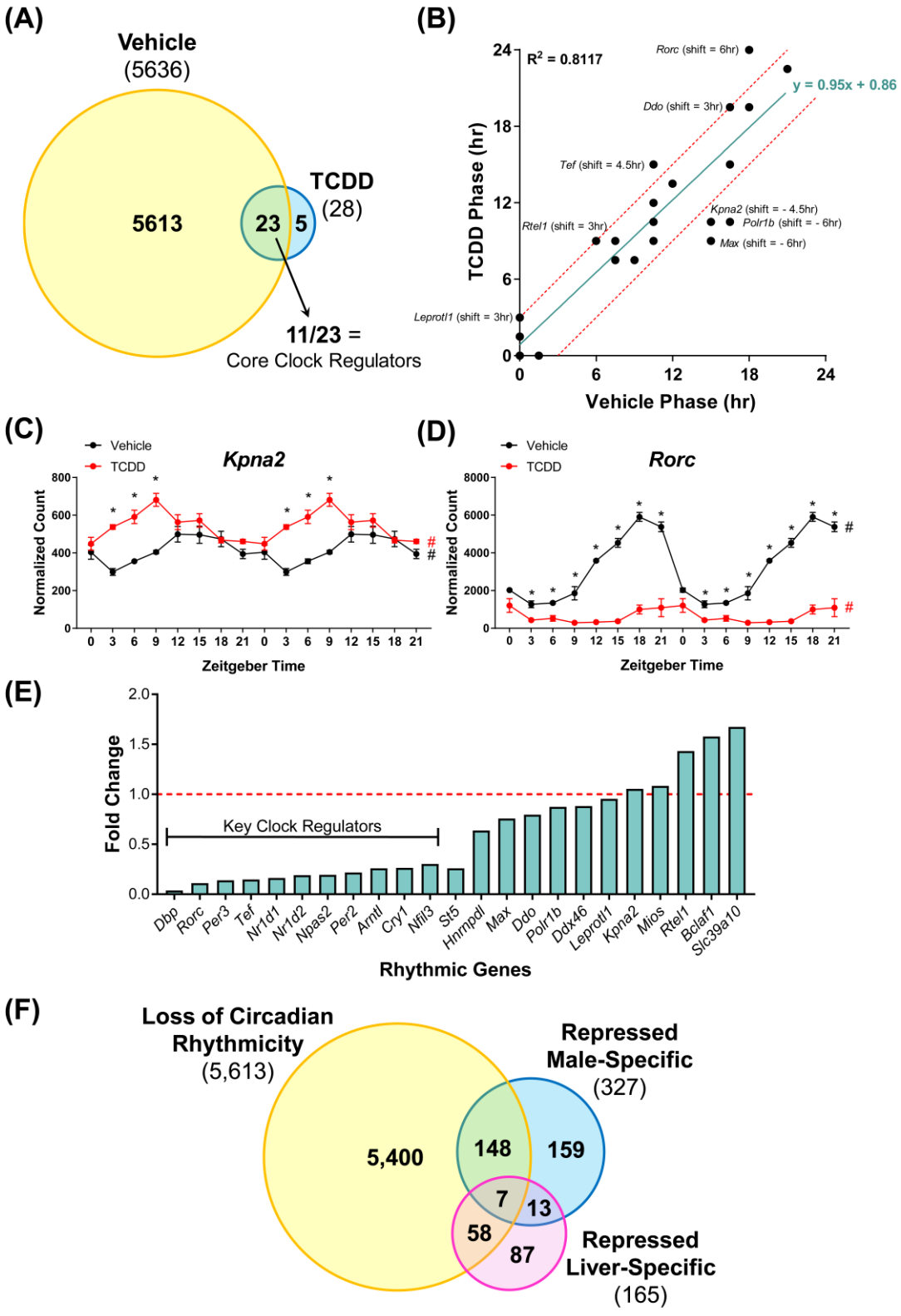

FIGURE 42. THE EFFECT OF TCDD ON THE CIRCADIAN RHYTHMICITY OF HEPATIC GENE EXPRESSION

FIGURE 42 (cont'd)

Male C57BL/6 mice orally gavaged with sesame oil vehicle or 30 μg/kg TCDD every 4 days for 28 days. (A) The number of hepatic genes which exhibited rhythmic expression in vehicle- and TCDD-treated mice. 5,613 of 5,636 (99.6%) rhythmic genes lost their circadian oscillation pattern following treatment, while 23 genes exhibited rhythmicity in both vehicle- and TCDD-treated mice. Rhythmicity was determined using JTK_CYCLE (BH q ≤ 0.1). (B) Correlation between the acrophases (time at which cycle peaks/crests) of rhythmic expression in vehicle- and TCDD-treated mice. The linear regression line is shown in green, while the red dashed lines represent acrophase shifts of ± 3h. Genes falling within the red dashed lines exhibited negligible acrophase shifts of ≤ 1.5h. TCDD decreased the acrophase of (C) *Kpna2* (as well as *Polr1b* and *Max*, not shown), while increasing the acrophase of (D) *Rorc* (as well as *Leprotl1*, *Rtel1*, *Tef*, and *Ddo*, not shown). Data points represent the average of 3 biological replicates ± standard error of the mean. Posterior probabilities (* P1(t) ≥ 0.80) comparing vehicle and TCDD were determined using an empirical Bayes method. Circadian rhythmicity was assessed using JTK_CYCLE (# BH q ≤ 0.1). (E) Altered amplitudes (fold change) of hepatic genes exhibiting rhythmicity in both vehicle- and TCDD-treated mice. The red dashed line represents a fold change of 1 (i.e. treatment had no effect on amplitude). (F) Genes which lost rhythmicity were compared to previously identified sets of male-specific and liver-specific genes repressed by TCDD [52].

was appropriately designed to examine the effects of persistent AhR activation on the hepatic circadian clock.

TCDD abolished rhythmicity in 5613 hepatic genes, equivalent to 99.6% of the genes which exhibited circadian regulation in controls. Only 23 genes maintained rhythmicity following TCDD treatment, while 5 acquired rhythmic expression (*Sdhaf2, Nsrp1, Marveld3, Folr1,* and *Gm17068*) (Figure 42A). Linear regression analysis comparing gene acrophases (time at which cycle peaks/crests) between vehicle- and TCDD-treated animals revealed a slope of 0.95, suggesting TCDD had little effect on the acrophase of the majority of genes. For example, of the 23 genes which maintained rhythmicity, 15 exhibited similar acrophases (±1.5h) between control and TCDD-treated animals (Figure 42B). TCDD increased the acrophase of *Rorc, Tef, Leprotl1*, *Rtel1*, and *Ddo* ≥ 3h (+ve phase shift), and decreased the acrophase of *Kpna2, Max,* and *Polr1b* ≥ 4.5h (-ve phase shift) (Figure 42C,D). In contrast to limited effects on acrophase, TCDD altered the amplitude of most rhythmic genes. Of the 23 genes identified as rhythmic in both controls and treated mice, 15 exhibited a ≥ 1.3-fold reduction in amplitude, while only 3 genes increased in amplitude (*Rtel1, Bclaf1, Slc39a10;* 1.4-, 1.6-, 1.7-fold) (Figure 42E). Overall, TCDD abolished the rhythmicity of the vast majority of clock-controlled hepatic genes, while those that continued oscillating following treatment exhibited reduced amplitudes (in most cases). Beyond the collapse of hepatic circadian rhythmicity, TCDD also causes the loss of liver-specific and sexually dimorphic gene expression [52]. Comparison of these gene sets revealed 47% of repressed male-specific genes and 39% of repressed liver-specific genes exhibited rhythmicity in vehicle- but not TCDD-treated mice (Figure 42F).

TCDD dampened rhythmicity of hepatic core clock regulators

The striking global loss in hepatic gene expression rhythmicity is likely due to the dampened expression of core circadian clock regulators. Notably, TCDD repressed hepatic expression of all 16 core clock regulators at one or more timepoint (Figure 43; Table 9).

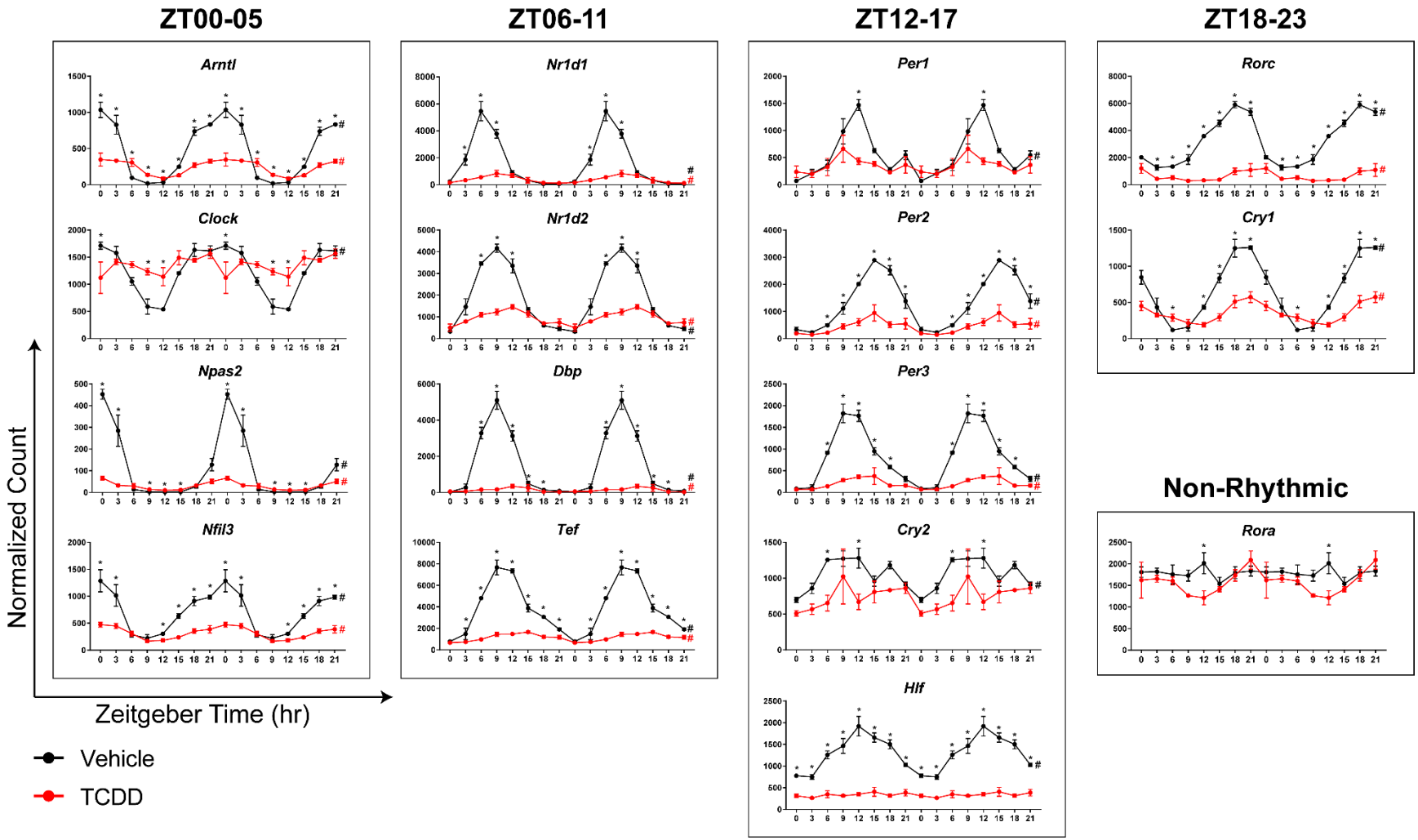

FIGURE 43. TCDD DAMPENED THE RHYTHMIC EXPRESSION OF THE CORE CLOCK REGULATORS

FIGURE 43 (cont'd)

RNA-Seq analysis of core hepatic clock regulators in male C57BL/6 mice orally gavaged with sesame oil vehicle or 30 µg/kg TCDD every 4 days for 28 days. Data points represent the average of 3 biological replicates ± standard error of the mean. Posterior probabilities (* P1(t) ≥ 0.80) comparing vehicle and TCDD were determined using an empirical Bayes method. Circadian rhythmicity was assessed using JTK_CYCLE (# BH q ≤ 0.1). Genes are grouped by their acrophase (time at which cycle peaks/crests) in vehicle mice. Data is plotted twice to more easily visualize effects on rhythmicity.

TABLE 9. THE EFFECT OF TCDD ON HEPATIC EXPRESSION AND RHYTHMICITY OF CORE CLOCK GENES

Gene	Differentially Expressed? (TCDD vs. VEH)	Number of pDREs[a]	AhR Enrichment[b]?	AhR Enrichment at a pDRE?	Rhythmic[c] in VEH?	Rhythmic[c] after TCDD?	Phase Shift (h) (TCDD - VEH)	Amplitude Fold Change (TCDD/VEH)
Arntl	Yes	2	Yes	No	Yes	Yes	1.5	-3.9
Clock	Yes	10	Yes	Yes	Yes	No	N/A	N/A
Npas2	Yes	14	Yes	No	Yes	Yes	0	-5.2
Nr1d1	Yes	1	Yes	Yes	Yes	Yes	1.5	-6.1
Nr1d2	Yes	0	Yes	No	Yes	Yes	1.5	-5.3
Rora	Yes	9	Yes	No	No	No	N/A	N/A
Rorc	Yes	3	Yes	No	Yes	Yes	6	-9.1
Per1	Yes	2	Yes	Yes	Yes	No	N/A	N/A
Per2	Yes	4	Yes	Yes	Yes	Yes	-1.5	-4.6
Per3	Yes	7	No	No	Yes	Yes	1.5	-7.2
Cry1	Yes	4	Yes	No	Yes	Yes	1.5	-3.8
Cry2	Yes	13	Yes	Yes	Yes	No	N/A	N/A
Nfil3	Yes	1	Yes	No	Yes	Yes	0	-3.3
Dbp	Yes	3	Yes	No	Yes	Yes	0	-27.3
Tef	Yes	5	Yes	Yes	Yes	Yes	4.5	-6.8
Hlf	Yes	2	Yes	Yes	Yes	No	N/A	N/A

[a] Putative dioxin response elements (pDREs; MSS ≥ 0.856) were identified by computationally querying the mouse genome [42].

[b] AhR genomic enrichment was determined through ChIP-Seq analysis of male livers 2h after treatment with 30 μg/kg TCDD [27].

[c] Rhythmicity was determined using JTK_CYCLE (BH q-value ≤ 0.1; period = 21-24h) [44].

Furthermore, the rhythmic expression of all core clock regulators was diminished by TCDD, involving either a ≥ 3.3-fold reduction in amplitude (*Arntl*, *Npas2*, *Nr1d1, Nr1d2, Rorc*, *Per2*, *Per3, Cry1, Nfil3, Dbp,* and *Tef*) or a complete loss of oscillation (*Clock*, *Per1*, *Cry2*, and *Hlf*). For example, the amplitude of *Dbp Rorc*, and *Per3* was repressed 27.3-, 9.1-, and 7.2-fold by TCDD (Figure 43; Table 9).

Capillary electrophoresis (WES ProteinSimple System) was used to evaluate the effect of TCDD on hepatic protein levels of select clock regulators. JTK_CYCLE analysis (BH q-value ≤ 0.1; period = 21-24 h) confirmed ARNTL, REV-ERBα, and NFIL3 protein levels exhibited rhythmic oscillations in control samples. TCDD reduced hepatic ARNTL and NFIL3 protein levels 14.4- and 80.6-fold, respectively, while REV-ERBα protein was undetected in TCDD-treated mouse liver samples at every timepoint (Figure 44). Furthermore, TCDD abolished the circadian rhythmicity of these three proteins, consistent with reduced amplitudes in gene expression.

ChIP-PCR was used to evaluate hepatic ARNTL genomic enrichment following persistent AhR activation over 28d. In control livers, oscillating genomic ARNTL binding within previously identified target genes was confirmed, with peak binding detected at ZT9. TCDD reduced ARNTL binding within *Per1*, *Dbp*, and *Nr1d1* 3.4-, 4.0-, and 3.7-fold, respectively. Moreover, ARNTL binding rhythmicity was abolished within *Per1* and *Dbp*, while the amplitude of rhythmicity at *Nr1d1* was reduced 5.9-fold (Figure 45A-C). The specificity of the ARNTL immunoprecipitation was confirmed using a negative control region on chromosome 6 (Figure 45D). These results demonstrate that TCDD dampened *Arntl* transcriptional rhythmicity, reduced ARNTL protein levels, and impaired ARNTL's ability to bind to genomic regions within target genes.

Enriched AhR binding within core clock genes

A previously published time-course hepatic RNA-seq analysis revealed differential expression of several E-box-containing core clock genes 4h after TCDD treatment, suggesting direct AhR regulation of the hepatic clock. Specifically, TCDD repressed *Per1* (2.0-fold; not-

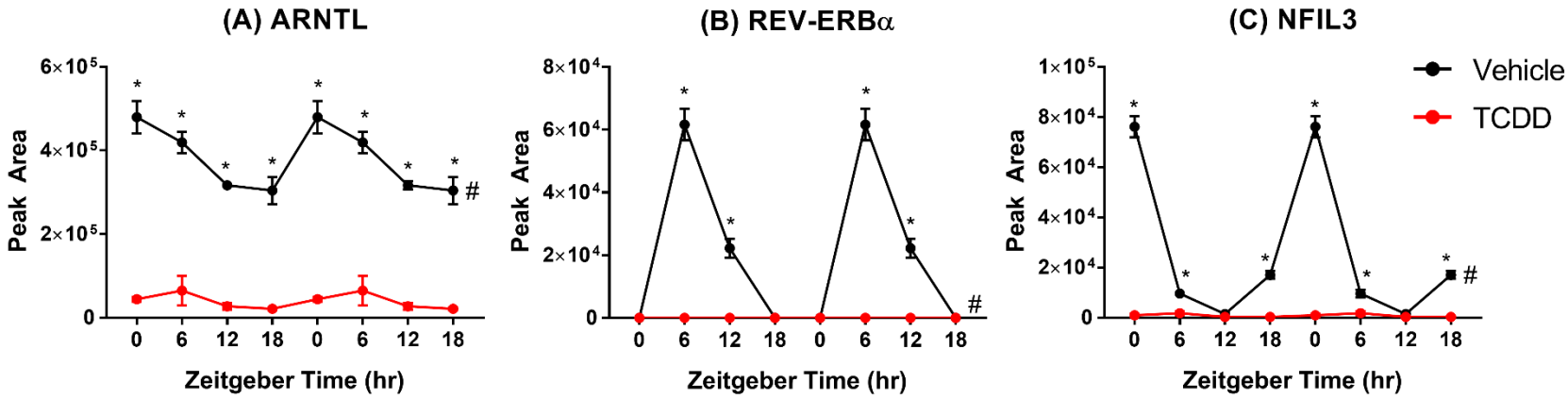

FIGURE 44. TCDD ABOLISHED THE RHYTHMICITY OF THE CORE CLOCK AT THE PROTEIN LEVEL

Hepatic protein levels of (A) ARNTL, (B) REV-ERBα, and (C) NFIL3 in male C57BL/6 mice orally gavaged with sesame oil vehicle or 30 µg/kg TCDD every 4 days for 28 days. Data points represent the average of 3 biological replicates ± standard error of the mean measured using capillary electrophoresis (WES ProteinSimple System). Statistical significance (* $p \leq 0.05$) between vehicle and TCDD was determined using a two-way ANOVA analysis followed by Sidak's multiple comparison test. Circadian rhythmicity was assessed using JTK_CYCLE (# BH $q \leq 0.1$). Data is plotted twice to more easily visualize effects on rhythmicity.

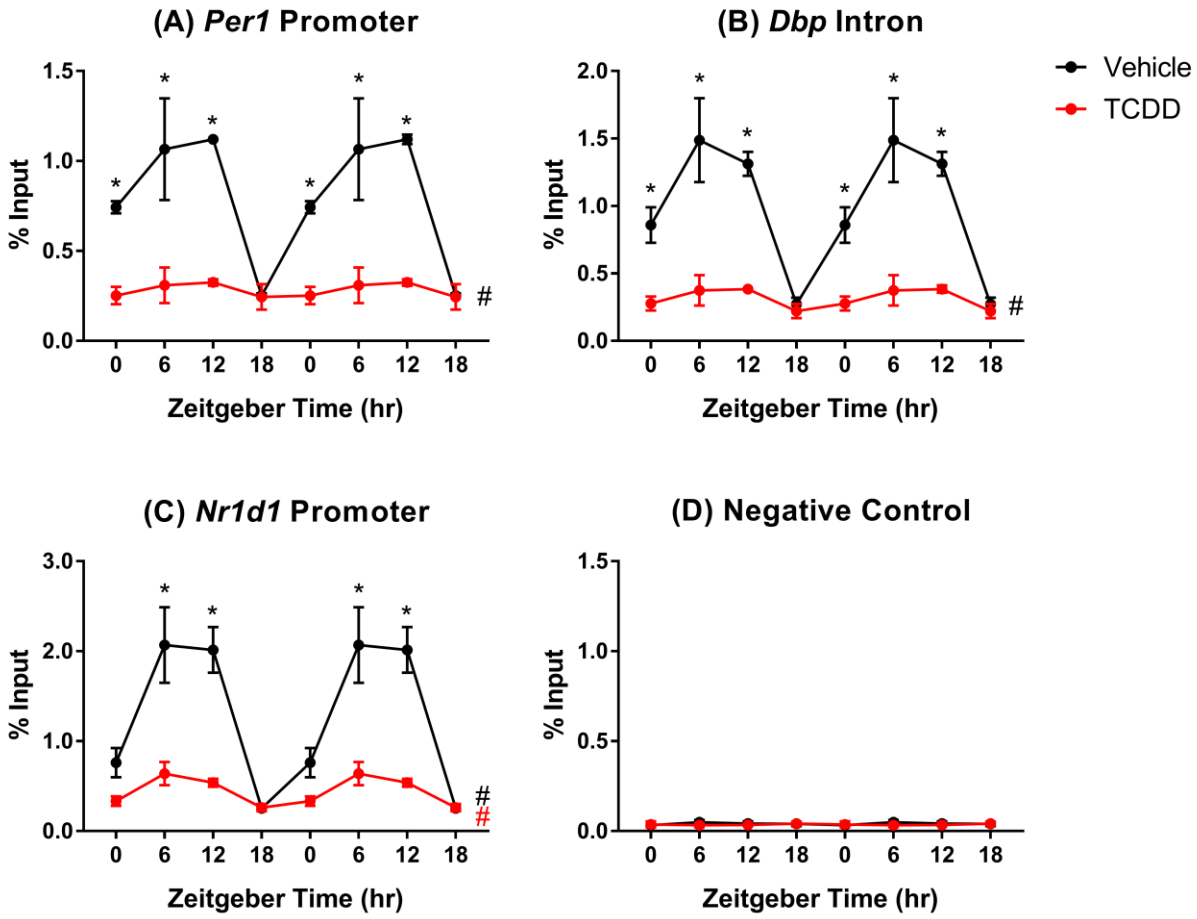

FIGURE 45. TCDD DAMPENED THE RHYTHMICITY OF ARNTL GENOMIC ENRICHMENT

ARNTL genomic enrichment within target genes assessed using chromatin immunoprecipitation (ChIP). Liver samples were collected from male C57BL/6 mice following oral gavage with sesame oil vehicle or 30 µg/kg TCDD every 4 days for 28 days. Genomic enrichment for ARNTL was quantified by qRT-PCR using primers targeting previously identified ARNTL binding sites within (A) the *Per1* promoter (site 2), (B) a *Dbp* intron, and (C) the *Nr1d1* promoter as described in Table 8. (D) A negative control region on chromosome 6 was used to confirm the specificity of the ANRTL immunoprecipitation. Data points represent the average % input of 3 biological replicates ± standard error of the mean. Statistical significance (* $p \leq 0.05$) between vehicle- and TCDD-treated mice was determined using a two-way ANOVA analysis followed by Sidak's multiple comparison test. Circadian rhythmicity was assessed using JTK_CYCLE (# BH $q \leq 0.1$). Data is plotted twice to more easily visualize effects on rhythmicity.

significant), *Per3* (3.0-fold), *Dbp* (3.3-fold), and *Tef* (1.8-fold) at 4h, while *Per2* was induced 3.0-fold [53]. At least one pDRE (MSS ≥ 0.856) was found within each core clock gene with the exception of *Nr1d2*, determined by a computational query of the mouse genome [42]. Similarly, ChIP-Seq analysis of male liver samples at 2h detected AhR genomic enrichment within the loci of all core clock regulators except *Per3* [27], providing further evidence AhR may directly interfere with the rhythmic expression of hepatic core clock regulators. However, only 7 of these 15 core clock genes exhibited AhR enrichment at a site containing a pDRE, while 8 genes only exhibited AhR enrichment at regions lacking a pDRE (Table 9). Therefore, TCDD-elicited disruption of hepatic rhythmicity may involve both canonical and non-canonical AhR signaling pathways.

In vitro studies using Hepa1c1c7 cells treated with β-naphthoflavone (βNF) for 1.5h report AhR interacts with ARNTL and binds at E-box response elements within the *Per1* promoter. This is reported to decrease the formation and binding of the ARNTL/CLOCK heterodimer at 2 of 3 E-boxes within the promoter of *Per1*, repressing its expression [41]. To further investigate non-canonical mechanisms involved in circadian dysregulation *in vivo*, ChIP-PCR was used to compare AhR, ARNTL, and CLOCK genomic binding in liver samples of male mice orally gavaged with TCDD for 2h. The primers described by Xu *et al* (2010) were used to assess binding within the *Per1* promoter at a site containing a canonical E-box but no pDRE (promoter site 1) [41]. In contrast to *in vitro* βNF treatment, *in vivo* TCDD treatment had no effect on AhR, CLOCK, or ARNTL enrichment within this region (Figure 46A). A 3.4-fold increase in AhR binding was detected further upstream of the Per1 transcription start site (promoter site 2), near a canonical E-box and pDRE. However, neither CLOCK nor ARNTL binding were affected by TCDD (Figure 46B). Similarly, 2.1-fold enrichment in AhR binding was detected at a non-canonical E-box (5'-CACGTT-3' [54]) within the promoter of *Per2*, despite a lack of pDREs within the area. Again, this AhR binding did not interfere with CLOCK or ARNTL binding (Figure 46C). AhR binding was also enriched 21.8-fold at a pDRE within a *Per2* intron. Despite a lack of canonical E-boxes within this region, CLOCK and ARNTL binding were detected but unaffected by TCDD (Figure 46D).

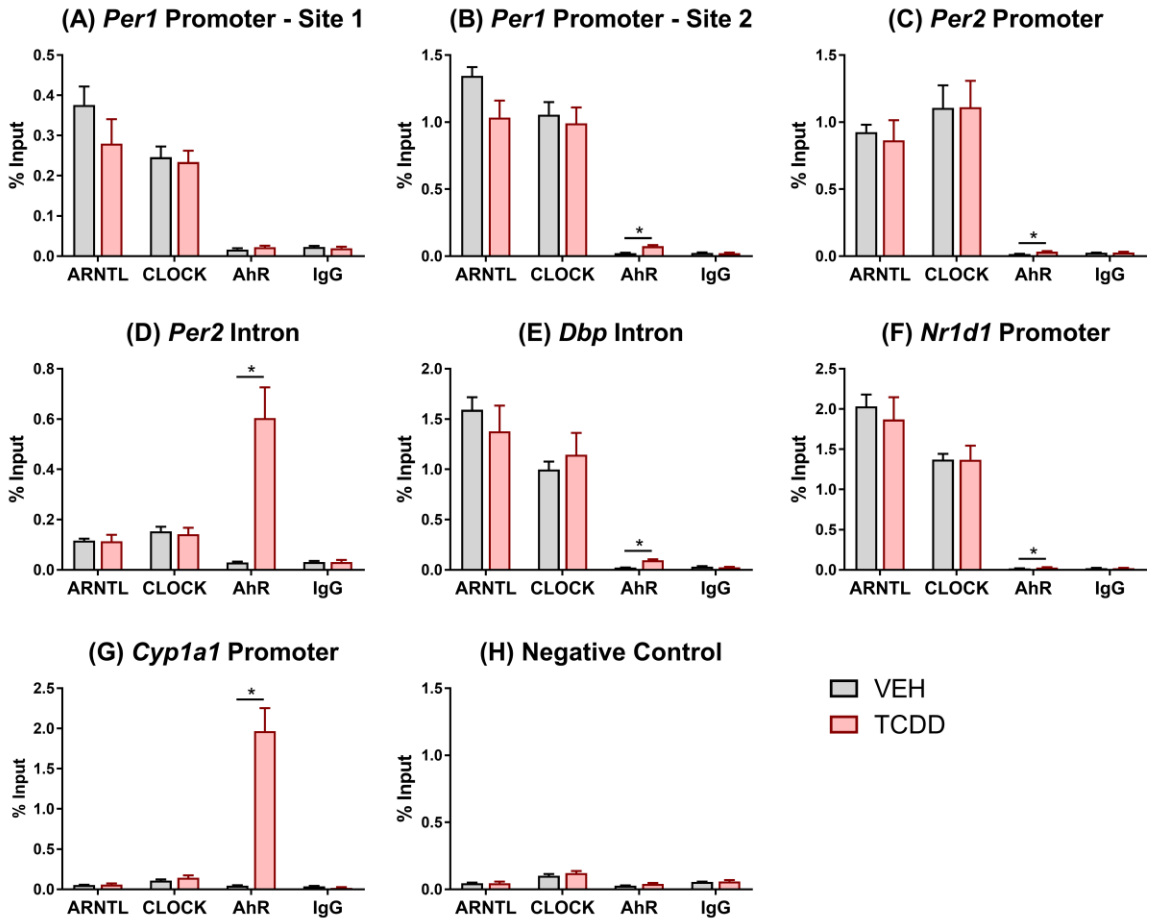

FIGURE 46. COMPARISON OF ARNTL, CLOCK, AND AHR GENOMIC ENRICHMENT

Genomic enrichment of ARNTL, CLOCK, and AhR within target genes assessed using chromatin immunoprecipitation (ChIP). Liver samples were collected between ZT4 and ZT6 from male C57BL/6 mice 2h following a single bolus dose of sesame oil vehicle or 30 µg/kg TCDD. Genomic enrichment was quantified by qRT-PCR using primers targeting regions within (A,B) *Per1*, (C,D) *Per2*, (E) *Dbp*, and (F) *Nr1d1* as described in Table 8. (G) *Cyp1a1* was used as a positive control for AhR binding, while (H) a negative control region on chromosome 6 was used to confirm the specificity of each immunoprecipitation. Data points represent the average % input of 4-5 biological replicates ± standard error of the mean. Statistical significance (* $p \leq 0.05$) between vehicle- and TCDD-treated mice was determined using a two-way ANOVA analysis followed by Sidak's multiple comparison test.

Additionally, AhR enrichment was increased 4.3- and 1.8-fold within a *Dbp* intron and the *Nr1d1* promoter, respectively, with no effect on CLOCK or ARNTL binding (Figure 46E,F). A 43.8-fold increase in AhR binding at a pDRE within the *Cyp1a1* promoter served as a positive control (Figure 46G), while no enrichment was detected in the negative control region on chromosome 6 (Figure 46H). Overall, TCDD-activated AhR did not interfere with ARNTL or CLOCK binding at the regions examined in this study.

TCDD disrupts circadian regulation of hepatic metabolism

To identify circadian-controlled biological processes and metabolic pathways affected by TCDD, a functional enrichment analysis was performed on 2,804 hepatic genes that: (i) exhibited rhythmicity in controls but not TCDD-treated mice and (ii) were differentially expressed (fold change ≥ 1.5; P1(t) ≥ 0.8) by TCDD at three or more timepoints. DAVID identified 19 enriched functional clusters (ES ≥ 1.3) that included metabolism of lipids (e.g. fatty acids, phospholipids, cholesterol/sterols, and sphingolipids), glycogen, and heme, as well as oxidation-reduction reactions and DNA repair (Figure 47A). Indeed, the hepatic peripheral clock is known to regulate expression of genes associated with nutrient metabolism, oxidative defense, and DNA repair, facilitating synchronization with feeding/fasting cycles and ultraviolet (UV) radiation exposure during daylight [3].

The effect of TCDD on circadian-controlled hepatic metabolism was further evaluated through an untargeted metabolomics analysis of male liver samples collected at 3h intervals over a 24h period. Negative mode electrospray ionization of polar hepatic extract detected a total of 6,569 metabolite peaks, of which 1,638 (24.9%) were identified as rhythmic by JTK_CYCLE (BH q-value ≤ 0.1; period = 21-24 h). Similarly, positive mode electrospray ionization detected 5,055 metabolite peaks, where 900 (17.8%) were identified as rhythmic in controls (Figure 47B). This fraction of rhythmic metabolites within the hepatic metabolome is comparable to the percentage of oscillating hepatic genes detected (25.7%), but lower than the ~50% reported in a targeted

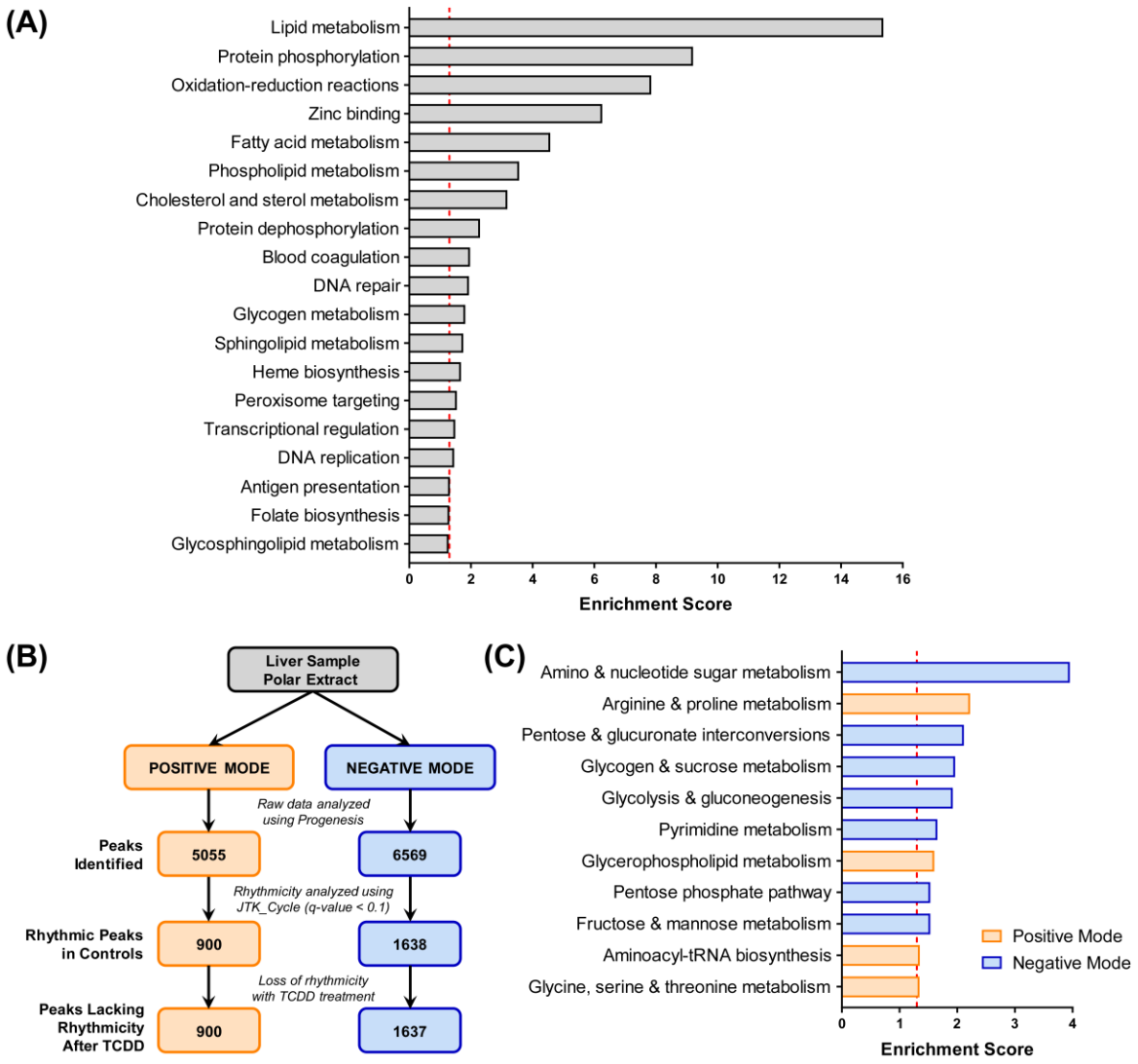

FIGURE 47. FUNCTIONAL ANALYSIS OF HEPATIC GENES AND METABOLITES WHICH LOST THEIR RHYTHMICITY

Transcriptomic and metabolomic changes were assessed in male C57BL/6 mice orally gavaged with sesame oil vehicle or 30 µg/kg TCDD every 4 days for 28 days. (A) The Database for Annotation, Visualization, and Integrated Discovery (DAVID) v6.8 was used to identify enriched functional clusters within 2,804 hepatic genes with abolished rhythmicity and TCDD-elicited differential expression at three or more timepoints. (B) Flow chart summarizing the analysis of an untargeted metabolomics assessment of polar hepatic extracts run in both positive and negative mode. (C) The *mummichog* algorithm in MetaboAnalyst v4.0 (MS Peaks to Pathways) was used to identify enriched KEGG pathways in the 900 and 1,637 oscillating peaks identified in positive (orange) and negative (blue) mode, respectively, which lost their rhythmicity following TCDD treatment. Scores ≥ 1.3 (red dotted line) were considered significantly enriched.

metabolomics study [12]. Following TCDD treatment, 1,637 of the 1,638 oscillating peaks detected in negative mode lost rhythmicity (99.9%). Similarly, 100% of the oscillating peaks identified in positive mode were arrhythmic following treatment (Figure 47B). Peaks which lost rhythmicity were assessed for enriched metabolic KEGG pathways using the *mummichog* algorithm within MetaboAnalyst [46]. A total of 11 enriched pathways were identified (7 in negative mode, 4 in positive mode), including several related to the biological processes enriched at the gene expression level (Figure 47C). Glucose and glycogen metabolism, bile acid homeostasis, heme biosynthesis, and redox homeostasis were examined further through the integration of transcriptomic, metabolomic, and enzymatic analyses.

(i) Glucose and glycogen metabolism

During the active phase, glucose is primarily obtained through the consumption of dietary polysaccharides, while the breakdown of glycogen (glycogenolysis) and *de novo* glucose biosynthesis (gluconeogenesis) provide glucose during the fasting phase. Circadian regulation of systemic glucose homeostasis is entrained by several factors such as autonomous nervous system (ANS) signaling between the SCN and the liver, rhythmic feeding and nutrient availability, hormones (e.g. insulin, glucagon, and glucocorticoids), and the peripheral hepatic clock [55]. Specifically, the transcription of several key gluconeogenesis genes including phosphoenolpyruvate carboxykinase 1 (*Pck1*) and glucose-6-phosphatase (*G6pc*) is directly regulated by core clock transcription factors (e.g. REV-ERBα), as well as the circadian-regulated transcriptional activators Krüppel-like factor 15 (KLF15) and cAMP responsive element binding protein 3-like 3 (CREB3L3) [56-58]. Both *Klf15* and *Creb3l3* lost rhythmicity and were repressed (3.1- and 3.0-fold, respectively) by TCDD. Accordingly, hepatic *Pck1* and *G6pc* were repressed 17.7- and 6.9-fold, respectively, consistent with results reported in KLF15 and CREB3L3 knockout models [56, 58]. *Pck1* rhythmic oscillation was concurrently abolished, while *G6pc* was classified as arrhythmic in both control and treated animals (Figure 48). KLF15 also controls the availability

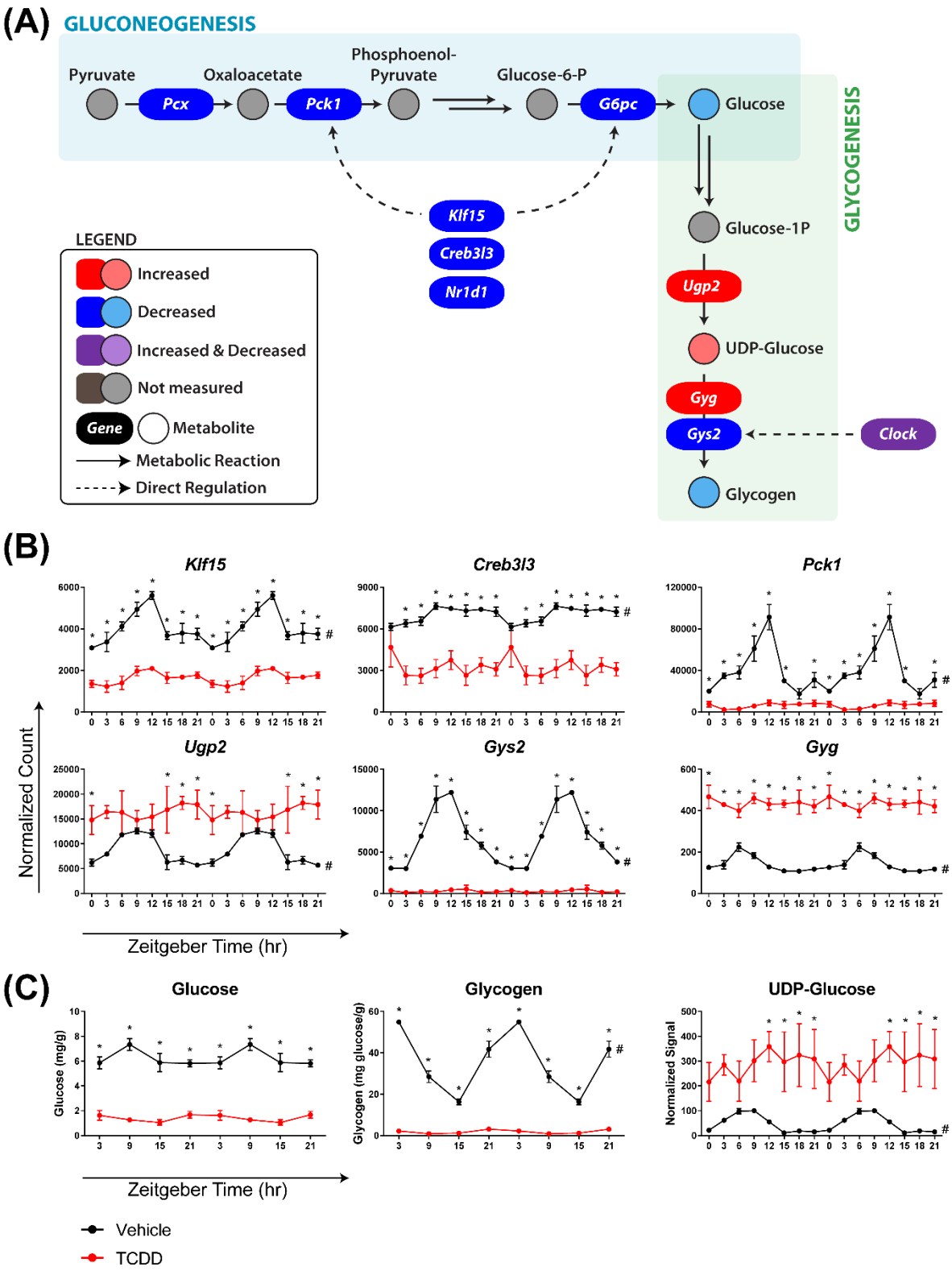

FIGURE 48. TCDD DISRUPTS THE CIRCADIAN REGULATION OF GLUCOSE HOMEOSTASIS

FIGURE 48 (cont'd)

Male C57BL/6 mice were orally gavaged with sesame oil vehicle or 30 µg/kg TCDD every 4 days for 28 days. (A) The effect of TCDD on hepatic gluconeogenesis and glycogenesis. TCDD-elicited changes in hepatic (B) genes and (C) metabolites involved in gluconeogenesis and glycogenesis. For genes, data points represent the average of 3 biological replicates ± standard error of the mean (SEM), where posterior probabilities (* P1(t) ≥ 0.80) comparing vehicle and TCDD were determined using an empirical Bayes method. For metabolites, data points represent the average of 3-5 biological replicates ± SEM, where statistical significance (* $p \leq 0.05$) between vehicle and TCDD was determined using a 2-way ANOVA analysis followed by Sidak's multiple comparison test. Circadian rhythmicity was assessed using JTK_CYCLE (# BH $q \leq 0.1$). Data is plotted twice to more easily visualize effects on rhythmicity.

of gluconeogenic precursors (e.g. pyruvate) by regulating gene expression associated with amino acid catabolism and nitrogenous waste excretion (i.e. urea cycle). Several KLF15 target genes were repressed including glutamic pyruvic transaminase (*Gpt*; encodes ALT; 12.3-fold), 4-hydroxyphenylpyruvic acid dioxygenase (*Hpd;* 3.7-fold), proline dehydrogenase (*Prodh;* 5.4-fold), tryptophan 2,3-dioxygenase (*Tdo2;* 2.0-fold) and ornithine transcarbamylase (*Otc;* 57.9-fold), impairing amino acid catabolism and limiting the availability of gluconeogenic precursors. Consistent with repression of key gluconeogenesis enzymes and regulators, hepatic glucose levels were reduced (up to 5.8-fold) at each timepoint (Figure 48).

Excess glucose consumed during the active phase can be stored as glycogen and called upon as an energy source during fasting. As such, hepatic glycogen levels oscillate in a circadian manner peaking at the end of the active phase (ZT0) (Figure 48). TCDD not only decreased hepatic glycogen levels at all timepoints (up to 31.4-fold), but also abolished its rhythmic oscillation pattern. This is consistent with the repression (88.7-fold) and loss of rhythmicity in glycogen synthase 2 (Gys2) (Figure 48), the rate-limiting step of hepatic glycogenesis which is directly regulated by CLOCK-mediated transcriptional activation [59]. Loss of circadian regulation in both hepatic *Gys2* expression and glycogen content was also observed in CLOCK mutant mice [59]. Paradoxically, glycogenin (*Gyg*), the core protein required for the initiation of glycogenesis, was induced 4.1-fold while losing its oscillation pattern. Additionally, the circadian-controlled enzyme UDP-glucose pyrophosphorylase 2 (*Ugp2*) was induced 3.1-fold. Accordingly, hepatic levels of UDP-glucose, the activated glucose monomer required for glycogen synthesis, were persistently increased 26.7-fold (Figure 48). Continuous induction of *Gyg* and *Ugp2* may represent an attempt to increase glycogenesis to restore depleted glycogen levels. The inability to store glucose during the active/feeding phase would compromise energy availability during fasting and limit effective nutrient utilization. This, combined with impaired gluconeogenesis and reprogramming of central carbon metabolism, suggests carbohydrate and amino acid metabolism

have been decoupled from feeding/fasting cycles, consistent with reports of lower circulating glucose levels and altered glucose tolerance in TCDD treated mice [27, 60].

(ii) Bile acid homeostasis

Several genes associated with bile acid biosynthesis and transport are circadian-regulated, allowing bile homeostasis to be synchronized with lipid consumption. For example, hepatic transcription of *Cyp7a1*, the rate-limiting step of primary bile acid biosynthesis, is regulated by REV-ERBα, DBP, and NFIL3 [61, 62]. In turn, daily fluctuations in the concentration and composition of the hepatic and serum bile acid pools influence the rhythmicity of bile acid metabolizing genes through farnesoid X receptor (FXR) signaling [63]. In agreement with dampened *Nr1d1*, *Dbp*, and *Nfil3* oscillations, TCDD repressed hepatic *Cyp7a1* 38.8-fold and abolished its rhythmic expression. Several hepatic bile acid transporters also lost rhythmicity and were repressed including blood-to-liver importer *Slc10a1* and liver-to-bile canaliculus exporter *Abcb11* (31.3- and 7.0-fold, respectively), while the liver-to-blood exporter *Abcc4* was induced 134.9-fold (Figure 49). These disruptions in enterohepatic circulation are consistent with the observed hepatic accumulation and loss of circadian oscillations in several bile acids including a primary taurine conjugate (3.8-fold), a secondary taurine conjugate (not-significant), and a cholic acid derivative (225.4-fold) (Figure 49), similar to previous studies [28, 64]. This loss of circadian regulation of bile acid homeostasis is further evidence of the decoupling between nutrient absorption, hepatic metabolism, and nuclear receptor signaling.

(iii) Heme biosynthesis

Heme regulates circadian cycling by serving as a cofactor for REV-ERBα/β, NPAS2, CLOCK, and PER2 [30-33], and in turn, several key clock components regulate heme biosynthesis. Specifically, NPAS2, ARNTL, PER1, and PER2 regulate the rhythmic expression of aminolevulinic acid synthase 1 (*Alas1*), the rate-limiting enzyme of hepatic heme biosynthesis

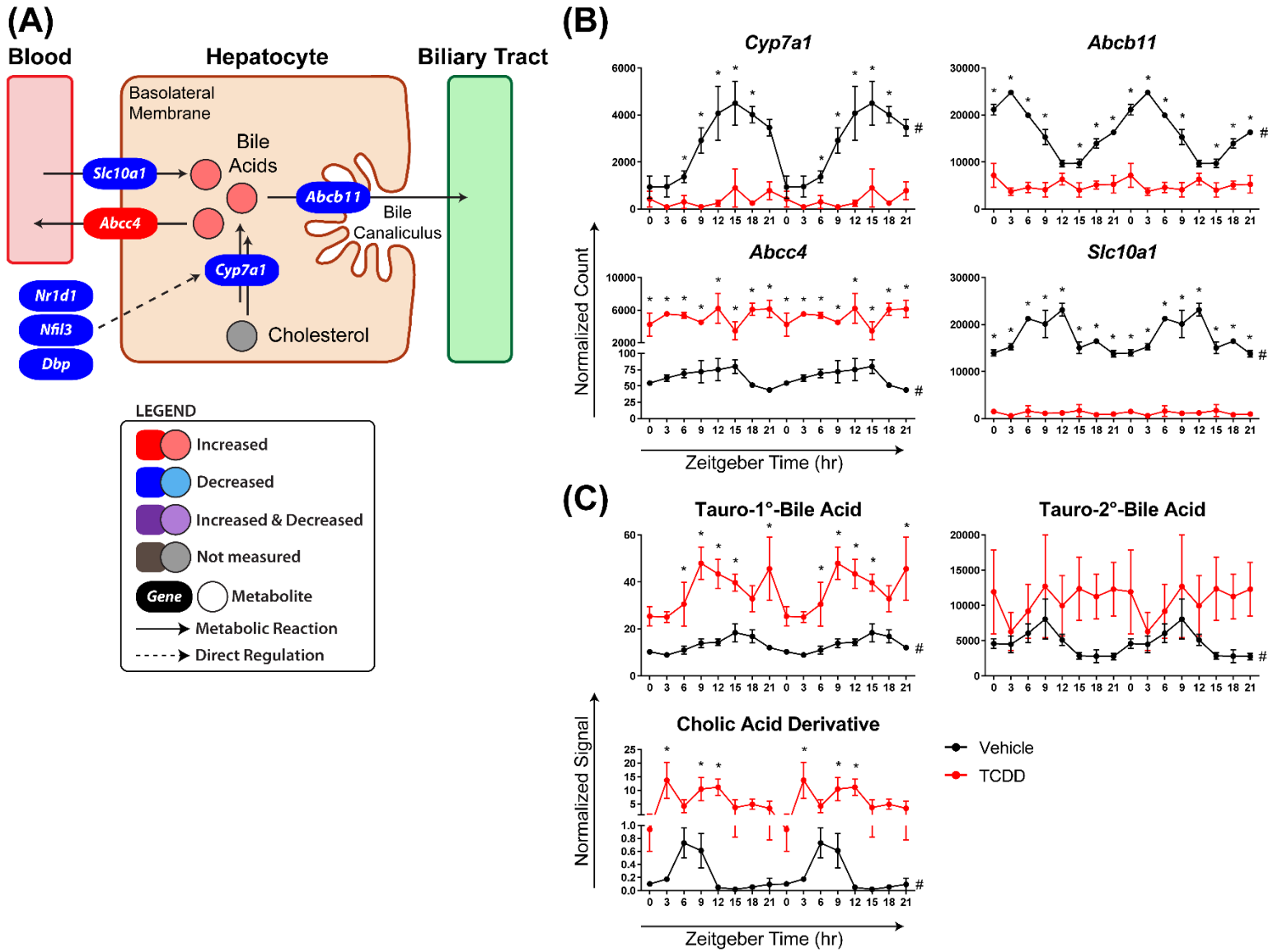

FIGURE 49. TCDD DISRUPTS THE CIRCADIAN REGULATION OF BILE ACID HOMEOSTASIS

FIGURE 49 (cont'd)

Male C57BL/6 mice were orally gavaged with sesame oil vehicle or 30 µg/kg TCDD every 4 days for 28 days. (A) The effect of TCDD on bile acid biosynthesis and hepatic transport. TCDD-elicited changes in hepatic (B) genes and (C) metabolites involved in bile acid homeostasis. For genes, data points represent the average of 3 biological replicates ± standard error of the mean (SEM), where posterior probabilities (* $P1(t) \geq 0.80$) comparing vehicle and TCDD were determined using an empirical Bayes method. For metabolites, data points represent the average of 3-5 biological replicates ± SEM, where statistical significance (* $p \leq 0.05$) between vehicle and TCDD was determined using a 2-way ANOVA analysis followed by Sidak's multiple comparison test. Circadian rhythmicity was assessed using JTK_CYCLE (# BH $q \leq 0.1$). Data is plotted twice to more easily visualize effects on rhythmicity.

[65]. In accordance with the diminished rhythmicity of *Npas2*, *Arntl, Per1*, and *Per2*, TCDD abolished the oscillating pattern of *Alas1*, leading to an 8.2-fold induction in hepatic expression. As a result, hepatic levels of protoporphyrinogen IX and heme were arrhythmic and increased 88.3- and 176.8-fold, respectively, following treatment (Figure 50), consistent with our report of hepatic hemin accumulation [27]. *Alas1* expression is also directly regulated by PPAR coactivator 1α (PPARGC1A; aka PGC-1α), which is transcriptionally regulated by nutrient availability [66]. Consequently, heme serves as a signal of nutritional status, allowing the peripheral hepatic clock to respond to nutrient availability. Interestingly, *Ppargc1a* was repressed 4.0-fold by TCDD, indicating the link between *Ppargc1a* and *Alas1* expression was disrupted. As a result, heme levels no longer accurately reflect nutrient availability, rendering the clock unresponsive to nutritional status.

Beyond *Alas1*, the remaining downstream heme biosynthesis genes were repressed by TCDD at one or more timepoints: (Alad; 4.0-fold), (Hmbs; 1.7-fold), (Uros; 3.1-fold), (Urod; 1.8-fold), (Cpox; 2.9-fold), (Ppox; 1.8-fold), and (Fech; 1.5-fold), consistent with previous reports [27, 67]. Four of the seven downstream genes (*Uros, Cpox, Ppox,* and *Fech*) exhibited rhythmicity in control mice, however oscillating expression was abolished by TCDD (Figure 50). *Uros* and *Urod* repression promotes the conversion of heme precursors to uroporphyrin metabolites, leading to hepatic porphyrin accumulation. Indeed, hepatic uroporphyrin I, III, and/or IV were detected in TCDD-treated mice but not in controls. Overall, TCDD-elicited dysregulation of heme biosynthesis not only disrupted the normal rhythmicity of the hepatic clock machinery, but also impaired entrainment with nutrient availability.

(iv) Redox homeostasis

The antioxidant proteins peroxiredoxin (PRDX) and thioredoxin (TXN), which exhibit daily oscillations in their oxidation states, are part of the common circadian ancestral system conserved across all domains of life [68, 69]. Interestingly, abolishment of the PRDX clock system in *S.*

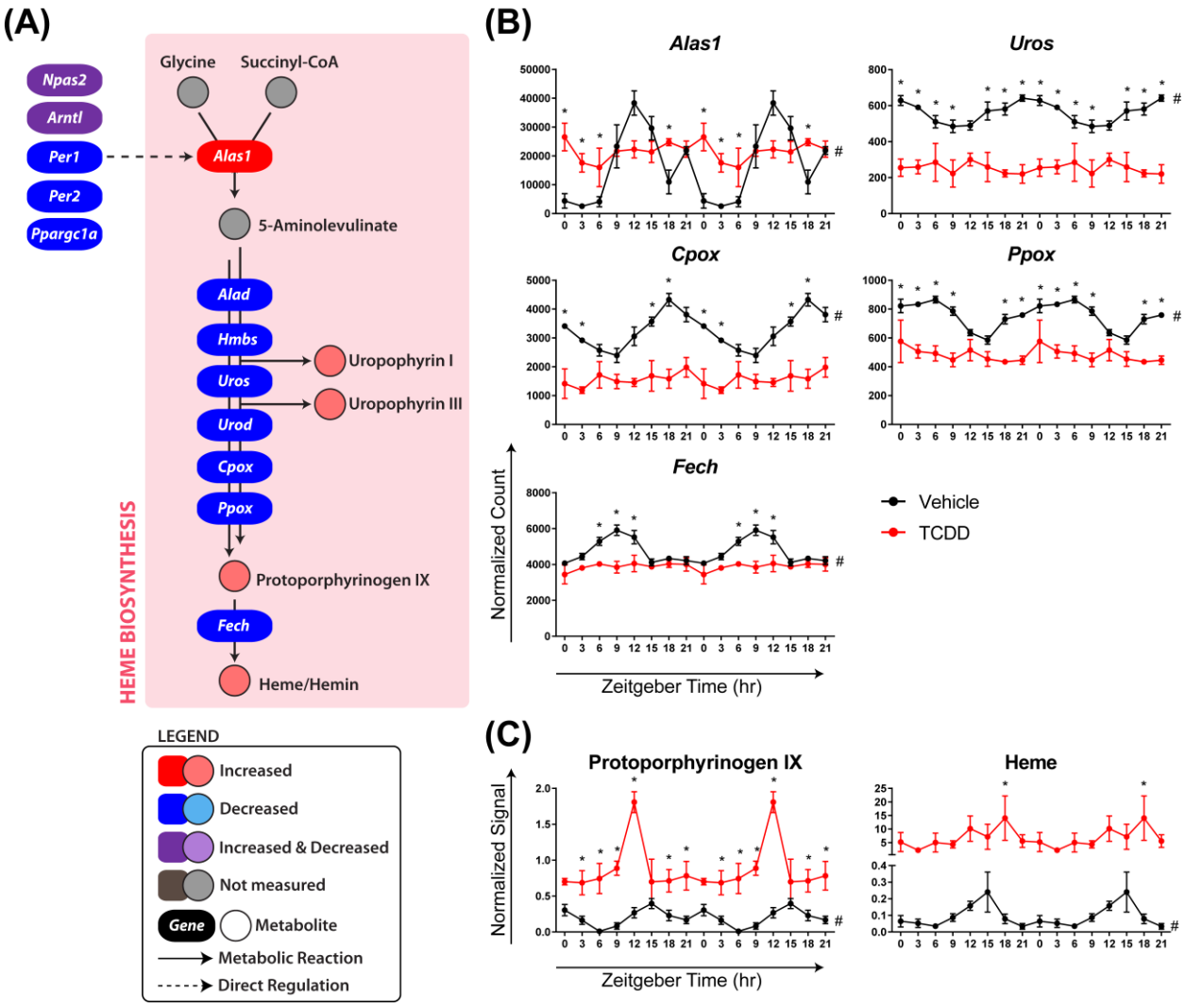

FIGURE 50. TCDD DISRUPTS THE CIRCADIAN REGULATION OF HEME BIOSYNTHESIS

Male C57BL/6 mice were orally gavaged with sesame oil vehicle or 30 µg/kg TCDD every 4 days for 28 days. (A) The effect of TCDD on hepatic heme biosynthesis. TCDD-elicited changes in hepatic (B) genes and (C) metabolites involved in heme biosynthesis. For genes, data points represent the average of 3 biological replicates ± standard error of the mean (SEM), where posterior probabilities (* P1(t) ≥ 0.80) comparing vehicle and TCDD were determined using an empirical Bayes method. For metabolites, data points represent the average of 3-5 biological replicates ± SEM, where statistical significance (* $p \leq 0.05$) between vehicle and TCDD was determined using a 2-way ANOVA analysis followed by Sidak's multiple comparison test. Circadian rhythmicity was assessed using JTK_CYCLE (# BH $q \leq 0.1$). Data is plotted twice to more easily visualize effects on rhythmicity.

elongatus and *A. thaliana* alters the amplitude or phase of core clock gene expression, demonstrating an intertwined yet poorly understood relationship between PRDX cycling and the clock's transcriptional feedback loops [68]. TCDD flattened and repressed hepatic expression of peroxiredoxin 4 (*Prdx4*; 2.9-fold) and 6 (*Prdx6*; 2.0-fold). Additionally, the predominant hepatic thioredoxin reductase *Txnrd1* was persistently induced 3.0-fold, while *Txnrd2* and *Txnrd3* were arrhythmic and repressed (4.0- and 5.3-fold respectively) following treatment (Figure 51). In mammals, intracellular redox status also directly regulates the core clock feedback loops, where the reduced forms of nicotinamide adenine dinucleotide (NADH) and nicotinamide adenine dinucleotide phosphate (NADPH) enhance the DNA-binding activity of the ARNTL/CLOCK and ARNTL/NPAS2 heterodimers [70]. TCDD repressed (2.3-fold) and flattened hepatic expression of nicotinamide phosphoribosyltransferase (*Nampt*), which catalyzes the rate-limiting conversion of nicotinamide (NAM) to nicotinamide mononucleotide (NMN). This led to loss of rhythmicity in hepatic NAM and NAD^+ levels. In addition, TCDD reduced hepatic NADPH levels 12.0-fold and abolished its oscillations (Figure 51). Perturbations in NAD coenzyme rhythmicity may compromise the redox-regulated entrainment of the core clock machinery. However, further studies investigating TCDD-elicited changes in the cyclic ratios of the oxidized to reduced forms (i.e. NAD^+:NADH; $NADP^+$:NADPH) are required.

Given that redox status entrains circadian rhythmicity, it is not surprising that the circadian clock regulates reactive oxygen species (ROS) homeostasis and antioxidant responses such as glutathione (GSH) biosynthesis [69]. GSH is synthesized from cysteine, glutamate, and glycine in a two-step enzymatic process catalyzed by glutamate-cysteine ligase (*Gclc*) and glutathione synthetase (*Gss*), both of which are circadian regulated. TCDD persistently induced *Gclc* and *Gss* 4.8- and 3.8-fold, respectively, abolishing their rhythmicity. Glutathione reductase (*Gsr*), responsible for recycling oxidized glutathione disulfide (GSSG) back to GSH, also lost rhythmicity and was induced 6.2-fold (Figure 52). The sustained induction of *Gclc* and *Gss* is in accordance with a 7.0-fold increase and loss of rhythmicity in the GSH precursor γ-glutamyl-cysteine (Figure

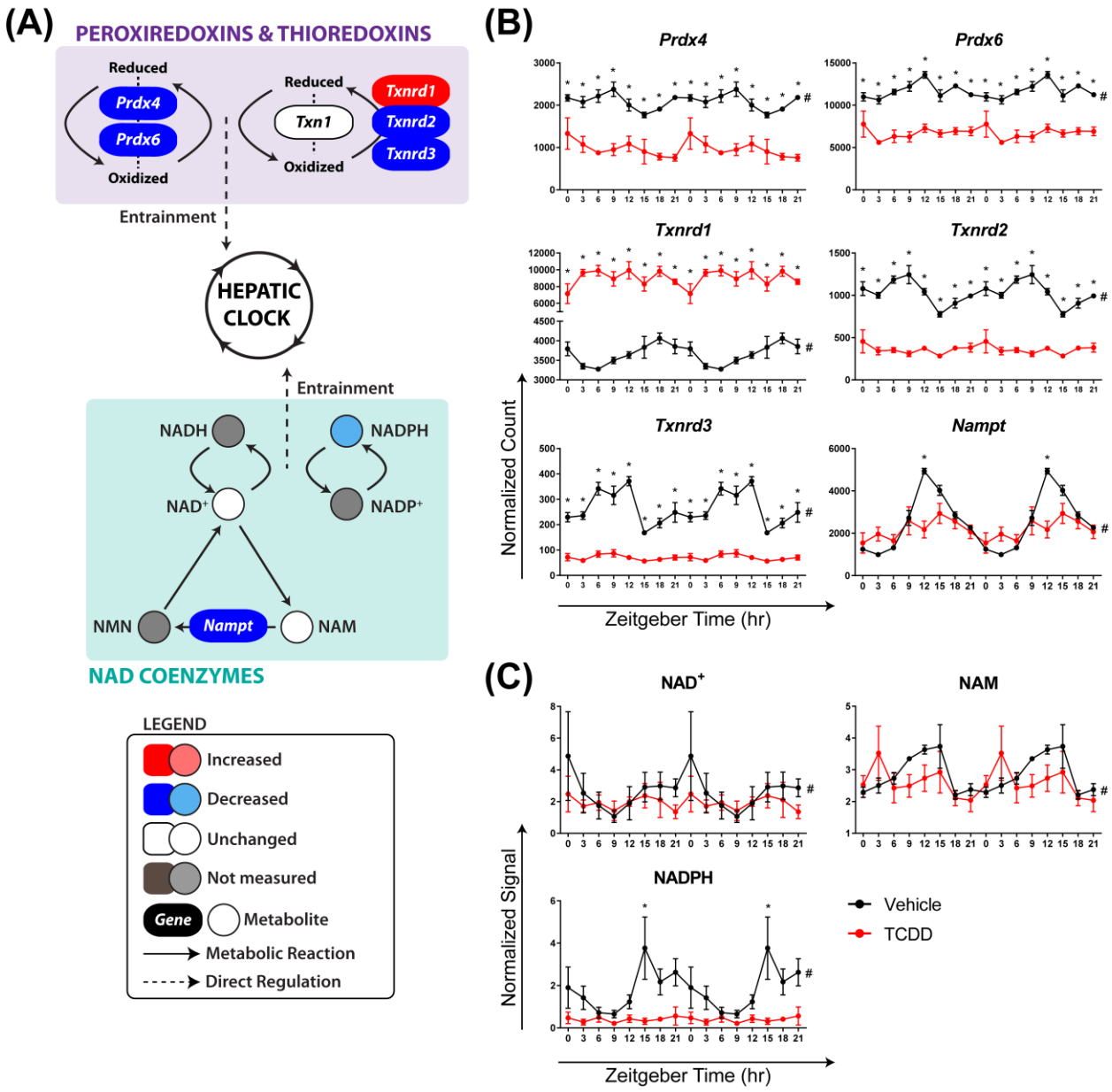

FIGURE 51. TCDD DISRUPTS REDOX-MEDIATED ENTRAINMENT OF HEPATIC CLOCK CYCLING

FIGURE 51 (cont'd)

Male C57BL/6 mice were orally gavaged with sesame oil vehicle or 30 µg/kg TCDD every 4 days for 28 days. (A) The effect of TCDD on the peroxiredoxins (*Prdx*), thioredoxin reductases (*Txnrd*), and nicotinamide adenine dinucleotide (NAD) coenzymes. TCDD-elicited changes in hepatic (B) genes and (C) metabolites associated with the redox cycling of PRDX, TXN, and NAD coenzymes. For genes, data points represent the average of 3 biological replicates ± standard error of the mean (SEM), where posterior probabilities (* P1(t) ≥ 0.80) comparing vehicle and TCDD were determined using an empirical Bayes method. For metabolites, data points represent the average of 3-5 biological replicates ± SEM, where statistical significance (* $p \leq 0.05$) between vehicle and TCDD was determined using a 2-way ANOVA analysis followed by Sidak's multiple comparison test. Circadian rhythmicity was assessed using JTK_CYCLE (# BH $q \leq 0.1$). Data is plotted twice to more easily visualize effects on rhythmicity.

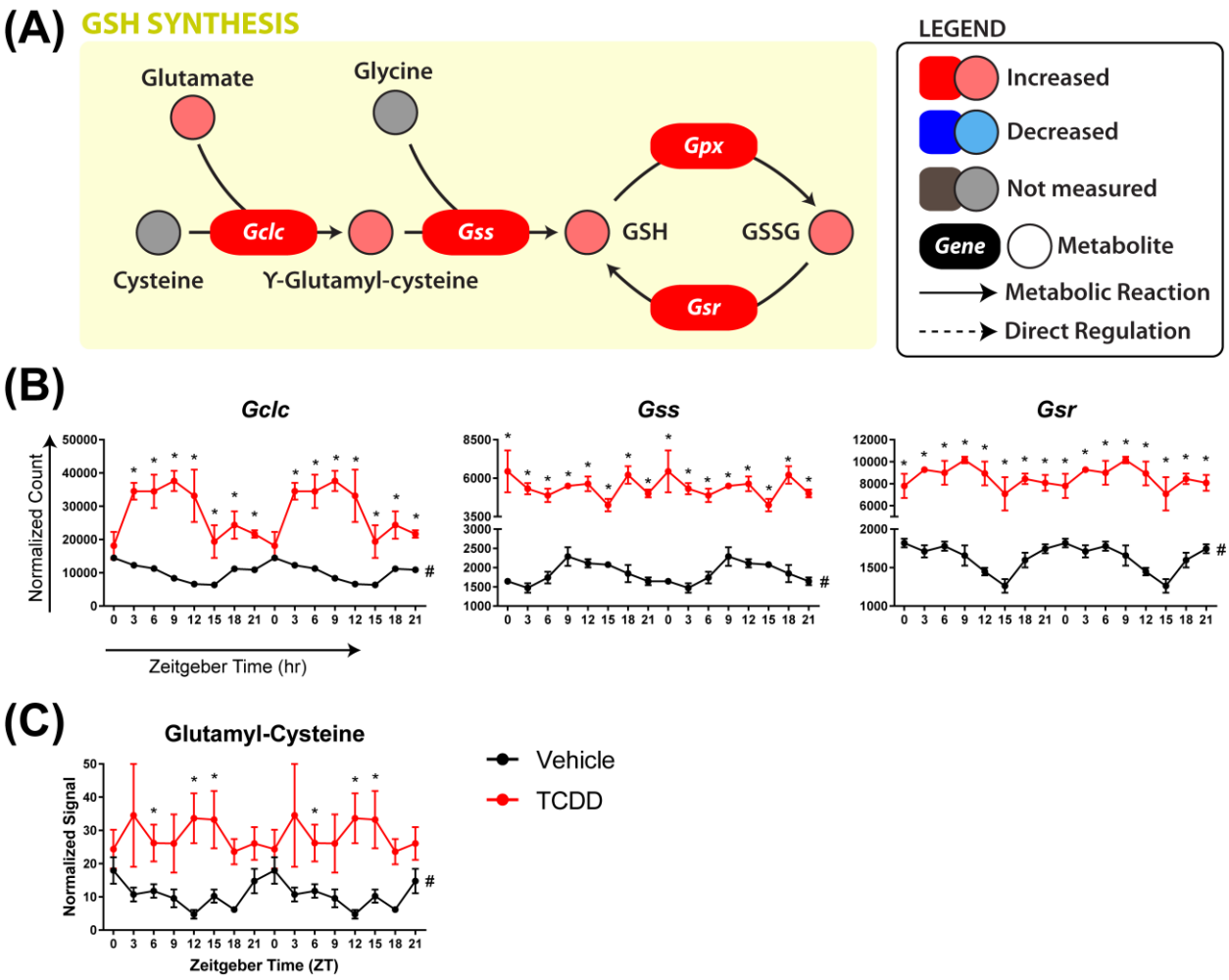

FIGURE 52. TCDD DISRUPTS THE CIRCADIAN REGULATION OF GLUTATHIONE (GSH) HOMEOSTASIS

Male C57BL/6 mice were orally gavaged with sesame oil vehicle or 30 µg/kg TCDD every 4 days for 28 days. (A) The effect of TCDD on GSH biosynthesis and recycling. TCDD-elicited changes in hepatic (B) genes and (C) metabolites involved in GSH biosynthesis. For genes, data points represent the average of 3 biological replicates ± standard error of the mean (SEM), where posterior probabilities (* P1(t) ≥ 0.80) comparing vehicle and TCDD were determined using an empirical Bayes method. For metabolites, data points represent the average of 3-5 biological replicates ± SEM, where statistical significance (* $p \leq 0.05$) between vehicle and TCDD was determined using a 2-way ANOVA analysis followed by Sidak's multiple comparison test. Circadian rhythmicity was assessed using JTK_CYCLE (# BH $q \leq 0.1$). Data is plotted twice to more easily visualize effects on rhythmicity.

52). Moreover, independent studies by our group detected a 1.3-fold increase in total hepatic GSH (GSH and GSSG) following TCDD treatment [42], as well as a 3.4-fold increase in hepatic glutamate (Fling *et al*., in preparation). Although increased antioxidant capacity is advantageous in response to TCDD-elicited oxidative stress, de-synchronization between the peripheral circadian clock and redox homeostasis may compromise cell signaling and overall liver function.

Beyond GSH, redox homeostasis is also affected by levels of uric acid, a breakdown product of purine nucleosides. In plasma, uric acid is a strong reducing agent that scavenges ROS, while intracellular uric acid promotes oxidative stress and stimulates pro-inflammatory pathways [71]. Several circadian-controlled genes involved in uric acid metabolism were affected by TCDD. Specifically, TCDD abolished the oscillation of ecto-5'-nucleotidase (*Nt5e*; induced 21.9-fold) and cytosolic II 5'-nucleotidase (*Nt5c2*; repressed 1.8-fold), which catalyze the hydrolysis of xanthosine monophosphate (XMP) to xanthosine. Purine-nucleoside phosphorylase (*Pnp*), which converts xanthosine to xanthine, also lost its rhythmicity. The oxidation of xanthine by xanthine dehydrogenase/xanthine oxidase (XDH/XO) yields uric acid, which is further oxidized to allantoin by urate oxidase (*Uox*). *Xdh* was induced 1.4-fold by TCDD, consistent with previous reports that *Xdh* induction contributes to AhR-mediated oxidative stress [42, 72]. TCDD also flattened *Uox* rhythmic oscillation, with a 35.0-fold reduction in expression. Accordingly, hepatic levels of uric acid and its upstream metabolites xanthosine and xanthine were reduced 45.9-, 157.6-, and 5.6-fold by TCDD, while concurrently losing their circadian oscillations (Figure 53). Overall, uric acid metabolism was shut down by TCDD, suggesting purine nucleosides may be shunted toward alternative metabolic pathways.

DISCUSSION

The hepatic circadian clock synchronizes metabolism with feeding/fasting cycles, ensuring efficient nutrient utilization and energy storage [3]. In this study, 25.7% of the hepatic transcriptome and ~20% of the polar hepatic metabolome exhibited circadian rhythmicity in

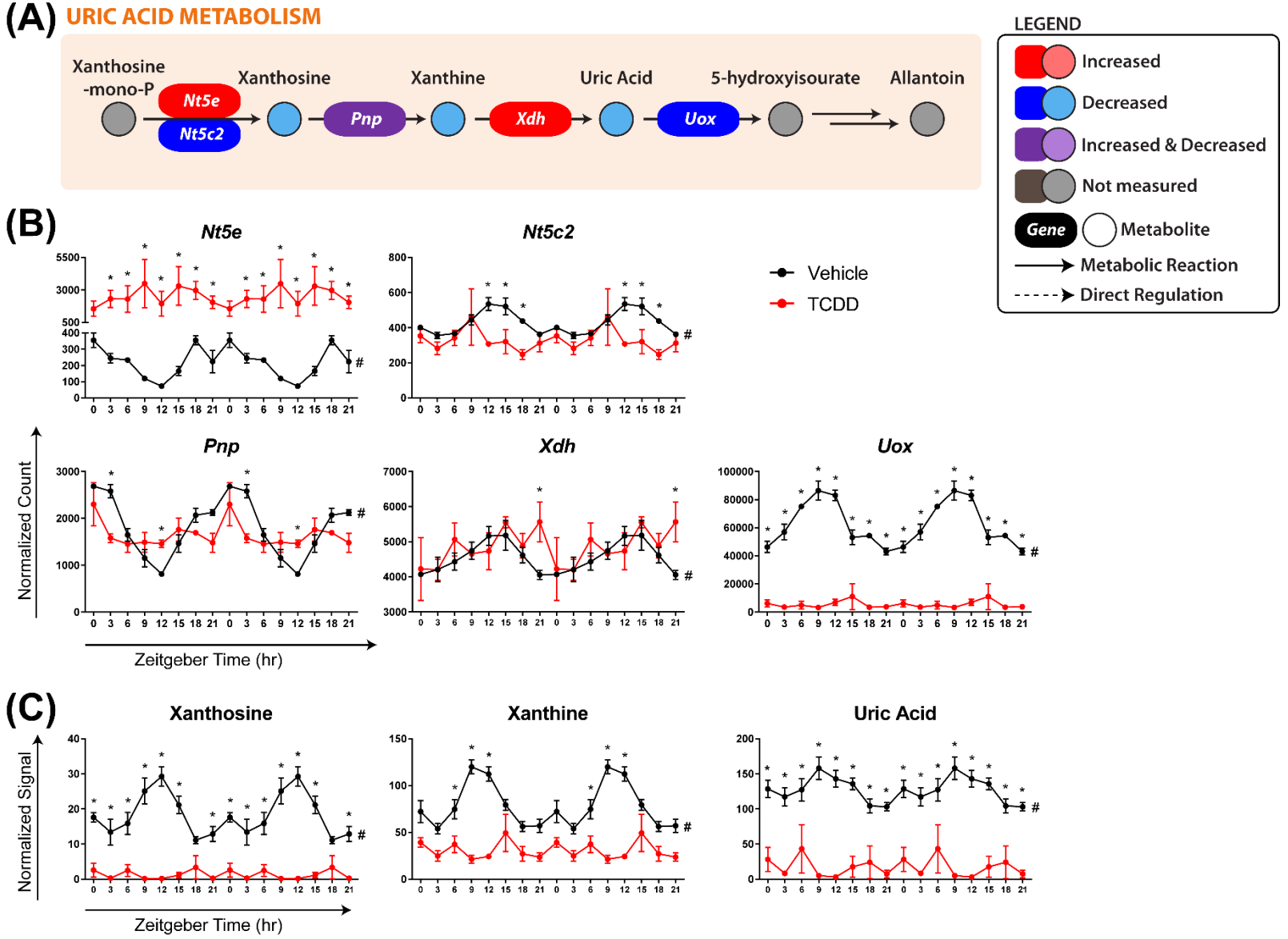

FIGURE 53. TCDD DISRUPTS CIRCADIAN REGULATION OF URIC ACID METABOLISM

FIGURE 53 (cont'd)

Male C57BL/6 mice were orally gavaged with sesame oil vehicle or 30 µg/kg TCDD every 4 days for 28 days. (A) The effect of TCDD on purine metabolism and uric acid biosynthesis. TCDD-elicited changes in hepatic (B) genes and (C) metabolites involved in uric acid metabolism. For genes, data points represent the average of 3 biological replicates ± standard error of the mean (SEM), where posterior probabilities (* P1(t) ≥ 0.80) comparing vehicle and TCDD were determined using an empirical Bayes method. For metabolites, data points represent the average of 3-5 biological replicates ± SEM, where statistical significance (* $p \leq 0.05$) between vehicle and TCDD was determined using a 2-way ANOVA analysis followed by Sidak's multiple comparison test. Circadian rhythmicity was assessed using JTK_CYCLE (# BH $q \leq 0.1$). Data is plotted twice to more easily visualize effects on rhythmicity.

control 9-10-week-old male C57BL/6 mice. These estimates fall in the middle of the range of previous reports [10-12]. Interestingly, ≥ 50% of the top selling pharmaceuticals in the United States target products of rhythmic genes [11]. Moreover, several drug-metabolizing enzymes are circadian-regulated including cytochrome P450s, UDP-glucuronosyltransferases, and GSH-S-transferases [73]. Consequently, time of administration and time of sample collection may be just as important as dose in assessing efficacy and mode of action, although not typically considered during safety or mechanistic studies. This may be yet another factor contributing to irreproducible results between studies [74, 75].

In rodents, AhR activation dysregulates not only the SCN master clock, but also the peripheral clocks of tissues such as the liver [22, 24]. The current study investigated the effects of TCDD on the rhythmicity of the hepatic transcriptome and metabolome in mice. We report that AhR activation by TCDD dampened the rhythmic expression of 15 hepatic core clock genes, involving either a decrease in amplitude or complete loss of oscillation. In turn, circadian oscillations in hepatic core clock protein levels were abolished, while genomic binding of ARNTL was reduced in the regulatory regions of known target genes. This is consistent with previous studies demonstrating AhR activation decreased the amplitude of core clock regulators (e.g. *Arntl*, *Per1*, and *Per2*) in the liver, ovaries, and bone marrow [24-26], while AhR deficiency increased the amplitude of oscillation [19]. To our knowledge, this is the first AhR study to demonstrate a complete loss of rhythmicity in core clock regulators at either the mRNA or protein level. Impaired cycling of the core clock machinery abolished the rhythmicity of virtually all circadian-controlled hepatic genes and polar metabolites. Moreover, this collapse of the hepatic clock was even detected at the gross pathology level, where RLW was also devoid of daily oscillations.

Hepatic ChIP-Seq studies identified AhR enrichment 2h after TCDD treatment in the majority of core clock genes, suggesting AhR directly alters the hepatic clock's transcriptional feedback loops [27]. Interestingly, approximately half of these core clock genes only exhibited AhR binding at sites lacking a pDRE, suggesting non-canonical AhR signaling [42]. βNF-activated

AhR has been shown to interact with ARNTL in mouse Hepa1c1c7 cells, which decreases ARNTL/CLOCK heterodimerization, reduces CLOCK binding at E-boxes within the *Per1* promoter, and represses *Per1* expression [41]. Heterodimerization between AhR and ARNTL is not surprising given the substantial sequence homology shared by ARNTL and AhR's canonical partner ARNT [15, 16]. In our study, ChIP-PCR analysis confirmed co-binding of AhR, ARNTL, and CLOCK at regulatory regions within *Per1*, *Per2*, *Nr1d1*, and *Dbp* 2h after TCDD treatment, including sites containing an E-box but no pDRE. However, AhR enrichment had no effect on the binding of CLOCK or ARNTL, suggesting ARNTL/CLOCK heterodimerization was not impaired by TCDD at the regions examined. Therefore, this non-canonical AhR mechanism may be ligand- and/or model-specific. Alternatively, AhR binding near ARNTL/CLOCK heterodimers may hinder co-activator recruitment, leading to repression of core clock genes, disruption of circadian regulation, and loss of rhythmicity in clock-controlled genes and metabolite levels.

In addition to dampening the transcriptional rhythmicity of the core clock feedback loops, TCDD dysregulated factors responsible for entraining the hepatic clock with the external environment. Gut-derived nutrients including glucose and amino acids reset the phase of the hepatic peripheral clock, allowing synchronization with feeding times [76]. For example, nutrient availability regulates co-activator PPARGC1A (aka PGC-1α) expression, which controls the transcription of several metabolic enzymes including *Alas1*, the rate-limiting step of heme biosynthesis [66]. Heme is a cofactor for REV-ERBα/β, NPAS2, CLOCK, and PER2, facilitating synchronization with nutrient availability [30-33]. TCDD abolished the oscillating expression of *Alas1* and downstream *de novo* heme biosynthesis genes, resulting in loss of rhythmicity in hepatic protoporphyrinogen IX and heme levels. Consequently, heme levels no longer reflect nutrient availability, decoupling synchronization with intestinal luminal contents. Additionally, TCDD alters segment-specific expression of intestinal nutrient transporters (e.g. fatty acid transporter *Cd36,* amino acid transporter *Slc36a1*, glucose transporter *Slc2a9*) [27, 49], and may therefore also interfere with rhythmic nutrient absorption. Intracellular redox homeostasis,

including oxidative cycling of PRDXs, TXNs, NADH, and NADPH, also entrains the core clock. TCDD not only abolished *Prdx*, *Txnrd*, and NAD co-enzyme rhythmicity, but also disrupted circadian regulation of key redox pathways including GSH biosynthesis and uric acid metabolism. This may alter the intracellular balance between pro- and anti-oxidants, affecting both hepatic clock entrainment and ROS-mediated gene regulation. The complex interactions between the core transcription-translation feedback loops, the conserved PRDX/TXN ancestral circadian system, and metabolite entrainment signals confound identification of the primary AhR targets that precipitate the collapse of hepatic circadian regulation.

AhR-mediated alterations in lipid, glucose, heme, bile acid, purine, and GSH metabolism contribute to the development and progression of TCDD-elicited NAFLD [27, 28, 42, 60, 77]. Beyond metabolic reprogramming, this study demonstrates AhR activation by TCDD disrupts circadian regulation of these pathways, leading to the loss of rhythmicity in gene expression and metabolite levels. As a result, hepatic metabolism and energy homeostasis are no longer synchronized with feeding/fasting cycles and nutrient availability, despite the lack of an effect on food consumption. Previous studies also report TCDD had no effect on food consumption [50], while others show that decreased consumption at high TCDD doses was insufficient to account for the observed weight loss and altered hepatic metabolism [78, 79]. Taken together, this suggests TCDD-induced wasting and hepatotoxicity may involve inefficient nutrient metabolism and the inability to store energy. For example, inhibition of glycogenesis and beta oxidation would limit energy availability during fasting. Meanwhile, central carbon intermediates are redirected to sustain the induction of heme and GSH biosynthesis, further compromising energy conservation during nutrient-rich periods.

In summary, AhR activation by TCDD abolished or dampened the rhythmic expression of hepatic core clock regulators and disrupted multiple clock entrainment cues, resulting in the collapse of hepatic circadian regulation. Consequently, hepatic metabolism was decoupled from feeding/fasting cycles, reducing metabolic efficiency and nutrient utilization. Our results

demonstrate that TCDD-activated AhR directly interferes with the hepatic clock's transcriptional feedback loops, however the primary targets have not been identified. Perturbations in circadian rhythm have been associated with multiple adverse effects including changes in the gut microbiome, increased intestinal permeability, NAFLD, obesity, cancer, and accelerated aging [4, 5, 80-83]. Therefore, AhR-mediated dysregulation of circadian rhythm may be a unifying mechanism which contributes to TCDD-elicited NAFLD, wasting syndrome, hepatocellular carcinoma, and gut dysbiosis. Collectively, the AhR may be central to an axis that regulates circadian rhythm, hepatic metabolism, and intestinal homeostasis. Additional studies are needed to determine if this extends to other tissues, as well as the relevance of AhR-mediated dysregulation of circadian rhythm in humans.

REFERENCES

REFERENCES

1. Partch, C.L., C.B. Green, and J.S. Takahashi, *Molecular architecture of the mammalian circadian clock.* Trends Cell Biol, 2014. 24(2): p. 90-9.

2. Roenneberg, T. and M. Merrow, *The Circadian Clock and Human Health.* Curr Biol, 2016. 26(10): p. R432-43.

3. Tong, X. and L. Yin, *Circadian rhythms in liver physiology and liver diseases.* Compr Physiol, 2013. 3(2): p. 917-40.

4. Savvidis, C. and M. Koutsilieris, *Circadian rhythm disruption in cancer biology.* Mol Med, 2012. 18: p. 1249-60.

5. Kondratov, R.V., A.A. Kondratova, V.Y. Gorbacheva, O.V. Vykhovanets, and M.P. Antoch, *Early aging and age-related pathologies in mice deficient in BMAL1, the core componentof the circadian clock.* Genes Dev, 2006. 20(14): p. 1868-73.

6. Lamont, E.W., D. Legault-Coutu, N. Cermakian, and D.B. Boivin, *The role of circadian clock genes in mental disorders.* Dialogues Clin Neurosci, 2007. 9(3): p. 333-42.

7. Hastings, M.H., E.S. Maywood, and M. Brancaccio, *Generation of circadian rhythms in the suprachiasmatic nucleus.* Nat Rev Neurosci, 2018. 19(8): p. 453-469.

8. Buijs, R.M., F.A. Scheer, F. Kreier, C. Yi, N. Bos, V.D. Goncharuk, and A. Kalsbeek, *Organization of circadian functions: interaction with the body.* Prog Brain Res, 2006. 153: p. 341-60.

9. Dibner, C., U. Schibler, and U. Albrecht, *The mammalian circadian timing system: organization and coordination of central and peripheral clocks.* Annu Rev Physiol, 2010. 72: p. 517-49.

10. Fang, B., L.J. Everett, J. Jager, E. Briggs, S.M. Armour, D. Feng, A. Roy, Z. Gerhart-Hines, Z. Sun, and M.A. Lazar, *Circadian enhancers coordinate multiple phases of rhythmic gene transcription in vivo.* Cell, 2014. 159(5): p. 1140-52.

11. Zhang, R., N.F. Lahens, H.I. Ballance, M.E. Hughes, and J.B. Hogenesch, *A circadian gene expression atlas in mammals: implications for biology and medicine.* Proc Natl Acad Sci U S A, 2014. 111(45): p. 16219-24.

12. Krishnaiah, S.Y., G. Wu, B.J. Altman, J. Growe, S.D. Rhoades, F. Coldren, A. Venkataraman, A.O. Olarerin-George, L.J. Francey, S. Mukherjee, S. Girish, C.P. Selby, S. Cal, U. Er, B. Sianati, A. Sengupta, R.C. Anafi, I.H. Kavakli, A. Sancar, J.A. Baur, C.V. Dang, J.B. Hogenesch, and A.M. Weljie, *Clock Regulation of Metabolites Reveals Coupling between Transcription and Metabolism.* Cell Metab, 2017. 25(5): p. 1206.

13. Takahashi, J.S., *Transcriptional architecture of the mammalian circadian clock.* Nat Rev Genet, 2017. 18(3): p. 164-179.

14. Fribourgh, J.L. and C.L. Partch, *Assembly and function of bHLH-PAS complexes.* Proc Natl Acad Sci U S A, 2017. 114(21): p. 5330-5332.

15. Takahata, S., K. Sogawa, A. Kobayashi, M. Ema, J. Mimura, N. Ozaki, and Y. Fujii-Kuriyama, *Transcriptionally active heterodimer formation of an Arnt-like PAS protein, Arnt3, with HIF-1a, HLF, and clock.* Biochem Biophys Res Commun, 1998. 248(3): p. 789-94.

16. Hogenesch, J.B., Y.Z. Gu, S. Jain, and C.A. Bradfield, *The basic-helix-loop-helix-PAS orphan MOP3 forms transcriptionally active complexes with circadian and hypoxia factors.* Proc Natl Acad Sci U S A, 1998. 95(10): p. 5474-9.

17. Wei, Y.D., U. Rannug, and A. Rannug, *UV-induced CYP1A1 gene expression in human cells is mediated by tryptophan.* Chem Biol Interact, 1999. 118(2): p. 127-40.

18. Tischkau, S.A., *AHR and the Circadian Clock*, in *The AH Receptor in Biology and Toxicology*, R. Pohjanvirta, Editor. 2011.

19. Jaeger, C., A.Q. Khazaal, C. Xu, M. Sun, S.L. Krager, and S.A. Tischkau, *Aryl Hydrocarbon Receptor Deficiency Alters Circadian and Metabolic Rhythmicity.* J Biol Rhythms, 2017. 32(2): p. 109-120.

20. Denison, M.S. and S.R. Nagy, *Activation of the aryl hydrocarbon receptor by structurally diverse exogenous and endogenous chemicals.* Annu Rev Pharmacol Toxicol, 2003. 43: p. 309-34.

21. Hankinson, O., *The aryl hydrocarbon receptor complex.* Annu Rev Pharmacol Toxicol, 1995. 35: p. 307-40.

22. Miller, J., D. Settachan, L. Frame, and R. Dickerson, *2,3,7,8-Tetrachlorodobenzo-p-dioxin phase advance the deer mouse (Peromyscus maniculatus) circadian rhythm by altering expression of clock proteins.* Organohalogen Compounds,, 1999. 42: p. 23-28.

23. Mukai, M., T.M. Lin, R.E. Peterson, P.S. Cooke, and S.A. Tischkau, *Behavioral rhythmicity of mice lacking AhR and attenuation of light-induced phase shift by 2,3,7,8-tetrachlorodibenzo-p-dioxin.* J Biol Rhythms, 2008. 23(3): p. 200-10.

24. Sato, S., H. Shirakawa, S. Tomita, Y. Ohsaki, K. Haketa, O. Tooi, N. Santo, M. Tohkin, Y. Furukawa, F.J. Gonzalez, and M. Komai, *Low-dose dioxins alter gene expression related to cholesterol biosynthesis, lipogenesis, and glucose metabolism through the aryl hydrocarbon receptor-mediated pathway in mouse liver.* Toxicol Appl Pharmacol, 2008. 229(1): p. 10-9.

25. Garrett, R.W. and T.A. Gasiewicz, *The aryl hydrocarbon receptor agonist 2,3,7,8-tetrachlorodibenzo-p-dioxin alters the circadian rhythms, quiescence, and expression of clock genes in murine hematopoietic stem and progenitor cells.* Mol Pharmacol, 2006. 69(6): p. 2076-83.

26. Tischkau, S.A., C.D. Jaeger, and S.L. Krager, *Circadian clock disruption in the mouse ovary in response to 2,3,7,8-tetrachlorodibenzo-p-dioxin.* Toxicol Lett, 2011. 201(2): p. 116-22.

27. Fader, K.A., R. Nault, M.P. Kirby, G. Markous, J. Matthews, and T.R. Zacharewski, *Convergence of hepcidin deficiency, systemic iron overloading, heme accumulation, and REV-ERBalpha/beta activation in aryl hydrocarbon receptor-elicited hepatotoxicity.* Toxicol Appl Pharmacol, 2017. 321: p. 1-17.

28. Fader, K.A., R. Nault, C. Zhang, K. Kumagai, J.R. Harkema, and T.R. Zacharewski, *2,3,7,8-Tetrachlorodibenzo-p-dioxin (TCDD)-elicited effects on bile acid homeostasis: Alterations in biosynthesis, enterohepatic circulation, and microbial metabolism.* Sci Rep, 2017. 7(1): p. 5921.

29. Nault, R., K.A. Fader, and T. Zacharewski, *RNA-Seq versus oligonucleotide array assessment of dose-dependent TCDD-elicited hepatic gene expression in mice.* BMC Genomics, 2015. 16(1): p. 373.

30. Kitanishi, K., J. Igarashi, K. Hayasaka, N. Hikage, I. Saiful, S. Yamauchi, T. Uchida, K. Ishimori, and T. Shimizu, *Heme-binding characteristics of the isolated PAS-A domain of mouse Per2, a transcriptional regulatory factor associated with circadian rhythms.* Biochemistry, 2008. 47(23): p. 6157-68.

31. Dioum, E.M., J. Rutter, J.R. Tuckerman, G. Gonzalez, M.A. Gilles-Gonzalez, and S.L. McKnight, *NPAS2: a gas-responsive transcription factor.* Science, 2002. 298(5602): p. 2385-7.

32. Lukat-Rodgers, G.S., C. Correia, M.V. Botuyan, G. Mer, and K.R. Rodgers, *Heme-based sensing by the mammalian circadian protein CLOCK.* Inorg Chem, 2010. 49(14): p. 6349-65.

33. Raghuram, S., K.R. Stayrook, P. Huang, P.M. Rogers, A.K. Nosie, D.B. McClure, L.L. Burris, S. Khorasanizadeh, T.P. Burris, and F. Rastinejad, *Identification of heme as the ligand for the orphan nuclear receptors REV-ERBalpha and REV-ERBbeta.* Nat Struct Mol Biol, 2007. 14(12): p. 1207-13.

34. Sorg, O., M. Zennegg, P. Schmid, R. Fedosyuk, R. Valikhnovskyi, O. Gaide, V. Kniazevych, and J.H. Saurat, *2,3,7,8-tetrachlorodibenzo-p-dioxin (TCDD) poisoning in Victor Yushchenko: identification and measurement of TCDD metabolites.* Lancet, 2009. 374(9696): p. 1179-85.

35. Wolfe, W.H., J.E. Michalek, J.C. Miner, J.L. Pirkle, S.P. Caudill, D.G. Patterson, Jr., and L.L. Needham, *Determinants of TCDD half-life in veterans of operation ranch hand.* J Toxicol Environ Health, 1994. 41(4): p. 481-8.

36. Gasiewicz, T.A., L.E. Geiger, G. Rucci, and R.A. Neal, *Distribution, excretion, and metabolism of 2,3,7,8-tetrachlorodibenzo-p-dioxin in C57BL/6J, DBA/2J, and B6D2F1/J mice.* Drug Metab Dispos, 1983. 11(5): p. 397-403.

37. Birnbaum, L.S., *Distribution and excretion of 2,3,7,8-tetrachlorodibenzo-p-dioxin in congenic strains of mice which differ at the Ah locus.* Drug Metab Dispos, 1986. 14(1): p. 34-40.

38. Boverhof, D.R., L.D. Burgoon, C. Tashiro, B. Chittim, J.R. Harkema, D.B. Jump, and T.R. Zacharewski, *Temporal and dose-dependent hepatic gene expression patterns in*

mice provide new insights into TCDD-Mediated hepatotoxicity. Toxicol Sci, 2005. 85(2): p. 1048-63.

39. Matthews, J., B. Wihlen, J. Thomsen, and J.A. Gustafsson, *Aryl hydrocarbon receptor-mediated transcription: ligand-dependent recruitment of estrogen receptor alpha to 2,3,7,8-tetrachlorodibenzo-p-dioxin-responsive promoters.* Mol Cell Biol, 2005. 25(13): p. 5317-28.

40. Rey, G., F. Cesbron, J. Rougemont, H. Reinke, M. Brunner, and F. Naef, *Genome-wide and phase-specific DNA-binding rhythms of BMAL1 control circadian output functions in mouse liver.* PLoS Biol, 2011. 9(2): p. e1000595.

41. Xu, C.X., S.L. Krager, D.F. Liao, and S.A. Tischkau, *Disruption of CLOCK-BMAL1 transcriptional activity is responsible for aryl hydrocarbon receptor-mediated regulation of Period1 gene.* Toxicol Sci, 2010. 115(1): p. 98-108.

42. Nault, R., K.A. Fader, M.P. Kirby, S. Ahmed, J. Matthews, A.D. Jones, S.Y. Lunt, and T.R. Zacharewski, *Pyruvate Kinase Isoform Switching and Hepatic Metabolic Reprogramming by the Environmental Contaminant 2,3,7,8-Tetrachlorodibenzo-p-Dioxin.* Toxicol Sci, 2016. 149(2): p. 358-71.

43. Teoh, S.T., M.P. Ogrodzinski, C. Ross, K.W. Hunter, and S.Y. Lunt, *Sialic Acid Metabolism: A Key Player in Breast Cancer Metastasis Revealed by Metabolomics.* Front Oncol, 2018. 8: p. 174.

44. Hughes, M.E., J.B. Hogenesch, and K. Kornacker, *JTK_CYCLE: an efficient nonparametric algorithm for detecting rhythmic components in genome-scale data sets.* J Biol Rhythms, 2010. 25(5): p. 372-80.

45. Huang da, W., B.T. Sherman, and R.A. Lempicki, *Systematic and integrative analysis of large gene lists using DAVID bioinformatics resources.* Nat Protoc, 2009. 4(1): p. 44-57.

46. Li, S., Y. Park, S. Duraisingham, F.H. Strobel, N. Khan, Q.A. Soltow, D.P. Jones, and B. Pulendran, *Predicting network activity from high throughput metabolomics.* PLoS Comput Biol, 2013. 9(7): p. e1003123.

47. Sinturel, F., A. Gerber, D. Mauvoisin, J. Wang, D. Gatfield, J.J. Stubblefield, C.B. Green, F. Gachon, and U. Schibler, *Diurnal Oscillations in Liver Mass and Cell Size Accompany Ribosome Assembly Cycles.* Cell, 2017. 169(4): p. 651-663 e14.

48. Kast, A., J. Nishikawa, T. Yabe, H. Nanri, and H. Albert, *Circadian rhythm of liver parameters (cellular structures, mitotic activity, glycogen and lipids in liver and serum) during three consecutive cycles in phenobarbital-treated rats.* Chronobiol Int, 1988. 5(4): p. 363-85.

49. Fader, K.A., R. Nault, D.A. Ammendolia, J.R. Harkema, K.J. Williams, R.B. Crawford, N.E. Kaminski, D. Potter, B. Sharratt, and T.R. Zacharewski, *2,3,7,8-Tetrachlorodibenzo-p-Dioxin Alters Lipid Metabolism and Depletes Immune Cell Populations in the Jejunum of C57BL/6 Mice.* Toxicol Sci, 2015. 148(2): p. 567-80.

50. Chapman, D.E. and C.M. Schiller, *Dose-related effects of 2,3,7,8-tetrachlorodibenzo-p-dioxin (TCDD) in C57BL/6J and DBA/2J mice.* Toxicol Appl Pharmacol, 1985. 78(1): p. 147-57.

51. Takeda, Y., R. Jothi, V. Birault, and A.M. Jetten, *RORgamma directly regulates the circadian expression of clock genes and downstream targets in vivo.* Nucleic Acids Res, 2012. 40(17): p. 8519-35.

52. Nault, R., K.A. Fader, J.R. Harkema, and T. Zacharewski, *Loss of liver-specific and sexually dimorphic gene expression by aryl hydrocarbon receptor activation in C57BL/6 mice.* PLoS One, 2017. 12(9): p. e0184842.

53. Nault, R., C.M. Doskey, K.A. Fader, C.E. Rockwell, and T. Zacharewski, *Comparison of Hepatic NRF2 and Aryl Hydrocarbon Receptor Binding in 2,3,7,8-Tetrachlorodibenzo-p-dioxin-Treated Mice Demonstrates NRF2-Independent PKM2 Induction.* Mol Pharmacol, 2018. 94(2): p. 876-884.

54. Yoo, S.H., C.H. Ko, P.L. Lowrey, E.D. Buhr, E.J. Song, S. Chang, O.J. Yoo, S. Yamazaki, C. Lee, and J.S. Takahashi, *A noncanonical E-box enhancer drives mouse Period2 circadian oscillations in vivo.* Proc Natl Acad Sci U S A, 2005. 102(7): p. 2608-13.

55. Kalsbeek, A., S. la Fleur, and E. Fliers, *Circadian control of glucose metabolism.* Mol Metab, 2014. 3(4): p. 372-83.

56. Takashima, M., W. Ogawa, K. Hayashi, H. Inoue, S. Kinoshita, Y. Okamoto, H. Sakaue, Y. Wataoka, A. Emi, Y. Senga, Y. Matsuki, E. Watanabe, R. Hiramatsu, and M. Kasuga, *Role of KLF15 in regulation of hepatic gluconeogenesis and metformin action.* Diabetes, 2010. 59(7): p. 1608-15.

57. Yin, L., N. Wu, J.C. Curtin, M. Qatanani, N.R. Szwergold, R.A. Reid, G.M. Waitt, D.J. Parks, K.H. Pearce, G.B. Wisely, and M.A. Lazar, *Rev-erbalpha, a heme sensor that coordinates metabolic and circadian pathways.* Science, 2007. 318(5857): p. 1786-9.

58. Kim, H., Z. Zheng, P.D. Walker, G. Kapatos, and K. Zhang, *CREBH Maintains Circadian Glucose Homeostasis by Regulating Hepatic Glycogenolysis and Gluconeogenesis.* Mol Cell Biol, 2017. 37(14).

59. Doi, R., K. Oishi, and N. Ishida, *CLOCK regulates circadian rhythms of hepatic glycogen synthesis through transcriptional activation of Gys2.* J Biol Chem, 2010. 285(29): p. 22114-21.

60. Nault, R., K.A. Fader, D.A. Ammendolia, P. Dornbos, D. Potter, B. Sharratt, K. Kumagai, J.R. Harkema, S.Y. Lunt, J. Matthews, and T. Zacharewski, *Dose-Dependent Metabolic Reprogramming and Differential Gene Expression in TCDD-Elicited Hepatic Fibrosis.* Toxicol Sci, 2016. 154(2): p. 253-266.

61. Lavery, D.J. and U. Schibler, *Circadian transcription of the cholesterol 7 alpha hydroxylase gene may involve the liver-enriched bZIP protein DBP.* Genes Dev, 1993. 7(10): p. 1871-84.

62. Duez, H., J.N. van der Veen, C. Duhem, B. Pourcet, T. Touvier, C. Fontaine, B. Derudas, E. Bauge, R. Havinga, V.W. Bloks, H. Wolters, F.H. van der Sluijs, B. Vennstrom, F. Kuipers, and B. Staels, *Regulation of bile acid synthesis by the nuclear receptor Rev-erbalpha.* Gastroenterology, 2008. 135(2): p. 689-98.

63. Zhang, Y.K., G.L. Guo, and C.D. Klaassen, *Diurnal variations of mouse plasma and hepatic bile acid concentrations as well as expression of biosynthetic enzymes and transporters.* PLoS One, 2011. 6(2): p. e16683.

64. Ma, K., R. Xiao, H.T. Tseng, L. Shan, L. Fu, and D.D. Moore, *Circadian dysregulation disrupts bile acid homeostasis.* PLoS One, 2009. 4(8): p. e6843.

65. Kaasik, K. and C.C. Lee, *Reciprocal regulation of haem biosynthesis and the circadian clock in mammals.* Nature, 2004. 430(6998): p. 467-71.

66. Handschin, C., J. Lin, J. Rhee, A.K. Peyer, S. Chin, P.H. Wu, U.A. Meyer, and B.M. Spiegelman, *Nutritional regulation of hepatic heme biosynthesis and porphyria through PGC-1alpha.* Cell, 2005. 122(4): p. 505-15.

67. Fader, K.A., R. Nault, S. Raehtz, L.R. McCabe, and T.R. Zacharewski, *2,3,7,8-Tetrachlorodibenzo-p-dioxin dose-dependently increases bone mass and decreases marrow adiposity in juvenile mice.* Toxicol Appl Pharmacol, 2018. 348: p. 85-98.

68. Edgar, R.S., E.W. Green, Y. Zhao, G. van Ooijen, M. Olmedo, X. Qin, Y. Xu, M. Pan, U.K. Valekunja, K.A. Feeney, E.S. Maywood, M.H. Hastings, N.S. Baliga, M. Merrow, A.J. Millar, C.H. Johnson, C.P. Kyriacou, J.S. O'Neill, and A.B. Reddy, *Peroxiredoxins are conserved markers of circadian rhythms.* Nature, 2012. 485(7399): p. 459-64.

69. Stangherlin, A. and A.B. Reddy, *Regulation of circadian clocks by redox homeostasis.* J Biol Chem, 2013. 288(37): p. 26505-11.

70. Rutter, J., M. Reick, L.C. Wu, and S.L. McKnight, *Regulation of clock and NPAS2 DNA binding by the redox state of NAD cofactors.* Science, 2001. 293(5529): p. 510-4.

71. Sautin, Y.Y. and R.J. Johnson, *Uric acid: the oxidant-antioxidant paradox.* Nucleosides Nucleotides Nucleic Acids, 2008. 27(6): p. 608-19.

72. Sugihara, K., S. Kitamura, T. Yamada, S. Ohta, K. Yamashita, M. Yasuda, and Y. Fujii-Kuriyama, *Aryl hydrocarbon receptor (AhR)-mediated induction of xanthine oxidase/xanthine dehydrogenase activity by 2,3,7,8-tetrachlorodibenzo-p-dioxin.* Biochem Biophys Res Commun, 2001. 281(5): p. 1093-9.

73. Gachon, F. and D. Firsov, *The role of circadian timing system on drug metabolism and detoxification.* Expert Opin Drug Metab Toxicol, 2011. 7(2): p. 147-58.

74. Gumz, M.L., *Taking into account circadian rhythm when conducting experiments on animals.* Am J Physiol Renal Physiol, 2016. 310(6): p. F454-5.

75. Matveyenko, A.V., *Consideration for Circadian Physiology in Rodent Research.* Physiology (Bethesda), 2018. 33(4): p. 250-251.

76. Oike, H., K. Oishi, and M. Kobori, *Nutrients, Clock Genes, and Chrononutrition.* Curr Nutr Rep, 2014. 3: p. 204-212.

77. Nault, R., K.A. Fader, T.A. Lydic, and T.R. Zacharewski, *Lipidomic Evaluation of Aryl Hydrocarbon Receptor-Mediated Hepatic Steatosis in Male and Female Mice Elicited by 2,3,7,8-Tetrachlorodibenzo-p-dioxin.* Chem Res Toxicol, 2017. 30(4): p. 1060-1075.

78. McConnell, E.E., J.A. Moore, J.K. Haseman, and M.W. Harris, *The comparative toxicity of chlorinated dibenzo-p-dioxins in mice and guinea pigs.* Toxicol Appl Pharmacol, 1978. 44(2): p. 335-56.

79. Harris, M.W., J.A. Moore, J.G. Vos, and B.N. Gupta, *General biological effects of TCDD in laboratory animals.* Environ Health Perspect, 1973. 5: p. 101-9.

80. Summa, K.C., R.M. Voigt, C.B. Forsyth, M. Shaikh, K. Cavanaugh, Y. Tang, M.H. Vitaterna, S. Song, F.W. Turek, and A. Keshavarzian, *Disruption of the Circadian Clock in Mice Increases Intestinal Permeability and Promotes Alcohol-Induced Hepatic Pathology and Inflammation.* PLoS One, 2013. 8(6): p. e67102.

81. Voigt, R.M., C.B. Forsyth, S.J. Green, E. Mutlu, P. Engen, M.H. Vitaterna, F.W. Turek, and A. Keshavarzian, *Circadian disorganization alters intestinal microbiota.* PLoS One, 2014. 9(5): p. e97500.

82. Froy, O., *Metabolism and circadian rhythms--implications for obesity.* Endocr Rev, 2010. 31(1): p. 1-24.

83. Mazzoccoli, G., S. De Cosmo, and T. Mazza, *The Biological Clock: A Pivotal Hub in Non-alcoholic Fatty Liver Disease Pathogenesis.* Front Physiol, 2018. 9: p. 193.

CHAPTER 7: CONCLUSIONS AND FUTURE RESEARCH

Accumulating evidence demonstrates that exposure to environmental contaminants such as 2,3,7,8-tetrachlordibenzo-*p*-dioxin (TCDD) and related aryl hydrocarbon receptor (AhR) agonists is associated with complex metabolic disorders including non-alcoholic fatty liver disease (NAFLD) [1-4]. Historically, the majority of studies investigating AhR-mediated hepatotoxicity, NAFLD, and hepatocellular carcinoma have focused entirely on the liver without considering interactions between hepatic and intestinal homeostasis. The studies in this report demonstrate that TCDD-elicited AhR activation leads to segment-specific transcriptional and functional changes along the intestinal tract that promote the development of hepatic steatosis with progression to steatohepatitis and fibrosis (Figure 54). These perturbations in the intestine-liver axis not only provide novel insight into the underlying mechanisms involved in NAFLD but may also represent potential therapeutic targets. Overall, this report provides compelling evidence that dysregulation of both the intestine-liver axis and the host-microbiota relationship play underappreciated roles in AhR-mediated NAFLD.

TCDD ELICITS SEGMENT-SPECIFIC EFFECTS ALONG THE INTESTINE-LIVER AXIS

TCDD elicits alterations along the intestine-liver axis which contribute to the development and progression of AhR-mediated NAFLD (Figure 55). TCDD-elicited repression of hepatic hepcidin allowed continuous duodenal absorption of dietary iron, leading to systemic iron accumulation and hepatic oxidative stress (Chapter 5). Moreover, increased paracellular permeability of the gastroduodenal region may increase passive nutrient and mineral absorption, further contributing to iron overloading (Chapter 4). In the jejunal epithelium, TCDD induced several genes associated with dietary lipid digestion (e.g. *Pnlip, Clps*) and fatty acid absorption (e.g. *Cd36*), consistent with hepatic dietary lipid accumulation (Chapter 3). Induction of ileal transporters responsible for bile acid reabsorption (e.g. *Slc10a2*, *Slc51a*), combined with hepatic induction of liver-to-blood exporters (e.g. *Abcc4*) and repression of blood-to-liver importers (e.g. *Slc10a1*, *Slco1a1*) dysregulated enterohepatic circulation, contributing to bile acid accumulation

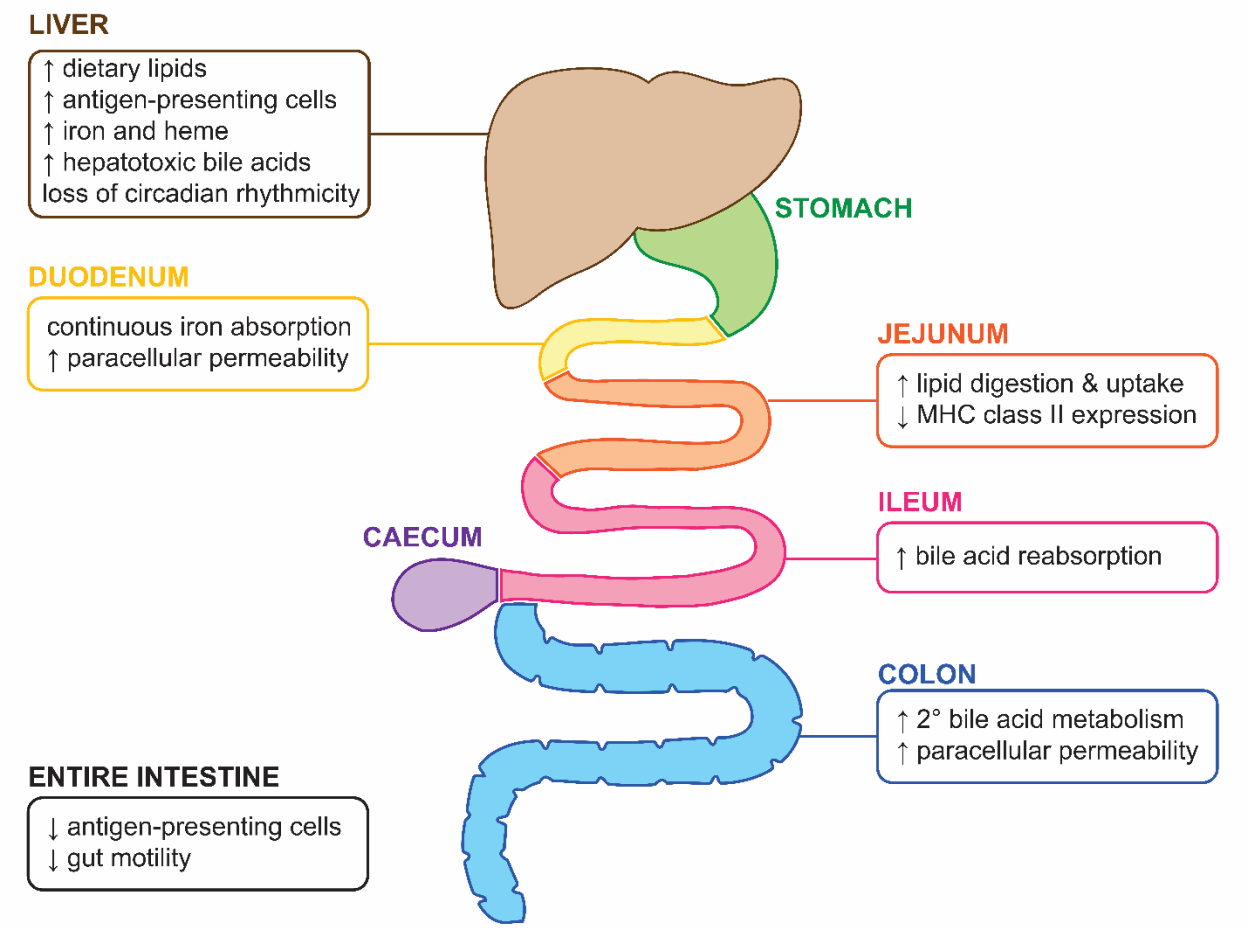

FIGURE 54. SUMMARY OF TCDD-ELICITED SEGMENT-SPECIFIC EFFECTS ALONG THE INTESTINE-LIVER AXIS

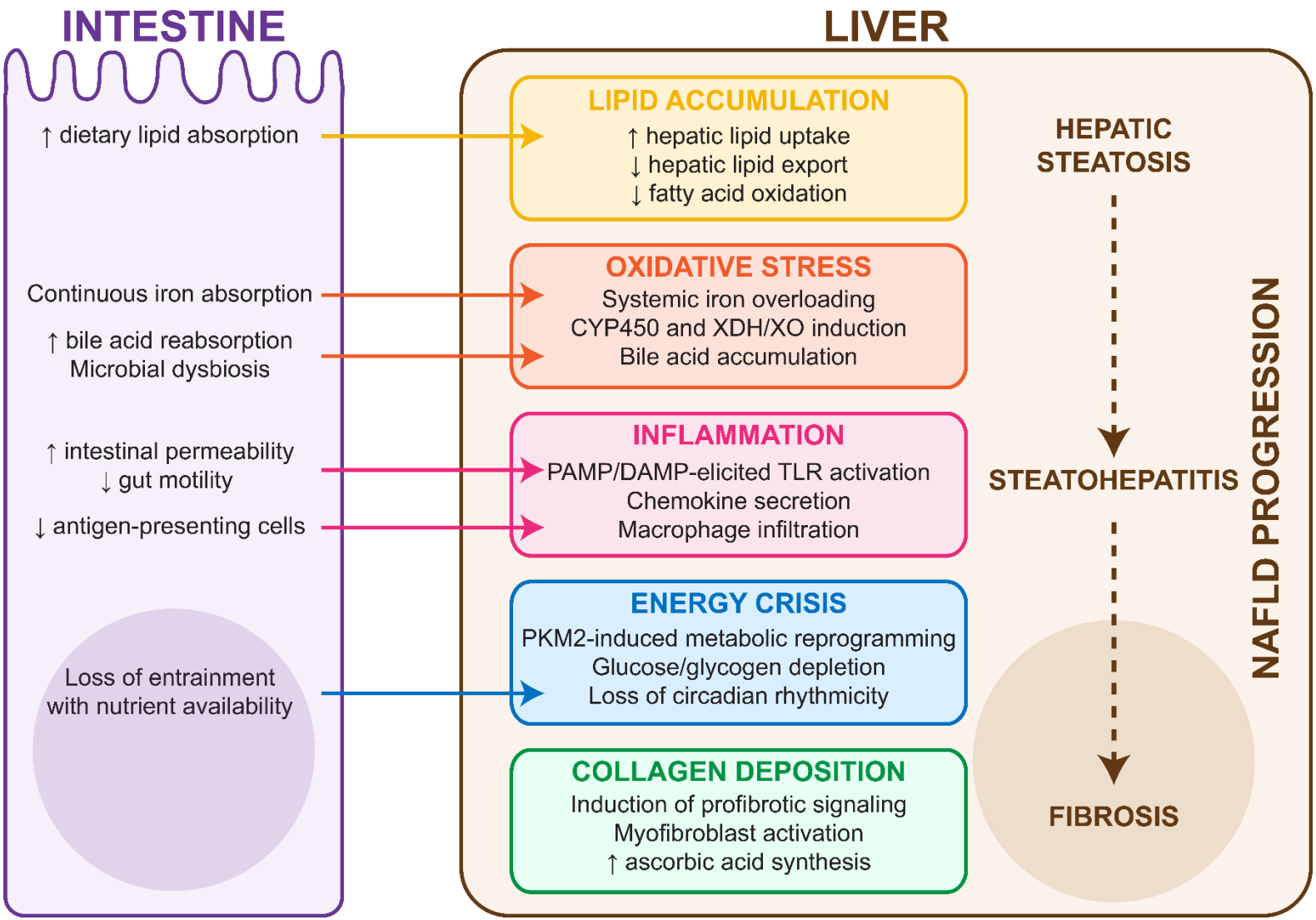

FIGURE 55. TCDD-ELICITED ALTERATIONS IN INTESTINAL FUNCTION PROMOTE KEY HEPATIC FEATURES OF NAFLD

in the liver and serum (Chapter 4). Moreover, increased colonic levels of microbial *bsh* and *baiCD* were consistent with accumulation of hepatotoxic secondary bile acid species such as taurolithocholic acid, which has been linked with bile duct proliferation, cholestasis, and oxidative stress (Chapter 4). TCDD also increased colonic paracellular permeability, which could promote increased translocation of bacteria and bacterial products (e.g. lipopolysaccharide (LPS)) across the intestinal barrier and initiate an innate immune response (Chapter 4).

In addition to segment-specific effects, TCDD decreased gut motility, which may contribute to microbial dysbiosis and increase nutrient absorption (Chapter 4). Moreover, TCDD depleted antigen-presenting cells (APCs) including macrophages and dendritic cells within the lamina propria of the small intestine, consistent with decreased jejunal transcript levels of major histocompatibility complex (MHC) class II genes (Chapter 3). Given the reciprocal infiltration of macrophages into the liver, combined with hepatic induction of several chemokines and chemokine receptors, it is tempting to speculate that APCs may migrate from the intestine to the liver via the portal vein. However, it is also possible that intestinal APCs migrated into mesenteric lymph nodes following exposure to a foreign antigen, leading to T cell activation and secretion of pro-inflammatory cytokines. Regardless of the underlying mechanism responsible, these reciprocal changes suggest the intestine may play a role in TCDD-elicited hepatic immune cell infiltration. These changes in intestinal function occurred in the absence of overt morphological toxicity to the intestinal mucosa, as assessed through hematoxylin and eosin (H&E) staining.

Beyond the effects on intestinal transcription and function, TCDD also disrupted synchronization between the intestine and the liver by abolishing hepatic circadian rhythmicity. Persistent AhR activation dampened the rhythmic expression of the core clock regulators and altered cues responsible for entraining hepatic cycling (Chapter 6). For example, TCDD increased hepatic heme levels while abolishing the circadian regulation of *de novo* heme biosynthesis, thereby rendering the clock less responsive to changes in feeding times and nutrient availability (Chapter 5,6). In turn, virtually all circadian-regulated genes and metabolites lost rhythmicity,

decoupling hepatic metabolism from feeding/fasting cycles. Specifically, the circadian regulation of dietary lipid metabolism, bile acid homeostasis, and glycogen synthesis was abolished, further dysregulating enterohepatic circulation and metabolic efficiency (Chapter 6). Moreover, recent studies have reported that perturbations in circadian rhythm increase intestinal permeability and alter the gut microbiome, further contributing to NAFLD development [5, 6]. Overall, TCDD-elicited AhR activation dysregulates hepatic metabolism, intestinal homeostasis, and circadian rhythmicity through multiple interlinked mechanisms.

This report contributes to the AhR field by demonstrating that the intestine is an important yet underappreciated target of TCDD-elicited toxicity. AhR activation alters the transcriptome of the intestinal epithelium in a segment-specific manner, leading to changes in intestinal functions such as nutrient absorption and enterohepatic circulation. TCDD-elicited dysfunction of the epithelial barrier, gut motility, innate immune defenses, and the microbiome further dysregulate the homeostasis of the gastrointestinal system. Given its critical function as a barrier to the external luminal contents, these changes impact the metabolic status of other organ systems, as well as the systemic homeostasis of the entire body. Therefore, intestinal dysfunction should be considered when investigating the toxicity of classical AhR targets such as the liver. Further studies will be needed to distinguish direct AhR effects on the intestinal epithelium versus secondary changes in response to systemic dysregulation.

FUTURE STUDIES

This report identified multiple mechanisms through which alterations in intestinal function may promote the development and progression of AhR-mediated NAFLD. However, the relative contributions of intestinal vs. hepatic alterations in driving the TCDD-elicited hepatic phenotype remain unclear. Tissue-specific tamoxifen-inducible AhR knockout (KO) models could be utilized to provide insight into the contributions of AhR-mediated intestinal dysfunction. This would involve comparing TCDD-elicited hepatotoxicity in wild type mice against that of the following models: (i)

whole body AhR KO, (ii) hepatocyte-specific AhR KO where Cre recombinase expression is driven by the albumin promoter ($Ahr^{flox/flox}$; *Alb-Cre*/ERT2) [7], and (iii) intestinal enterocyte-specific AhR KO where Cre recombinase expression is driven by the villin 1 promoter ($Ahr^{flox/flox}$; *Vil1-Cre*/ERT2) [8]. The use of tamoxifen-inducible Cre recombinase allows AhR to be knocked out during adulthood, thereby avoiding the developmental side-effects reported in AhR-null mice [9-11]. Additionally, the TCDD-elicited hepatic phenotypes observed in these tissue-specific AhR KOs could also be compared against antibiotic-mediated sterilized mice to examine the relative contribution of the gut microbiome to NAFLD progression [12, 13]. Insight into the tissue-specific and microbial roles in NAFLD development could help identify effective targets for preventative and therapeutic strategies.

AhR activation not only perturbs the rhythmicity of the hepatic clock as described in Chapter 6, but is also reported to alter the expression of core clock genes within other peripheral tissues such as the ovaries and bone marrow [14, 15]. However, the effects of AhR activation on the rhythmicity of the gastrointestinal clock have not been examined. Interestingly, the circadian clock is known to regulate several important intestinal functions including: (i) gut motility, (ii) maintenance and restoration of the intestinal barrier, (iii) expression and secretion of digestive enzymes, (iv) nutrient absorption (e.g. lipids), and (v) intestinal immune responses [16, 17]. Transcriptomic, proteomic, and/or metabolomic analyses of the intestinal epithelium at 3-hour (h) intervals over a 24h period could provide insight into whether AhR-mediated dysregulation of the intestinal clock contributes to TCDD-elicited alterations in these circadian-controlled functions. Furthermore, the interplay between circadian rhythmicity and the microbiome warrants further investigation. For example, it is reported that the gut microbiome regulates the cycling of the circadian transcription factor NFIL3, which controls daily oscillations in enterocyte lipid absorption, metabolism, and export [18]. It would be interesting to examine whether this regulatory mechanism plays a role in TCDD-elicited increases in dietary lipid absorption.

Chapter 4 suggests that TCDD-elicited dysbiosis of the gut microbiome promotes AhR-mediated NAFLD, where increased abundance of microbial bile acid metabolism genes (*bsh*, *baiCD*) likely contributes to the accumulation of hepatotoxic secondary bile acid species. Beyond bile acid metabolism, alterations in the microbial metabolism of short chain fatty acids (SCFAs) and choline have also been associated with NAFLD [19-22], however the effects of AhR activation on these metabolic pathways have not been investigated. Similar to the targeted approach employed for *bsh* and *baiCD* quantification, degenerate qRT-PCR could be used to assess the abundance of trimethylamine (TMA)-producing microbial genes including choline-TMA-lyase (*cutC*) and carnitine monooxygenase (*cntA*), as well as genes involved in SCFA metabolism such as butyryl-CoA:acetate CoA-transferase (*but*) and butyrate kinase (*buk*) [23, 24]. Alternatively, shotgun metagenomic sequencing followed by a function-based analysis (e.g. Xander, shotgunFunctionalizeR) could be used to assess global TCDD-elicited changes in the gut microbiome [25, 26]. Assessment of the fecal or caecal metabolome would also provide further insight into AhR-mediated dysregulation of microbial metabolism, potentially leading to the identification of additional metabolic pathways which promote NAFLD development and progression.

CONSIDERATIONS FOR MECHANISTIC INVESTIGATIONS OF NAFLD PATHOGENESIS

In Chapter 6, transcriptomic and metabolomic analyses revealed that ~25% and ~20% of hepatic genes and polar metabolites exhibit circadian oscillations, while previous studies report that ~40% of all genes in the mouse genome exhibit rhythmicity in at least one tissue [27]. In addition, more than half of the top selling pharmaceuticals in the United States target rhythmic metabolites, while several drug-metabolizing enzymes are circadian-regulated [27, 28]. Time of administration and time of sample collection may therefore affect efficacy, toxicity, and mechanism of action, and should be considered and controlled during mechanistic and safety studies [29, 30]. Furthermore, given the global effects associated with circadian rhythm

perturbation [31-34], the nocturnal nature of mice and rats should be considered when scheduling animal handling procedures during a study. For example, working with rodents in the middle of the lights on period will disrupt their sleeping phase, while turning on the lights during their active phase will disrupt light/dark cues, potentially introducing confounding effects into the study [35, 36]. To minimize such disruptions, animal handling should be limited to the transition between the lights off/lights on period (or vice versa) if possible, particularly when investigating circadian rhythm, metabolism/metabolic disorders, and/or behavior.

This report, as well as numerous other studies, have demonstrated that alterations in intestinal homeostasis play an important role in the development of metabolic disorders including NAFLD, diabetes, and obesity [37-40]. These studies highlight the dependence of hepatic homeostasis on nutrients, metabolites, and systemic cues originating from other tissues. Consequently, it is crucial to consider tissue interactions while researching complex metabolic disorders, rather than focusing on the primary target organ in isolation. Moreover, accumulating evidence including studies in Chapter 4 suggests that alterations in the gut microbiome contribute to NAFLD development, and thus host-microbiota relationships should also be considered [19-21, 41].

The TCDD-elicited effects on intestinal function described in this report (e.g. increased intestinal permeability, dysbiosis of the gut microbiome, dysregulation of bile acid homeostasis, iron overloading) are similar to alterations detected in human epidemiological studies of NAFLD patients [37, 42-44]. Moreover, the hepatic phenotype which develops following TCDD-treatment mimics the full spectrum of histopathological features associated with human NAFLD, where hepatic steatosis progresses to steatohepatitis with fibrosis as the dose and duration of exposure increase [45-50]. Therefore, AhR activation induced by ligands such as TCDD represents a relevant model to study NAFLD development and progression. In contrast to other NAFLD rodent models such as those induced by diet (e.g. high-fat, high-sucrose, choline-deficient), genetics (e.g. *foz/foz*), or chemicals (e.g. carbon tetrachloride), AhR activation dysregulates the intestine-

liver axis, mirroring the tissue interactions involved in human metabolic disorders. AhR activation also recapitulates the multifactorial nature of human disease development, involving altered nutrient absorption, oxidative stress, endocrine disruption, and gut dysbiosis [51-55]. Furthermore, AhR-mediated differential expression of target genes such as *Cd36* and *Hamp* mimics human genetic variants, where polymorphisms and/or altered expression of *CD36* and *HFE* are associated with increased susceptibility to NAFLD [56-59]. Taken together, ligand-induced AhR activation should be considered a valuable tool for investigating the development and progression of human NAFLD.

REFERENCES

REFERENCES

1. Casals-Casas, C. and B. Desvergne, *Endocrine disruptors: from endocrine to metabolic disruption.* Annu Rev Physiol, 2011. 73: p. 135-62.

2. Cave, M., S. Appana, M. Patel, K.C. Falkner, C.J. McClain, and G. Brock, *Polychlorinated biphenyls, lead, and mercury are associated with liver disease in American adults: NHANES 2003-2004.* Environ Health Perspect, 2010. 118(12): p. 1735-42.

3. Chen, J.Q., T.R. Brown, and J. Russo, *Regulation of energy metabolism pathways by estrogens and estrogenic chemicals and potential implications in obesity associated with increased exposure to endocrine disruptors.* Biochim Biophys Acta, 2009. 1793(7): p. 1128-43.

4. Grun, F. and B. Blumberg, *Endocrine disrupters as obesogens.* Mol Cell Endocrinol, 2009. 304(1-2): p. 19-29.

5. Summa, K.C., R.M. Voigt, C.B. Forsyth, M. Shaikh, K. Cavanaugh, Y. Tang, M.H. Vitaterna, S. Song, F.W. Turek, and A. Keshavarzian, *Disruption of the Circadian Clock in Mice Increases Intestinal Permeability and Promotes Alcohol-Induced Hepatic Pathology and Inflammation.* PLoS One, 2013. 8(6): p. e67102.

6. Voigt, R.M., C.B. Forsyth, S.J. Green, E. Mutlu, P. Engen, M.H. Vitaterna, F.W. Turek, and A. Keshavarzian, *Circadian disorganization alters intestinal microbiota.* PLoS One, 2014. 9(5): p. e97500.

7. Walisser, J.A., E. Glover, K. Pande, A.L. Liss, and C.A. Bradfield, *Aryl hydrocarbon receptor-dependent liver development and hepatotoxicity are mediated by different cell types.* Proc Natl Acad Sci U S A, 2005. 102(49): p. 17858-63.

8. el Marjou, F., K.P. Janssen, B.H. Chang, M. Li, V. Hindie, L. Chan, D. Louvard, P. Chambon, D. Metzger, and S. Robine, *Tissue-specific and inducible Cre-mediated recombination in the gut epithelium.* Genesis, 2004. 39(3): p. 186-93.

9. Murray, I.A., R.G. Nichols, L. Zhang, A.D. Patterson, and G.H. Perdew, *Expression of the aryl hydrocarbon receptor contributes to the establishment of intestinal microbial community structure in mice.* Sci Rep, 2016. 6: p. 33969.

10. Lahvis, G.P., S.L. Lindell, R.S. Thomas, R.S. McCuskey, C. Murphy, E. Glover, M. Bentz, J. Southard, and C.A. Bradfield, *Portosystemic shunting and persistent fetal vascular structures in aryl hydrocarbon receptor-deficient mice.* Proc Natl Acad Sci U S A, 2000. 97(19): p. 10442-7.

11. Fernandez-Salguero, P., T. Pineau, D.M. Hilbert, T. McPhail, S.S. Lee, S. Kimura, D.W. Nebert, S. Rudikoff, J.M. Ward, and F.J. Gonzalez, *Immune system impairment and hepatic fibrosis in mice lacking the dioxin-binding Ah receptor.* Science, 1995. 268(5211): p. 722-6.

12. Seki, E., S. De Minicis, C.H. Osterreicher, J. Kluwe, Y. Osawa, D.A. Brenner, and R.F. Schwabe, *TLR4 enhances TGF-beta signaling and hepatic fibrosis.* Nat Med, 2007. 13(11): p. 1324-32.

13. Cani, P.D., R. Bibiloni, C. Knauf, A. Waget, A.M. Neyrinck, N.M. Delzenne, and R. Burcelin, *Changes in gut microbiota control metabolic endotoxemia-induced inflammation in high-fat diet-induced obesity and diabetes in mice.* Diabetes, 2008. 57(6): p. 1470-81.

14. Tischkau, S.A., C.D. Jaeger, and S.L. Krager, *Circadian clock disruption in the mouse ovary in response to 2,3,7,8-tetrachlorodibenzo-p-dioxin.* Toxicol Lett, 2011. 201(2): p. 116-22.

15. Garrett, R.W. and T.A. Gasiewicz, *The aryl hydrocarbon receptor agonist 2,3,7,8-tetrachlorodibenzo-p-dioxin alters the circadian rhythms, quiescence, and expression of clock genes in murine hematopoietic stem and progenitor cells.* Mol Pharmacol, 2006. 69(6): p. 2076-83.

16. Konturek, P.C., T. Brzozowski, and S.J. Konturek, *Gut clock: implication of circadian rhythms in the gastrointestinal tract.* J Physiol Pharmacol, 2011. 62(2): p. 139-50.

17. Balakrishnan, A., A. Tavakkolizadeh, and D.B. Rhoads, *Circadian clock genes and implications for intestinal nutrient uptake.* J Nutr Biochem, 2012. 23(5): p. 417-22.

18. Wang, Y., Z. Kuang, X. Yu, K.A. Ruhn, M. Kubo, and L.V. Hooper, *The intestinal microbiota regulates body composition through NFIL3 and the circadian clock.* Science, 2017. 357(6354): p. 912-916.

19. Turnbaugh, P.J., R.E. Ley, M.A. Mahowald, V. Magrini, E.R. Mardis, and J.I. Gordon, *An obesity-associated gut microbiome with increased capacity for energy harvest.* Nature, 2006. 444(7122): p. 1027-31.

20. Spencer, M.D., T.J. Hamp, R.W. Reid, L.M. Fischer, S.H. Zeisel, and A.A. Fodor, *Association between composition of the human gastrointestinal microbiome and development of fatty liver with choline deficiency.* Gastroenterology, 2011. 140(3): p. 976-86.

21. Cho, I., S. Yamanishi, L. Cox, B.A. Methe, J. Zavadil, K. Li, Z. Gao, D. Mahana, K. Raju, I. Teitler, H. Li, A.V. Alekseyenko, and M.J. Blaser, *Antibiotics in early life alter the murine colonic microbiome and adiposity.* Nature, 2012. 488(7413): p. 621-6.

22. Wang, Z., E. Klipfell, B.J. Bennett, R. Koeth, B.S. Levison, B. Dugar, A.E. Feldstein, E.B. Britt, X. Fu, Y.M. Chung, Y. Wu, P. Schauer, J.D. Smith, H. Allayee, W.H. Tang, J.A. DiDonato, A.J. Lusis, and S.L. Hazen, *Gut flora metabolism of phosphatidylcholine promotes cardiovascular disease.* Nature, 2011. 472(7341): p. 57-63.

23. Rath, S., B. Heidrich, D.H. Pieper, and M. Vital, *Uncovering the trimethylamine-producing bacteria of the human gut microbiota.* Microbiome, 2017. 5(1): p. 54.

24. Vital, M., C.R. Penton, Q. Wang, V.B. Young, D.A. Antonopoulos, M.L. Sogin, H.G. Morrison, L. Raffals, E.B. Chang, G.B. Huffnagle, T.M. Schmidt, J.R. Cole, and J.M.

Tiedje, *A gene-targeted approach to investigate the intestinal butyrate-producing bacterial community.* Microbiome, 2013. 1(1): p. 8.

25. Wang, Q., J.A. Fish, M. Gilman, Y. Sun, C.T. Brown, J.M. Tiedje, and J.R. Cole, *Xander: employing a novel method for efficient gene-targeted metagenomic assembly.* Microbiome, 2015. 3: p. 32.

26. Kristiansson, E., P. Hugenholtz, and D. Dalevi, *ShotgunFunctionalizeR: an R-package for functional comparison of metagenomes.* Bioinformatics, 2009. 25(20): p. 2737-8.

27. Zhang, R., N.F. Lahens, H.I. Ballance, M.E. Hughes, and J.B. Hogenesch, *A circadian gene expression atlas in mammals: implications for biology and medicine.* Proc Natl Acad Sci U S A, 2014. 111(45): p. 16219-24.

28. Gachon, F. and D. Firsov, *The role of circadian timing system on drug metabolism and detoxification.* Expert Opin Drug Metab Toxicol, 2011. 7(2): p. 147-58.

29. Matveyenko, A.V., *Consideration for Circadian Physiology in Rodent Research.* Physiology (Bethesda), 2018. 33(4): p. 250-251.

30. Gumz, M.L., *Taking into account circadian rhythm when conducting experiments on animals.* Am J Physiol Renal Physiol, 2016. 310(6): p. F454-5.

31. Fonken, L.K. and R.J. Nelson, *The effects of light at night on circadian clocks and metabolism.* Endocr Rev, 2014. 35(4): p. 648-70.

32. Summa, K.C., M.H. Vitaterna, and F.W. Turek, *Environmental perturbation of the circadian clock disrupts pregnancy in the mouse.* PLoS One, 2012. 7(5): p. e37668.

33. Ebihara, S. and K. Tsuji, *Entrainment of the circadian activity rhythm to the light cycle: effective light intensity for a Zeitgeber in the retinal degenerate C3H mouse and the normal C57BL mouse.* Physiol Behav, 1980. 24(3): p. 523-7.

34. Brainard, G.C., M.K. Vaughan, and R.J. Reiter, *Effect of light irradiance and wavelength on the Syrian hamster reproductive system.* Endocrinology, 1986. 119(2): p. 648-54.

35. Stenvers, D.J., R. van Dorp, E. Foppen, J. Mendoza, A.L. Opperhuizen, E. Fliers, P.H. Bisschop, J.H. Meijer, A. Kalsbeek, and T. Deboer, *Dim light at night disturbs the daily sleep-wake cycle in the rat.* Sci Rep, 2016. 6: p. 35662.

36. Roedel, A., C. Storch, F. Holsboer, and F. Ohl, *Effects of light or dark phase testing on behavioural and cognitive performance in DBA mice.* Lab Anim, 2006. 40(4): p. 371-81.

37. Miele, L., V. Valenza, G. La Torre, M. Montalto, G. Cammarota, R. Ricci, R. Masciana, A. Forgione, M.L. Gabrieli, G. Perotti, F.M. Vecchio, G. Rapaccini, G. Gasbarrini, C.P. Day, and A. Grieco, *Increased intestinal permeability and tight junction alterations in nonalcoholic fatty liver disease.* Hepatology, 2009. 49(6): p. 1877-87.

38. Ridlon, J.M., J.M. Alves, P.B. Hylemon, and J.S. Bajaj, *Cirrhosis, bile acids and gut microbiota: unraveling a complex relationship.* Gut Microbes, 2013. 4(5): p. 382-7.

39. Musso, G., R. Gambino, and M. Cassader, *Obesity, diabetes, and gut microbiota: the hygiene hypothesis expanded?* Diabetes Care, 2010. 33(10): p. 2277-84.

40. Kirpich, I.A., L.S. Marsano, and C.J. McClain, *Gut-liver axis, nutrition, and non-alcoholic fatty liver disease.* Clin Biochem, 2015. 48(13-14): p. 923-30.

41. Leung, C., L. Rivera, J.B. Furness, and P.W. Angus, *The role of the gut microbiota in NAFLD.* Nat Rev Gastroenterol Hepatol, 2016. 13(7): p. 412-25.

42. Mouzaki, M., A.Y. Wang, R. Bandsma, E.M. Comelli, B.M. Arendt, L. Zhang, S. Fung, S.E. Fischer, I.G. McGilvray, and J.P. Allard, *Bile Acids and Dysbiosis in Non-Alcoholic Fatty Liver Disease.* PLoS One, 2016. 11(5): p. e0151829.

43. Doulberis, M., G. Kotronis, D. Gialamprinou, J. Kountouras, and P. Katsinelos, *Non-alcoholic fatty liver disease: An update with special focus on the role of gut microbiota.* Metabolism, 2017. 71: p. 182-197.

44. George, D.K., S. Goldwurm, G.A. MacDonald, L.L. Cowley, N.I. Walker, P.J. Ward, E.C. Jazwinska, and L.W. Powell, *Increased hepatic iron concentration in nonalcoholic steatohepatitis is associated with increased fibrosis.* Gastroenterology, 1998. 114(2): p. 311-8.

45. Pierre, S., A. Chevallier, F. Teixeira-Clerc, A. Ambolet-Camoit, L.C. Bui, A.S. Bats, J.C. Fournet, P. Fernandez-Salguero, M. Aggerbeck, S. Lotersztajn, R. Barouki, and X. Coumoul, *Aryl hydrocarbon receptor-dependent induction of liver fibrosis by dioxin.* Toxicol Sci, 2014. 137(1): p. 114-24.

46. Boverhof, D.R., L.D. Burgoon, C. Tashiro, B. Chittim, J.R. Harkema, D.B. Jump, and T.R. Zacharewski, *Temporal and dose-dependent hepatic gene expression patterns in mice provide new insights into TCDD-Mediated hepatotoxicity.* Toxicol Sci, 2005. 85(2): p. 1048-63.

47. Kopec, A.K., D.R. Boverhof, R. Nault, J.R. Harkema, C. Tashiro, D. Potter, B. Sharratt, B. Chittim, and T.R. Zacharewski, *Toxicogenomic evaluation of long-term hepatic effects of TCDD in immature, ovariectomized C57BL/6 mice.* Toxicol Sci, 2013. 135(2): p. 465-75.

48. Hashimoto, E., M. Taniai, and K. Tokushige, *Characteristics and diagnosis of NAFLD/NASH.* J Gastroenterol Hepatol, 2013. 28 Suppl 4: p. 64-70.

49. Nault, R., K.A. Fader, M.P. Kirby, S. Ahmed, J. Matthews, A.D. Jones, S.Y. Lunt, and T.R. Zacharewski, *Pyruvate Kinase Isoform Switching and Hepatic Metabolic Reprogramming by the Environmental Contaminant 2,3,7,8-Tetrachlorodibenzo-p-Dioxin.* Toxicol Sci, 2016. 149(2): p. 358-71.

50. Nault, R., K.A. Fader, D.A. Ammendolia, P. Dornbos, D. Potter, B. Sharratt, K. Kumagai, J.R. Harkema, S.Y. Lunt, J. Matthews, and T. Zacharewski, *Dose-Dependent Metabolic Reprogramming and Differential Gene Expression in TCDD-Elicited Hepatic Fibrosis.* Toxicol Sci, 2016. 154(2): p. 253-266.

51. Stohs, S.J., *Oxidative stress induced by 2,3,7,8-tetrachlorodibenzo-p-dioxin (TCDD).* Free Radic Biol Med, 1990. 9(1): p. 79-90.

52. Lefever, D.E., J. Xu, Y. Chen, G. Huang, N. Tamas, and T.L. Guo, *TCDD modulation of gut microbiome correlated with liver and immune toxicity in streptozotocin (STZ)-induced hyperglycemic mice.* Toxicol Appl Pharmacol, 2016. 304: p. 48-58.

53. Angrish, M.M., B.D. Mets, A.D. Jones, and T.R. Zacharewski, *Dietary fat is a lipid source in 2,3,7,8-tetrachlorodibenzo-rho-dioxin (TCDD)-elicited hepatic steatosis in C57BL/6 mice.* Toxicol Sci, 2012. 128(2): p. 377-86.

54. Lee, J.H., T. Wada, M. Febbraio, J. He, T. Matsubara, M.J. Lee, F.J. Gonzalez, and W. Xie, *A novel role for the dioxin receptor in fatty acid metabolism and hepatic steatosis.* Gastroenterology, 2010. 139(2): p. 653-63.

55. Lu, P., J. Yan, K. Liu, W.G. Garbacz, P. Wang, M. Xu, X. Ma, and W. Xie, *Activation of aryl hydrocarbon receptor dissociates fatty liver from insulin resistance by inducing fibroblast growth factor 21.* Hepatology, 2015. 61(6): p. 1908-19.

56. Sheedfar, F., M.M. Sung, M. Aparicio-Vergara, N.J. Kloosterhuis, M.E. Miquilena-Colina, J. Vargas-Castrillon, M. Febbraio, R.L. Jacobs, A. de Bruin, M. Vinciguerra, C. Garcia-Monzon, M.H. Hofker, J.R. Dyck, and D.P. Koonen, *Increased hepatic CD36 expression with age is associated with enhanced susceptibility to nonalcoholic fatty liver disease.* Aging (Albany NY), 2014. 6(4): p. 281-95.

57. Ramos-Lopez, O., S. Roman, E. Martinez-Lopez, N.A. Fierro, K. Gonzalez-Aldaco, A. Jose-Abrego, and A. Panduro, *CD36 genetic variation, fat intake and liver fibrosis in chronic hepatitis C virus infection.* World J Hepatol, 2016. 8(25): p. 1067-74.

58. Lee, S.H., S.H. Jeong, D. Lee, J.H. Lee, S.H. Hwang, Y.A. Cho, Y.S. Park, J.H. Hwang, J.W. Kim, N. Kim, D.H. Lee, and W. Kang, *An epidemiologic study on the incidence and significance of HFE mutations in a Korean cohort with nonalcoholic fatty liver disease.* J Clin Gastroenterol, 2010. 44(7): p. e154-61.

59. Valenti, L., P. Dongiovanni, A.L. Fracanzani, G. Santorelli, E. Fatta, C. Bertelli, E. Taioli, G. Fiorelli, and S. Fargion, *Increased susceptibility to nonalcoholic fatty liver disease in heterozygotes for the mutation responsible for hereditary hemochromatosis.* Dig Liver Dis, 2003. 35(3): p. 172-8.